

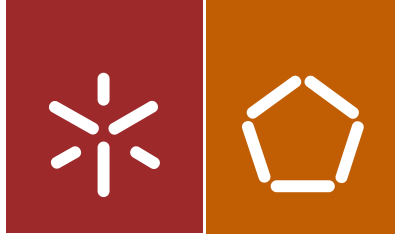


Universidade do Minho
Escola de Engenharia

Leonardo Avila Velez

Seismic behavior of
concrete block masonry buildings

Dezembro de 2014



Universidade do Minho
Escola de Engenharia

Leonardo Avila Velez

Seismic behavior of
concrete block masonry buildings

Tese de Doutoramento
Engenharia Civil

Trabalho efectuado sob a orientação de
Professora Doutora Graça Vasconcelos
Professor Doutor Paulo B. Lourenço

Dezembro de 2014

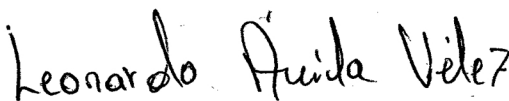
Statement of integrity

I hereby declare having conducted my thesis with integrity. I confirm that I have not used plagiarism or any form of falsification of results in the process of the thesis elaboration.

I further declare that I have fully acknowledged the Code of Ethical Conduct of the University of Minho

University of Minho, 15/Dezembro/2014

Full name: Leonardo Avila Velez

Signature:  Leonardo Avila Velez

...to my grandmother, my parents and my wife

ACKNOWLEDGEMENTS

First of all, I am always thankful with God to give me during all my live the persons, the moments and the situations that made of me who I am right now, all of them have been in the correct time even if at that time I did not think it was like that.

I want to thanks my supervisor, Professor Graça Vasconcelos for all the discussions, help, support, patience, readings and advices during all these years.

To my co-supervisor, Professor Paulo Lourenço for believe in me, providing me with financial opportunities and for all the suggestions, guidance and careful readings.

To Professor Daniel Bedoya, my mentor and friend in Colombia for all his advices and guidance since the first time we meet and for trusted on me to apply for a young research grant.

To the Portuguese Agency of Innovation (ADI), which financed the present work developed in the scope of the national project ALVEST (n°5456), “Development of solutions for structural masonry”.

The experimental research of this work was performed at the National Laboratory for Civil Engineering, in the Earthquake Engineering and Structural Dynamic Division (LNEC-NESDE) in Lisbon, and at the structural lab from University of Minho (LEST) in Guimarães, Portugal. Those works would not have been successful without the assistance of the laboratories technicians, to whom I am grateful. I also would like to thanks the help of all the masons that worked in the construction of the four buildings, especially to Pedro and Jerson for their friendship during and after their working time.

To Costa & Almeida Lda, for the provision of materials and workmanship for the experimental campaign.

To my colleague and friend Nuno Mendes, for all the discussions and suggestions. Without them, this work would have been quite more difficult.

To my PhD friends Thomas and Elisa, for their friendship and all the adventures in the good and bad moments.

I wish to acknowledge all the colleagues and friends I meet in Guimarães, both inside and outside the university, especially to my neighbors, Ms. Fernanda and Mr. Torcato, for their support, friendship and for having made my life in Portugal even better.

I´m grateful with my parents and family for be part of my live, and to my wife for the patience, love and unconditional support.

Finally, I express my sincere gratitude to my grandmother Rosa Elena Segura, who has always taken care of me, even in the distance. For the encouragement and support during all my life and mainly during the execution of this work.

ABSTRACT

Masonry buildings are one of the most representative constructive systems since the early ages of civilization. Through time, they have exhibited worldwide structural deficiencies, severe damage and collapse during strong earthquake events. It is known that their brittle behavior together with its low frictional resistance, which is mainly due to the combination of low tensile strength, large mass and insufficient connection between structural elements, are the main limitations for its structural implementation in residential buildings. Nevertheless, masonry also offers several advantages like thermal and acoustic efficiency, excellent fire behavior, economy, durability and a simple construction technology. Then, if the deficiencies are overcome, it can be effectively considered as an alternative low cost structural solution.

Following past researches dealing with the proposal of an innovative solution in structural masonry for low to medium rise residential buildings, based on concrete block masonry units and truss type reinforcement, the main objective of the present work is to study the seismic behavior of masonry buildings built with this system. For this, an enlarged experimental campaign and numerical analysis were planned. It is commonly found that research on masonry under seismic loading has been mostly focused on experimental and numerical analyses of structural masonry elements, namely masonry walls. Lesser research has been developed in relation to the global seismic behavior of masonry buildings, particularly in case of new masonry buildings, to which special laboratory facilities like shaking tables are needed. Therefore, this work is an attempt to fill this research gap. The experimental study of the dynamic behavior of masonry buildings is based on shaking table tests of four masonry buildings, to which incremental seismic inputs are imposed. From the tests, the main seismic performance features are derived. It is intended that the tested experimental models be representative of low to medium rise prototype residential buildings with distinct levels of geometrical complexity and different reinforcement solutions.

Complementary, a numerical simulation, which encompasses a full nonlinear dynamic time history analysis by phases, is performed. The numerical model considers masonry as homogeneous material and it is calibrated on experimental results. With this methodology, the damage from a previous input is the initial condition for a new input, being possible to describe the accumulation of damage also seen in the experimental dynamic tests. Accelerations, displacements and damage are obtained and compared with the experimental results. From them, accurate and satisfactory results were obtained.

Finally, typical seismic design considerations for masonry buildings are discussed. Here, linear elastic and nonlinear static analyses are discussed, namely regarding the behavior factor “ q ” to be used in a linear elastic analysis and the nonlinear “pushover” analysis as a simplification of the complete nonlinear dynamic analysis. Comparison and discussion of the principal differences found from the two analyses are presented.

RESUMO

Os edifícios de alvenaria são um dos sistemas construtivos mais utilizados desde os primeiros tempos da civilização. A ocorrência de sismos em diferentes regiões do mundo evidenciaram as deficiências estruturais, traduzindo-se em danos consideráveis e mesmo colapso. O comportamento frágil, juntamente com a sua baixa resistência ao corte e flexão, devida à baixa resistência à tração, grande massa e insuficiente ligação entre os elementos estruturais, são as principais factores de vulnerabilidade que têm limitado a sua aplicação. No entanto, a alvenaria também oferece várias vantagens como a eficiência térmica e acústica, o comportamento excelente ao fogo, economia, durabilidade e uma tecnologia de construção simples. Então, se as deficiências forem ultrapassadas, considera-se que a alvenaria estrutural pode ser efetivamente uma solução construtiva alternativa de baixo custo.

Na sequência de estudos anteriores, que tiveram como objectivo central o desenvolvimento de uma solução em alvenaria estrutural para edifícios residenciais de baixa a média altura, com base em unidades de bloco de betão e armaduras pré-fabricadas, o principal objetivo do presente trabalho é estudar o comportamento sísmico de edifícios de alvenaria construídos com o sistema de alvenaria estrutural proposto. Para isso, foi planeada uma alargada campanha experimental e consequente análise numérica. Encontram-se na literatura vários trabalhos onde é feito o estudo experimental e numérico de elementos estruturais de alvenaria, nomeadamente paredes de alvenaria. Menos trabalhos se encontram relativos à avaliação do comportamento global à acção sísmica de edifícios de alvenaria, em particular de novos edifícios de alvenaria, que pressupõe a existência de instalações de laboratório especiais, como mesas sísmicas. Assim, pretende-se com este trabalho contribuir para o estudo global da alvenaria à acção sísmica com base em edifícios. O estudo experimental do comportamento dinâmico de edifícios de alvenaria é baseado em testes de mesa sísmica de quatro edifícios de alvenaria, aos quais se impõem carregamentos sísmicos incrementais. A partir destes ensaios, pretende-se obter as principais características do desempenho sísmico. Pretende-se que os modelos experimentais sejam representativos de edifícios residenciais de baixa a média altura com distintos níveis de complexidade geométrica e soluções de reforço diferentes.

Complementarmente, efectua-se a uma simulação numérica do comportamento dinâmico não linear com integração no tempo por fases. O modelo numérico considera a alvenaria como material homogéneo e é calibrado em base aos resultados experimentais. Com esta metodologia, os danos resultantes dos vários carregamentos sísmicos são tidos em conta, sendo possível descrever a acumulação de danos. Acelerações, deslocamentos e os danos são obtidos e comparados com os resultados experimentais.

Finalmente, são discutidas algumas considerações de dimensionamento sísmico para edifícios de alvenaria, nomeadamente dimensionamento elástico lineares e não lineares. A este respeito é discutida a obtenção do coeficiente comportamento "q" para ser usado numa análise elástica linear e feita uma análise não-linear "pushover" como uma simplificação da análise não linear dinâmica.

Faz-se uma comparação entre a análise linear estática e dinâmica e apresenta-se uma discussão sobre as principais diferenças encontradas.

Contents

ACKNOWLEDGEMENTS	vii
ABSTRACT	ix
RESUMO	xi
LIST OF SYMBOLS.....	xvii
LIST OF ABBREVIATIONS.....	xix
LIST OF FIGURES	xxi
LIST OF TABLES.....	xxix
Chapter 1 Introduction.....	1
1.1 Motivation for the study of masonry buildings.....	2
1.1.1 An overview of shaking table testing on masonry buildings.....	3
1.1.2 Numerical simulation of masonry buildings and design principles	4
1.2 Objectives and methodology	6
1.3 Outline of the thesis	8
Chapter 2 Description of experimental program.....	11
2.1 Introduction.....	12
2.2 An overview of the proposed constructive system	13
2.3 Buildings' prototypes	14
2.4 Considerations about scale	16
2.5 Shaking table testing	19
2.5.1 Design of building models.....	19
2.5.2 Construction of experimental buildings	22
2.5.3 Test setup	28
2.5.4 Seismic inputs and test procedure	34
2.6 Experimental characterization of materials	38
2.6.1 Concrete and steel bars	38
2.6.2 Truss type reinforcement	38
2.6.3 Mortar	39
2.6.4 Concrete block units	40
2.6.5 Mechanical characterization of masonry.....	40
2.7 Conclusions	47

Chapter 3 Experimental investigation of symmetric masonry buildings	49
3.1 Introduction.....	50
3.2 Objectives and methodology	51
3.3 Validation of the seismic input - Theoretical input vs. real input	51
3.3.1 Analysis of the seismic inputs	51
3.3.2 Signal processing.....	52
3.4 Dynamic Properties	56
3.5 Damage patterns and failure modes	59
3.5.1 RM model.....	59
3.5.2 UM model	62
3.5.3 Comparison of damage between UM and RM models.....	66
3.5.4 Variation of the frequency and damping along the seismic inputs.....	68
3.6 Seismic performance.....	71
3.6.1 Amplification factors from the accelerations	72
3.6.2 Analysis of deformation of the buildings	74
3.6.3 Base shear vs. displacement diagrams	87
3.7 Conclusions	89
Chapter 4 Experimental investigation of asymmetric masonry buildings	91
4.1 Introduction.....	92
4.2 Objectives and methodology	92
4.3 Validation of the seismic input - Theoretical input vs. real input	93
4.3.1 Signal processing.....	93
4.3.2 Analysis of the seismic inputs	94
4.4 Dynamic Properties	96
4.5 Damage patterns and failure modes	98
4.5.1 RM model.....	99
4.5.2 UM model	105
4.5.3 Comparison of damage between UM and RM models.....	109
4.5.4 Variation of the frequency and damping along the seismic inputs.....	110
4.6 Seismic performance.....	114
4.6.1 Amplification factors from the accelerations	114
4.6.2 Analysis of deformation of the buildings	117

4.6.3	Base shear vs. displacement diagrams.....	131
4.7	Conclusions	134
Chapter 5	Numerical modeling of the seismic behavior of masonry buildings	137
5.1	Introduction.....	138
5.2	Objectives and methodology	139
5.3	Construction of the numerical model	140
5.4	Calibration of the numerical model	143
5.5	Phased nonlinear dynamic simulation	149
5.5.1	A brief introduction	149
5.5.2	Constitutive model for the simulation of masonry.....	151
5.5.3	Material properties.....	152
5.5.4	Analysis procedures.....	153
5.6	Results and validation against experimental data.....	158
5.6.1	Accelerations	158
5.6.2	Displacements.....	161
5.6.3	Capacity curves	164
5.6.4	Damage	167
5.7	Concluding remarks	169
Chapter 6	Seismic design considerations	171
6.1	Introduction.....	172
6.2	Objectives and methodology	173
6.3	Seismic resistance verification	174
6.4	Structural behavior factor q for seismic analysis.....	174
6.4.1	Experimental behavior factor q for the symmetric UM model.....	176
6.5	Nonlinear static “pushover” analysis.....	180
6.5.1	Capacity curves of the symmetric UM building.....	180
6.5.2	Analysis of damage.....	183
6.5.3	Analysis of in-plane deformation - interstory drifts	186
6.6	Conclusions	188
Chapter 7	Conclusions, final remarks and future works	189
7.1	Conclusions	190
7.1.1	Experimental research	191

- 7.1.2 Numerical simulation..... 193
- 7.1.3 Seismic design considerations 195
- 7.2 Future works 196
- REFERENCES.....199
- APPENDIX A Final project for the construction of the symmetric buildings.....209
- APPENDIX B Final project for the construction of the asymmetric buildings.....221

LIST OF SYMBOLS

A	Area
a	Acceleration
C	Damping matrix
D	Displacement
E	Modulus of elasticity or Young's Modulus
E_{\perp}	Modulus of elasticity normal to the bed joints
F	Force
f_t	Tensile strength
f_c	Compressive Strength
$f_{c\perp}$	Compressive Strength normal to bed joints
$f_{c\parallel}$	Compressive Strength parallel to bed joints
F_i	Frequency
G_f^I	Mode-I fracture energy
G_c	Compressive fracture energy
g	Gravity acceleration
h	Crack bandwidth
K	Stiffness matrix
L	Length
M	Moment
M	Mass matrix
m	Mass
m_{ω}	Number of eigen frequencies
m_{ϕ}	Number of mode shapes
T	Time
T_i	Period
V	Volume

ν	Poisson ' s Ratio
ν	Velocity
W	Weight
$\omega_{i,N}$	Numerical eigen frequencies values
$\omega_{i,E}$	Experimental eigen frequencies values
$W_{w,i}$	Global weighting diagonal matrixes for the frequency values
$W_{\phi,i}$	Global weighting diagonal matrixes for mode shapes ' displacements
α	Coefficient value: mass-proportional damping
β	Coefficient value: stiffness-proportional damping
ε	Strain
ζ_i	Damping ratio
λ	Scale factor
ρ	Specific mass
σ	Stress
u	Displacement vector
\dot{u}	velocity vector
\ddot{u}	acceleration vector
ϕ^E	Experimental mode shapes ' vectors
ϕ^N	Numerical mode shapes ' vectors
$\phi_{i,N}$	Numerical mode shapes ' displacements
$\phi_{i,E}$	Experimental mode shapes ' displacements
Δt	Time step
Δu	Displacement increment

LIST OF ABBREVIATIONS

DC	Direct Current
BS	Base Shear
BSC	Base Shear Coefficient
CV	Coefficient of Variance
LDP	Linear Dynamic Procedure
LEST	Structural Laboratory From The University Of Minho
LNEC	National Laboratory for Civil Engineering - Portugal
LSP	Linear Static Procedure
LVDT	Linear Variable Differential Transformer - Displacement Transducers
MAC	Modal Assurance Criterion
NDP	Nonlinear Dynamic Procedure
NESDE	Earthquake Engineering and Structural Dynamic Division
NSP	Nonlinear Static Procedure (pushover analysis)
PBEE	Performance-Based Earthquake Engineering
PGA	Peak Ground Acceleration
PGD	Peak Ground Displacement
POD	Plane Of Degradation
PSD	Position-Sensitive Detectors
RM	Reinforced masonry
RMS	Root Mean Square
SDOF	Single Degree Of Freedom
UM	Unreinforced Masonry

LIST OF FIGURES

Figure 2.1 – Geometry details and dimensions of real block unit (in cm)	13
Figure 2.2 – Details of the constructive system based on concrete block masonry: (a) unit block, half unit block and steel truss type reinforcement, (b) sample of block and reinforcement disposition, (c) traditional masonry bond with truss type reinforcement, (d) alternative masonry bond composed of continuous vertical joints formed by the frogged ends of the concrete blocks	14
Figure 2.3 – Geometrical configurations for the buildings considered in the present thesis: (a) symmetric and (b) asymmetric	15
Figure 2.4 – Adopted geometry for symmetric buildings: (a) dimensions for UM and RM models, (b and c) reinforcement distribution in west - east and north – south, respectively	18
Figure 2.5 - Adopted geometry for asymmetric buildings: (a and b) dimensions for UM and RM models, (c and d) reinforcement distribution for all walls	18
Figure 2.6 – Example of twin houses using the adopted asymmetric configuration	19
Figure 2.7 – Geometrical dimension (in cm) for ring beam foundations: (a) symmetric buildings and (b) asymmetric buildings	20
Figure 2.8 – Masonry bond patterns: (a) RM models and (b) UM models	21
Figure 2.9 – Masonry buildings for the experimental campaign: (a, b) symmetric and (c, d) asymmetric	22
Figure 2.10 – Construction of foundation: (a) wooden sticks for leveling, (b) formwork boards with smooth surface, (c) placing of steel reinforcement	23
Figure 2.11 – Foundation construction: (a) vertical tubes positioning and (b) box-like formwork and suspension pieces already installed	24
Figure 2.12 – Vertical truss type reinforcement for masonry: (a) bent of anchorage, (b) anchorage to foundation 's reinforcement and (c) final position on foundation before casting	24
Figure 2.13 – Foundation construction: (a) internal restraining metal poles, (b) external restraining metal poles, (c) concrete pouring and (d) spreading with vibrators	25
Figure 2.14 – Construction process: (a) foundation with vertical steel, (b) installation of first masonry row, (c) horizontal joint with reinforcement and (d) detail of mortar covering reinforcement	26
Figure 2.15 – Construction of slab: (a) wood scaffold and smooth board formwork, (b) perimeter supporting beams, (c) first masonry story with slab 's formwork, (d) view before casting and (d) view of slab after concrete pouring and smoothing	27
Figure 2.16 – Concrete block masonry building for experimental shaking table test	28

Figure 2.17 – Shaking table: (a) rigid body and (b) general view of the full system i.e. table, guidance (torque tubes) and actuators. (Adapted from LNEC-NESDE website http://www.lnec.pt/organizacao/de/nesde/ptriaxialdescricao . retrieved June, 2014).....	30
Figure 2.18 – Piezoelectric accelerometer: (a) model 393A03 and (b) typical cut-away view.....	31
Figure 2.19 – Captive guided displacement transducer	32
Figure 2.20 - Position-sensitive detectors (PSD): (a) controller and camera, (b) optical sensor (Hamamatsu 2014).....	33
Figure 2.21 – Masonry buildings instrumentation for shaking table tests: (a, b) symmetric buildings and (c, d) asymmetric buildings	34
Figure 2.22 - Designed seismic inputs: (a) standard and scaled elastic response spectrum; (b) artificial spectrum for the North-South direction (NS); (c) artificial spectrum for the East-West direction (EW); (d) artificial time histories NS direction and (e) artificial time histories for EW direction	36
Figure 2.23 – Inputs (white noise) for dynamic identification: (a) North-South direction and (b) East-West direction.....	37
Figure 2.24 – Masonry specimens: (a) steel distribution in RM samples. Distances are in cm, (b) instrumentation distribution. Numbers refer to LVDTs and (c) final setup at laboratory	42
Figure 2.25 – Cracking pattern during direct compression tests: (a, b) UM specimens, (c, d) RM specimens and (e, f) specimens taken from experimental buildings	43
Figure 2.26 – Vertical and horizontal stress-displacement diagram from direct compression: (a) UM specimens and (b) RM specimens	43
Figure 2.27 – Masonry specimen for diagonal tests: (a) instrumentation distribution. Distances are in cm. Numbers refers to LVDTs and (b) final test setup.....	44
Figure 2.28 - Cracking pattern during diagonal compression tests: (a, b) UM specimens, (c, d) RM specimens and (e, f) specimens taken from the buildings.....	46
Figure 2.29 – Results from diagonal tests: (a, b) strain-stress curves for UM and RM specimens and (c, d) top and bottom horizontal opening for UM and RM specimens.....	47
Figure 3.1 - Diagrams correlating the peak accelerations at the base of buildings and PGA targets: (a) longitudinal direction and (b) transverse direction	55
Figure 3.2 - Diagrams correlating the peak displacements at the base of buildings and PGD targets: (a) longitudinal direction and (b) transverse direction.....	55
Figure 3.3 - Transfer function curves for: a) RM building and b) UM building.....	57
Figure 3.4 - Global mode shapes of both masonry buildings: (a) first mode - transverse direction and (b) second mode - longitudinal direction	58
Figure 3.5 - Damage observed after each seismic input test for the RM model (100% and 150%) ..	59

Figure 3.6 - Damage observed after each seismic input test for the RM model (from 250% to 400%)	60
Figure 3.7 – Damage in the middle of the walls affecting unit blocks	61
Figure 3.8 – Damage at the bottom of the walls, mainly at corners affecting unit blocks.....	61
Figure 3.9 – Unit failure after input test of: (a) 400% and (b) 400% 2	61
Figure 3.10 - Damage observed after each seismic input test for the UM model (from 100% to 200%)	63
Figure 3.11 - Damage observed after each seismic input test for the UM model (250% and 250% 2)	64
Figure 3.12 – Damage around openings at second floor during seismic test of 250%: (a) crack opening during test, (b) final stage at the end of the test, (c) detachment of units at upper corner and (d) cracks in unit block at lower corner	65
Figure 3.13 – Damage in corners during the test of 250%	65
Figure 3.14 – Final damage of the east and north walls.....	66
Figure 3.15 – Final damage west wall at second floor (between openings)	66
Figure 3.16 - Final damage patterns in: (a, b) RM building and (c, d) UM building.....	67
Figure 3.17 - Crack patterns after the seismic input of 250%: (a, b) RM building and (c, d) UM building	68
Figure 3.18 - Simplified damage indicator for RM building	71
Figure 3.19 - Measured accelerations for each level: (a) RM model 100%-long; (b) UM model 100%- long; (c) RM model 250%-long and (d) UM model 250%-long.....	72
Figure 3.20 - Story accelerations and dynamic amplification factors versus PGA of RM model: (a) longitudinal direction and (b) transverse direction	73
Figure 3.21 - Story accelerations and dynamic amplification versus PGA of UM model: (a) longitudinal direction and (b) transverse direction	74
Figure 3.22 - In-plane displacements in walls of RM building: (a) north façade, (b) west façade, (c) south façade and (d) east façade	76
Figure 3.23 - In-plane displacements in walls of UM building: (a) north façade, (b) west façade, (c) south façade and (d) east façade	76
Figure 3.24 - Interstory drifts for RM model: (a) north façade, (b) west façade, (c) south façade and (d) east façade.....	77
Figure 3.25 - Interstory drifts for UM model: (a) north façade, (b) west façade, (c) south façade and (d) east façade.....	78
Figure 3.26 - Damage of the UM model in south and east façades after: (a) test run of 200% (PGA=1.11g) and (b) test run of 250% (1.33g).....	79

Figure 3.27 - Global and relative out-of-plane displacements for RM model: (a, b) south façade, (c, d) west B and (e, f) west C	80
Figure 3.28 - Global and relative out-of-plane displacements for UM model: (a, b) south façade, (c, d) west A and (e, f) west C	81
Figure 3.29 - Biaxial displacement trajectories in the horizontal plane at north-east corner for test run of 250% in: (a) RM model at second story, (b) UM model at second story, (c) RM model at first story and (d) UM model at first story	83
Figure 3.30 - Displacement amplification versus PGA: (a, b, c, d) longitudinal direction and (e, f, g, h) transverse direction	85
Figure 3.31 - Base shear coefficient versus top displacement/height in percentage for 100% seismic input	87
Figure 3.32 – Experimental hysteresis envelopes curves for RM and UM buildings: (a) longitudinal direction and (b) transversal direction.....	89
Figure 4.1 - Diagrams correlating the peak accelerations at the base of buildings and PGA targets: (a) longitudinal direction and (b) transverse direction.....	95
Figure 4.2 - Diagrams correlating the peak displacements at the base of buildings and PGD targets: (a) longitudinal direction and (b) transverse direction	95
Figure 4.3 - Global mode shapes for both asymmetric masonry buildings: (a) first: transversal, (b) second: longitudinal and (c) third: torsional	98
Figure 4.4 – Different crack widths developed in the RM model	99
Figure 4.5 – Damage observed after each seismic input test for the RM model (from 75% to 200%)	100
Figure 4.6 – Damage observed after each seismic input test for the RM model (from 250% to 300%)	101
Figure 4.7 – Wall west 2 at first level after seismic input of: (a) 250% and (b) 300%	102
Figure 4.8 – Crush failure (west wall) during seismic input of 300% 2.....	103
Figure 4.9 – Lost of mortar joints at the first floor of the east wall: (a) left pier of the window; (b, c and d) right pier of the window.....	103
Figure 4.10 – Out-of-plane failures; (a) separation of the north wall at the corner with the east wall; (b) left pier of west 1 wall (c) out-of-plane detachment and separation of the west 1 and north 2 walls; (d) separation between west and south wall; (e) out-of-plane cracking at the south wall.	104
Figure 4.11 – Damage on steel; (a and b) dowel effect in vertical reinforcement; (c) deformation on horizontal reinforcement due to cycle movements; (d) failure of horizontal reinforcement at welding connection	104
Figure 4.12 – Damage on RM model during shaking table test of 300%_2.....	105

Figure 4.13 - Damage observed after each seismic input test for the UM model (50% to 150%) ...	106
Figure 4.14 - Damage observed after repetition of the seismic input of 150%	107
Figure 4.15 – Final damage in the asymmetric unreinforced masonry building: (a) north 1, (b) north 2, (c) west 2 at second level, (d) corner between west 2 and south walls, (e) south wall and (f) east wall at second floor	108
Figure 4.16 – Sliding mechanism evidence at second floor after final input test on UM model: (a) north 1, (b and c) east and (d) west 2 walls.....	108
Figure 4.17 - Final damage patterns for the asymmetric: (a, b) reinforced building and (c, d) unreinforced building. Note that different seismic input applies.....	109
Figure 4.18 - Crack patterns of the RM and UM models at 150%: (a, b) RM model; (c, d) UM model	110
Figure 4.19 – Damage indicator for: (a) RM and (b) UM	113
Figure 4.20 - Measured accelerations in the longitudinal direction: (a) RM model at 100%; (b) UM model at 100%; (c) RM model at 150% and (d) UM model at 150%1	115
Figure 4.21 - Story accelerations and dynamic amplification factors versus PGA of RM model: (a) longitudinal direction and (b) transverse direction	116
Figure 4.22 - Story accelerations and dynamic amplification versus PGA of UM model: (a) longitudinal direction and (b) transverse direction	116
Figure 4.23 - In-plane displacements for RM in façade: (a) north, (b) west2, (c) south and (d) east	118
Figure 4.24 - In-plane displacements for UM model in façade: (a) north, (b) west2, (c) south and (d) east.....	119
Figure 4.25 - Interstory drifts for RM in façade: (a) north, (b) west2, (c) south and (d) east	121
Figure 4.26 - Interstory drifts for UM in façade: (a) north, (b) west2, (c) south and (d) east.....	122
Figure 4.27 - Global and relative out-of-plane displacements for RM in façade: (a, b) south, (c, d) west2 and (e, f) east.....	124
Figure 4.28 - Global and relative out-of-plane displacements for UM in façade: (a, b) south, (c, d) west2 and (e, f) east	125
Figure 4.29 - Biaxial displacement trajectories in the horizontal plane at south-west corner in: (a, b) RM building at first and second story for input of 150%, (c, d) UM model at first and second story for input of 150% and (e, f) RM model at first and second story for input of 300%2. Note the different scale for the last plots	126
Figure 4.30 - Displacement amplification versus PGA for: (a, b, c, d) longitudinal direction and (e, f, g, h) transverse direction	128
Figure 4.31 – LVDTs position on asymmetric buildings at east wall.....	129

Figure 4.32 - Base shear coefficient versus top displacement/height in percentage, for the asymmetric buildings during the seismic input of 100%	132
Figure 4.33 - Experimental hysteresis envelopes curves for the asymmetric RM and UM buildings: (a) longitudinal direction and (b) transversal direction	133
Figure 5.1 – Curved shell element (CQ40S): a) Example of element implemented for walls and slabs, b) in-plane Gauss integration for quadrilateral elements	141
Figure 5.2 – Thickness integration schemes for quadrilaterals: a) Gauss (2-point) and Simpson (more than 2 points) integration, b) example for slabs ´ integration 2 x 2 x 2.....	142
Figure 5.3 – Mesh of the numerical model: (a) 3D view and (b) detailed view	142
Figure 5.4 – Location and distribution of interfaces elements	147
Figure 5.5 – Mode shapes of: (a, b) experimental results, (c, d) numerical results	148
Figure 5.6 – Optimization ´s results: (a) frequency errors between experimental and numerical values, (b) MAC matrix for the mode shapes	149
Figure 5.7 – Micro modeling approach.....	150
Figure 5.8 – Modeling behaviors of masonry when subjected to a force or combination of forces: (a, c, d) micro modeling and (b, d, f) macro modeling approach	150
Figure 5.9 – Stress-strain curves: (a) Secant and elastic unloading in a tension-softening curve, (b) Parabolic compressive behavior (c) Exponential tensile behavior	152
Figure 5.10 – Stress-strain curve with loading-unloading relationship	153
Figure 5.11 – Signals inputs implemented in the numerical simulation.....	154
Figure 5.12 – Rayleigh damping implemented in the numerical simulation	157
Figure 5.13 – Numerical and experimental peak acceleration values: (a) North façade – longitudinal direction and (b) West façade – transverse direction.....	159
Figure 5.14 - RMS acceleration values comparison: (a) North façade – longitudinal direction and (b) West façade – transverse direction.....	161
Figure 5.15 – Comparison between numerical and experimental relative peak displacements: (a) North façade – longitudinal direction and (b) West façade – transverse direction.....	162
Figure 5.16 - Comparison between numerical and experimental relative RMS displacements: (a) North façade – longitudinal direction and (b) West façade – transverse direction.....	163
Figure 5.17 – Experimental and numerical time history signals for point W2.1 during test of 250%_1	164
Figure 5.18 – Hysteretic response in longitudinal direction for input signal of 100% in: (a) experimental building and (b) numerical model	165
Figure 5.19 – Capacity curves relating base shear coefficient and top normalized displacement: (a) longitudinal direction and (b) transverse direction	166

Figure 5.20 – Maximum principal tensile strain for every input	168
Figure 5.21 – Final damage for the experimental unreinforced masonry building	169
Figure 6.1 – Definition of the structural behavior factor.....	176
Figure 6.2 – Experimental hysteresis envelopes for the symmetric buildings: (a) longitudinal direction and (b) transverse direction	178
Figure 6.3 – Evaluation of the structural behavior factor for the UM model: (a) longitudinal direction and (b) transverse direction	178
Figure 6.4 – Capacity curve comparison for the experimental, nonlinear dynamic and pushover analyses: (a) longitudinal direction and (b) transverse direction.....	182
Figure 6.5 - Maximum principal tensile strain: (a) pushover from north to south (positive orientation) and (b) pushover from south to north (negative orientation)	183
Figure 6.6 - Minimum principal compression strain: (a) pushover from north to south (positive orientation) and (b) pushover from south to north (negative orientation)	184
Figure 6.7 - Maximum principal tensile strain: (a) pushover from west to east (positive orientation) and (b) pushover from east to west (negative orientation)	184
Figure 6.8 - Minimum principal compression strain: (a) pushover from west to east (positive orientation) and (b) pushover from east to west (negative orientation)	185
Figure 6.9 - Final damage patterns in symmetric unreinforced masonry building: (a) north – west façades and (b) south – east façades	186
Figure 6.10 - Maximum principal tensile strain for the nonlinear dynamic analysis of 200%	186
Figure 6.11 – Interstory drifts comparison for the maximum values of experimental, nonlinear dynamic and pushover analyses in the UM model for: (a) longitudinal direction and (b) transverse direction	187

LIST OF TABLES

Table 2.1 – Scale factors of the similitude laws (Carvalho 1999)	17
Table 2.2 – Description of actuators for the shaking table at LNEC	30
Table 2.3 – Characteristics of actuators	30
Table 2.4 – Accelerometer specification (PCB 2014).....	32
Table 2.5 – LVDT specification (RDP 2014).....	32
Table 2.6 – Seismic input sequence	37
Table 2.7 – Mechanical properties of mortar	39
Table 2.8 – Mechanical properties of block and half block units (adapted from manufacturer and Haach (2009)).....	40
Table 2.9 – Mechanical properties of masonry from direct compression tests	42
Table 2.10 – Mechanical properties of masonry from diagonal tests	45
Table 3.1 - Input series and corresponding PGA	52
Table 3.2 – Dynamic properties	58
Table 3.3 - Evolution of the frequency and damping coefficient	69
Table 3.4 - Maximum values of the displacements measured by LVDTs (in mm)	86
Table 4.1 - Input series and corresponding PGA for the asymmetric buildings	94
Table 4.2 – Dynamic properties	97
Table 4.3 - Evolution of the frequency and damping coefficient	111
Table 4.4 - Maximum values of the displacements measured by LVDTs (in mm)	130
Table 5.1 – Linear elastic material properties.....	143
Table 5.2 – Parameters for calibration in option 1	145
Table 5.3 – Percentage (from reference value) needed for optimal solution using option 4	145
Table 5.4 – Parameter for calibration in option 5.....	146
Table 5.5 – Normal stiffness for the interfaces	147
Table 5.6 – Normal stiffness for the interfaces at the base of the numerical model	147
Table 5.7 – Experimental and numerical frequency values.....	148
Table 5.8 – Tensile material properties	153
Table 5.9 – Compressive material properties	153
Table 5.10 – Integration schemes.....	157

Table 6.1 – Values of structural behavior factor in terms of force..... 179

Table 6.2 – Values of structural behavior factor in terms of ductility..... 179

Chapter 1

Introduction

1.1 Motivation for the study of masonry buildings

Masonry is considered as the oldest building material used in the world. In particular, masonry buildings are the most representative constructive system since the early ages of humankind. Most of them are unreinforced masonry (URM) buildings constructed without the consideration of earthquake design requirements or reference to any particular design code. The analyses made on the damages of buildings after several earthquakes through the history have revealed the high seismic vulnerability of this type of construction (Bruneau 1994). It is common that total or partial collapse of unreinforced masonry buildings occurs during an earthquake due to poor quality of materials and construction technology, lack of connection between the intersection walls and between walls and floors and ceilings (Costa et al. 2006; Lang 2000; Lourenço and Roque 2006; Mendes and Lourenço 2009). This situation contributed for the progressive reduction of construction in unreinforced masonry, namely in several European countries, together with the introduction of the reinforced concrete. In Portugal, structural masonry almost disappeared in the last decades, being used almost only as non-loadbearing masonry walls in reinforced concrete frame structural systems (Haach 2009; Lourenço 2004b).

The low tensile strength, limited ductility and limited ability to dissipate energy are the main reasons for the European codes limit the use of unreinforced masonry in high seismicity regions, typically with PGA above 0.2g (Eurocode 8 2004; Eurocode 6 2005; Magenes 2006). However, according to Magenes (2006), new construction in structural masonry in several European countries is far from being marginal, even in countries with high seismic hazard in which masonry remained as a relevant construction system for residential buildings, such as in Italy, Germany and Switzerland. In Portugal, the national annex of Eurocode 8 (2004) poses severe limitations for structural masonry, allowing unreinforced masonry only for one-story buildings in low seismicity areas ($PGA \leq 0.1g$) and enforcing strict rules about types and dimensions of units, geometrical and distributional parameters of walls. Notice that in terms on behavior factor “q”, no higher values than 1.5 are allowed for unreinforced masonry. This seems insufficiently grounded in observations and testing.

Masonry has several advantages as a structural material, such as thermal and acoustic efficiency, economy, simple construction technology, excellent fire behavior and, usually, relatively low embedded energy. Masonry has good durability and adequate performance with respect to healthy indoor environment. It can be effectively considered as an alternative low cost structural solution for low to medium rise residential buildings (Lourenço et al. 2010). Recent research efforts have been made to support the development and use of new solutions in structural masonry for the European construction market (Da Porto et al. 2011; Haach et al. 2010; Lourenço et al. 2010).

The acceptance of a new solution in structural masonry by the construction market, such as the one proposed in this work, requires the masonry materials, construction technology guidelines and a valid design procedure. Experimental and numerical validation can assist in the development of innovative solutions, especially in case of seismic actions. With this respect, it should be mentioned that the consideration of buildings, instead of individual structural elements, provides the mechanical performance of the overall system, including namely walls and floor to walls connections, in-plane

and out-of-plane resisting mechanisms and their interaction, and effect of openings. Therefore, whenever possible, consideration of prototypes or models is appealing.

1.1.1 An overview of shaking table testing on masonry buildings

In the scope of seismic experimental research, distinct testing approaches have been used to study the failure and resisting mechanism of masonry, such as quasi-static monotonic or cyclic tests, pseudo-dynamic tests and dynamic shaking table tests (Paquette and Bruneau 2006). Each of them has advantages and disadvantages, namely in the pseudo-dynamic test, the velocity at which the structure is deformed are two or three orders of magnitude smaller than the one occurring during a real situation, being the test not able to capture important parameters like the strain rate effects. In general, the most important difference between static and dynamic tests is the time dependency of the dynamic approach. Then, in the last one, the response of the structure is directly associated to the time history accelerations that take place due to the inertial forces in which the mass, stiffness and damping play an important role (Carvalho 1999). Tomazevic et al. (1996a) carried out an extensive experimental testing program on lateral in-plane behavior of masonry walls under different lateral load histories, namely static (monotonic and cyclic) and dynamic. It was concluded that the results were dependent on the shape and velocity of application of the induced lateral load patterns. Comparison between static and dynamic procedures showed higher values of lateral resistance in case of dynamic loads (fast rate of application of loads) than in case of static load (low rate of application of loads), whereas minor differences were found regarding lateral deformations. According to Calvi et al. (1996) dynamic tests simulate more accurately the seismic action than quasi-static cyclic tests. Differences are expected to be found on strength, stiffness, damage propagation and energy dissipation. Quasi-static tests are more conservative than dynamic tests, as lower lateral strength and more damage are found. An extensive experimental program was performed in Elgawady et al. (2004) in the scope of retrofitting unreinforced masonry walls, indicating that dynamic and static cyclic tests provide similar failure modes. The same conclusion was pointed out in Vasconcelos et al. (2006) for dry stacked stone masonry walls.

Examples of static cyclic tests carried out on full-scale buildings also exist (Abrams 1986; Moon et al. 2007; Yi et al. 2006). Still, the results of shaking table tests provide the most realistic dynamic behavior of masonry buildings under seismic actions and they are often used for calibration of numerical models (Mendes and Lourenço 2009). The most adequate simulation of earthquake movements can be made through a shaking table device, being possible to introduce any particular base motion (Bairrao and Vaz 2000; Carvalho 1999; Henderson et al. 2003). Then, the dynamic tests performed by this device are considered as the most accurate and representative option for subjecting a structural model to any particular base motion, constituting an invaluable source of information, in particular, for the understanding of the dynamic behavior of buildings. Even if no soil-structure interaction is taken into account, the structure is exposed to physical shaking as the one produced during an actual seismic event, with the presence of inertial forces similar to the one induced to structures by earthquakes. This experimental approach enables also to analyze the nonlinear interaction between the distinct structural elements, being possible to apply in-plane and

out-of-plane movements using a bidirectional shaking table. Limitations are also attributed to shaking table testing such as the need to use scaled models and the high cost, usually leading to a low number of specimens (Žarnić et al. 2001).

Shaking tables date back to the 19th century but they have been effective for the assessment of the dynamic and seismic behavior of civil engineering structures only since the 1960s, after overcoming limitations concerning mainly with the power needed to reproduce dynamic forces. The use of shaking table testing has revealed itself to be versatile as reference point of evaluation, measurement and assessment, for buildings in all types of materials like reinforced concrete, steel, unreinforced and reinforced masonry and even wood (Bairrão and Falcão Silva 2009; Krstevska et al. 2010; Pei and van de Lindt 2011; Zhou and Li 2010). This experimental approach has been followed by different authors and has been revealed valuable to analyze the behavior of ancient masonry buildings and to assess the performance of strengthening techniques or even the effect of enclosure masonry walls on the behavior of reinforced concrete frames (Benedetti et al. 1998; Tomazevic and Klemenc 1997; Tomažević et al. 2009; Tomažević et al. 1993; Žarnić et al. 2001). With respect to masonry structures, an analysis of the effect of different diaphragms on the dynamic behavior of stone masonry buildings was performed by Tomažević et al. (1993) through testing of four 1:4 scale simplified models of two-story unreinforced stone masonry buildings. The models were tested in a one-dimensional shaking table with distinct types of wooden floors. Abrams (2000) reported results of shaking table tests carried out on reduced scale, unreinforced clay-unit two stories masonry buildings with distinct number of openings and dimensions leading to variable pier sizes and aspect ratios. More recently, shaking table tests were carried out on a half scale two-story unreinforced brick masonry building, representative of unreinforced masonry buildings in Christchurch, New Zealand (Bothara et al. 2010). In general, good performance of the buildings was achieved, even for high levels of peak ground acceleration, if adequate bond of masonry and adequate stiffness of the diaphragms are provided. In this case, a ductile and energy dissipating in-plane resisting mechanism is found, avoiding premature out-of-plane collapse of the walls.

The efficiency of distinct retrofitting systems applied to ancient masonry buildings, namely glass and carbon fibers reinforced polymer overlays has also been evaluated based on shaking table tests (Bairrao and Vaz 2000; Benedetti et al. 1998; Tomažević et al. 2009). Tomažević and Weiss (2010) have used the results of shaking table tests carried out on confined and unconfined masonry buildings as the basis for the assessment of the behavior factor q proposed in Eurocode 8 (2004) to obtain the design response spectrum. Finally, shaking table tests have been also adopted for the evaluation of the effectiveness of masonry infill walls to strengthen reinforced concrete frames (Lee and Woo 2002; Tu et al. 2010; Žarnić et al. 2001).

1.1.2 Numerical simulation of masonry buildings and design principles

For the numerical simulation of masonry structures, different types of analysis have been proposed. Indeed, advanced analysis methods have been developed combining accurate material description and structural models, particularly in the field of finite element analysis. Complementary, finite element analysis has been developed by providing robust nonlinear models that assist in the better

understanding of the dynamic behavior of masonry buildings (Calderini and Lagomarsino 2006; Mendes and Lourenço 2009; Sucuoglu and Erberik 1997). Despite the progress in this area, it is noticed that finite element analyses requires high expertise and it is hard to apply them directly into the design of masonry buildings due to high computation effort and time.

The assessment of the seismic behavior of masonry buildings can be obtained by applying a static or dynamic method of analysis with linear or nonlinear behavior. Additionally, masonry buildings can be studied by limit analysis in order to obtain the collapse mechanism and the structural load failure. The structural design must balance the representativeness of the building with the time-consuming and cost of the analysis. Thus, different modeling strategies for masonry structures are proposed like the fiber element method, discrete element method, micro and macro modeling, and the continuum. All modeling strategies have advantages and disadvantages. The selection of one modeling technique over another depends on the objective of the study, the financial resources, the available input data and the level of experience of the engineer. Here, the availability of input data is a key issue so that the validation of the numerical models against reliable experimental information is possible.

In brief, the fiber element method used an equivalent system of beam elements in order to model the entire structure. After the structure is discretized into rectilinear beams, each beam is subdivided into longitudinal fibers. Its application in masonry structures include mainly bridges (Felice 2009; Santis and Felice 2014) and reinforced concrete frames with infill masonry (Lu et al. 2012). The discrete method is considered a discontinuous approach developed for the analysis of structures composed by blocks. In fact, it has been increasingly applied in numerical models aimed at representing the mechanical behavior of system composed of multiple bodies, blocks or particles (Lemos 2007). It is specially suitable for structures in which the relative motion between the blocks significantly influences the collapse mechanism (Azevedo and Sincaian 2000). The micro modeling approach permits the separate characterization of unit, bed joint mortar and head joint mortar. It is considered as the best tool available to analyze and understand the real behavior of masonry in terms of local response. This method requires the implementation of constitutive laws for each material component. Then, it is suitable to represent explicitly the stress and deformation behavior of the mortar and units in a more strict way (Berto et al. 2004). In the macro modeling approach, the structure is divided into blocks with a considerable size and each block represents a large portion of masonry. This method involves simple analytical models to simulate the overall force-deformation behavior (or stress-strain). This strategy is more practice-oriented due to the reduced time to generate the model and performing the analysis. Furthermore, it provides a user-friendly mesh generation and a considerable less computational effort (Lourenço 2004a). Finally, in the continuum modeling approach, masonry is modelled as an equivalent material, being ideal for distributed failure patterns. Its mesh is made of continuum elements and it is possible to use material models like Rankine-Hill (anisotropic model), smeared crack models and Maekawa damage (plasticity models). This strategy is usually followed when a global analysis of a large-scale structure is required (Lemos 2007).

Any prediction obtained by a numerical model presents deviations to the real behavior. Nevertheless, it is always important to have a numerical model capable of representing, as much as possible, the

effective behavior of the structure in order to get reliable predictions. The best strategy to achieve this objective is validating the numerical model with measurements obtained during load tests, taking profit that the loading is perfectly known and controlled. To sum up, it is possible to use different modeling strategies with different aims in distinct cases of structure to be analyzed (Lourenço 2004a). For masonry buildings, it depends mainly of the planned objectives and type of analysis.

The earthquake engineering, as a field of technological endeavor for the design and construction of buildings, took several decades in be developed until today´s codes. This evolution was aided by parallel developments in computer science, information technology, and developments with regard the inelastic behavior of materials. As known, earthquakes are unpredictable and uncontrollable, and then the main defense against them is prevention.

For the seismic design of masonry buildings, the Eurocode 8 (2004) considers linear analysis methods (as the equivalent lateral force method, which makes use of the behavior factor “q” and the modal response spectrum analysis) and nonlinear analysis methods (as the nonlinear static “pushover” analysis and nonlinear dynamic analysis). The full nonlinear dynamic time history analysis is the most advanced numerical simulation that can be developed for the seismic analysis of structures. However, it should be stressed that static methods prevail over dynamic as they are more suitable to be used in common practice (Magenes 2006). In this regard, in recent years commercial software programs based on equivalent frame or macro-elements idealization of masonry (nonlinear macro-elements) and displacement-based methodologies (pushover analysis) have been proposed enabling the global analysis and assessment of masonry buildings (Galasco et al. 2006; Lagomarsino et al. 2006; Magenes et al. 2006). More recently, the design of masonry structures have been performed following the response spectrum methods as described by Fajfar (2000).

1.2 Objectives and methodology

The present thesis addresses the seismic performance of a new masonry structural system developed for residential and public buildings. The use of structural masonry, in particular for the Portuguese construction market, requires a deeper insight on the seismic behavior of masonry buildings, as Portugal is a medium to high seismic hazard country. Additionally, complete background on seismic design of masonry buildings is needed. Notice that a reason that contributes to the absence of structural masonry is the lack of academic training.

The idea is the proposal of an earthquake-resistant new masonry system that ensures good mechanical performance, ensuring that no-collapse and damage limit states are fulfilled, and that provides an economical and simple solution. Studies on the lateral in-plane behavior of concrete block masonry walls have already been done on masonry elements (Haach 2009; Haach et al. 2010). Those studies provided useful information about the cyclic behavior of masonry walls but validation of the seismic behavior of masonry buildings built with the proposed masonry system solution is still missing. Therefore, in view of this status the main aims of the proposed research program are: (1) experimental validation of masonry buildings with the proposed constructive

system; (2) assessment of the main parameters defining the seismic performance of the masonry buildings; (3) obtain a better insight on the numerical modelling approaches for the masonry buildings; (4) provide some design guidelines for the design of new masonry buildings. Based on the complexity of the dynamic behavior of structures and especially of masonry buildings, the accomplishment of a solution to be used in zones with different seismic hazard necessarily involves the experimental dynamic characterization and the numerical nonlinear analysis, being both techniques powerful tools for the understanding of the global behavior of structures subjected to seismic action. Therefore, aiming at obtaining the seismic behavior of a structural solution for concrete block masonry buildings, an extensive experimental testing program based on shaking table tests, complemented with a detailed numerical nonlinear dynamic time history analysis was planned and carried out.

To accomplish these objectives, the work methodology to be followed encompasses the following steps:

1. Design an experimental program for the characterization of the seismic response of structural masonry buildings based on shaking table tests. More than walls and piers, it is important to fully understand the global behavior of masonry buildings under seismic loading, namely at the level of the connections among intersection walls and between masonry walls and slabs. It should be stressed that seismic behavior of masonry buildings is only well studied through dynamic analysis.
2. Shaking table testing of different typologies of masonry buildings to assess: (1) the influence of the geometry configuration on the seismic behavior of the concrete block masonry buildings; (2) the influence of the reinforcing system composed of vertical and horizontal truss type reinforcements. For this, in addition to symmetric geometries, asymmetric geometrical configurations should be considered as it directly influences the distribution of masses and stiffness. This irregular redistribution increases the probability of torsional movements during earthquake events, causing stress concentration and damage in setbacks corners. Besides, as masonry presents typical brittle behavior, with low ductile capacity and energy dissipation, current design codes recommend the addition of minimum percentages of steel reinforcement, depending of the seismic zone in which the building is constructed.
3. Development of a numerical model based on finite elements to describe the seismic behavior of concrete block masonry buildings. Here, the nonlinear dynamic time history analysis is adopted as it is considered the most advanced numerical simulation that better represents the dynamic behavior of masonry structures.
4. Assessment of the seismic design procedures recommended in the codes for masonry buildings; i.e. Eurocode 6 (2005) and Eurocode 8 (2004). With this respect, an assessment of the behavior factor, q , to be used in the seismic design of the unreinforced masonry is provided based on the results of the seismic response of symmetric buildings. Additionally, a comparison between the numerical results of the dynamic nonlinear analysis and the results obtained in the simpler nonlinear static “pushover” analysis is made. Notice that the

European code suggest the use of this simplified approach for practical purposes, if more information is needed that the simple linear analysis.

1.3 Outline of the thesis

The research investigation of the seismic behavior of concrete block masonry buildings that is presented in this thesis is organized in seven chapters. Therefore, besides this introductory Chapter, where the motivation for the study and a brief background about the studies of the seismic behavior of masonry as structural material are given, the thesis is composed of the following chapters: (2) Description of the experimental program; (3) Experimental investigation of symmetric masonry buildings; (4) Experimental investigation of asymmetric masonry buildings; (5) Numerical modeling of the seismic behavior of masonry buildings; (6) Design considerations and (7) Conclusions, final remarks and future works. In the following, a brief description of the work proposed in each chapter is provided:

- **Chapter 2** is dedicated to the detailed description of the experimental campaign performed on the shaking table for four masonry buildings. Firstly, the constructive masonry system and the prototypes buildings are presented. Secondly, the design and construction of the models are discussed. Additionally, a description of the shaking table setup, the instrumentation of the buildings, the seismic inputs imposed and the test procedure implemented is presented. Furthermore, the experimental characterization of the material properties is also discussed.
- **Chapter 3** presents the analyses procedures performed, and results of the experimental campaign carried out on symmetric masonry buildings. Descriptions of the evolution of the damage and failure mechanisms are presented. The identification of the dynamic modal parameters is performed before any seismic input and after each incremental input. From these identifications, the stiffness degradation and its relation with the damage are studied. The seismic performance of the buildings is extensively discussed in terms of accelerations and displacements. In-plane, out-of-plane, interstory drifts, amplification factors and force vs displacements diagrams are some of the parameters discussed.
- **Chapter 4** describes the analyses procedures and results of the experimental campaign of geometrical asymmetric masonry buildings. Similar to the analyses procedures performed in chapter 3, the damage observed and the modal parameters were obtained after each seismic input. Then, relations between stiffness degradation and evolution of damage are discussed. The seismic performance of both buildings is studied based on accelerations and displacements. In-plane, out-of-plane, interstory drifts, amplification factors and force vs displacements diagrams, among other

parameters are discussed. A comparison is made between symmetric and asymmetric buildings.

- **Chapter 5** presents the numerical simulation for the symmetric unreinforced masonry building, in which nonlinear dynamic time history analysis is performed. Previously, the experimental building was tested through a sequence of incremental seismic inputs. Then, for the numerical simulation, a phase analysis procedure is implemented to account for the accurate evolution of damage between inputs. Thus, each incremental test is simulated in an individual phase. Description of the construction and calibration of the numerical model is presented. The constitutive model implemented and the analysis procedures are discussed. Results in terms of accelerations, displacements, capacity curves and damage are presented and compared with the experimental results.
- **Chapter 6** addresses the design verification of the symmetric unreinforced masonry building. Following codes procedures, two design methods are discussed, namely a linear dynamic analysis in which the behavior factor “q” is obtained based on the experimental results obtained in the symmetric buildings and a nonlinear static “pushover” analysis with a lateral load proportional to the mass of the structure. For the linear simulation, force reduction factors based on base shear capacity and energy dissipation are obtained and compared with code limitations. From the pushover analysis, the interstory drifts, capacity curves and damage are obtained and directly compared with the experimental and the nonlinear dynamic results. Important conclusions regarding the implementation of simplified methods for the design of masonry buildings are discussed.
- **Chapter 7** presents the main conclusions and the final remarks from the full research investigation. Furthermore, suggestions for future works are also given.

Chapter 2

Description of experimental program

Abstract

The first step for the validation of a new constructive solution is the detailed and safe evaluation of its structural behavior. As a residential solution, a building must provide security and safety for the designer, the constructor and the final user (building's residents). Few or no damage and that never collapse are the minimum requirements expected during its life-span design period. To accomplish this objective, the self-weight, occupancy, wind and earthquake loads are taken into account during the design process.

As a new constructive system, an optimal validation includes not only different types of loads, but also different types of building configurations. The experimental evaluation of the constructive system studied in this thesis includes four masonry buildings. On them, dynamic shaking table tests were performed. A complete description from the design process of the buildings, through the experimental campaign, until the analysis performed is discussed

2.1 Introduction

The constructive system based on concrete block masonry (reinforced and unreinforced) to be studied in this work was firstly proposed by researchers of the civil engineering department at the University of Minho in Portugal (Haach et al. 2010; Haach et al. 2011). A previous extensive research work was developed by Haach (2009) based on detailed experimental and numerical evaluation of the system in individual structural components, namely shear walls and beam elements. For this, static cyclic tests and static monotonic tests were performed, resulting in the complete validation of the constructive system applied in structural components (walls and beams) under in-plane loading.

As a new constructive solution to be used in residential building, it is required the full assessing of its structural behavior as a whole, more than for individual structural elements. The interaction within connecting elements (i.e. wall-wall and wall-slab), the distribution of stresses, the combination of in-plane and out-of-plane forces and the transmission of loads between structural components are interactions that can be evaluated only when the entire building is studied.

Regulatory codes around the world focus firstly on the safety of buildings' occupants. For this purpose, design norms require rigorous structural calculations in which the quality of the materials, the appropriate method of construction and the external forces that the structure is going to face are the main aspects to consider. In general, design procedures include a complete background study of the area in which the building will be constructed. In that study, several conditions like surrounding environments, natural activity (wind, seismic, extreme weather, along with others) and soil conditions are taken into account. All design regulations are based on data from past earthquakes, which are periodically revised and updated. The no implementation of these regulations for the design, construction and maintenance of buildings has widely demonstrated deplorable performance of them, with dangerous and catastrophic consequences that in some cases have resulted in fatal repercussions.

A dangerous situation that any building can undergo is the natural and unpredictable seismic wave's movements on earth that occur during earthquakes. Earthquakes are the result of a sudden motion of the tectonic plates that causes a violent shaking of the earth. From this motion, large elastic strain energy releases and spreads out in the form of seismic waves, causing the undesirable and risky motion of everything attached to the earth surface. Dedicated research has been focused in the study and understanding of these sudden movements. Today's technology can perform accurate measurements of seismic waves by locating digital instruments - called seismographs - on specific places on earth. However, the prediction of the occurrence of any earthquake is far away from being possible. Aware of the problem, constructive norms promote the prevention as the most rational and logical option to deal with next seismic events.

With the introduction and implementation of the European standards (Eurocodes) for the design and construction of civil structures, the European community of civil engineers has reference guidelines for the prevention and technical procedure to be followed during the different stages of the construction process. Hence, aiming at evaluating the seismic performance of concrete block masonry buildings, a detailed experimental campaign has been planned in a controlled laboratory

environment. To account for the influence of geometry configuration and steel reinforcement, four different buildings were designed. The buildings were designed and constructed following the Eurocodes and its earthquake resistance performance was studied. For this, dynamic tests by using a shaking table were performed. The design, construction, earthquake simulations and signal processing made for the experimental campaigns are discussed in this chapter.

2.2 An overview of the proposed constructive system

The constructive system solution for structural masonry is based on three-cell concrete block units (Figure 2.1), truss type steel reinforcement (when applied) and modified general-purpose mortar used for both laying masonry units and filling the vertical hollow cells (when reinforcement is added), see Figure 2.2a,b. The three-cell concrete blocks present frogged ends with a dimension that enables to form vertical cells in which vertical reinforcement can be placed, see Figure 2.2c and d. Furthermore, the units possess a conic shape in their cells resulting in one face with higher area than the opposite; then, if the unit block is observed as in Figure 2.1, the top horizontal face has more net area than the bottom horizontal face. This will determine their constructive position during installation, as it is in the face with higher net area that the mason should place the mortar (and steel reinforcement). The masonry units have geometry of 40cm length x 20cm thickness x 19cm height. Due to its characteristics, the concrete masonry units belong to group two of the classification given by the Eurocode 6 (2005), with an average percentage of vertical perforation of 46% and an average thickness of shells and webs of about 30mm.

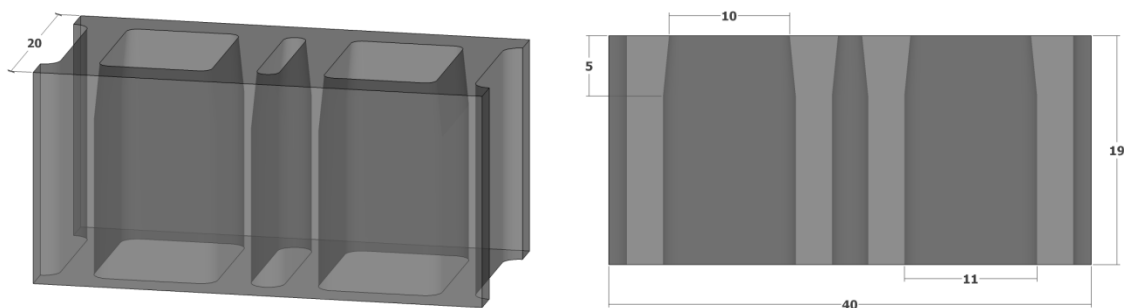


Figure 2.1 – Geometry details and dimensions of real block unit (in cm)

With this constructive system different possibilities for masonry bond can be adopted, namely traditional masonry bond in which vertical reinforcements can be placed simultaneously in internal vertical cells and in cells formed by the frogged ends or an alternative masonry bond composed of continuous vertical joints formed by the frogged ends of the blocks. The latter masonry bond makes the construction technology easier when steel reinforcement is implemented, and is preferable as good performance is found in masonry shear wall tests (Haach et al. 2010). For unreinforced masonry solutions, it is planned that dry joints are used for head joints, as the construction is much faster in this way.

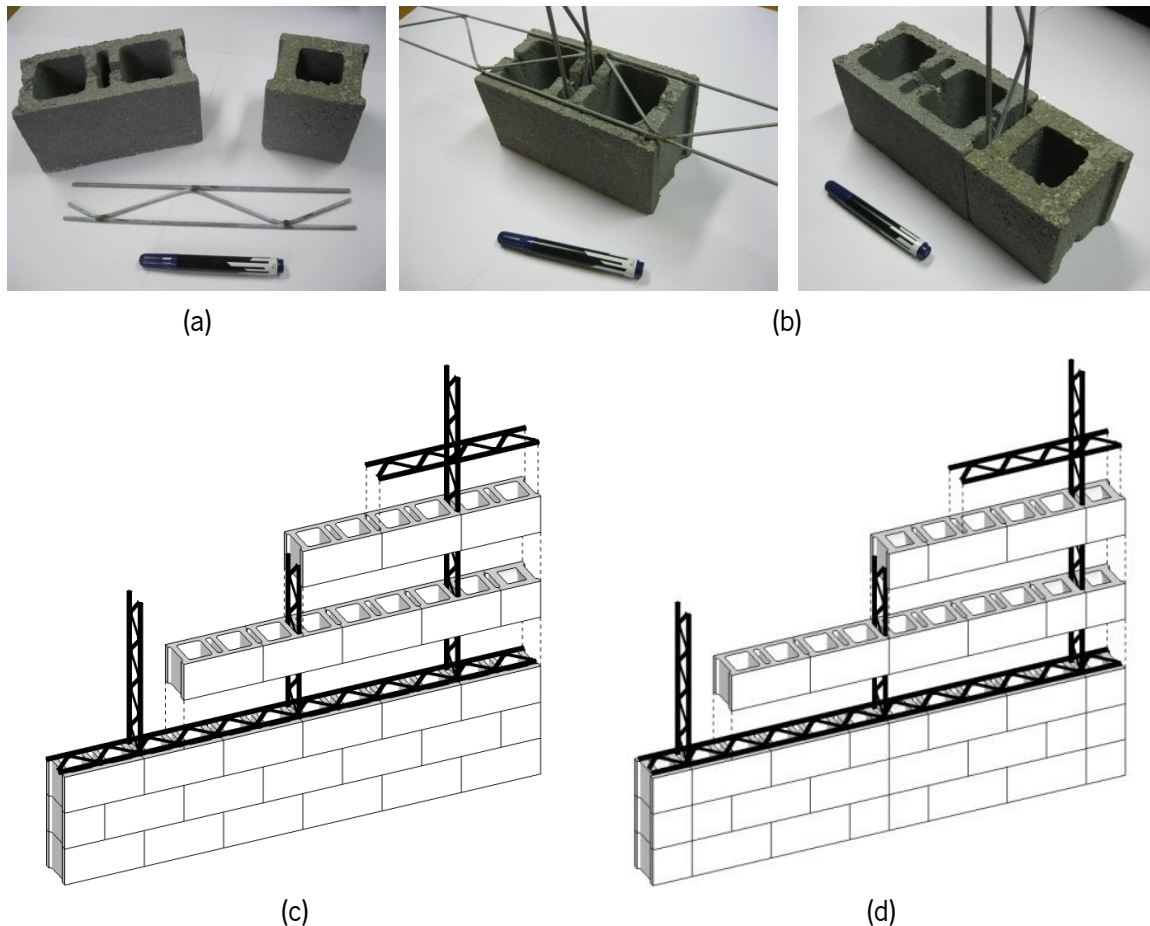


Figure 2.2 – Details of the constructive system based on concrete block masonry: (a) unit block, half unit block and steel truss type reinforcement, (b) sample of block and reinforcement disposition, (c) traditional masonry bond with truss type reinforcement, (d) alternative masonry bond composed of continuous vertical joints formed by the frogged ends of the concrete blocks

The reinforced masonry solution uses pre-fabricated truss type steel reinforcement. It consists in two parallel wires welded to a continuous zigzag wire and can be used for both head and bed joints, see Figure 2.2b. The dimensions of this reinforcement depend on the design requirements and the geometry of the units. Reinforced vertical cells should be filled with mortar and the vertical reinforcement should be adequately anchored to the concrete beams and concrete slabs.

2.3 Buildings' prototypes

From past earthquakes, it has become clear that the geometrical configuration of buildings has an important influence in the global behavior of these structures. The damage observed and subsequent analyses of their causes show that besides the quality of the structural materials, building configuration is of relevance. It is common that house buildings present regular geometrical configuration but in many real situations, an asymmetric configuration for the structural layout of buildings is also found. In numerous circumstances due to land configurations, architectural plans or owner objectives, just to mention some cases, the possibility of constructing a geometrically regular building is no longer feasible.

The Eurocodes consider specific criteria for the geometrical configuration in plan and in elevation of the buildings. Two categories, namely regular and non-regular configurations, are found with specific limitation for each of them. Mainly setbacks (re-entrant corners or edge recesses) in plan and in elevation are controlled. For the earthquake design of buildings, some of the principles to be applied encompass:

- Bi-directional resistance and stiffness,
- Torsional resistance and stiffness,
- Diaphragmatic behavior at story level

With these concepts in mind, two different geometrical configurations are considered for the present study. A regular symmetric in plan and in elevation building and a non-regular asymmetric in plan (but symmetric in elevation) building are considered, see Figure 2.3. The construction system for both is the same, i.e. structural resistant masonry walls with reinforced concrete slabs working as rigid diaphragms.

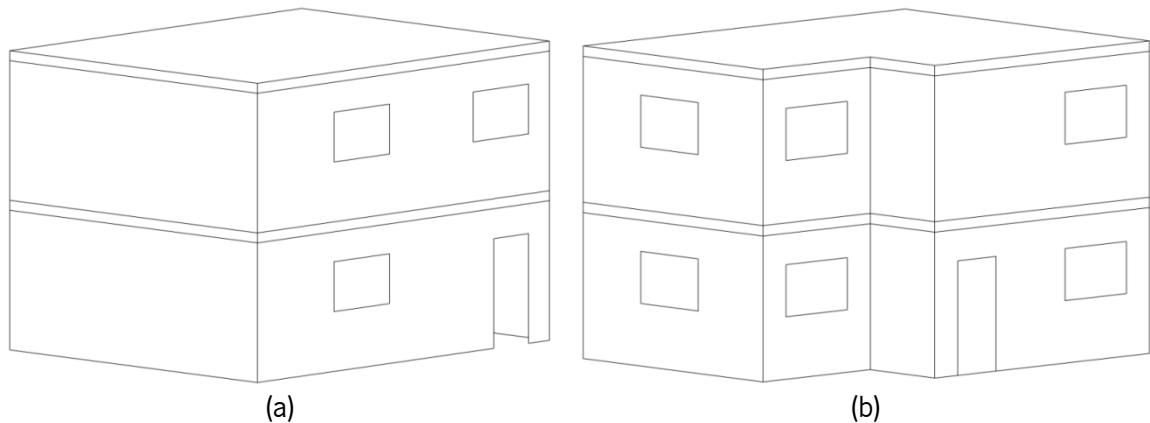


Figure 2.3 – Geometrical configurations for the buildings considered in the present thesis: (a) symmetric and (b) asymmetric

The concrete block masonry buildings are to be used mainly in low to medium rise residential areas. Then, the adopted residential prototypes have about 60m² of plan area. They are individual structures without any other surrounding structures attached to them. They have a maximum of two floor levels, with an interstory height of 3m and with a percentage of openings of approximately of 14% of the wall's area in which they are located.

The symmetric building presents two opposite walls without openings, representing a configuration in which neighboring houses can be attached to it. This is a very common distribution in modern residential row buildings. The asymmetric building has only one wall with similar characteristics i.e. without openings, representing a configuration in which another house can be attached there. This arrangement is commonly known as twins or geminate houses. The asymmetric geometrical configuration presents only one setback at one corner, its design and construction follow area's limitations imposed by the Eurocodes.

Finally, because the buildings can be located in different geographical zones with different seismic actions, a study of the influence of steel reinforcement is performed. This comparison allows a more open discussion of their seismic performance. Then, from each individual configuration i.e. regular and non-regular, an unreinforced and a reinforced buildings will be studied. Thus, in the present thesis four structural masonry buildings are proposed. They will be designed, constructed, tested, analyzed and numerically represented in order to validate the construction system here implemented. A recap of the buildings to be studied is, namely a (1) symmetric plan geometry with no reinforcement; (2) symmetric plan geometry with reinforcement; (3) asymmetric plan geometry with no reinforcement; (4) asymmetric plan geometry with reinforcement.

2.4 Considerations about scale

Due to testing restrictions, such as the size and payload of the table platform, most shaking table tests are carried out on scaled models that can be considered representative of the prototype structures. As will be discussed later in this chapter, the shaking table of the National Laboratory for Civil Engineering (LNEC) in Lisbon - Portugal will be used for carrying out the experimental tests. This table is among the largest in Europe with a platform plan dimensions of 4.6m x 5.6m and a payload capacity of 400KN. It was therefore decided to build reduced 1:2 scale models for all the proposed prototypes, taking into account adequate scaling laws. Applying a similitude scale law between the model and the real building guarantees that the structural behavior, including the damage patterns and failure mechanisms, obtained from dynamic testing of the scaled model are similar to those observed on the real building (prototype) after an earthquake.

The usual similitude laws in experimental dynamic problems are the Cauchy and Froude similitudes. As can be seen in Equation 2.1 and Equation 2.2, the relation between inertial forces and elastic restoring forces is given by the Cauchy similitude, whereas the relation between inertial forces and gravity are given by the Froude similitude (Carvalho 1999).

$$Cauchy\ value = \frac{(\rho L^3 v^2 / L)}{EL^2} = \frac{\rho v^2}{E} \quad 2.1$$

$$Froude\ value = \frac{(\rho L^3 v^2 / L)}{\rho L^3 g} = \frac{v^2}{Lg} \quad 2.2$$

In which ρ is specific mass, v is the velocity, E is the modulus of elasticity, L is the length and g is the acceleration of gravity.

For a rigorous scale of the buildings' prototypes, both similitude laws must be respected. However, the necessary specific mass required to accomplish both laws is inversely proportional to the geometric scale, as observed in Table 2.1. The limitations of the shaking table do not allow the implementation of a Cauchy-Froude law, because the model's mass plus the additional mass required is larger than the payload capacity of the table. Therefore, it was decided to consider only

the Cauchy similitude law, which has been adopted in many masonry buildings testing programs (Candeias et al. 2004; Mendes and Lourenço 2009; Tomažević 2000; Tomažević et al. 2009).

By using the Cauchy scale factors, the experimental buildings have dimensions of 4.20m x 3.40m in plan (polygonal convex line for the asymmetric buildings) and 3.0m in total height, with walls and slabs' thicknesses of 0.1m. The interstorey height is 1.4m with windows openings of 0.8m length x 0.5m height and door openings of 0.5m length x 1.1m height, see Figure 2.4 and Figure 2.5.

To account for an accurate simulation of geometry and the stress-strain relationship, the material properties of the experimental models should be equal to the prototypes, namely in terms of compressive strength, shear strength and modulus of elasticity. Thus, in addition to produce masonry units at reduced 1:2 scale (with final dimensions of 200mm length x 100mm thickness x 95mm height), the composition of the micro-concrete for the blocks was tailored to replicate the compressive strength of the units, with a minimum value of 10MPa. The maximum size of the aggregates was half of the aggregates size used for full-scale blocks, given the lower thickness of the shells and webs. The final scaled block unit has a net area of 110.14cm² and a weight of 2.12Kg.

Table 2.1 – Scale factors of the similitude laws (Carvalho 1999)

Parameter	Symbol	Relation Prototype/Model	Cauchy scale factor	Cauchy + Froude scale factor
Length	L	L_p/L_M	λ	λ
Young's Modulus	E	E_p/E_M	1	1
Specific mass	ρ	ρ_p/ρ_M	1	λ^{-1}
Area	A	A_p/A_M	λ^2	λ^2
Volume	V	V_p/V_M	λ^3	λ^3
Mass	m	m_p/m_M	λ^3	λ^2
Displacement	D	d_p/d_M	λ	λ
Velocity	v	v_p/v_M	1	$\lambda^{1/2}$
Acceleration	a	a_p/a_M	λ^{-1}	1
Weight	W	w_p/w_M	λ^3	λ^2
Force	F	F_p/F_M	λ^2	λ^2
Moment	M	M_p/M_M	λ^3	λ^3
Stress	σ	σ_p/σ_M	1	1
Strain	ε	$\varepsilon_p/\varepsilon_M$	1	1
Time	T	t_p/t_M	λ	$\lambda^{1/2}$
Frequency	F	F_p/F_M	λ^{-1}	$\lambda^{-1/2}$

In particular, for the symmetric buildings the mortar used fine sand to comply with the reduced scale of the bed joints. A cement mortar of a mix 1:3 (cement : sand) with a water/cement ratio of 0.9 was used so that appropriate flowability and workability was achieved, enabling to use the mortar also in the reinforced hollow cells (pre-mixed mortar with similar characteristics and resistance was implemented for the asymmetric buildings). The truss type reinforcement was scaled with respect to

the distance of the diagonal bar (see Figure 2.2a) being reduced to half of the usual value; thus, following the same geometrical scale reduction of the unit blocks.

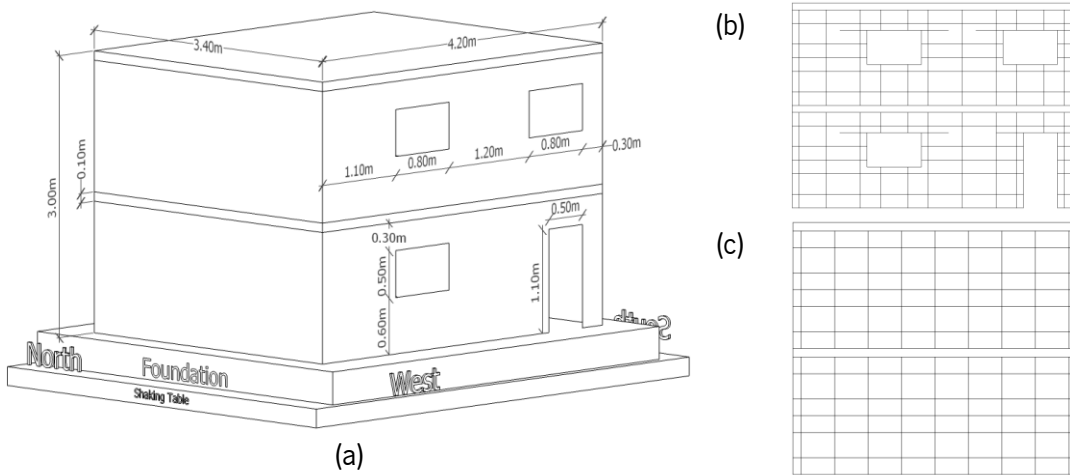


Figure 2.4 – Adopted geometry for symmetric buildings: (a) dimensions for UM and RM models, (b and c) reinforcement distribution in west - east and north – south, respectively

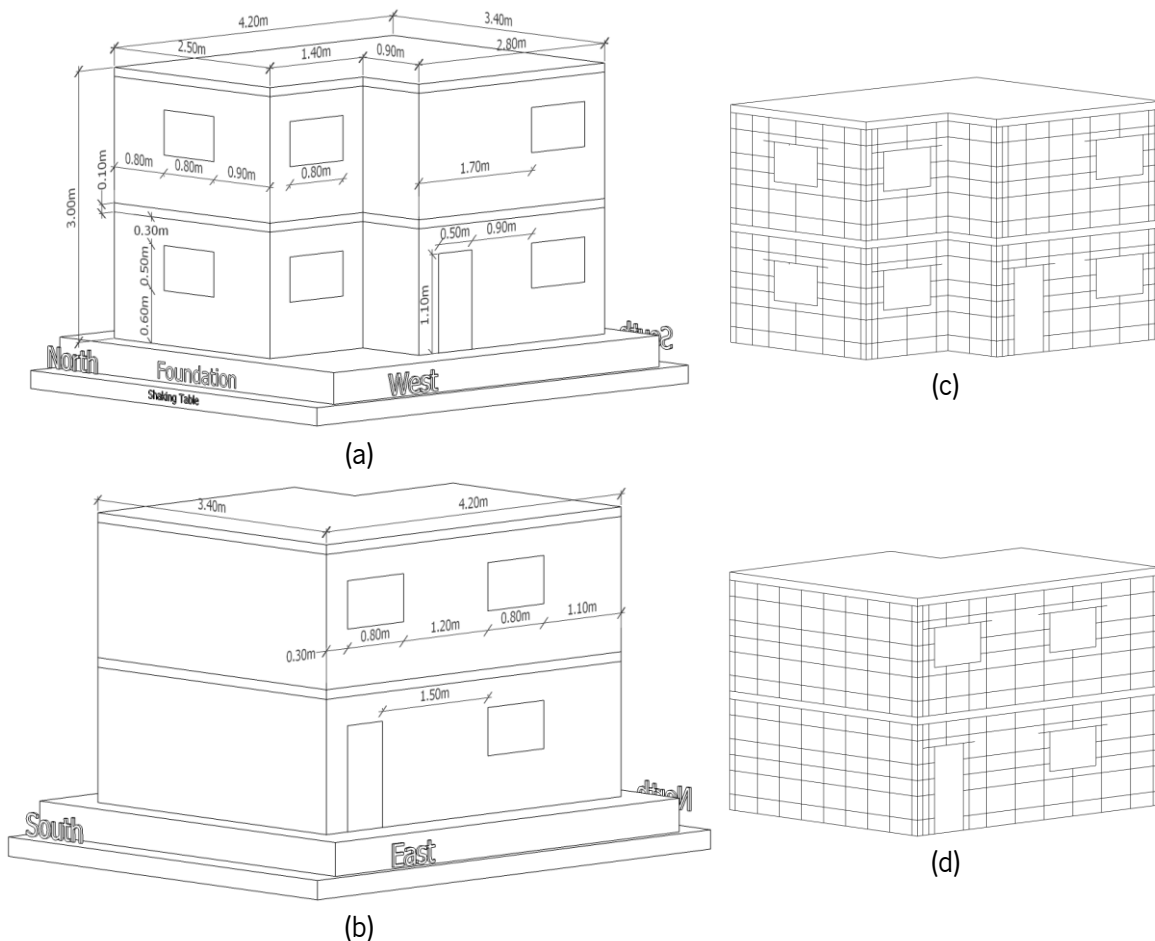


Figure 2.5 - Adopted geometry for asymmetric buildings: (a and b) dimensions for UM and RM models, (c and d) reinforcement distribution for all walls

2.5 Shaking table testing

Each experimental model was designed and built individually. The European regulations for design and construction of seismic resistant structures were followed (Eurocode 2 2004; Eurocode 8 2004; Eurocode 6 2005; Eurocode 6 2006). The same regulations were taken for the seismic actions applied to the models through the shaking table tests. Major attention was taken regarding recommendations and specific rules for masonry buildings including materials and detailing. Specific descriptions of their design and construction together with test setups and final signal processes performed are discussed.

2.5.1 Design of building models

The first step in the process of designing was the selection of the geometrical configurations. The two arrangements (regular and non-regular) were selected from a series of options after studying the typical residential houses' distribution in Portugal. This study included mainly the distribution and location of walls, windows (in relation with the spaces with natural light) and doors. The final geometrical configurations, presented in Figure 2.4 and Figure 2.5, encompasses only the necessary structural walls with their respective openings. Both models present walls with no openings, allowing the future coupling of neighboring houses attached to them as observed in Figure 2.6. In the symmetric option it is even possible the configuration of continue row buildings.

With the geometry of the buildings defined, the next step was the design of their foundations. It was planned one foundation for each configuration i.e. one foundation for the symmetric buildings and one foundation for the asymmetric buildings. This obeys mainly to the cost and necessary time of construction and curing of the concrete. Apart from their geometrical dimensions, the design and construction of both foundations have the same basis. In addition to the necessary weight they have to support (self-weight plus masonry buildings) and the connecting function between the shaking table and the models, the most relevant stage of their design are the displacements' control during the model's transportation between the construction site (located around 10m far from the table) and the shaking table.

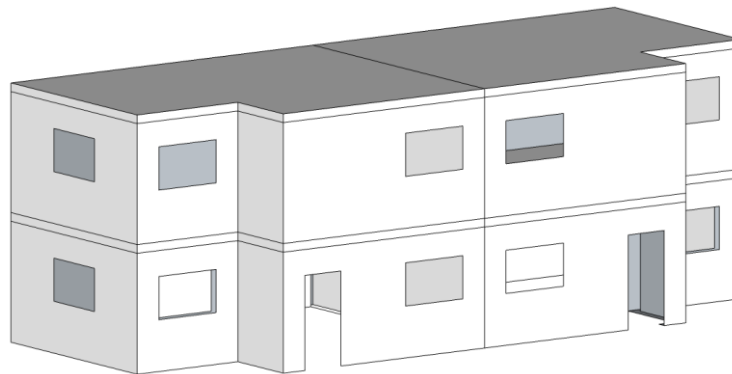


Figure 2.6 – Example of twin houses using the adopted asymmetric configuration

Instead of a full slab as foundation, a perimeter grid of beam foundations was selected for each model. The limitations on middle span deformations were imposed in order to avoid damage of the models, in particular cracking of masonry, during transportation (carried out from the four corners of the foundations). An arrangement of several holes was planned for the fixation to the shaking table. The final geometrical dimensions for both foundations are presented in Figure 2.7. A geometrical representation of the final position of the masonry buildings is also observed.

For the final configurations of both foundations, it was used the maximum dimensions allowed by the table. The transportation of models was carried out by using an overhead crane with two parallel hoists that takes the models from the four pieces of suspension. The thickness of both foundations is the same (thickness of 35cm). The reinforced concrete foundations were also used to connect the models to the shaking table through post-tensioned steel rods. The holes observed on each foundation were used for that fixation.

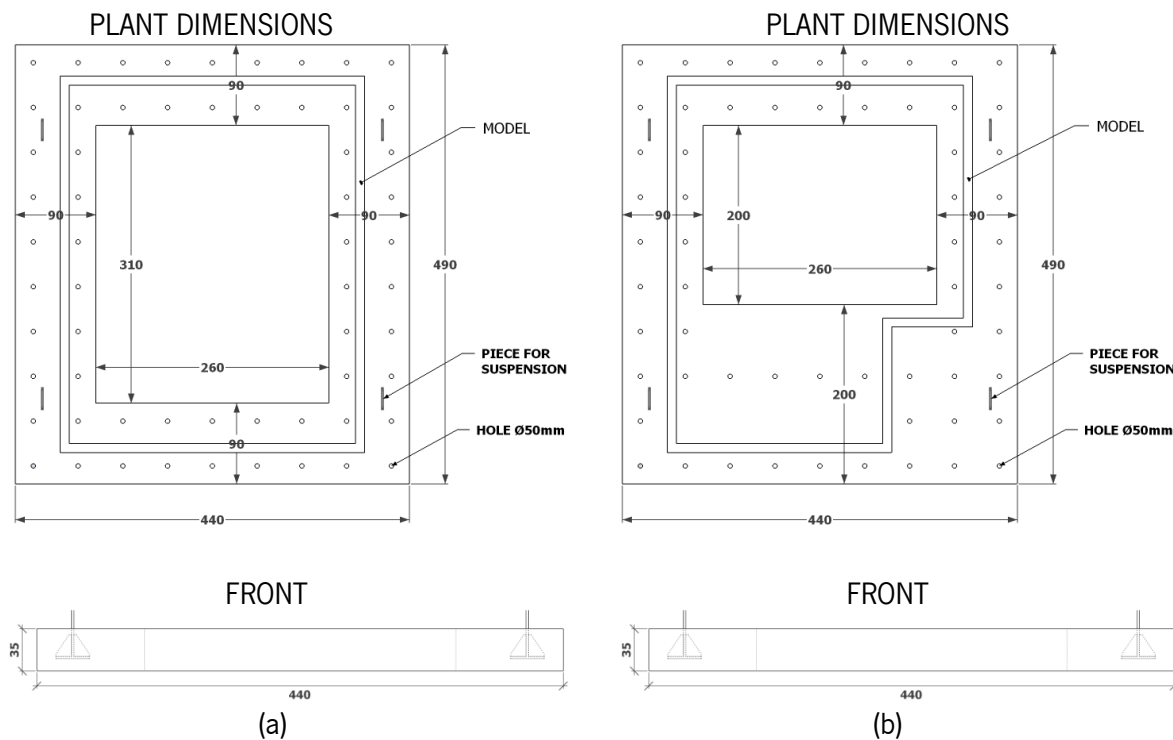


Figure 2.7 – Geometrical dimension (in cm) for ring beam foundations: (a) symmetric buildings and (b) asymmetric buildings

Apart from masonry, the other structural elements that make part of the buildings are the reinforced concrete slabs. A couple of slabs were designed and constructed for each configuration, similarly to the foundations (one for each story). In this way, the slabs of the RM models will be used again in the UM model. The slabs have the main aim of working as rigid diaphragms at the top of each story. They also serve as connecting point for structural walls and as structural elements for the transmission of forces between stories, contributing to the good global behavior of the masonry buildings. They were designed as reinforced concrete two-way solid slabs, having structural strength in the two orthogonal directions. In the design, it was assumed that slabs are supported on their four sides by the masonry walls, making a more economical design. As known, the moment of bending

in each direction will depend on the ratio of the two spans and the conditions of restraint at each support. Then, span and effective depth ratios were taken into account controlling excessive deflections.

Both reinforced concrete structures, i.e. foundations and slabs were verified by using the software SAP2000 (2009). On the numerical models, similar conditions to the ones that should occur in the experimental models were adopted. Furthermore, incremental forces based on design coefficients were taken into account. In a final check, these coefficients were increased about twice its original value to account for the suspension period they will afford, i.e. during models' transportation to the table for the foundations, and between reinforced – unreinforced buildings' constructions for the slabs.

Regarding masonry, vertical continuous joints were considered for the reinforced masonry buildings; whereas traditional run masonry bond was used for the unreinforced masonry buildings, see Figure 2.8. The bond adopted for reinforced masonry makes the construction technology easier. As continuous head joints were adopted, vertical reinforcements were applied around the openings and at corner walls. Additionally, flexural horizontal reinforcements were added to masonry lintels above openings, see Figure 2.4b and Figure 2.5c and d for details.



Figure 2.8 – Masonry bond patterns: (a) RM models and (b) UM models

The truss type steel reinforcement was designed in accordance with the minimum reinforcement ratios recommended by the Eurocode 6 (2005) and Eurocode 8 (2004). Suggestions about overlaps, laps and anchorages were also followed for both vertical and horizontal reinforcements. The final steel configuration provides an average of 0.07% for vertical reinforcement and of 0.05% for horizontal reinforcement. The final designs for the construction of the symmetric and asymmetric buildings are presented in Appendix A and Appendix B respectively. Figure 2.9 shows the symmetric and asymmetric experimental buildings before testing.

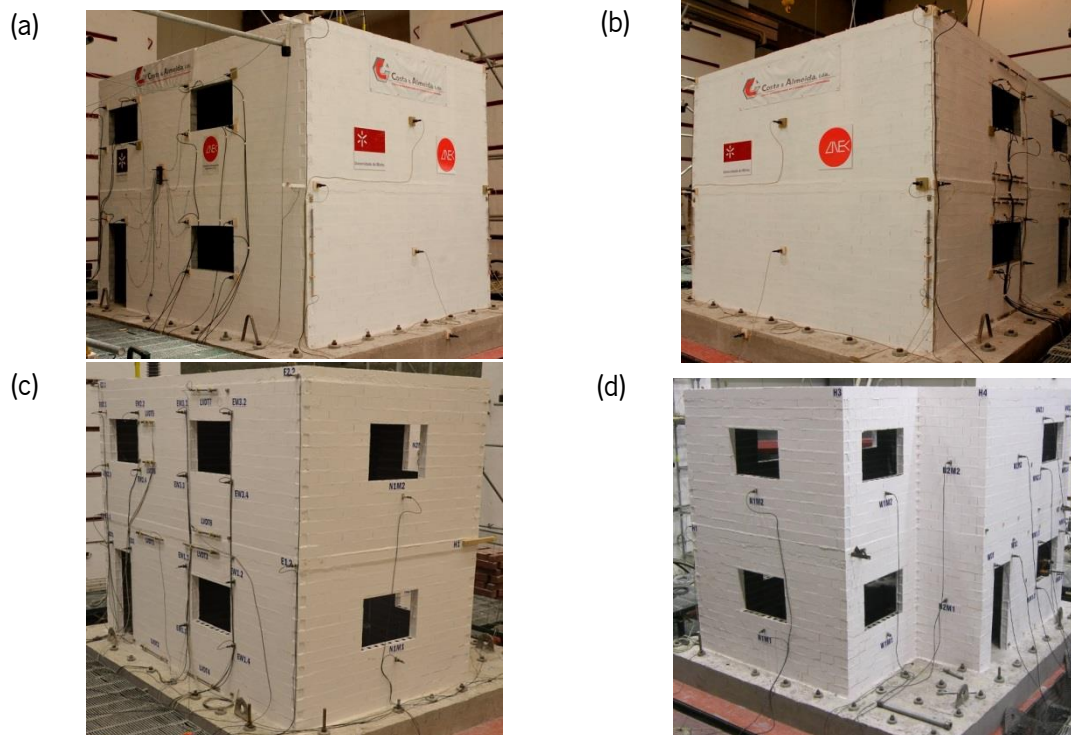


Figure 2.9 – Masonry buildings for the experimental campaign: (a, b) symmetric and (c, d) asymmetric

2.5.2 Construction of experimental buildings

In case of reinforced masonry buildings, their foundations were essential for the anchorage of the vertical reinforcements. Then, it was decided to start the construction of the models by the reinforced model to anchor the vertical reinforcement to the foundation before concrete casting. After construction, testing and demolition of the reinforced buildings, the reinforced concrete slabs and foundations were recovered. The remaining steel tips on them are totally removed by using a saw blade. Finally, the foundation and the slabs were reused for the construction of the unreinforced buildings.

The construction of all buildings presents similar procedures. They were made at the same location and with similar conditions, i.e. inside the LNEC facilities. The general construction process developed for all the buildings is described below and, when justified, minor differences or construction variation among models will be pointed out.

The LNEC facilities involve the 3D shaking table platform and a strong reinforced concrete floor adjacent to it. This strong floor was used for the construction of the models. It was designed to resist high load weights and was constructed with an ideal leveling. However, due to wear and tear after several years of loading and unloading from previous buildings' models, the floor has no longer an acceptable leveling, which is mandatory for a good fixation to the table platform. Then, the first step was the floor's leveling for the construction of the grid foundations. The leveling was performed by using wooden sticks, as observed in Figure 2.10a.

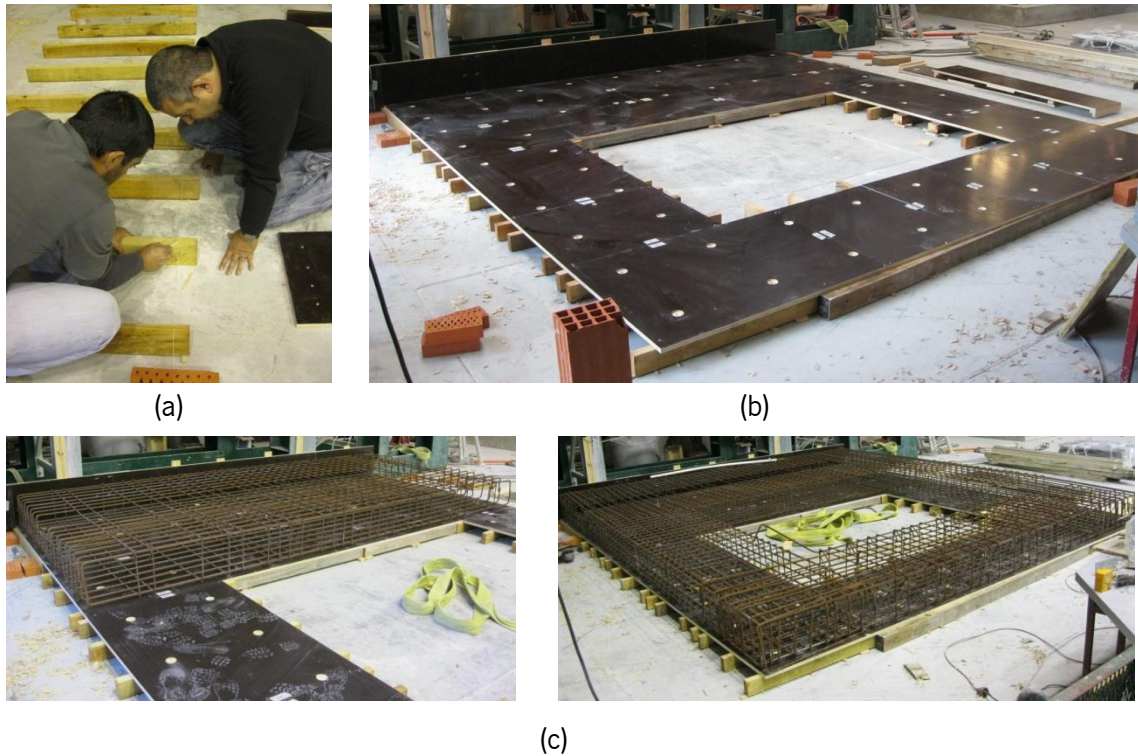


Figure 2.10 – Construction of foundation: (a) wooden sticks for leveling, (b) formwork boards with smooth surface, (c) placing of steel reinforcement

To improve the leveling process and to obtain a good finishing, a smooth material formwork was used. On it, circle marks for the placement of vertical plastic tubes were defined through which steel rods were later introduced to the fixation of the foundation to the table. The formwork board was installed over the wooden sticks as seen in Figure 2.10b. The steel reinforcement for the foundation is then placed (Figure 2.10c)

The steel reinforcement was previously bent and tied in a job site and only its application and positioning was needed during the construction. The installation of the vertical formwork was performed making a box-like setup. To control cover protection for steel, small concrete pieces were used to hold the reinforcing steel bars away from the bottom and sides of the formwork. Furthermore, it was placed the metal suspensions' pieces and the vertical plastic tubes. For the last ones, special care was taken. The tubes must be vertical and located with a precision of ± 1 mm. To accomplish this, an additional arrangement of wooden sticks was made. The sticks have holes where the tubes were introduced, being located with precision, minimizing position errors or movements during the concrete pouring, see Figure 2.11.

Finally, before the foundation's concrete casting, the anchorage for the truss type vertical reinforcement of masonry was carried out. These pieces of steel were bent at one extreme to be tied to the lower foundation's reinforcement. In their final position, they were tied to the lower and upper foundation's reinforcement. Figure 2.12 presents a view of this process.

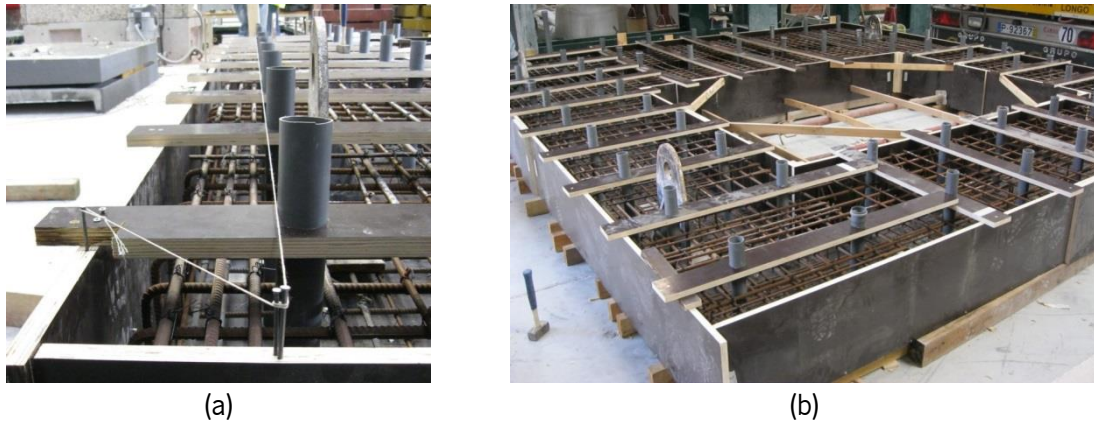


Figure 2.11 – Foundation construction: (a) vertical tubes positioning and (b) box-like formwork and suspension pieces already installed

The internal and external sides of the formwork were restrained by metal poles in order to fix the box-like shape of the foundation during the pouring of concrete and curing. Before pouring, it was spread out water in all the formwork in order to avoid water absorption by the wood. For the concrete, it was used a ready-mix concrete manufactured according with the design requirements in a factory near the LNEC. It was poured by using a concrete mixer. The pouring process was always followed by spreading operations in which electrical vibrators were used, see Figure 2.13. The top surface was leveled with a stainless steel trowels, obtaining a smooth concrete finishing.

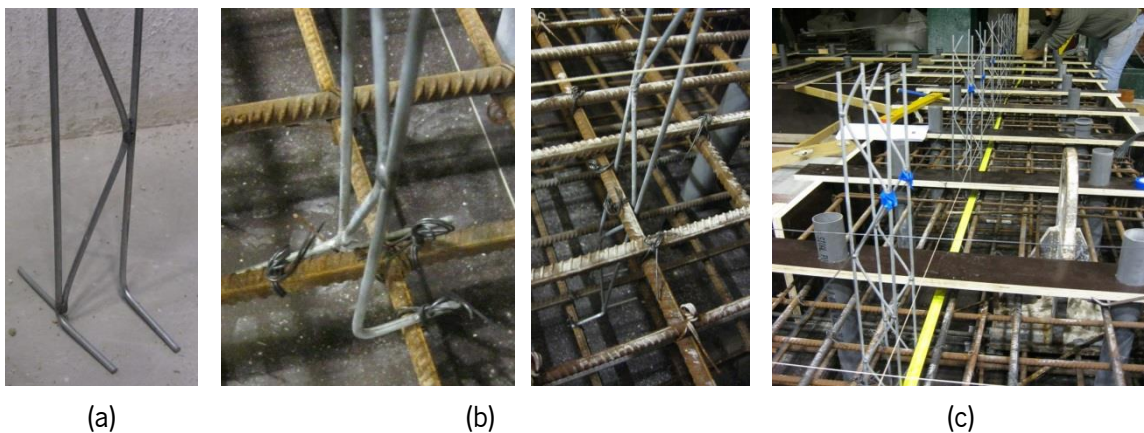


Figure 2.12 – Vertical truss type reinforcement for masonry: (a) bent of anchorage, (b) anchorage to foundation's reinforcement and (c) final position on foundation before casting

After three days of casting, the internal and external lateral boards of the formwork were removed, allowing airflow and appropriate environment conditions for the curing period. To prevent cracks during curing water was often spread over the foundation.

After curing time, the vertical reinforcement for the first story was tied to the steel tips previously anchored in the foundation (Figure 2.14a). This process was performed using traditional steel tie wire pieces and following overlap sizes. Next, detailed snapping of chalk lines on foundation as well as level and plumb's positions at the corners of the future masonry walls were carried out, after which the construction of masonry walls started.

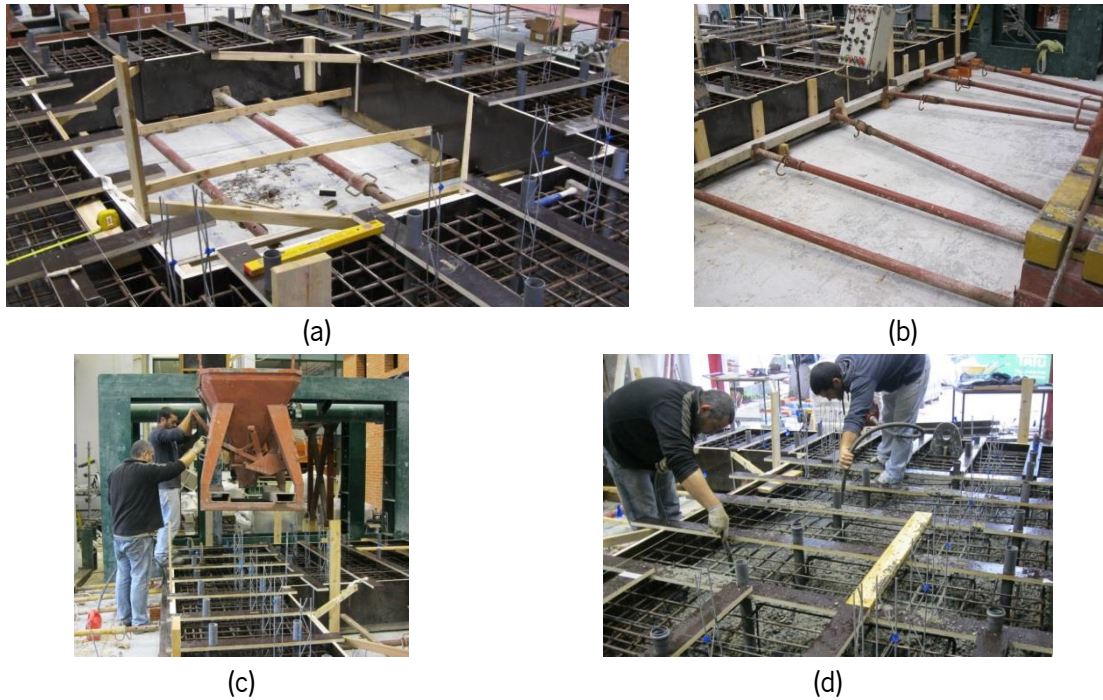


Figure 2.13 – Foundation construction: (a) internal restraining metal poles, (b) external restraining metal poles, (c) concrete pouring and (d) spreading with vibrators

It should be mentioned that for this process no specialist workmanship is required. The installation of masonry follows the common traditional methods applied in other constructive masonry solutions. However, care must be taken in the position of the unit blocks. As aforementioned, the concrete units possess a conic shape in their cells, resulting in a horizontal face with higher net area. Units should be placed with the biggest net area of the transversal webs up, so that the mortar of the bed joints is always placed on the face with higher area, and in case of reinforcement, it should result in a higher embedded steel area.

For the first masonry row, water was sprayed to the area of foundation in which the mortar was placed. The mortar was mixed with an electrical mortar mixer. Similar construction process was performed on every masonry row in which position and leveling was frequently verified. Then, the respective masonry bond (traditional or alternative, Figure 2.2c and d) was composed. On the reinforced masonry buildings, after finishing every masonry row, the vertical joints where steel reinforcement was placed were filled with mortar. The filling process was performed up until half block of the actual row constructed, in order to avoid weak planes at the horizontal joints of masonry. On the same buildings, according with design specifications, it was installed the horizontal truss type reinforcement, see Figure 2.14.

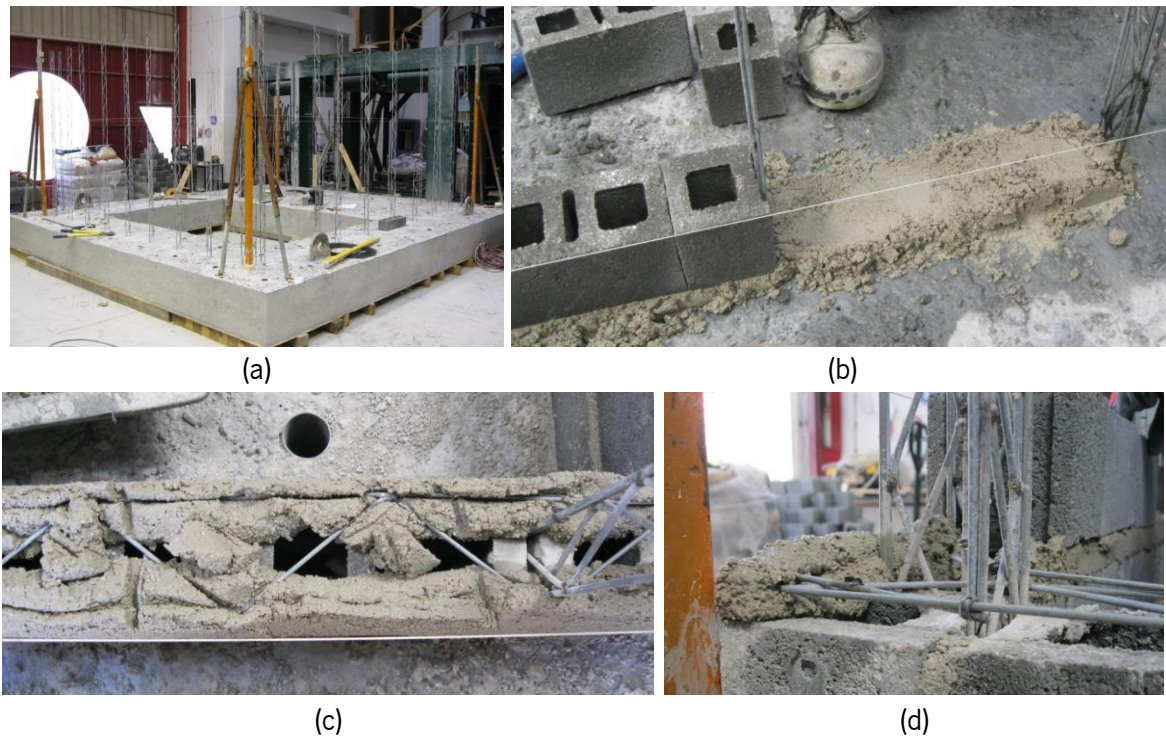


Figure 2.14 – Construction process: (a) foundation with vertical steel, (b) installation of first masonry row, (c) horizontal joint with reinforcement and (d) detail of mortar covering reinforcement

In all buildings, lintels were constructed above doors and windows' openings. Design specification for overlaps and joint thicknesses for steel covering were made. After 14 masonry rows, the construction of the first slab takes place. Its formwork includes the construction of a temporary scaffolding with vertical metal poles that support a wooden structure in which the smooth wood boards are located. Inside this box-like formwork, the steel reinforcement for the slab was placed. In addition to the flexural reinforcement along the two directions of the slab, it possesses border (tie) beams along the entire perimeter. These beams are used for the connection between the structural walls and the slab and are responsible for transmitting the slab's forces (reactions) to the walls.

The vertical truss type reinforcement of masonry crosses through the slabs thickness. Furthermore, a portion of the overlap for the vertical reinforcement of the second story was embedded into the slab, generating a structural connection and anchorage between the first and second floors. To avoid the falling of concrete through units' cells during slab's concrete pouring, it was placed polyurethane foam in all the cells of the last units' row. For the casting of the slabs, it was used a ready-mix manufactured concrete which was poured by using a concrete mixer. Arrangements, steel covering, vibration and smooth finishing process similar to the ones performed during the construction of the foundation were followed. Later, similarly to the foundation, the sides of the formwork were removed and a curing period was considered. A graphical overview of this construction process can be observed in Figure 2.15.

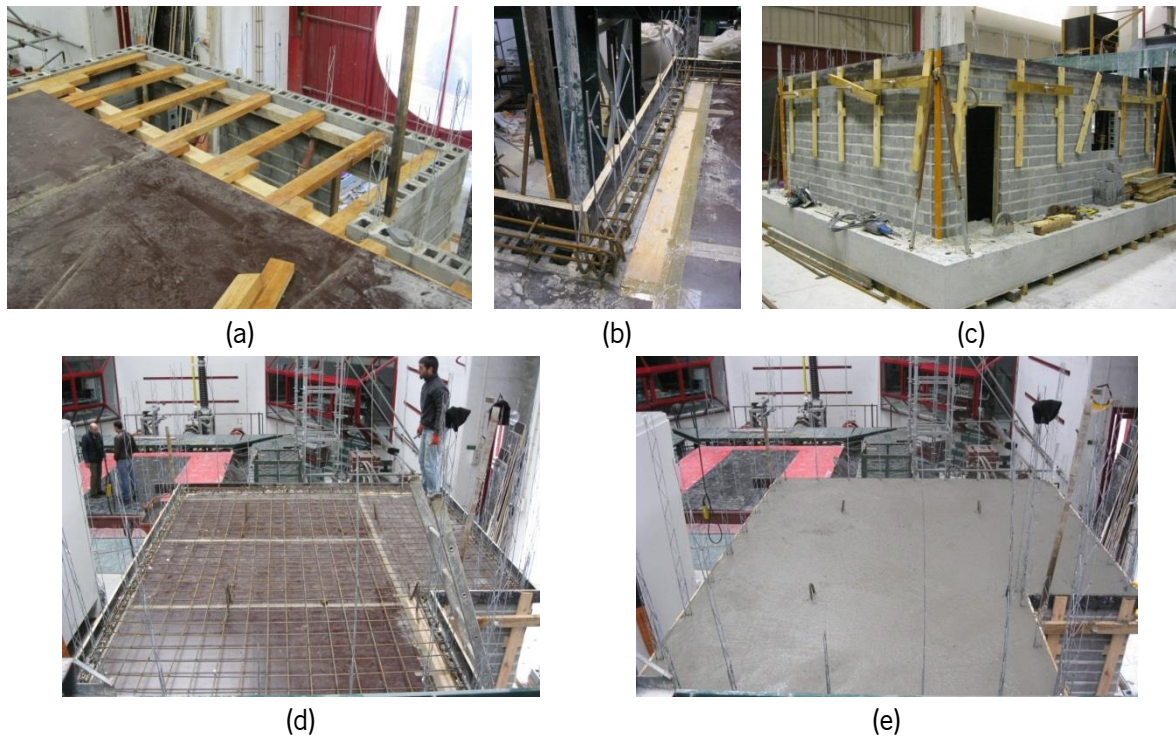


Figure 2.15 – Construction of slab: (a) wood scaffold and smooth board formwork, (b) perimeter supporting beams, (c) first masonry story with slab's formwork, (d) view before casting and (d) view of slab after concrete pouring and smoothing

As mentioned before, slabs were made only during the construction of reinforced buildings. Later, they were reused for the construction of the unreinforced buildings. On those buildings, it was clear that the walls-slab connection could not be based only on the horizontal mortar layer. Then, to improve the connection and seismic performance, steel dowels of 15cm long were placed every 50cm around the slab's perimeter and anchored with epoxy resin.

The construction of the second story followed an identical process. After finishing the construction of the buildings, and after an appropriate curing time, they were painted white color making the future identification and marking of cracks easier. An example of a final concrete block masonry building for shaking table tests is shown in Figure 2.16.

During the entire masonry construction, vertical and horizontal plumb of the walls was always checked. Furthermore, every two masonry rows mortar samples for compression and flexural tests were collected to control the construction quality. In addition, flow tests were frequently made in order to control the mortar's workability, which is particularly important for the filling of vertical reinforced joints. Some of the mortar samples taken were tested after 28 days of curing time and others were tested at the same time of buildings shaking table tests, giving more accurate strength values of mortar at that time. At this point, it should be mentioned that mortar joints on masonry buildings were frequently sprayed with water, avoiding loss of water during its curing time.



Figure 2.16 – Concrete block masonry building for experimental shaking table test

Throughout the construction of all masonry buildings, masonry specimens were built with the aim of characterizing the masonry under compression and shear through uniaxial and diagonal compression tests. Furthermore, after shaking table test some masonry samples were taken from the damaged buildings aiming at contributing for the materials characterization and comparison with the other built separately.

Before shaking table testing, two important processes were performed, namely the positioning of models on the table platform and the final fixation to the table. The movement of the models was carefully performed by using the two overhead bridge cranes. It consists in two parallel runways (along the lab) with two traveling bridges with their respective hoist. The models were lifted from the suspension pieces located in the corners' foundation (Figure 2.11b) and moved with very low rate velocity to their final position. The fixation to the table was made with steel rods installed through the plastic tubes located during construction at the foundation (Figure 2.11). As observed in Figure 2.7a and b, each building was attached to the table in 60 points by using post-tensioned steel rods.

After the final shaking table tests, a controlled demolition for each building was performed. It always took place above the shaking table. Adequate and practical safety requirements were followed. For the reinforced buildings, special care was taken in order to recover the foundation and slabs to be reused on the unreinforced buildings. Finally, from all demolitions, several masonry samples were taken for material characterization.

2.5.3 Test setup

The experimental testing for structural components improved significantly during the last decades. The study of phenomena like the dynamic performance of buildings during earthquakes is now performed under real-time controlled conditions. The era of computers and technology, have increased the range and precision of instrumentation devices for all kind of measurements. Modern and more specialized laboratories offer powerful mechanisms for the study of a huge quantity of physical and natural phenomena, increasing the level of knowledge in all sciences. One of the modern laboratories located in Europe, specialized in the study of the seismic behavior of structures, was the place for the construction and development of the experimental study carried out in this work. Test setups consist mainly in the shaking table itself and the devices implemented for the measurement of buildings' performance, both of them discussed below.

2.5.3.1 Shaking table

The shaking table tests of the buildings were performed at the Earthquake Engineering and Structural Dynamic Division (NESDE), which is part of the National Laboratory for Civil Engineering (LNEC) in Lisbon, Portugal. This facility has a triaxial shaking table, which features three independent translational degrees of freedom namely two horizontal (longitudinal and transversal) and one vertical, which are driven by hydraulic actuators. In particular, its rotational degrees of freedom are restrained by a passive system based on a set of high torsion stiffness tubes, one for each axis (roll, pitch and yaw).

The system is composed of three main components: (1) the table itself; (2) the guidance system and (3) the hydraulic actuators that include the control system.

The body of the shaking table is a rigid welded steel slab, with a shape similar to an inverted triangular prism, in which the top part is the table platform where the specimens can be installed and fixed, see Figure 2.17. The dimensions of this platform are 4.6m X 5.6m. The full body has a weight of 40ton and was designed to provide a high stiffness connection with the other components of the system; i.e. the guiding and the control system. It is supported by a system of rods, which technically are “rod end joints” with swivel balls that allow the translational movements of the table. This system serves as connection between the stiff torque tubes and the table platform.

The guidance system is composed by the system of torque tubes. They have a thickness of 2cm and a diameter of 1.2m for the tube that controls the horizontal movements and a diameter of 0.8m for the ones that control the vertical movements. The torque tubes are supported at both ends by bearings that allow them to rotate around their longitudinal axis. They are linked at each end by means of cranks to the system of rods. Then for example, when the platform moves vertically, it either pulls or pushes the connecting rods, rotating both cranks by the same angular displacement and the respective torque tube likewise. The guidance system ensures that the platform only moves in the desired translational degrees of freedom. It prevents the overturning rotation at the table by providing a large reaction force to any pair of vertical or horizontal forces developed through table rotation.

The system of actuators consists in the servo-controlled hydraulic actuators and their associated control system. Each actuator is composed by a hydraulic cylinder with double effect i.e. tension – compression, with one or more servo-valves and a set of hydraulic components for their connection, control and safety operation. A hydraulic pumping station provides the pressurized oil to all the shaking table’s actuators by an average pressure of about 20MPa and a flow rate of 690 liters/min. The pumping station is responsible for the oil-flow capacity of the system, which affect directly its velocity limit. The shaking table platform is driven by four actuators distributed as follow: (1) one vertical; (2) three horizontal, namely one in the longitudinal direction and two in the transverse direction.

The two actuators in the transverse direction are located “in-line” (one in front of the other) in a push-pull arrangement as presented in Figure 2.17. A description of the actuators is presented in Table 2.2.

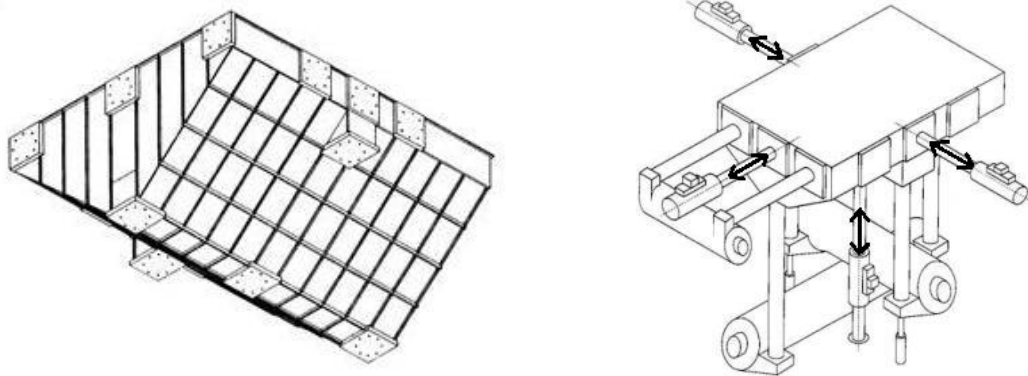


Figure 2.17 – Shaking table: (a) rigid body and (b) general view of the full system i.e. table, guidance (torque tubes) and actuators. (Adapted from LNEC-NESDE website <http://www.lnec.pt/organizacao/de/nesde/ptriaxialdescricao>. retrieved June, 2014)

Table 2.2 – Description of actuators for the shaking table at LNEC

Direction	Number of units	Total force (KN)	Manufacturer
Vertical	1	375	INSTRON
Horizontal - Longitudinal	1	1250	INSTRON
Horizontal - Transversal	2	750	INSTRON

All the actuators possess an effective stroke of 145mm, in which the safety margin of displacement is already taken into account. The specific characteristics of the actuators are described in Table 2.3.

The shaking table has a frequency range between 0.1Hz and 40Hz. It has a mixed (Analog/Digital) control system with a D/A capacity up to 8 channels ADC – 16 bits and an A/D capacity of 96 digital channels. In general, the actuators' performances during shaking table tests are compared with internal control sensors located in the table. From this comparison, updated factors are obtained and given to the system, increasing the accuracy performance of the table. As a whole, the shaking table can carry a maximum payload of 40ton, meaning that the horizontal actuators can have a force capacity of the order of two or three times the maximum payload of the table.

Table 2.3 – Characteristics of actuators

Direction	Stroke (mm _{pp}) (effective/maximum)	Maximum velocity (cm/s) (nominal/limit)	Maximum acceleration (m/s ²) (empty table)
Vertical	290/400	42.4/73.5	31.25
Horizontal - Longitudinal	290/400	41.9/72.6	9.38
Horizontal - Transversal	290/400	70.1/121.5	18.75

To summarize, the mechanical system of the shaking table is complex. Even it has been updated and improved based on previous experiences, the true representation of an actual seismic event is

still a challenge, not only for the LNEC table facilities but also for most of the European research centers. Thus for the present study, the vertical component of the seismic action, despite its significant importance, was not used in order to avoid more interference on the complex control system and the direct limitations in model weight as the vertical actuator has restrictions in its maximum force capacity, see Table 2.2.

2.5.3.2 Instrumentation and acquisition systems

In order to obtain complete data about the excitation of the models, they were instrumented with three different types of devices, namely accelerometers, displacement transducers (LVDT) and position-sensitive detectors (PSD). These measurement devices were used to monitor the accelerations, the local and global displacements. All these measuring devices have the important task of transforming physical quantities such as the accelerations and displacements in electric signals that can be recorded and posteriorly analyzed.

An accelerometer, also known as acceleration transducer is an electromechanical device that measures accelerations. It moves proportionally to the acceleration amplitude of a moving body. This amplitude of motion is detected and converted into an electrical signal in the form of voltage. There are five main types of accelerometers that, depending on their characteristics, are used for different applications. These five types are piezoelectric, piezoresistive, capacitive, force balance (also known as servo) and the strain gauge based. For the present study, only piezoelectric accelerometers were used (see Figure 2.18). Compared with others, the piezoelectric accelerometers have the advantages of not using external power source (active transducers), being stable, having a good signal-to-noise ratio and being linear over a wide frequency and dynamic range. The principal disadvantage concerns the impossibility of measuring the DC components i.e. response at 0Hz, like the permanent gravity acceleration g (Ramos 2007).

For all the buildings, the seismic ICP® accelerometers, model number 393A03 were used (PCB 2014)(Figure 2.18a). This accelerometer has a ceramic sensing element and a shear sensing geometry with hermetic stainless steel housing. It gives fixed voltage sensitivity, regardless of cable type or length, low-impedance output signal, which can be transmitted over long cables (even in harsh environments) with virtually no loss in signal quality and low-noise voltage output signal. A detailed description of its specification is given in Table 2.4.



Figure 2.18 – Piezoelectric accelerometer: (a) model 393A03 and (b) typical cut-away view

Accelerometers are generally used in civil engineering structures, partly because they provide accurate results with relative low cost. Moreover, it is possible to calculate displacements by numerical integration of the acceleration records.

Table 2.4 – Accelerometer specification (PCB 2014)

Specification	English	SI
Sensitivity ($\pm 5\%$)	1000mV/ <i>g</i>	102mV/(m/s ²)
Measurement range	± 5 <i>g</i> pk	± 49 m/s ² pk
Frequency Range ($\pm 5\%$)	0.5 to 2000 Hz	0.5 to 2000 Hz
Resonant Frequency	≥ 10000 Hz	≥ 10000 Hz
Temperature Range	-65 to +250 °F	-54 to +121 °C
Size - Hex	1 3/16 in	30.2 mm
Size - Height	2 3/16 in	55.6 mm
Weight	7.4 oz	210 gm

A Linear Variable Differential Transformer (LVDT) is an electrical linear position/displacement transducer used to measure linear displacements. An inductive LVDT sensor has no electrical connection across the sensing element ensuring clean data and a long life, it can even operate in extreme environments like submerged in sea waters and in temperatures of 600°C (1100°F). The LVDT converts a position or linear displacement from a mechanical reference (zero, or null position) into a proportional electrical signal containing phase (for direction) and amplitude (for distance) information. The advantage of not requiring an electrical contact, between the moving part (core assembly) and the coil assembly, is that it relies on electromagnetic coupling. Thus, because the sliding core does not touch the inside of the tube, it can move without friction, making the LVDT a highly reliable device.

Table 2.5 – LVDT specification (RDP 2014)

Type	Range (mm)	L (mm)	X (mm)	D3 (mm)	Total weight (gr)	TF (mm)	Sensitivity (nom)
ACT2000	± 50	295	76	4.75	511	15	1.5 V/V
ACT4000	± 100	452	127	4.75	710	15	3.2 V/V

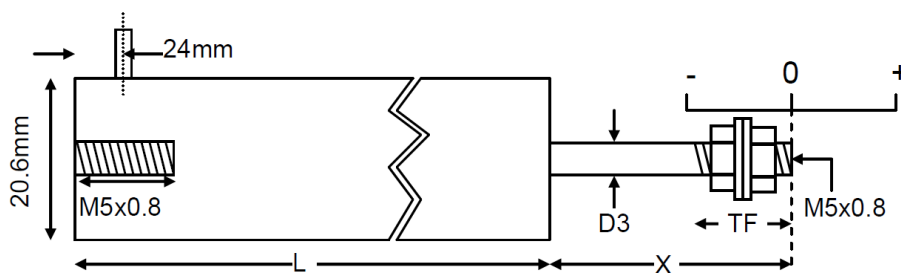


Figure 2.19 – Captive guided displacement transducer

For the masonry building tested, ACT LVDT displacement transducers were used. In particular it was used the captive guided version, which has bearings to guide the armature inside the measurement sensor (RDP 2014). A detailed description of the LVDTs that were used for the buildings instrumentation is made through Figure 2.19.

The PSD detectors are opto-electric position sensing units that measure the position of a single point (target) focused on a sensor's head (camera). Unlike the LVDTs, the PSD provides the advantage of measuring structure displacements related to an external reference point. The system is composed by a high-resolution camera, an optical sensor and a control unit, see Figure 2.20. For the shaking table tests two-dimensional PSD were used. The sensors use photodiode surface resistance providing continuous data (X and Y for the present study) featuring high position resolution and high-speed response.



Figure 2.20 - Position-sensitive detectors (PSD): (a) controller and camera, (b) optical sensor (Hamamatsu 2014)

For the masonry buildings, five PSDs were used. One sensor was attached to the concrete beam foundation; the other four were distributed at the two diagonally opposite corners of each slab (intersecting corner between north and east walls and intersecting corner between south and west walls). In this way, the global X and Y position of the models was always recorded.

During the experimental tests, a set of three video cameras was located about five meters far from the models, focusing from top to bottom at three corners. From the video records, damage evolution and damage mechanisms were possible to be identified. Furthermore, two photo cameras (with different resolution capacities) were used for the photographic record of cracks and damages. After each seismic test, global and detailed photographs of each wall were taken to document the damages.

The instrumentation of the masonry buildings was designed aiming at obtaining the most relevant and important measurements to assess their performance during the seismic tests. The accelerometers and LVDTs were mounted on the models whereas the Hamamatsu sensors use external reference frames where the sensors heads are mounted. The purpose of the accelerometers and its location was to obtain the time history accelerations and subsequent time history displacements, evaluating the in-plane and out-of-plane behavior of the structural masonry walls at both floor levels. Then, each building was instrumented with this device at most of their corners, openings corners and in some middle points of the walls. The LVDTs aim at obtaining local in-plane deformations and, thus they were placed in some piers at both floor levels. The PSDs were located with the objective to obtain external global displacements of the buildings, they were placed at diagonally opposite building's corners at both floor levels and at the concrete beam foundation.

The two buildings of each geometrical configuration were equally instrumented. The details of this instrumentation are presented in Figure 2.21.

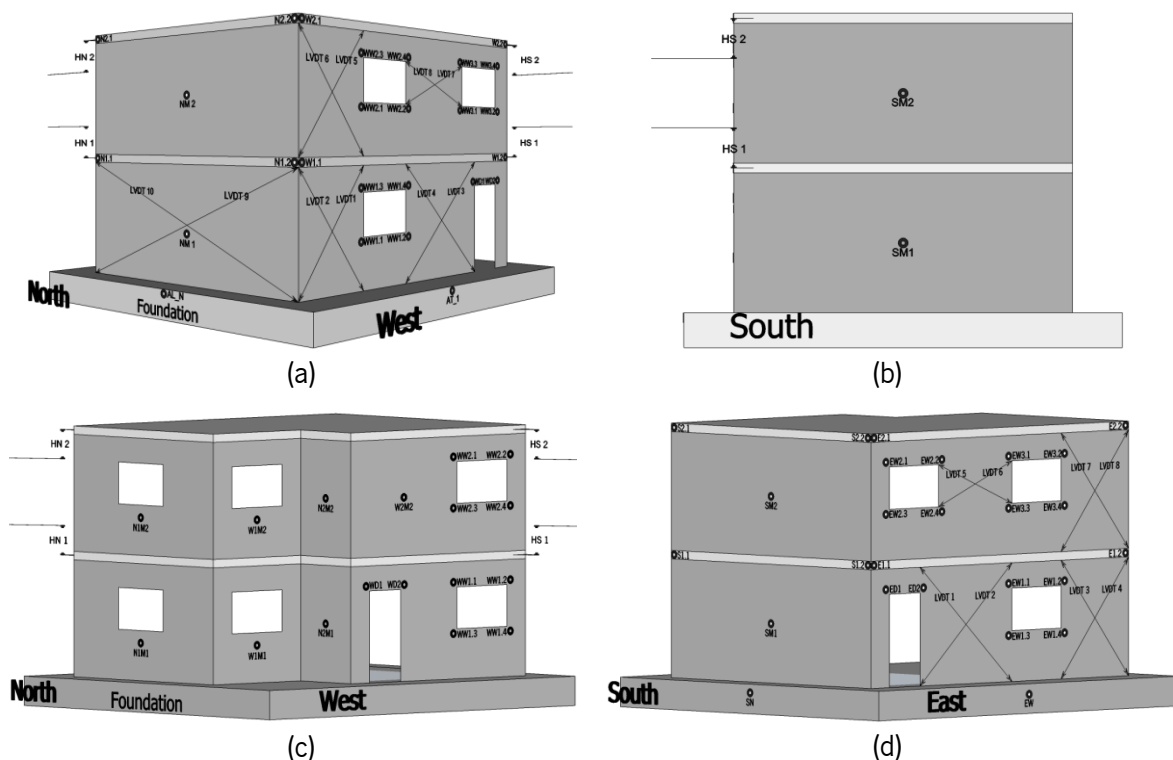


Figure 2.21 – Masonry buildings instrumentation for shaking table tests: (a, b) symmetric buildings and (c, d) asymmetric buildings

The designations HN, HS indicate Hamamatsu sensors in North and South facades. For the symmetric configuration a total of 28 accelerometers, 10 LVDTs and 4 PSD units were used for each building model. On the other hand, for the asymmetric configuration 43 accelerometers, 8 LVDTs and 5 PSD units were in total implemented. As observed, the main function of the LVDTs was to measure local displacements and crack openings in the piers. Finally, it should be mentioned that all devices were calibrated before every experimental test.

2.5.4 Seismic inputs and test procedure

The ground motion produced by an earthquake can be represented by three components, namely two horizontal and one vertical. There are unidirectional, bidirectional and three-dimensional shaking tables that can reproduce only one, two or the three components respectively. As discussed previously, the shaking table at LNEC has three degrees of freedom but, in the present study, the vertical component is not considered. This decision was taken after considering: (a) the necessary careful technical control of the hydraulic actuator that controls the vertical degree of freedom together with the horizontal ones; (b) the limitation in models' weight when this component is used (see Table 2.2) and (c) due to the fact that vertical components of the ground motion seem not to significantly affect the seismic behavior of regular structures, such as masonry buildings (Tomažević 2000).

Earthquakes are a stochastic phenomenon that depends on the source mechanism and local soil conditions, meaning that they do not occur twice in the same form. Aiming at avoiding selecting a natural earthquake that could be not representative of the conditions of a given site, artificial accelerograms (one longitudinal and one transverse) were considered as the input seismic load for the shaking table. These accelerograms were derived from the proposed elastic response spectrum provided in the Eurocode 8 (2004). The elastic response spectrum of Lisbon region (design ground acceleration = $1.5 \text{ m/s}^2 = 0.15g$) was adopted, considering type 1 seismic action, ground type A and 5% damping. For its implementation on the masonry building models, Cauchy similitude law (Table 2.1) was followed and the artificial accelerograms were compressed in time by a factor of 2 and the acceleration was multiplied by the scale factor 2 as well. The standard response spectrum and the response spectrum obtained from the compressed artificial accelerograms are shown in Figure 2.22a. From the previous task, two uncorrelated accelerograms with a total duration of about 15seg, one for each horizontal orthogonal direction of the models, was generated. The generation of the accelerograms was made by using the software LNEC-SPA (2007). A frequency range of 200Hz was considered and a Fourier filter between 0.7Hz and 40Hz was adopted. This filter is adopted in order to remove the displacement of a rigid body (low frequencies) and the noise (high frequencies) from the generated signal. It is observed that very good fitting of the generated response spectrum to the scaled one was obtained for each direction, see Figure 2.22b and c. The shaking table motion is controlled by displacements i.e. inputs are introduced to the actuators in form of displacement time histories. Then, the artificial accelerograms were processed by double integration in order to be possible to give to the table's system the corresponding displacements. The acceleration, velocity and displacement time histories of the final designed inputs are presented in Figure 2.22d and e.

The previous input was taken as the reference input for all the models. However, due to the cost involved on the project and the maximum desired information that is possible to be obtained from this type of test, this was not the only input introduced to the models. Instead, the seismic action was applied to the buildings in a phased procedure, with a sequence of incremental amplitude levels from the reference input. This procedure of load application, which is commonly described in literature, enables, among others, to follow the damage and deformation patterns for a sequence of increasing seismic action. Nevertheless, it is accepted that the nonlinear behavior can be influenced by the phased action and that damage accumulates during the tests. Table 2.6 summarizes the test sequence procedure for the masonry buildings, corresponding to distinct percentages of the reference seismic input. Severe damage of the models or limits of the shaking table in terms of actuators displacement capacity were the parameters for defining the last test run.

The last input test in all the buildings was repeated. However, in some of them due to the need of protecting the testing equipment, most of the instrumentation was removed anticipating a severe failure. Hence, data from those tests were not recorded. Further discussion will be done in next chapters.

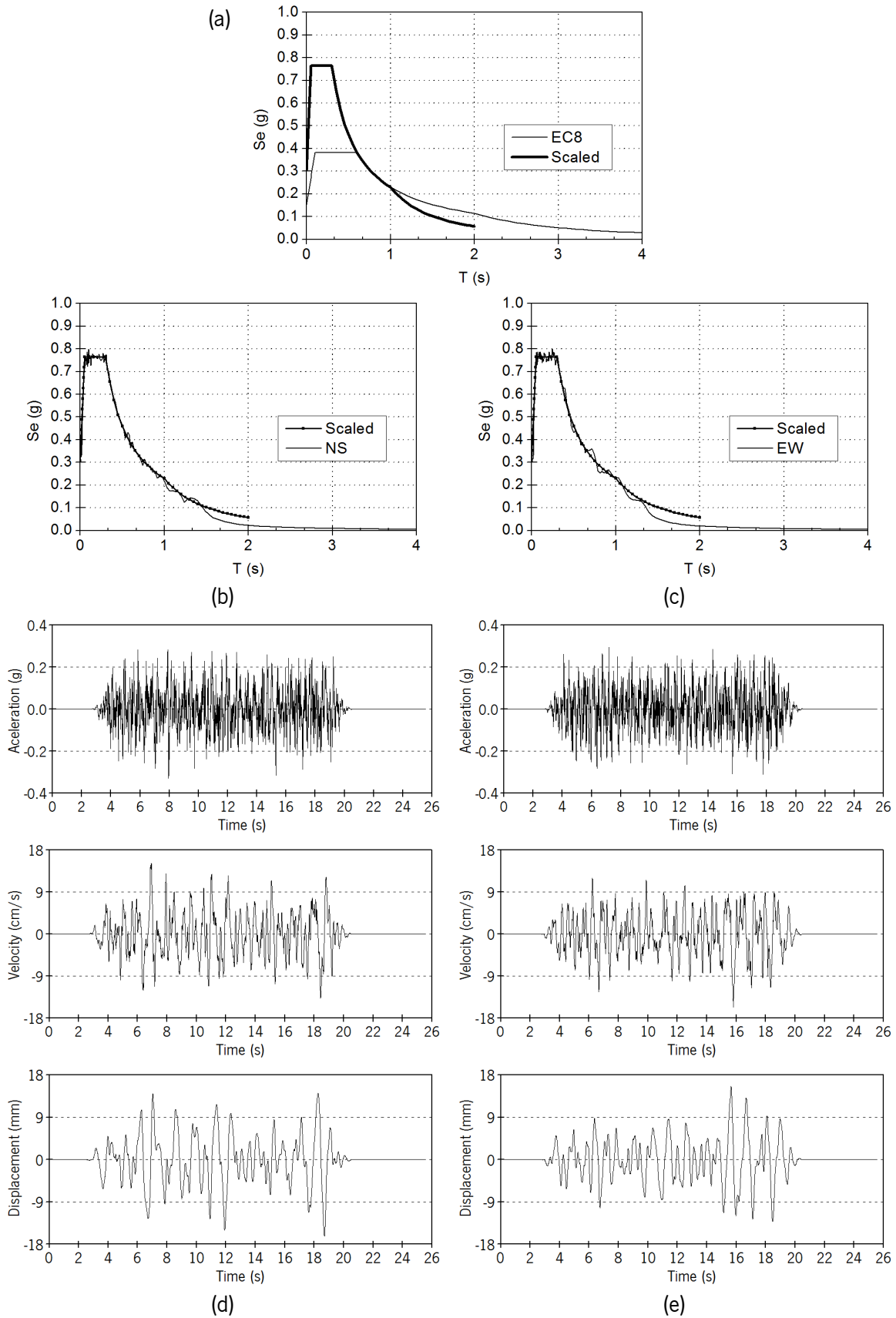


Figure 2.22 - Designed seismic inputs: (a) standard and scaled elastic response spectrum; (b) artificial spectrum for the North-South direction (NS); (c) artificial spectrum for the East-West direction (EW); (d) artificial time histories NS direction and (e) artificial time histories for EW direction

Table 2.6 – Seismic input sequence

% from reference input introduced to the shaking table	Symmetric Reinforced Masonry Building	Symmetric Unreinforced Masonry Building	Asymmetric Reinforced Masonry Building	Asymmetric Unreinforced Masonry Building
25%				☒
50%	☒	☒	☒	☒
75%	☒		☒	☒
(reference input) 100%	☒	☒	☒	☒
150%	☒	☒	☒	☒☒
200%	☒	☒	☒	
250%	☒	☒☒	☒	
300%	☒		☒☒	
400%	☒☒			

The dynamic characterization was performed before and after each seismic input test imposed to the buildings, obtaining their dynamic properties. The solution of the eigenvalue problem, i.e. yielding eigenvalues (natural frequencies), eigenvectors (mode shapes) and damping, gives an intuitive overview and a considerable insight into the dynamic features of the structure. Furthermore, relations between damage and stiffness degradation can help in the future formulation of design guidelines.

On the shaking table, the buildings were subjected to low level forced vibration tests, by means of uniform white noise signals in the two orthogonal directions. These signals, similarly to the inputs, were generated but unlike the inputs were directly designed to accomplish the scale law. Then, no scale modification was needed. Their low amplitude intends to avoid any damage on the experimental buildings. Additionally, the signals were processed with a low pass filter of 125Hz and imposed to the models with a sample frequency of 250Hz for about 2 minutes. The final inputs are presented in Figure 2.23. It can be observed that the maximum amplitude of the signal applied in North-South direction is, approximately, the double of the maximum amplitude of the signal applied in the East-West direction. This is related to the fact that the buildings are much stiffer in the North-South direction.

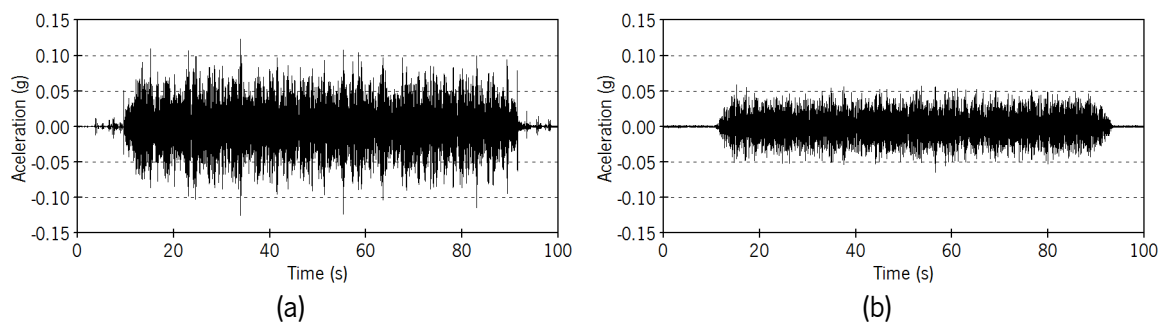


Figure 2.23 – Inputs (white noise) for dynamic identification: (a) North-South direction and (b) East-West direction

At each stage of the shaking table procedures, detailed visual inspection was performed. Cracks were labeled by using ink markers with different colors according with the input test, making easier the identification of the damage evolution. Lastly, a photographic record of this evolution for each wall was carried out.

2.6 Experimental characterization of materials

In addition to the experimental tests carried out on the masonry buildings models, mechanical evaluation of masonry components was also made. This study aims to obtain further information of the materials for numerical simulation. The European standards for design and construction, particularly the Eurocode 2 (2004), Eurocode 6 (2005) and Eurocode 8 (2004) request for minimum criteria in materials to be used in seismic zones for the construction of buildings. Therefore, this characterization is, as well, a validation of the quality and capacity of the materials to be used in the future construction of concrete block masonry buildings.

2.6.1 Concrete and steel bars

It was not made specific tests on the concrete and its steel reinforcement bars. As mentioned before, the concrete for the casting of foundations and slabs was a ready-mix product. However, the manufacturer was a certified company that gives a certified guaranty of the quality and qualities of the final product. For its preparation, design recommendations were given to the manufacturer. The concrete used in the construction of the slabs and foundation was according to Eurocode 2 (2004) a concrete of class C30/37 XC2(P) CL0.40 $D_{max}=12.5\text{mm}$ S2. This type of concrete has a characteristic compressive cylinder strength at 28 days of $f_{ck} = 30\text{MPa}$ and in cubes of $f_{ck,cube} = 37\text{MPa}$ with modulus of elasticity $E = 33\text{GPa}$. The XC2 refers to the exposure class related to the environment conditions. In this case, XC2 is related to the corrosion induced by carbonation in wet or rarely dry conditions and P corresponds to the country in which it was manufactured, in this case Portugal. CL refers to the contents of chlorides, which was 0.4. The maximum aggregate size was 12.5mm and the concrete slump test gives a consistency S2 (50mm – 90mm slump). For its manufacture, a cement type CEM II/A-L according with the EN 1015-3 (2004) was used. This is a Portland-limestone composite cement with compressive strength at 28 days higher than 42.5MPa. Finally, additions type II were used: pozzolanic or latent hydraulic additions. For example, materials like fly ash (fa) and ground granulated blastfurnace slag (ggbs). The reinforcing steel was provided by a company. It corresponds to a cold-formed welded and seamless carbon steel structural type A500 in form of ribs bars. It has characteristic yield strength of $f_{yk} = 500\text{MPa}$ and a density of approximately 7850 kg/m³.

2.6.2 Truss type reinforcement

The truss type reinforcement for masonry was bought already welded and provided by Bekaert®. The manufacturer reference is a Murfor RND_Z. The company meets quality certification as the

ISO9001. This reinforcement is a prefabricated wire especially designed for masonry. It consists of two longitudinal wires which are welded to a continuous zig-zag cross wire to form a lattice truss configuration. The cross wire is welded to the sides of the longitudinal wires so that the overall thickness does not exceed the diameter of the longitudinal wires. As the truss was manufactured with a reduced length of the diagonal bars, the welding was manual. This can be a weak point as mentioned by Haach (2009). The steel used is a high strength steel. The characteristic tensile strength is 500MPa. The shear resistance of each weld connecting the cross wire to the longitudinal wires is at least 2.5kN. The RND reference is related to the shape of the truss reinforcement. In this case, round wire for use with masonry with nominal 10mm thick mortar joints. The Z refers to its standard finishing. It means hot dipped galvanized wire with a zinc coating of at least 70g/m² designed for masonry exposed to a dry environment. The diameter of the longitudinal wires is 4mm and 3.75mm for the diagonal one. Its triangular shape makes it inflexible to forces in their horizontal plane, like flexion caused by wind or earthquakes. Finally, it has been demonstrated that its unique shape combined with its material properties increase the tensile strength of masonry. Detailed information about this truss type reinforcement can be found in [www.bekaert.com \(/construction/masonry_reinforcement/ Murfor\)](http://www.bekaert.com(/construction/masonry_reinforcement/Murfor)).

2.6.3 Mortar

Mortar is responsible for the connection between masonry blocks, the stress uniform distribution, correction of irregularities of blocks and accommodation of deformations associated to thermal expansions and shrinkage. In addition, mortar plays an important role in the crack initiation and progress. Then, mortar as one of the masonry's components plays an important role in its final behavior. During the construction of the masonry buildings, the first (and frequently) test performed was its consistency. This test is a control procedure during the construction process, since it presents a direct relation with the workability of mortar. The determination of the consistence of the fresh mortar was made by using the method of the flow table, following the European standard (EN 1015-3 2004). The average value obtained was 180mm with a coefficient of variation (CV) of 0.55%.

Additionally to the flow table, during the construction several samples of masonry were taken in order to evaluate its mechanical behavior. This evaluation was made by means of the determination of the flexural and compressive strength of the hardened mortar. Samples consist in rectangular prisms specimens of 40mm x 40mm x 160mm. They were made and tested according with EN 1052-1 (1999). From the results of more than 60 samples for the flexural test and more than 120 for the compressive test, it was obtained the average results that are given in Table 2.7.

Table 2.7 – Mechanical properties of mortar

	Flexural strength	Compressive strength
Average (MPa)	2.7	11.71
CV (%)	10	5

The previous results satisfied the requirements given by the Eurocode 8 (2004) regarding mortar for masonry structures to be used in seismic prone areas, which suggest minimum values in compression of 5MPa for unreinforced masonry and 10MPa for reinforced masonry.

2.6.4 Concrete block units

The manufacturer of the concrete block units is a certified company, specialized in the design and construction of concrete blocks for masonry structures, with more than 30 years of experience in the market. Even the block unit is a new solution, the company performs experimental tests following actual norms implemented in the validation and mechanical evaluation of commercial units. Furthermore, previous investigations regarding the individual components of the constructive system, including the concrete block units, were performed by Haach (2009). Uniaxial compressive test in the directions normal and parallel to the bed joints were carried out. As any concrete material, in the concrete block units a curing period of 28 days was taken in order to get its maximum resistance, even if the last one will also depend of the proportion's mixture of raw materials. For the present project, it was intending to use masonry units with sufficient robustness in order to avoid local brittle failure. Table 2.8 summarizes the average values of the mechanical properties of the concrete blocks. All mechanical properties were evaluated in relation to gross area of the specimens. On the table, f_t is tensile strength of the units, $f_{c\perp}$ is the mean compressive strength normal to the bed joints, E_{\perp} is the modulus of elasticity of the units normal to the bed joints and $f_{c\parallel}$ is the mean compressive strength of the units parallel to the bed joints.

Table 2.8 – Mechanical properties of block and half block units (adapted from manufacturer and Haach (2009))

	f_t (MPa)	$f_{c\perp}$ (MPa)	E_{\perp} (GPa)	$f_{c\parallel}$ (MPa)
Block unit	3.19	12.13	9.57	7.88
Half block unit	3.19	10.33	9.44	7.20

According to Eurocode 8 (2004), units used to build masonry structures in seismic areas should have a normalized compressive strength normal to bed joints not lower than 5MPa and a normalized compressive strength parallel to bed joints not lower than 2MPa. Then, the concrete block units used satisfy by far the minimum requirements of European standards.

2.6.5 Mechanical characterization of masonry

Destructive tests were carried out on masonry samples in order to characterize the masonry as a composite material. The characterization consists in the evaluation of the direct uniaxial compression strength and tensile and shear strength. Previously to the uniaxial compression tests, the specimens were submitted to non-destructive tests for the identification of modulus of elasticity. Three samples of unreinforced masonry (UM) and three samples of reinforced masonry (RM) were

built for each test. Specimens were built with 3 blocks of width and 6 courses height with 1cm-joints aiming at achieving as much as possible square geometry samples. Final dimensions of each sample are 60cm X 65cm. They were constructed with the same materials, by the same workers, at the same time, location and environment conditions of buildings construction.

In addition to the characterization on constructed samples, the masonry was characterized through small wallets removed from the damaged buildings tested on the shaking table. The wallets were removed from undamaged parts by using a circular saw. In most cases, their dimensions do not follow standard requirements for the elaboration of the tests. Nevertheless, the wallets were adjusted as much square as possible and tested. Their results have given an insight of the final mechanical properties from the buildings tested.

All the experimental campaign for the materials characterization was performed at the structural laboratory from the University of Minho (LEST). It was found a specific mass for unreinforced masonry of 1200Kg/m³ and a specific mass for reinforced masonry of 1300Kg/m³.

2.6.5.1 Uniaxial compression

The geometry of the specimen tested under uniaxial compression is shown in Figure 2.24a, b, including the steel arrangement used for reinforced specimens, which is similar to the typical distribution used in reinforced masonry buildings. The determination of the compressive strength of masonry was made by using the standard EN 1052-1 (1999). For this, a steel frame of 600kN load capacity to which a servo-actuator of 550kN is connected was used. All the samples were tested until failure or heavy damage and carried out under displacement control by means of a vertical LVDT connected to the actuator at a rate of 10µm/s. For the tests, all samples were placed between the strong floor of the laboratory facilities and the actuator. Besides, aiming at distributing the vertical load in the specimens, a steel beam was used at the top. Furthermore, a thin compensation layer of gypsum plaster was used to ensure the adequate alignment of the load and avoid possible in-plane rotation and thus avoid flexural effects, see Figure 2.24c. The horizontal and vertical deformations of the specimens were measured by 6 LVDTs, 4 for vertical displacements and 2 for horizontal displacements, respectively. The horizontal LVDTs were located between two units in order to measure head joints openings, they were located in different course position aiming at obtaining opening measures at different height of the samples.

The modulus of elasticity and compressive strength of masonry was always carried out in the perpendicular direction to the bed joints. The compressive load was applied up to 30% of the maximum load expected, and then it was kept constant for about 2 minutes to finally be unloaded. This loading – unloading sequence was applied for 3 times. With these results, the elastic modulus (E) was calculated through a linear regression of the data by using Equation 2.3. After this sequence, the specimens were loaded uniformly in compression until failure. From the last test, the evaluation of the compressive strength (f_c) of masonry was obtained through Equation 2.4. In both equations (A) is the loaded gross cross-section and (F_{max}) is the maximum load achieved, ε is the mean strain (from the 4 vertical LVDTs at each specimen) at one third of the maximum strength achieved.

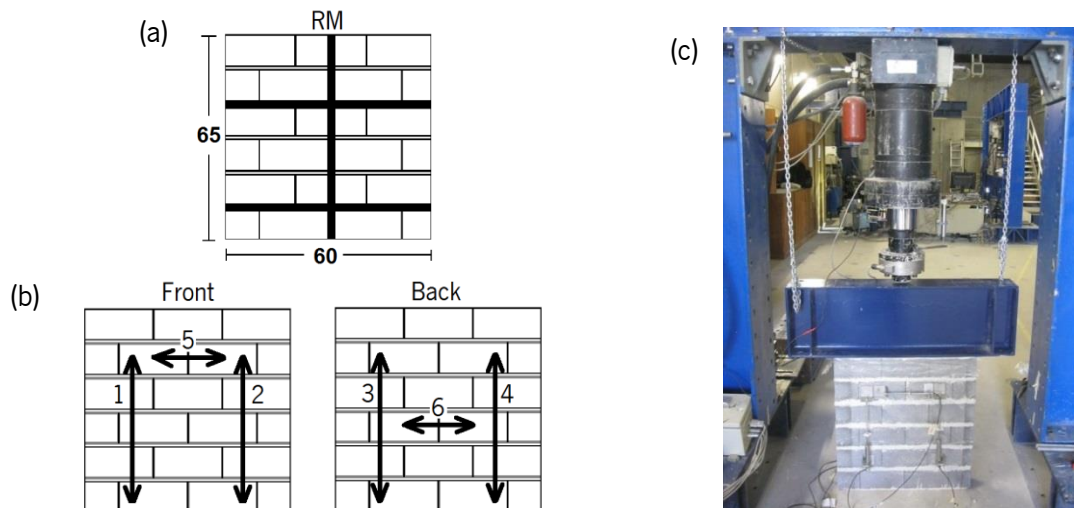


Figure 2.24 – Masonry specimens: (a) steel distribution in RM samples. Distances are in cm, (b) instrumentation distribution. Numbers refer to LVDTs and (c) final setup at laboratory

$$E_i = \frac{F_{i,max}}{3 \times \varepsilon_i \times A_i} \quad 2.3$$

$$f_c = \frac{F_{max}}{A} \quad 2.4$$

Table 2.9 summarizes the results obtained from uniaxial compression tests. The results from UM and RM were statistically grouped i.e. final results correspond to 6 masonry specimens (3 reinforced and 3 unreinforced). This was made after verified that the truss type steel reinforcement does not have influence in neither the elastic properties nor the maximum resistance to compression. The coefficient of variation (CV) gives an idea about the scatter in these results.

Table 2.9 – Mechanical properties of masonry from direct compression tests

	E_{\perp}	$f_{c\perp}$	$f_{c\perp}^*$
Average	5.3 (GPa)	5.95 (MPa)	7.60 (MPa)
CV (%)	24	4.8	15.8

* Samples from experimental buildings

Masonry presented a brittle behavior in most specimens. Figure 2.25 presents the damage patterns on UM specimens, on RM and specimens taken from the experimental buildings. In all of them, it was found a distribution of predominantly vertical cracks all over the masonry. At maximum strength the specimens open laterally (number 1 in Figure 2.25b), and progress until the complete loss resistance and further failure (number 3). It was common to observe how the internal cells of the blocks remained standing as seen in Figure 2.25d. The main difference between UM and RM specimens was the distribution of the initial cracks and the improvement in the final connection between the remained internal cells.

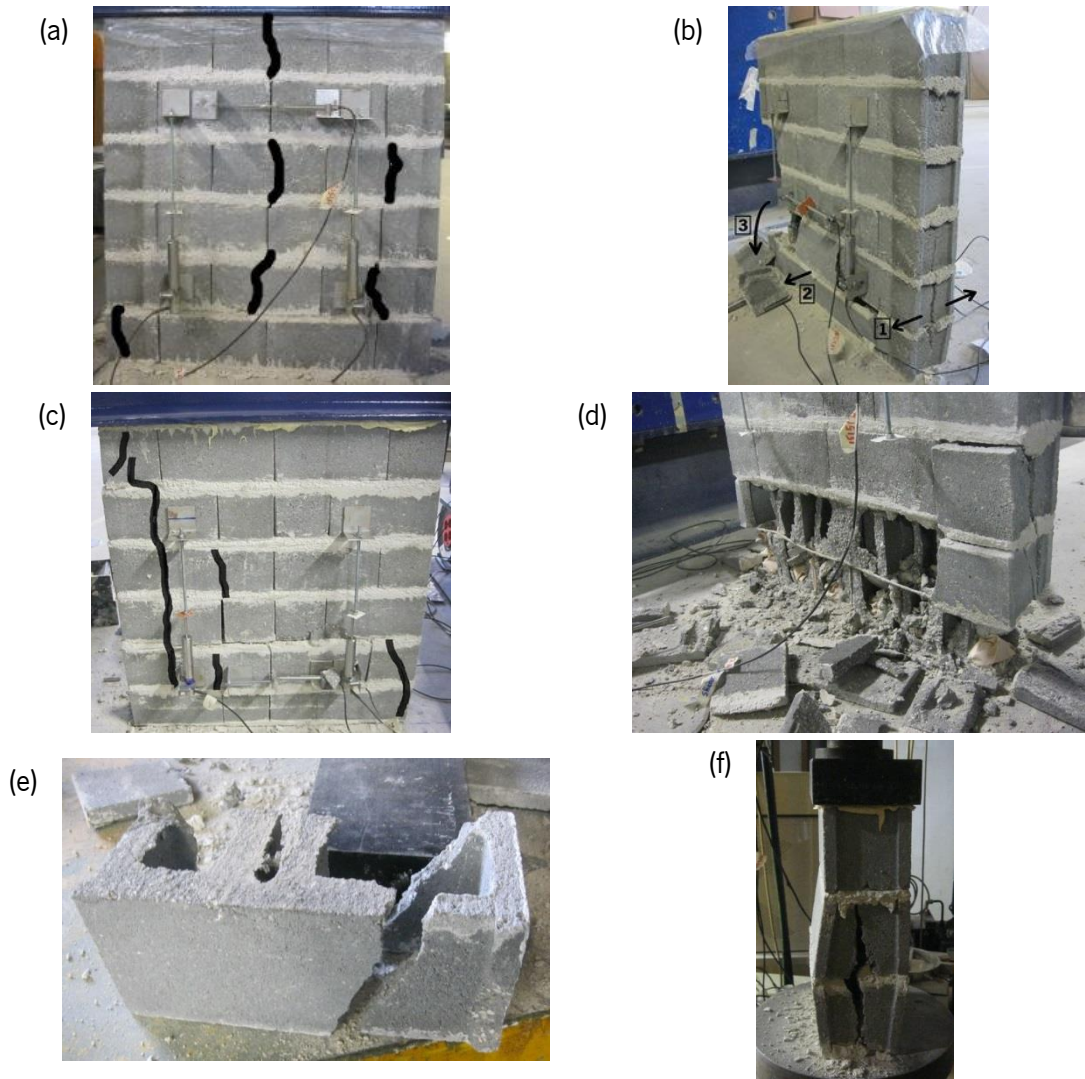


Figure 2.25 – Cracking pattern during direct compression tests: (a, b) UM specimens, (c, d) RM specimens and (e, f) specimens taken from experimental buildings

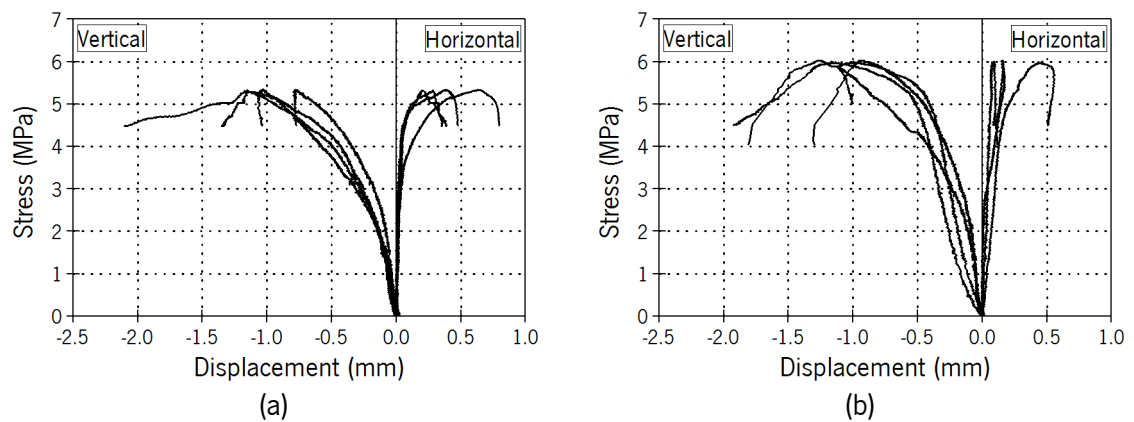


Figure 2.26 – Vertical and horizontal stress-displacement diagram from direct compression: (a) UM specimens and (b) RM specimens

The vertical and horizontal deformation from the specimens is presented in Figure 2.26. It can be observed a small increase on the maximum strength in case of RM specimens, when compared to UM specimens. However, no major differences were found in the displacements. The higher values of the reinforced masonry can be attributed to the effect of the steel in absorbing the tensile stresses of the masonry units, resulting from the triaxial stress state of the mortar joints.

2.6.5.2 Diagonal compression test

Diagonal compression tests in masonry samples were performed in laboratory following the standard ASTM E 519-02 (2002). These tests were carried out by using the same testing frame, actuator and measurement equipment used for uniaxial compression tests. Specimens were located between the strong floor of the laboratory and the actuator by using loading shoes of cold-rolled steel. The shoes help the samples to keep their diagonal position and to transmit the force from the actuator to the specimens. Furthermore, gypsum plaster was used between loading shoes and specimens to improve the distribution of stresses and load application, see Figure 2.27b. All the samples were tested until failure and carried out under displacement control by means of a vertical LVDT connected to the actuator at a rate of $2\mu\text{m/s}$. 2 LVDTs were used to measure the shortening of the vertical diagonal (one for face) and 2 LVDTs were used for the measuring the variation on the length of the horizontal diagonal. In addition, 2 horizontal LVDTs were located at the upper and lower positions to evaluate opening evolution. The instrumentation and setup for this test is presented in Figure 2.27.

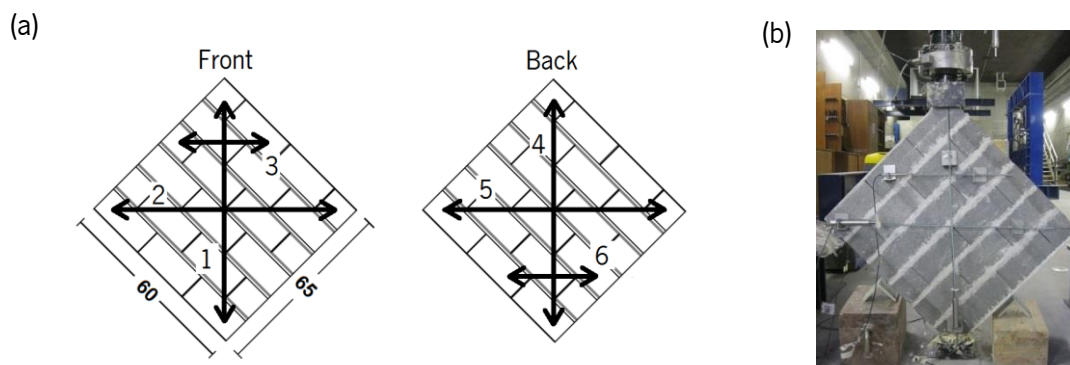


Figure 2.27 – Masonry specimen for diagonal tests: (a) instrumentation distribution. Distances are in cm. Numbers refers to LVDTs and (b) final test setup

This test procedure allows obtaining the shear and tensile strength of the specimens. The tensile strength is obtained by assuming that the specimen collapsed when the principal stress, at the center of the specimens achieves its maximum value. Its calculation is made by using Equation 2.5.

$$f_s = f_t = \frac{0.707P}{\left(\frac{w+h}{2}\right)t} \quad 2.5$$

Where f_s is the shear strength of the masonry, f_t is the tensile strength of the masonry, P is the applied force, w is the width of the specimen, h is the height of the specimen and t is the thickness of the specimen. In addition, the shear strain and shear modulus were calculated by using Equation 2.6 and Equation 2.7, respectively.

$$\gamma = \frac{\Delta V + \Delta H}{l_0} \quad 2.6$$

$$G = \frac{f_s}{\gamma} \quad 2.7$$

Where γ is the shear strain, ΔV is the vertical shortening, ΔH is the horizontal extension and l_0 is the vertical gage length and G is the shear modulus.

Table 2.10 presents the results obtained from diagonal tests on UM and RM specimens. In addition, results of samples taken from the experimental buildings are also given.

Table 2.10 – Mechanical properties of masonry from diagonal tests

	f_t (MPa)	CV (%)	G (GPa)	CV (%)
UM	0.12	7.9	1.76	8.1
RM	0.39	14	1.60	21.3
RM (From exp buildings – square geometry)	0.42	2.6		
RM (From exp buildings – no square geometry)	0.72	5.8		

It is observed that UM and RM specimens present distinct tensile strength. The presence of steel reinforcement together with mortar at its head joints seems to influence considerably this parameter. The tensile strength is 300% higher for RM specimens and in case of the samples taken from the buildings the differences in the tensile strength are 350% higher than in case of UM specimens. In general, tensile strength results presented satisfactory distribution, with a maximum CV of 14%. In agreement to what was expected for a linear property the shear modulus presents narrow differences between UM and RM samples. In this parameter, with a CV of 21.3% for RM specimens, it was found in some specimens similar values to the UM samples.

The presence of steel has also an important influence in the cracking pattern observed during tests. As observed in Figure 2.28a and b, UM samples presented a typical diagonal opening along the unit mortar interfaces in accordance with the load applied. All specimens failed through their joints and no cracks or damage was observed in block units. Cracks occur progressively starting with fissures in the top or bottom part of the specimens at their bed joints. This behavior continues spreading through the samples. Then, when these cracks (in the bed joints) made connection with the head joints (with no mortar) failure of the specimen occurred.

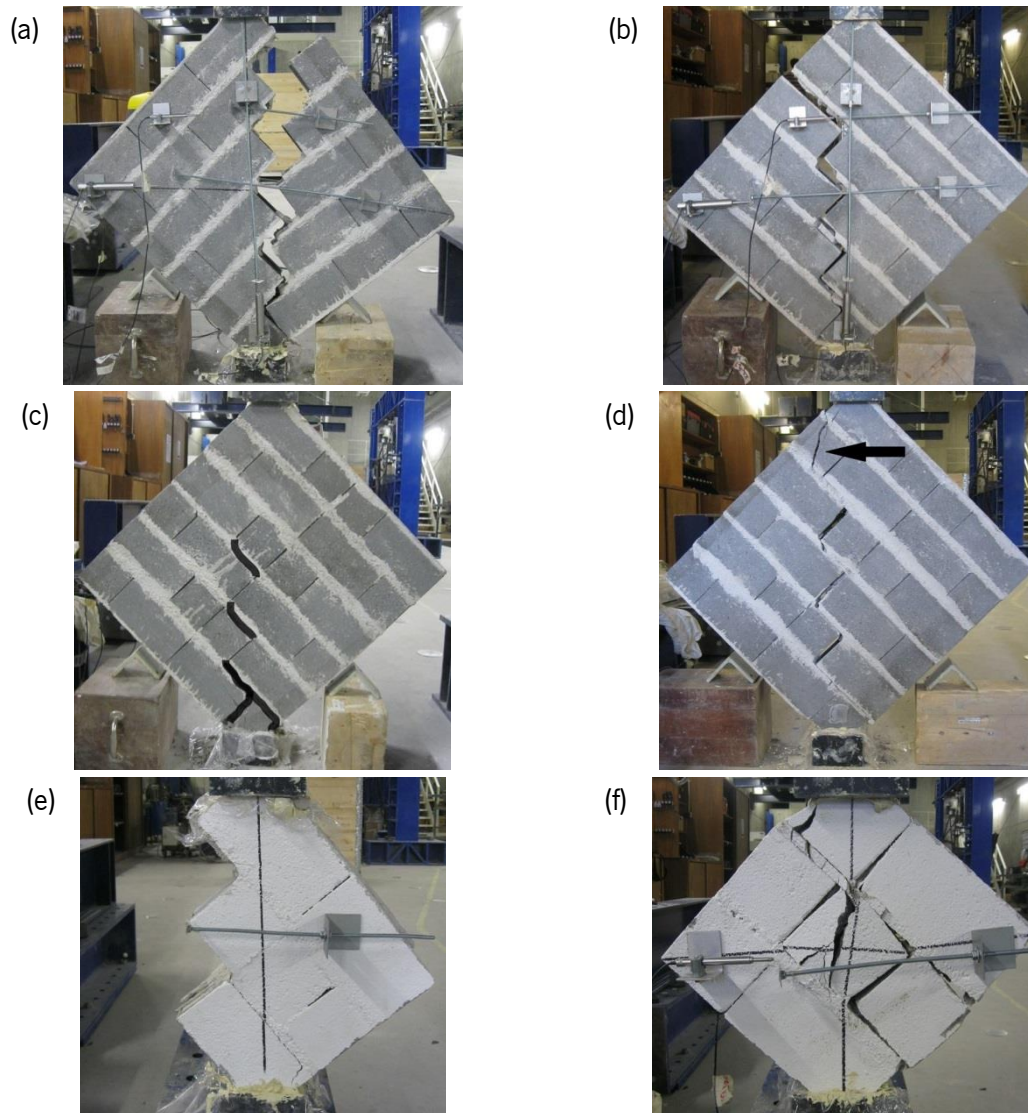


Figure 2.28 - Cracking pattern during diagonal compression tests: (a, b) UM specimens, (c, d) RM specimens and (e, f) specimens taken from the buildings

In case of reinforced specimens, the cracks tend to follow the diagonal direction of the load, but instead of failure at joints, it was observed failure at units, mainly at the ones in contact with the loading shoes. Similar behavior was observed in the samples taken from the buildings (Figure 2.28e and f), in which cracks also follow a diagonal path through loading projection and units' failure.

The strain-stress relations obtained from the diagonal tests, as well as the horizontal displacement registered at the top-bottom part of the specimens are presented in Figure 2.29. It is observed that the increase in shear strength is attributed to the presence of steel reinforcement at vertical joints. The influence of the filling of vertical joints is also an important factor contributing for the increase on the shear strength as pointed out by Haach (2009). The higher strength is also associated to a much higher deformation in case of RM specimens, see Figure 2.29b. These results are in accordance to the results obtained by Vasconcelos et al. (2012). Due to the size limitation of the masonry samples taken from the buildings, their vertical strain measurements were not possible. Thus, shear strain was not evaluated from those specimens.

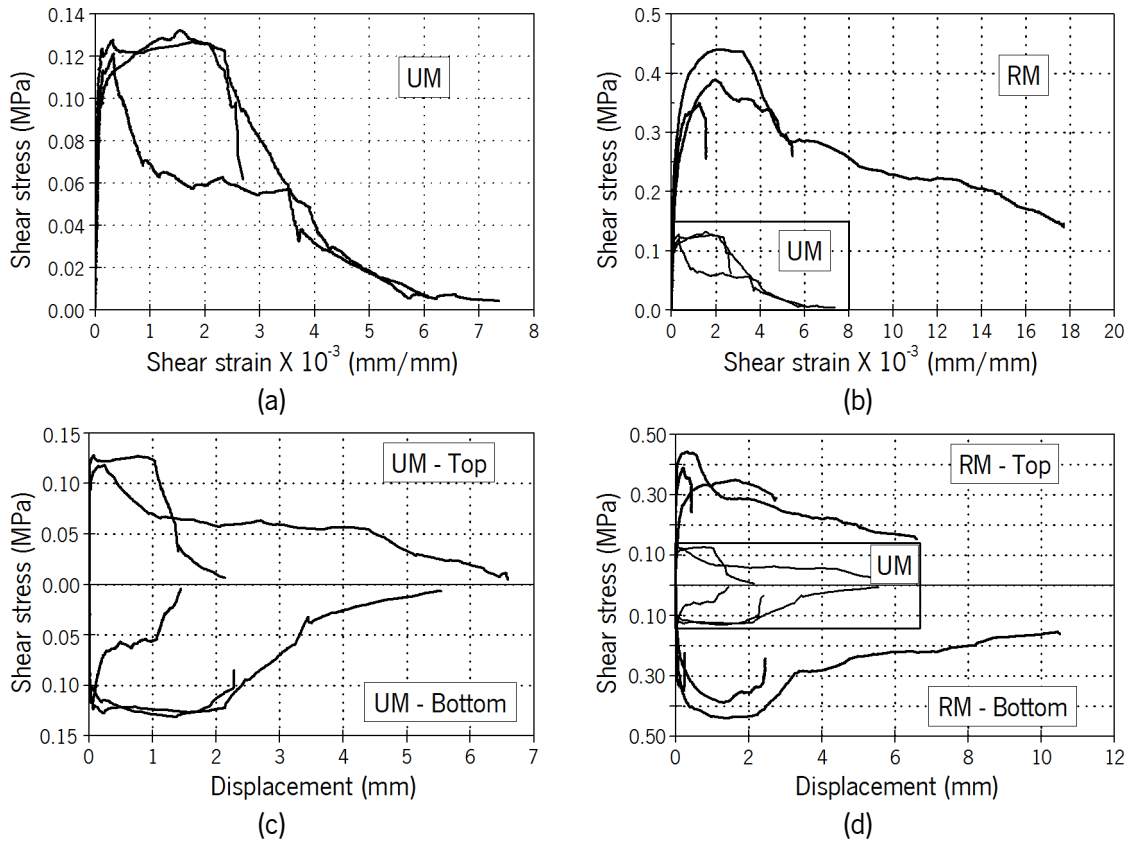


Figure 2.29 – Results from diagonal tests: (a, b) strain-stress curves for UM and RM specimens and (c, d) top and bottom horizontal opening for UM and RM specimens

2.7 Conclusions

The preparation of the experimental program constitutes one of the most critical parts of the mechanical evaluation of the constructive system. As a composite material, masonry needs to be studied and understood as an assemblage.

In this chapter the constructive masonry system to be used (through its individual components) was presented and described in detail, as well as the preparation of the experimental studies that were carried out on shaking table for the evaluation of the seismic performance of the masonry buildings. Four masonry buildings were designed intending to study not only the influence in geometry configuration but also the effects of steel reinforcement on seismic performance.

Detailed description of prototypes and design of buildings were presented. Construction of the experimental buildings and shaking table testing preparation and execution were also discussed. The experimental campaign was reviewed in detail regarding setup, equipment, input signals and test procedures. With this respect, special attention should be taken with the input signals for the shaking table tests, as they must be representative of the real seismic loading.

Finally, it was presented a detailed characterization of the mechanical behavior of masonry through direct compression and diagonal tests. It was seen that the vertical reinforcement influences the mechanical strength of masonry in both uniaxial and diagonal compression, increasing the

compressive and shear strength. However, the increase on the strength is particularly relevant in shear. At the same time, the shear deformation is considerably higher in case of reinforced masonry, which appears to indicate that reinforced masonry buildings should behave in a different manner when subjected to seismic loading, where shear resistance mechanism should control their seismic response.

Chapter 3

Experimental investigation of symmetric masonry buildings

Abstract

The present chapter deals with the experimental validation of a new structural solution for concrete block masonry buildings. Dynamic tests of two identical two-story concrete block masonry buildings were performed on a shaking table in reduced scale 1:2, with focus on the global behavior. The buildings are symmetric in both plan and in elevation. Both models were tested by imposing uncorrelated artificial accelerograms, compatible with the elastic response spectrum defined by the Eurocode 8 (2004), in the two orthogonal horizontal components. The first model was tested in reinforced conditions (RM) following the same code, while the second building was tested as an unreinforced solution (UM). The post-processing performed on the outputs signals from the shaking table is discussed. Furthermore, the identification of the dynamic properties using modal analysis (based on input-output techniques) as well as the seismic evaluation of both buildings is presented.

During the experimental tests, various input motions with incremental amplitude were implemented. The damage identification through stiffness degradation is studied. Thus, the experimental analysis encompasses parameters as the cracking patterns with consequence failure mechanisms. Accelerations, together with the in-plane and out-of-plane behavior in terms of displacements and interstory drifts are discussed. Findings related their structural capacity with the global dynamic behavior and comparisons between the results of the two buildings are also presented.

3.1 Introduction

The study of any constructive system must be completed with the study of its mechanical behavior when implemented in whole structures, in which interactions between the distinct structural elements play a central role in the global behavior of the structure. The Eurocode 6 (2005) makes the distinction between the masonry considered as a composite material resulting from the assemblage of units and mortar and the structural masonry elements. In case of structural elements (walls, beams and spandrels), the mechanical properties will depend not only of the intrinsic mechanical properties of it but also of the geometry of the element and the interaction of adjacent parts.

The seismic behavior of masonry structures has been systematically studied since 1980's (Abrams 1986; Tomažević 1999; Tomazevic and Klemenc 1997). The methods and experimental procedures implemented have been validated through the time. Nowadays, the experimental methods and analysis adopted in the evaluation of the seismic behavior of masonry buildings are well documented and scientifically accepted. In this scope, the earthquake resistance response of several construction systems composed of different materials has been evaluated experimentally by shaking table tests (Candeias et al. 2004; Gardone et al. 2004; Krstevska et al. 2010; Rezaifar et al. 2008). Nowadays, this mechanical device allows the most accurate simulation of seismic events, becoming the best tool for the earthquake resistance evaluation of structures. Regarding masonry buildings, the shaking table has been used in different types of constructive systems, with satisfactory results. Bothara et al. (2010) studied the seismic performance of a symmetric two story brick masonry house with timber floor and roof. The structure was subjected to incremental input motions on a shaking table. The in-plane and out-of-plane behavior were analyzed and related with the failure mechanisms, being the gable walls recognized as the most vulnerable parts. In addition, the influence of diaphragms and of the bond pattern to the global behavior of the masonry buildings was also analyzed. Benedetti et al. (2001) developed an enlarged experimental campaign in order to evaluate the seismic response of symmetric masonry buildings. For this, 12 stone and brick masonry buildings were subjected to 58 shaking table tests from which performance indexes were obtained and correlated with the damage. As important conclusion from this work, it was found that damage to spandrel beams produces more significant energy absorption than other types of damage. Concerning the use of steel reinforcement, Zonta et al. (2001) evaluated the ductility and seismic performance of symmetric plan reinforced masonry buildings in an experimental program including 33 shaking table tests for different reinforcing techniques. Behavior factors suggested as design parameters for this type of construction were also provided.

The shaking table tests were also selected in this study for the validation and analysis of seismic performance of the constructive system under study based on concrete block masonry. For this, reduced scale buildings were designed to be representative of housing buildings and further tested at the shaking table so that the global behavior could be evaluated. This is a step forward in the validation of the constructive system, as the interaction between the walls and walls and slabs is taken into consideration.

3.2 Objectives and methodology

The main aim of the present study is to develop a masonry system to be applied in new construction of residential houses that behaves adequately under moderate to high seismic intensity. As discussed in the previous chapter, the project is focused in the construction of residential buildings satisfying all the requirements from the European codes related to the no collapse and damage limitation. To accomplish this, it is mandatory to understand the global behavior of buildings (more than in individual elements) when subjected to dynamic loads, assessing its performance to earthquakes.

The experimental assessment of the seismic behavior of concrete block masonry buildings is carried out through shaking table tests. This experimental approach has been demonstrated to be adequate for different constructive systems like timber and concrete.

This chapter is focused on the analysis of the seismic response and performance assessment of residential masonry buildings with symmetric plan geometry. From the results, it is expected to get a better insight on the resistance and deformation parameters of the masonry buildings. It is the first step of the experimental validation and seems to be the best reference point for future studies regarding this new constructive masonry system.

For the experimental validation, two two-story concrete block masonry buildings were designed. One of the buildings was built with plain masonry and another one was built with the reinforcing system composed of truss type steel reinforcement, at the horizontal and vertical continuous joints. The seismic inputs were imposed to the models in two directions (longitudinal and transverse) simultaneously. It is expected that the addition of horizontal and vertical steel reinforcement help to provide higher ductility and lateral resistance to face seismic loads. Through the incremental seismic inputs, the identification of the dynamic parameters is carried out aiming at defining damage indicators that characterize the damage patterns of the buildings.

Finally, it should be mentioned that all results discussed in this chapter are related to the scaled models. Therefore, Cauchy similitude law presented in Table 2.1 should be considered in order to obtain the prototype 's values.

3.3 Validation of the seismic input - Theoretical input vs. real input

3.3.1 Analysis of the seismic inputs

The shaking table tests were performed by incremental seismic inputs. Table 3.1 summarizes the test sequence with the actual Peak Ground Acceleration (PGA) measured at the base of the two models, corresponding to distinct percentages of the reference seismic input. For each building, the results are presented in the longitudinal (NS) and transverse (EW) directions. The PGA value obtained for the 100% test, which has an average of about 0.4g for both buildings, depends on the characteristics of the physical model, given that the calibration of the seismic input was made with steel masses.

Table 3.1 - Input series and corresponding PGA

Test	Reinforced model		Unreinforced model	
	PGA NS (m/s ²)	PGA EW (m/s ²)	PGA NS (m/s ²)	PGA EW (m/s ²)
50%	2.06 (0.21g)	1.74 (0.18g)	2.62 (0.27g)	1.99 (0.20g)
75%	2.90 (0.30g)	2.82 (0.29g)	-	-
100%	3.84 (0.39g)	3.71 (0.38g)	5.01 (0.51g)	4.26 (0.43g)
150%	6.24 (0.64g)	5.53 (0.56g)	7.88 (0.80g)	6.64 (0.68g)
200%	9.80 (1.00g)	7.13 (0.73g)	10.90 (1.11g)	8.51 (0.87g)
250%	12.32 (1.26g)	8.90 (0.91g)	13.04 (1.33g)	10.42 (1.06g)
300%	13.03 (1.33g)	10.14 (1.03g)	-	-
400% 1	15.83 (1.61g)	12.71 (1.30g)	-	-
400% 2	15.49 (1.58g)	13.36 (1.36g)	-	-

With respect to the UM model, after the test run of 250%, an additional shaking table test with the same input was considered. This test was denoted by 250% 2. In this test, due to the need of protecting testing equipment, most of the instrumentation was removed anticipating a severe failure. Hence, the input-motion at the base of the model was not measured.

3.3.2 Signal processing

The local and global behavior of the buildings was analyzed quantitatively in terms of acceleration and displacements for all the seismic inputs. After all the tests were finished, the information from all the instrumentation devices was collected and organized. The analysis was carried out individually for each building and for each instrumentation device. The data was selected and organized according to the following methodology: (1) the data was separated according to the acquisition type, namely video and photo information for each building (RM and UM models); (2) the measured data was separated by type of device, namely Position-Sensitive Detectors (PSDs), accelerometers, LVDTs, video cameras and photo cameras and (3) to finally be organized and analyzed by each individual input test.

Experimental measurements are never perfect, even with sophisticated modern instruments. Two main types of measurement errors are recognized: (1) systematic errors, in which every measurement is either less than or greater than the true value by a fixed percentage or amount; (2) random errors, in which there are unpredictable variations in the measured signal from moment to moment or from measurement to measurement. This latter type of error is often called noise (Bendat and Piersol 2011). Then, one of the fundamental problems in signal analysis is distinguishing the noise from the true signal. Sometimes, both types of errors can be partly distinguished in the basis of frequency components. For example, the signal may contain mostly low-frequency components and the noise may be located in higher frequencies. The process of finding the most accurate true signal from a record is the basis of filtering a signal.

All the data acquired throughout the distinct measuring equipment was processed by using the software for signal processing LNEC-SPA (2007), which provides analysis tools for the removal of

quasi-static components and noise by means of filters, offset correction, signal crop, among others. The first signal processing was concerning the acceleration records. All the accelerometer devices take measurements in units of gravity or thousands of gravity. Signals were multiplied by scaled factors in order to obtain the same acceleration measurements in SI units and have a standard unit of comparison. The SI metric system was chosen since all the other equipment devices use this unit system as output.

The signal processing performed consisted mainly in the removal of the quasi-static components and noise by using a band pass Fourier filter between 0.6Hz and 35Hz, increasing the measurement accuracy. The quasi-static components are limited by the table itself. The process of finding the low limit for the frequency filter, and therefore removing of those components, consisted in a technique in which the displacements from the table (from high sensitive displacement devices attached to it) are compared with the displacements of the accelerometers at the base of the models (obtained from the numerical integration of the acceleration records). Indirectly, this process validates the displacements obtained from the accelerometers, reducing the mathematical error produced by the double integration. The upper limit of the filter band is based on the background noise found in the signals, in which mainly ambient noise inside and outside the laboratory is removed. As example, the laboratory is located just few kilometers away from an international airport. The noise produced by the planes' turbines during landing and takeoff procedures (planes pass over the laboratory during approximation to the airport) was sometimes registered by the sensitive accelerometer devices. This noise is not related with the buildings behavior and needs to be removed. The limitation in the band limit removes those unwanted components. Besides, the signal is less "heavy" for analysis by reducing its frequency contents. Special care was taken with the control of the sample frequency of the signals. Hence, avoiding the aliasing problem, no decimation was applied to any of them, so that a sampling frequency of 250Hz corresponding to a sampling rate of 0.004s was accepted. As final processes in the accelerometers, signal DC offset correction and boundary noise reduction, by means of cropping the extreme registered data, were carried out. After all, the total duration of each signal was confirmed and verified.

Following these processes, a detailed visual inspection in all the signal records was made in order to identify abnormal peaks or inconsistent signals, e.g. signals that do not make sense with the amplitudes and times of the experimental inputs. During this process the phase shift (or phase offset), and phase difference between signals were also revised and amended. The phase shift is validated through the initial angle of the sinusoidal function, normally at its origin. The difference in phase is typical for devices located in opposite façades, e.g. north and south, in which a positive value in one device is negative in the other in a phenomenon called anti-phase. In order to focus in quantities values and make easier the signal comparisons, those differences were corrected.

Displacements were obtained by numerical double integration of the acceleration records obtained during the seismic inputs tests. The importance of this parameter is related to the evaluation of the direct buildings' deformation. Then, aiming at obtaining as much as possible a valid and accurate analysis, all displacements were converted to millimeters (mm). The study of such detailed magnitude in 3-meter height buildings suggests a strong and reliable dynamic analysis.

For the purpose of identifying the modal parameters, a different signal processing was adopted on the accelerometers records. As discussed in 2.5.4 - Seismic inputs and test procedure, the inputs for the dynamic identification are different from the seismic tests. Therefore, its analysis encompasses a different methodology. The first step was the transformation of the signal from time (or spatial) domain to frequency domain from which frequencies and damping coefficients are obtained. This process is commonly called harmonic analysis. Some records exhibit periodic components that repeat at fixed intervals throughout the signal, like a sine wave. It is often useful to describe the amplitude and frequency of such periodic components exactly. Actually, it is possible to analyze any arbitrary set of data into periodic components, whether or not the data appear periodic. Harmonic analysis is conventionally based on the Fourier transform, which is a way of expressing a signal as a sum of sine and cosine waves. With this process it is possible to simplify the calculation of complex functions.

A primary modal analysis without any filter was carried out, aiming to identify the higher quantity of modes. However, for both buildings (RM and UM) no any clear mode was detected beyond the frequency capacity of the shaking table (40HZ). Then a low pass Fourier filter of 40Hz was applied to all the signals. Similar process of units, DC offset, phase and visual inspection to the ones aforementioned was carried out. The sampling frequency of these signals is equal to the one on the seismic tests, i.e. 250Hz (0.004s). Thus, the Nyquist frequency is equal to 125Hz, which is much higher than the upper limit frequency applied of 40Hz. As a result, no decimation was made. On the estimation of the frequency response functions, a reduction of leakage was executed by the introduction of a Hanning window with a standard frames' overlap of 2/3. On the frames, a value of 2^{10} ; i.e. 1024 samples per frame filled with a minimum number of zeroes (padding), was considered.

Concerning the Position-Sensitive Detectors (PSDs), they measure global position in centimeters. In order to have consistent units for all the analysis, they were converted to millimeters. These devices register signal information much before the input signal begins and ends much after it finish. Then, boundary signal cropping was also applied at the extremes of all the records. For a final analysis, the PSDs are plotted not against the time but its "X" values vs. its "Y" values given an idea of the actual global movements of the buildings during the seismic tests. Finally, the Linear Variable Differential Transformers (LVDTs) registered a direct signal in centimeters. They were converted to millimeters. In this signal, a DC offset correction process was necessary. Analogous to previous devices a cropping process was also performed.

As discussed, each individual signal for each device and for each seismic input was processed. In general, their scale, amplitude, frequency and phases were detailed studied, compared and corrected when needed. Unfortunately, during shaking table tests some devices fell down, were partially detached, were not working correctly or just not working at all. From those devices, no any signal could be taken or analyzed, generating some gaps on plots that are specifically reported later. These unwanted outcomes are not predictable, making certain part of any experimental research. Fortunately, those missing values did not affect substantially the analysis of the global behavior of the masonry buildings as will be seen in the following discussions. All these techniques of signal processing are necessary and mandatory for this type of experimental tests, aiming at obtained, as accurate and reliable as possible the performance of the proposed buildings to earthquakes events.

The theoretical input or target corresponds with the signals discussed in section 2.5.4. It is expected that the shaking table reproduce those signal with the maximum accuracy as possible. However, even though the shaking table possesses a sophisticated control of the oil-hydraulic actuators, the efficiency of this control was evaluated by comparing the measured accelerations and displacements at the base of the buildings (reinforced concrete beam) with the target values imposed to the shaking table, see Figure 3.1 and Figure 3.2. In the plots, the terminology AL and AT means acceleration in the longitudinal and transverse direction respectively, and similarly, DL and DT refer to longitudinal and transverse displacements. The terms RM and UM corresponds to reinforced and unreinforced masonry buildings, respectively.

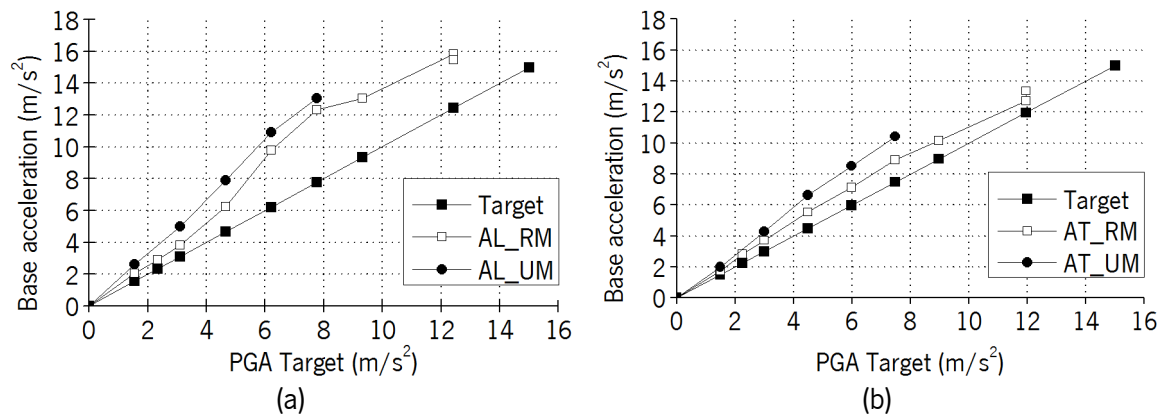


Figure 3.1 - Diagrams correlating the peak accelerations at the base of buildings and PGA targets: (a) longitudinal direction and (b) transverse direction

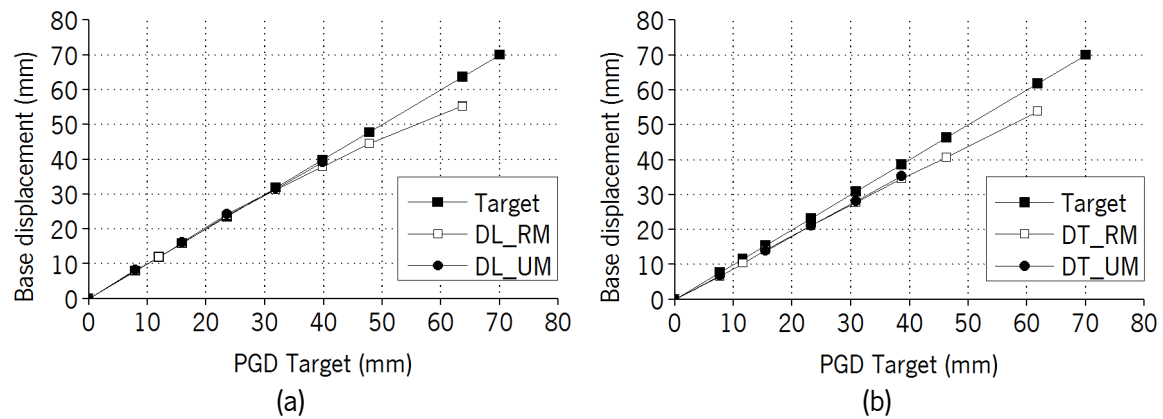


Figure 3.2 - Diagrams correlating the peak displacements at the base of buildings and PGD targets: (a) longitudinal direction and (b) transverse direction

The measurements at the base of the buildings allow assessing the actual accelerations and displacements for further analysis of the results. It is observed that the records of measured accelerations in longitudinal and transverse directions differ from the imposed accelerations. The recorded accelerations are always higher than the target ones, reaching a difference of about +60% for the longitudinal direction and about +30% for the transverse direction. On the other hand, the differences found between target and recorded displacements are lower, being the Peak Ground Displacement (PGD) on both directions smaller than the target values. For this parameter, it was

found maximum differences of about –15%. However, it should be noted that these differences were found at the last input tests suggesting an acceptable performance of the shaking table through the experimental campaign.

The differences found between the imposed and measured values of accelerations and displacements can be explained by two main reasons: (1) the calibration process of the seismic input, which is made by means of steel masses, before placing the buildings on the table. In this procedure, inert masses with a weight equal to the masonry buildings (including their foundation) are fixed over the shaking table. Then, input motions similar to the ones imposed to the buildings are imposed and calibrations of the shaking table's movements are based on the theoretical input introduced vs. actual input obtained on the table. Then, even the inert masses represent the weight of the buildings; they do not represent the real geometry of the buildings. Thus, it is expected that the inertial forces during buildings' tests caused slightly difference in the accelerations and displacements develop; (2) the distribution of the actuators on the shaking table. In the longitudinal direction, the table is controlled by only one actuator. The transverse direction is controlled by two actuators, resulting in the better control of the shaking table's movements.

The evaluation of the base ground motions of models is essential for the adequate analysis of the seismic response of the buildings. As will be discussed later in this chapter, most of the results studied from the shaking table are based on relative quantities, e.g. total acceleration at the top minus total acceleration at the base (obtaining relative accelerations). This methodology is work demanding, regarding values and process, but more reliable in terms of buildings' deformations. Therefore, the results obtained in the masonry building models will be evaluated based on the real ground motions recorded at their bases rather than on the theoretical artificial inputs imposed.

3.4 Dynamic Properties

Both buildings were transported and fixed to the shaking table. After fixation and instrumentation and before any seismic input, the identification of their dynamic properties was carried out. The identification is focused on the obtaining of natural frequencies, initial damping coefficients and fundamental mode shapes of the buildings. It is expected that the dynamic properties be related with the seismic performance of the structures.

For the identification of the modal parameters, the same instrumentation implemented for the seismic tests and described in Figure 2.21 was used. However, for this type of tests, only the accelerometers were activated for registering the data. Input-output techniques were implemented for the identification of these parameters in which the two white noises discussed in section 2.5.4 were introduced to the shaking table as inputs in the two horizontal directions. These identifications were based on the frequency response functions (FRFs), phases and coherences, estimated through traditional methods of signal analysis (Bendat and Piersol 2011). For all these analysis, the software LNEC-SPA (2007) was implemented.

Figure 3.3 shows the transfer function curves for the 28 accelerometers placed on the buildings. Due to the symmetry of the two buildings, only two essential natural frequencies were identified in the frequency range analyzed.

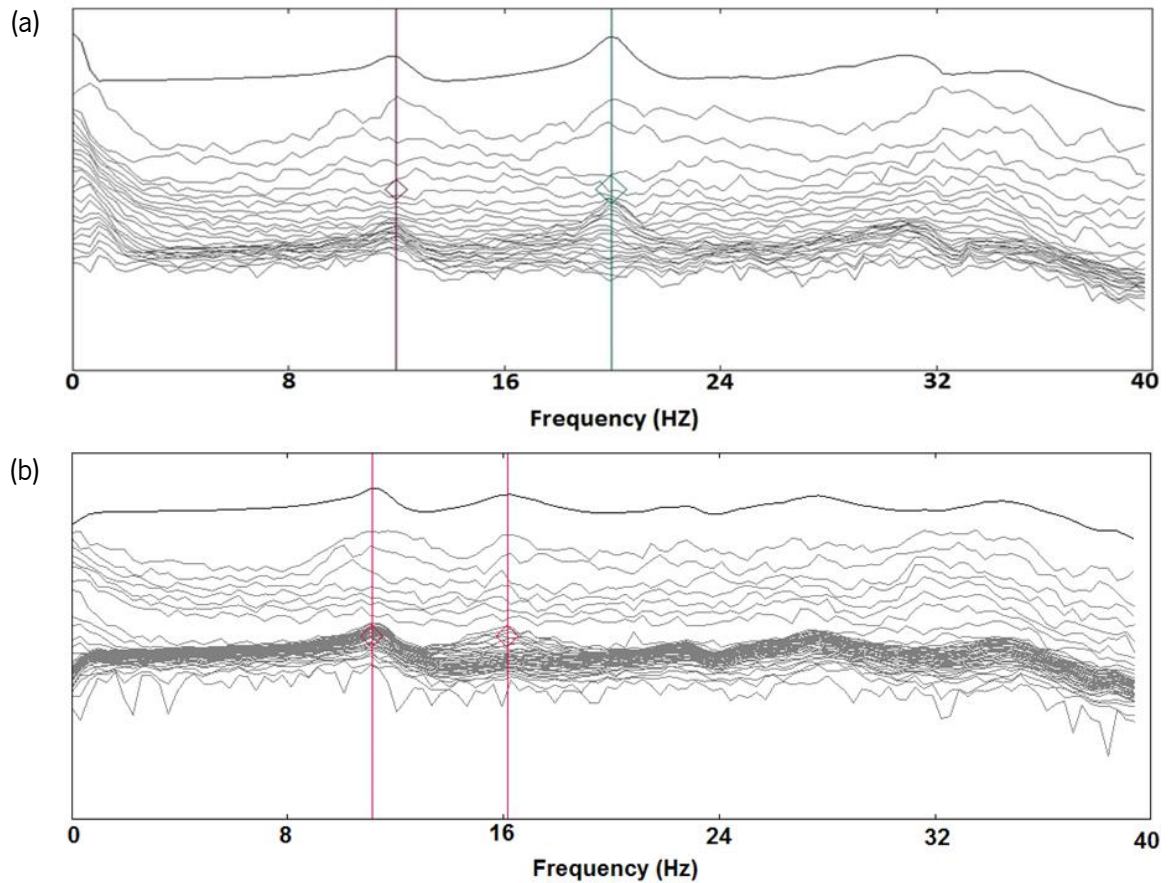


Figure 3.3 - Transfer function curves for: a) RM building and b) UM building

The dissipation of the kinetic and strain energy of the vibrating structure is representing by the damping ratio. In literature, it is possible to find different options for the estimation of the damping values. As a rule, difficulties come into its estimation as the energy is dissipated by various mechanisms that are not related to a unique physical phenomenon and make hardly possible to identify or describe mathematically each of these energy-dissipating mechanism in a real building. The damping depends on the hysteresis rule appropriate for the structure. Usually, for masonry structures, the damping ratio is taken as 3% related to critical damping, a value that has been supported by several investigations (Abrams and Costley 1994; Chopra 1995; Mazzon et al. 2009; Toranzo et al. 2009).

For the estimation of the coefficients of equivalent viscous damping, Half-Power bandwidth method has been used. The identification of damping ratios was made for each orthogonal direction in agreement with the frequency identification. It was found a value of 2.62% for the first mode in RM model and a value of 3.85% in the UM model. The second mode presents values of 1.34% and 3.52% in the RM and UM models respectively. Table 3.2 summarizes the frequencies and damping ratios found for each building.

Table 3.2 – Dynamic properties

Model	Direction	F (Hz)	ζ (%)
RM	Trans	11.90	2.62
	Long	20.02	1.34
UM	Trans	11.11	3.85
	Long	16.12	3.52

As seen, for the masonry buildings the first two natural frequencies are clearly identified by well-defined peaks, summarizing the frequency response of all the accelerometers. In a frequency around 30Hz, it was expected to find a third mode but after analyzing the mode shape in both cases it was concluded that a no logical behavior was related and it was not taken into account. For the buildings the first natural frequency occurs in the transversal direction, see Figure 3.4. The RM model registered a value of 11.90Hz and the UM model a value of 11.11Hz. The second frequency is associated to a mode shape in the longitudinal direction (in-plane with the walls with openings), exhibiting a value of 20.02Hz for RM model and value of 16.12Hz for the UM model. The first natural frequency presents no significant differences between buildings. Nevertheless, different situation occurs for the second frequency, in which the RM building presents a higher value.

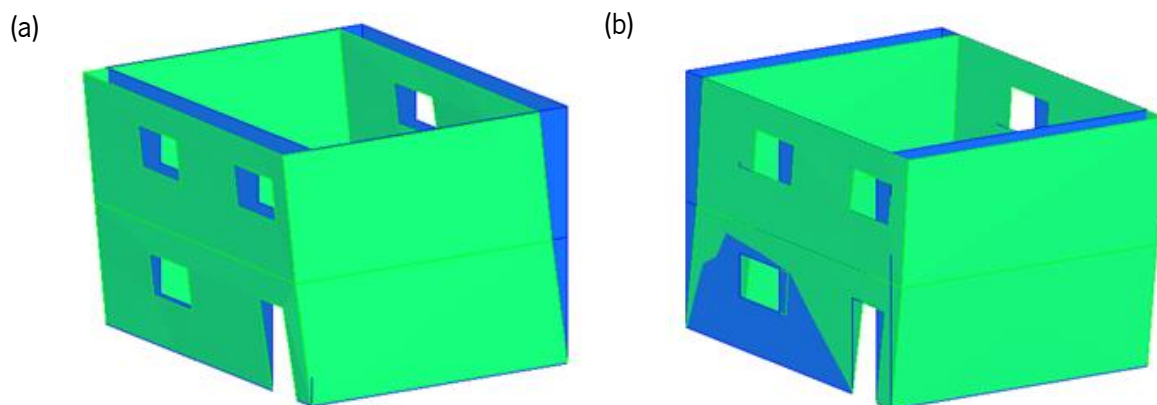


Figure 3.4 - Global mode shapes of both masonry buildings: (a) first mode - transverse direction and (b) second mode - longitudinal direction

It is seen that identical mode shapes were found in both building. The behavior obtained is considered global, even if it was found a small local behavior in the second mode for the lower part of the west wall in the first level in UM model, as seen in Figure 3.4b. For both models, it was noted that even the frequency values are different (a difference of 6.5% in the first mode between the RM and UM building and a difference of 19.4% in the longitudinal direction), the directions and shapes of the mode shapes are similar. In spite of the geometry and materials of both masonry buildings are the same, this behavior can possibly be explained by the filling of the vertical joints with mortar in case of the vertical joint in reinforced (RM model), to which a distinct masonry bond used (vertical continuous joints with vertical reinforcement). As the longitudinal walls are longer and are the ones with openings, higher concentration of reinforcement were placed on them in relation to the transverse walls. For the two mode shapes, opposite façades move in phase, presenting simple swinging movements. This global behavior in masonry is related to the reinforced concrete slabs that

work as rigid diaphragms on the buildings. The rotational mode was not clearly identified from the data obtained.

3.5 Damage patterns and failure modes

3.5.1 RM model

In this model, the first seismic tests of 50% (0.21g) and 75% (0.30g) did not cause any visible damage to the structure. It was on the test of 100% that the first cracks were observed. Figure 3.5 presents the cracks labeled after the seismic input of 100% and 150%. These inputs only affected the first level. After the input of 100% (0.39g), small horizontal cracks were observed at the bottom of the north-west corner and just a small crack at the lower part of the window in the east wall. The input of 150% (0.64g) caused the first cracks in the south wall, being located at the bottom of the wall. In the west wall, a horizontal crack was also found at the left pier of the window.



Figure 3.5 - Damage observed after each seismic input test for the RM model (100% and 150%)

The damage increased mainly in the longitudinal walls in subsequent seismic inputs (Figure 3.6). During the test of 250% (1.26g), additional horizontal cracks were observed only in the longitudinal walls. In particular, in the east wall two important cracks (40cm each) were observed at the lower part of the wall, one on the left and another one on the right pier of the window.

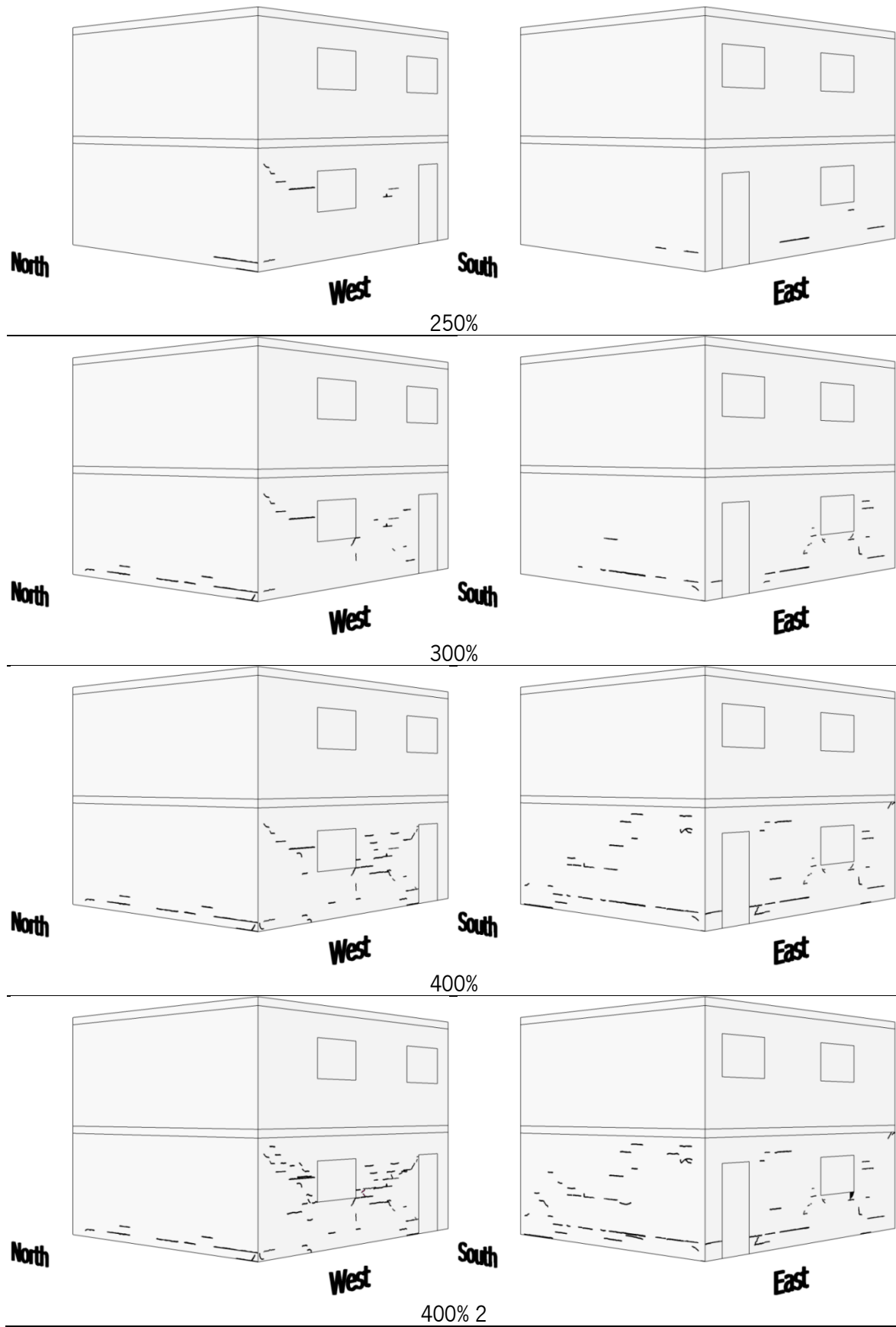


Figure 3.6 - Damage observed after each seismic input test for the RM model (from 250% to 400%)

The input test of 300% (1.33g) resulted in the increase of damage on the north and south walls, in which the bottom part of them were the most affected in all cases by discontinuous horizontal cracks. In the west façade, the right pier of the window was the most affected with the increase of small horizontal cracks over it. The east wall was also affected, but at lower level, by small cracks on both side piers of the window. The input test of 400% (1.61g) considerably increased the damage of the south wall, in which the horizontal cracks (maximum 20cm of length) spread over the entire wall at the first floor. In longitudinal direction, the increase of cracks developed mainly in the diagonal directions inside the piers. The final input test of 400% 2 (1.58g), in which was registered more than 1.5g, the damage was spread out mainly in the longitudinal walls at the first floor level, in which the piers were the most affected. No increment of damage was observed on the north façade. During this test, it was observed the only unit detachment happened in this building. It occurs in the lower right corner of the window at the first level of the east wall.



Figure 3.7 – Damage in the middle of the walls affecting unit blocks



Figure 3.8 – Damage at the bottom of the walls, mainly at corners affecting unit blocks

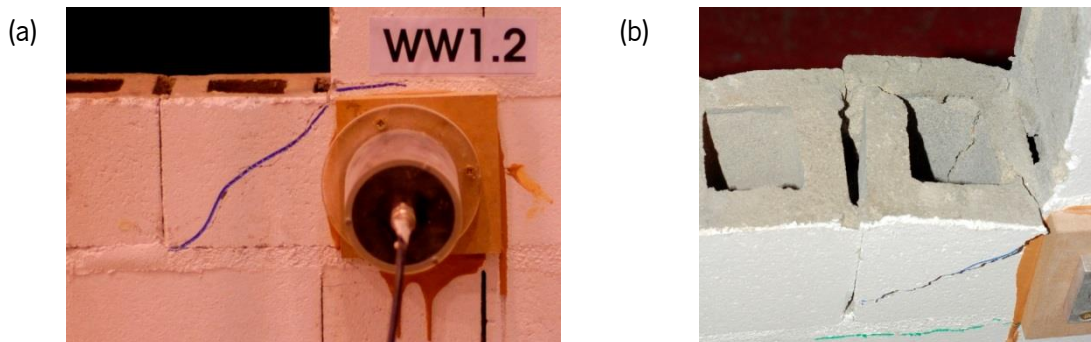


Figure 3.9 – Unit failure after input test of: (a) 400% and (b) 400% 2

The crack density is considerably higher in the west façade, where smeared small horizontal and inclined cracks developed along the diagonals between openings and between the corner north-west. In the east façade, only few small horizontal and inclined cracks are distributed along the diagonal between openings and between corner and the window (direction north-south). The major crack is a horizontal crack at the second course, appearing to be a continuation of the bed joint crack developed in south wall. In this building, damage has been concentrated at the first story level of the building and almost no damage developed in the second story. The density of cracks is clearly higher in case of the walls with openings. In the north façade only a horizontal crack developed at the first course with almost the full length of the wall, whereas in the south façade a horizontal continuous crack develop at the second course, accompanied by many smeared small horizontal cracks roughly located along the diagonal east-west. Additionally, it is noted that the building is very far away from collapse, with a maximum crack opening at the end of the tests lower than 1mm and no yielding of any reinforcement was seen. It should be stressed that almost all cracks developed along the unit-mortar interface, even if some concrete units were also affected with minor cracks. Horizontal cracks appear to be the result of in-plane flexural resisting mechanism associated with low values of vertical pre-compression. The tendency for smeared cracking along the diagonals is also associated to the presence of horizontal and vertical reinforcements. According to Haach et al. (2010), the presence of horizontal reinforcements leads to significant crack distribution, avoiding cracking localization.

3.5.2 UM model

The first seismic test of 50% (0.27g) did not cause any significant damage to the structure. It was during subsequent tests that important cracks were observed, as seen in Figure 3.10 and Figure 3.11. The input test of 100% (0.51g) presented cracks in all walls of the first story and in the walls with openings in the second story. In the north and south walls, the opened cracks are predominantly horizontal at the first course of units at the first floor level, with an approximately 50% length of the wall. Simultaneously, stepped diagonal cracks developed at the corners of these façades, which appear to be in continuation of diagonal cracks developing in the walls with openings (west and east façades). In the walls with openings, the first cracks were mainly shear diagonal stepped cracks developed at the unit-mortar interfaces, starting from the corners of the windows. After the seismic input of 150% (0.80g) all walls presented severe cracking. At the first story, the horizontal cracks in the transverse walls, at first course of units extend to the walls with openings. At this stage, the structure presents a horizontal crack at the first course of the first story with a length of approximately 80% of the perimeter of the building. In the north wall, a horizontal crack developed along the first course also at the second story in about 70% the length of the wall. This crack extends to the full length of the west wall (with openings) and to the pier between the corner and the window at the west façade up to the end of the stepped diagonal crack developed from the right bottom corner of the window. Stepped cracks appear also at the upper right corner of the north wall and at the upper and lower right corners of the south façade. The condition corresponding to the test input of 200% (1.11g) is characterized by the opening of a diagonal crack that developed in the north façade. This crack appeared from the upper right side of the second story to the lower left side of the

first story together with a horizontal crack along of the third course of units at the second level of the south façade. These failures extend to the walls with openings, connecting previous damage and increasing the horizontal division of the model. In particular, for each longitudinal wall, it can be observed the horizontal cracks that connect the windows at the second story. On the west wall, it connects the bottom corners and in the east wall, it connects the middle of the windows.

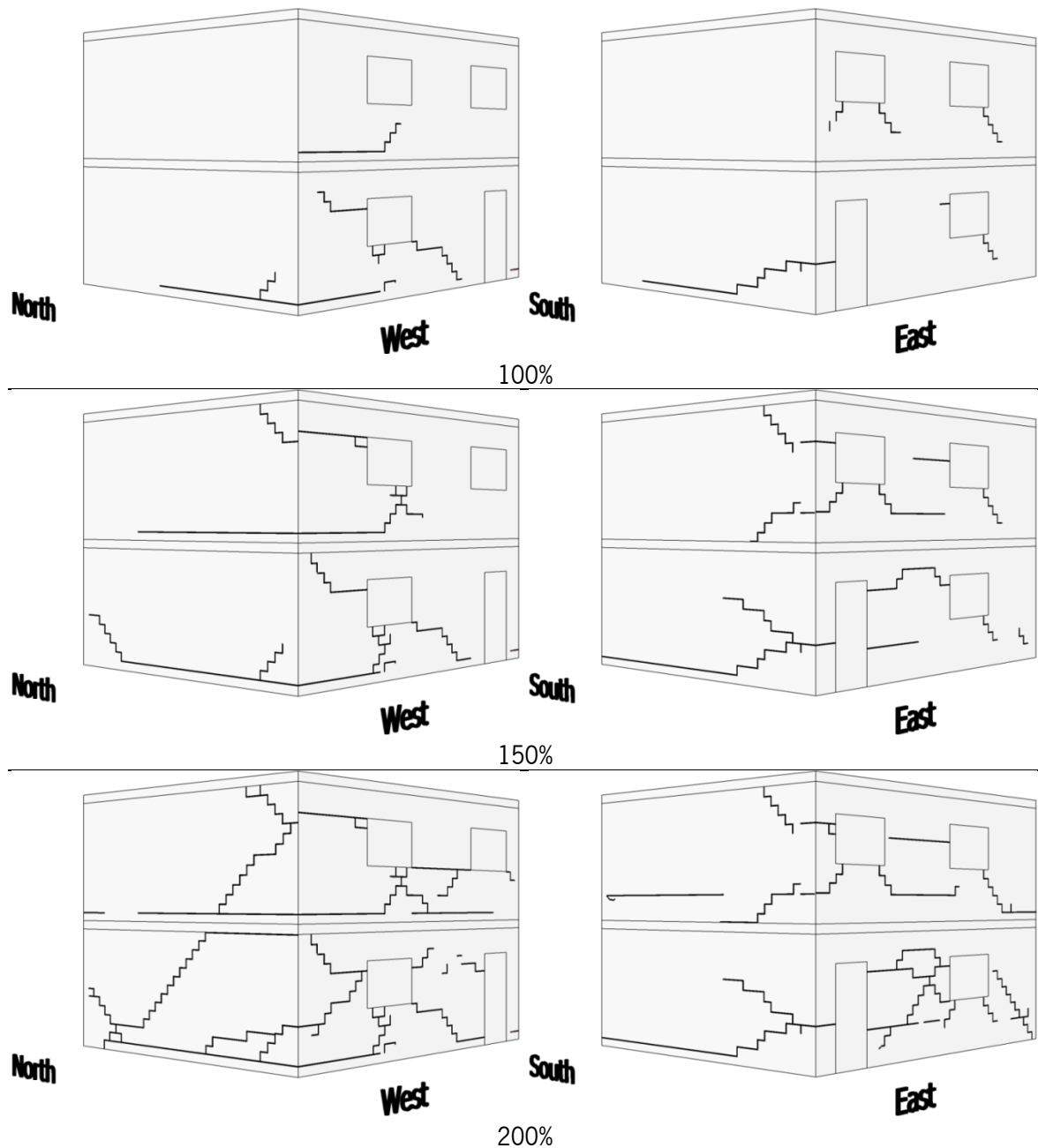


Figure 3.10 - Damage observed after each seismic input test for the UM model (from 100% to 200%)

The increase on input to the test of 250% (1.33g) results in the progress of damage to the corners of the building at the bottom of first story (north-west, south-west and south-east) with crushing and loss of concrete block units. At this stage of loading, horizontal cracks at fifth row from the top and at the third row from the bottom develop also in the south wall in the second story and also at fifth row from the top in the first story. Horizontal cracks at the same location developed also in the east

wall at second and first story. Similarly, a horizontal crack opened approximately at mid height of the second story in the north wall. The development of these almost continuous cracks at the unit-mortar interfaces appears to be related to the inertial forces, resulting from the out-of-plane behavior of the walls due to tensile stresses appearing in the normal direction to the bed joints. At the end of this stage of loading, cracking patterns of the walls are due to mixed in-plane and out-of-plane resisting mechanism of the walls. This combination of cracks divides the UM building in discrete almost horizontal blocks and promotes sliding resisting mechanisms during shaking tests.

The opening of the cracks during this test run was significant, with values of opening larger than 50mm. The repetition of the seismic test, corresponding to input of 250% 2, aimed at assessing the influence of the existing damage on the deformation mechanism of the UM model, to validate the ductility and energy dissipation of the solution, and the capacity to withstand aftershocks. This test clearly enabled to identify the sliding mechanism developing in both directions along the cracks defining the discrete blocks.

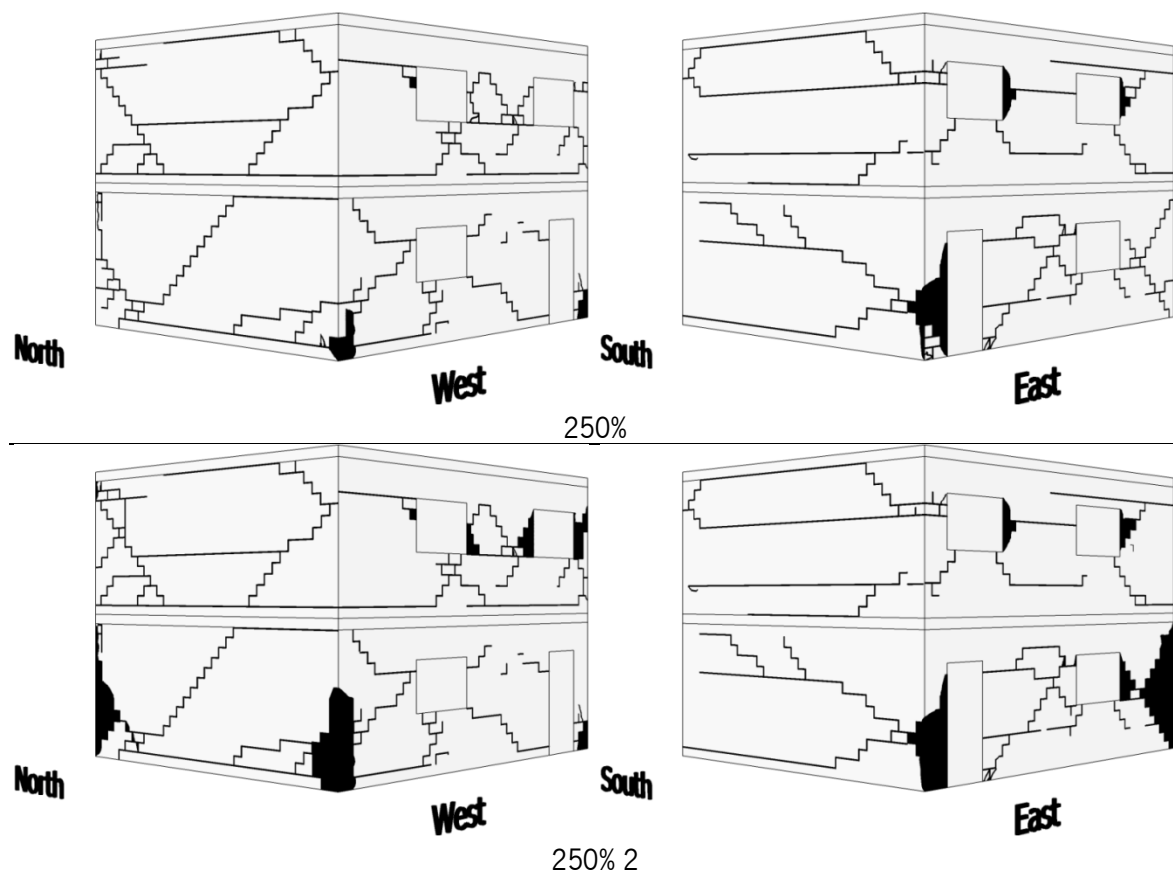


Figure 3.11 - Damage observed after each seismic input test for the UM model (250% and 250% 2)

In this test, it was also possible to observe the disintegration of three corners at first story. The most compromised damage was observed between north-east walls, in which about two-three units from the corner were lost. Additionally, more units were lost at the border of the windows of the east wall (first and second stories) and in the west wall (second story). It is stressed that global collapse of the UM building did not occurred, in spite of the very severe damage.

As observed, the building was affected at both levels. The detachments of units at the second floor, during the seismic input of 250% are presented in Figure 3.12. The failure affected mostly the piers of the windows, resulting from the combination of the in-plane and out-of-plane resisting mechanism. During this input test, the lower part of the building's corners were also severe affected. Figure 3.13 presents the damage on them after the seismic test, from where an important detachment of a block of units (9 units of height by 3 units of length) and crushing of units (about 2 units in each direction) were observed.

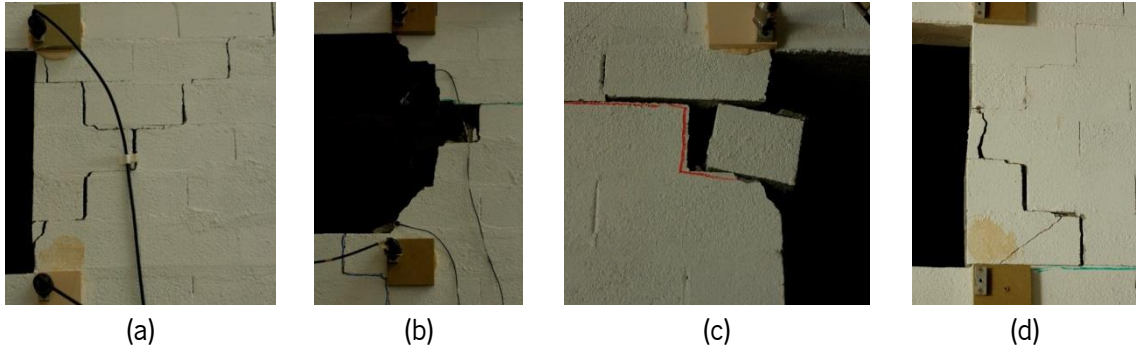


Figure 3.12 – Damage around openings at second floor during seismic test of 250%: (a) crack opening during test, (b) final stage at the end of the test, (c) detachment of units at upper corner and (d) cracks in unit block at lower corner



Figure 3.13 – Damage in corners during the test of 250%

Some pictures of the final damage stage of the building can be observed in Figure 3.14 and Figure 3.15 for the east and west walls, respectively. From them, it is possible to observe the considerable damage presented in the corners of the north façade, the diagonal cracks observed at the piers of two floor levels and the horizontal cracks connecting openings.

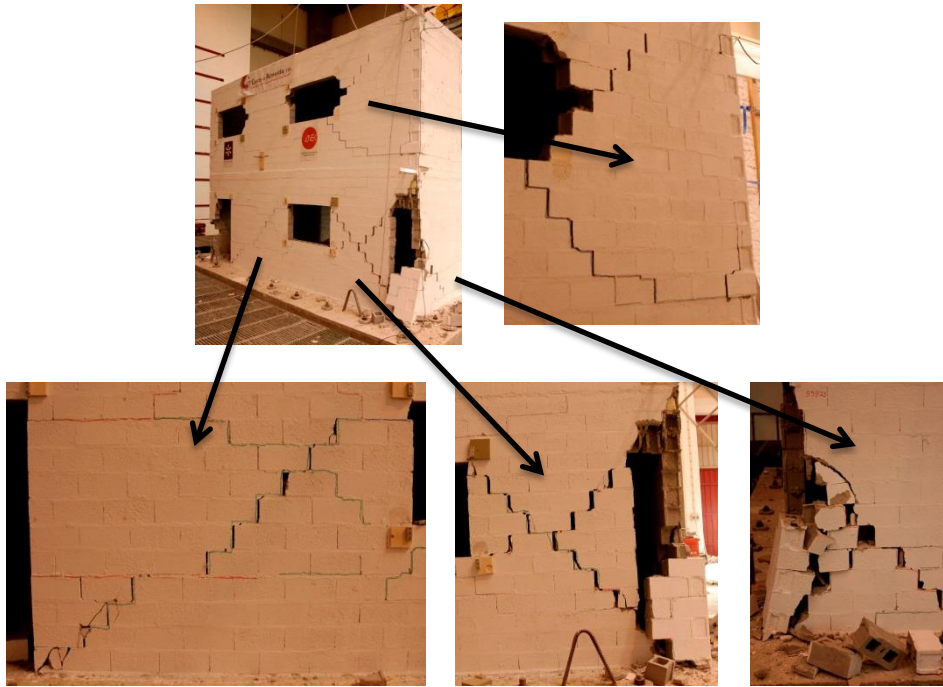


Figure 3.14 – Final damage of the east and north walls



Figure 3.15 – Final damage west wall at second floor (between openings)

3.5.3 Comparison of damage between UM and RM models

The crack and damage patterns obtained for the last stage of seismic inputs for the two masonry buildings are shown in Figure 3.16. For the RM model, the crack patterns correspond to the second test input of 400% and for the UM model, the crack patterns correspond to the second test input of 250%.

The comparison of the crack patterns reveals that a large difference in the cracking density and cracking path was found for the RM and UM models. The UM model presents much higher and important cracks and much more severe damage, even for low seismic loading, when compared with the reinforced building. The maximum input motion attained by the UM building represents 62.5% of the maximum input attained by the RM model. The important detachment of unit blocks at two floor levels and the development of the shear sliding mechanism was the final stage of the UM building. Besides the higher crack density recorded in the UM model, it is observed that the cracking

pattern significantly differs from the cracking observed in the RM model: (1) there is clear diagonal crack localization along the unit mortar interfaces; (2) the damage is spread over the entire model (all façades and the two stories); (3) the onset of cracking occurs for much earlier loading stage. Moreover, when the test was completed, the model was heavily damaged and difficult to repair (though perfectly standing). On the other hand, the RM buildings concentrate the damage only at the first floor level, in which small horizontal cracks were mainly presented: (1) at the diagonals of the piers of the longitudinal walls; (2) at the bottom part of the transverse walls (walls without openings).

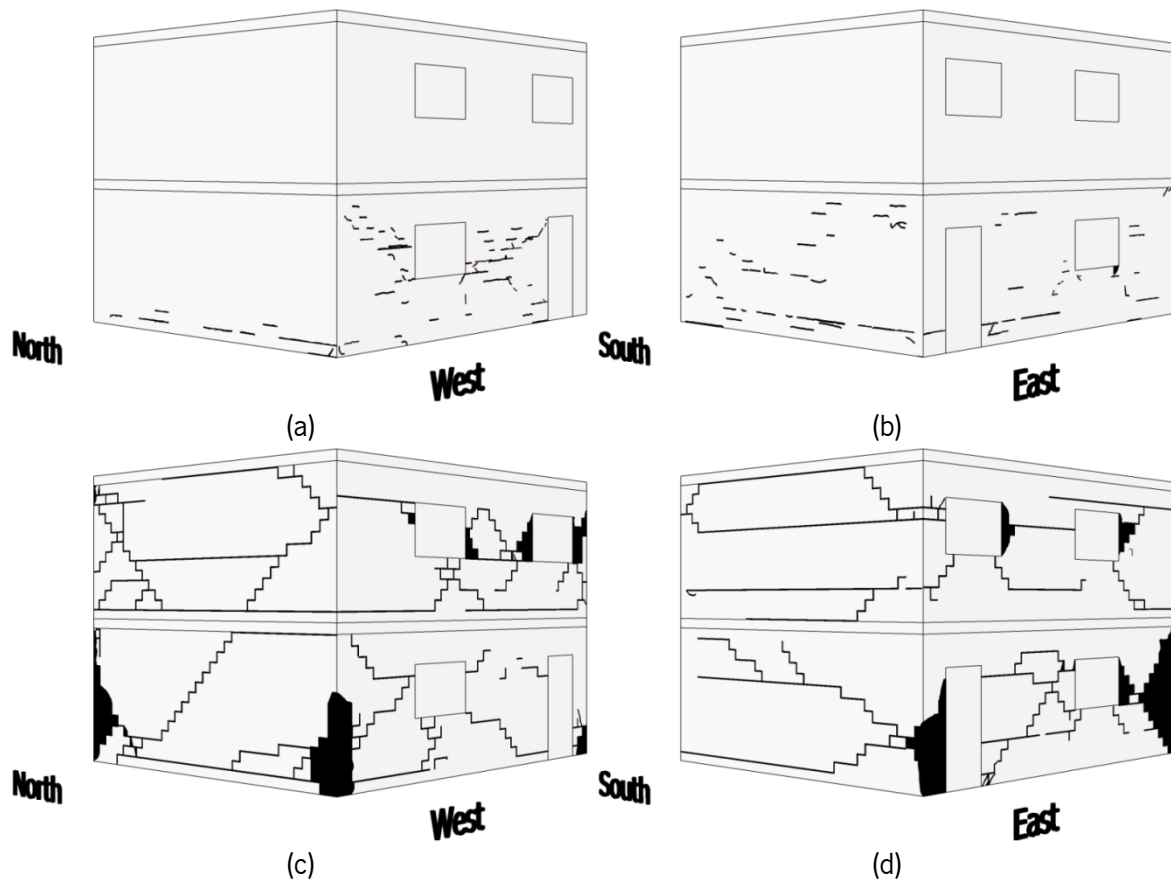


Figure 3.16 - Final damage patterns in: (a, b) RM building and (c, d) UM building

Aiming at having a better comparison of the damage presented in both buildings, the crack patterns observed in the reinforced masonry building after the input test of 250% and the damage presented in the unreinforced building after the first test of 250% are shown in Figure 3.17.

The differences observed for the same seismic input between masonry buildings are much considerable. The damage in the RM building is much more controlled as it presents only very few horizontal cracks at the first level, affecting mainly the lower part of the walls. Instead, for the same seismic input the UM building presented very difficult repairable damage, caused by the combination of the in-plane and out-of-plane resisting mechanisms. In particular, the damage included important cracks in all the walls at both floor levels, loss of unit blocks and interconnection between horizontal and diagonal cracks among walls.

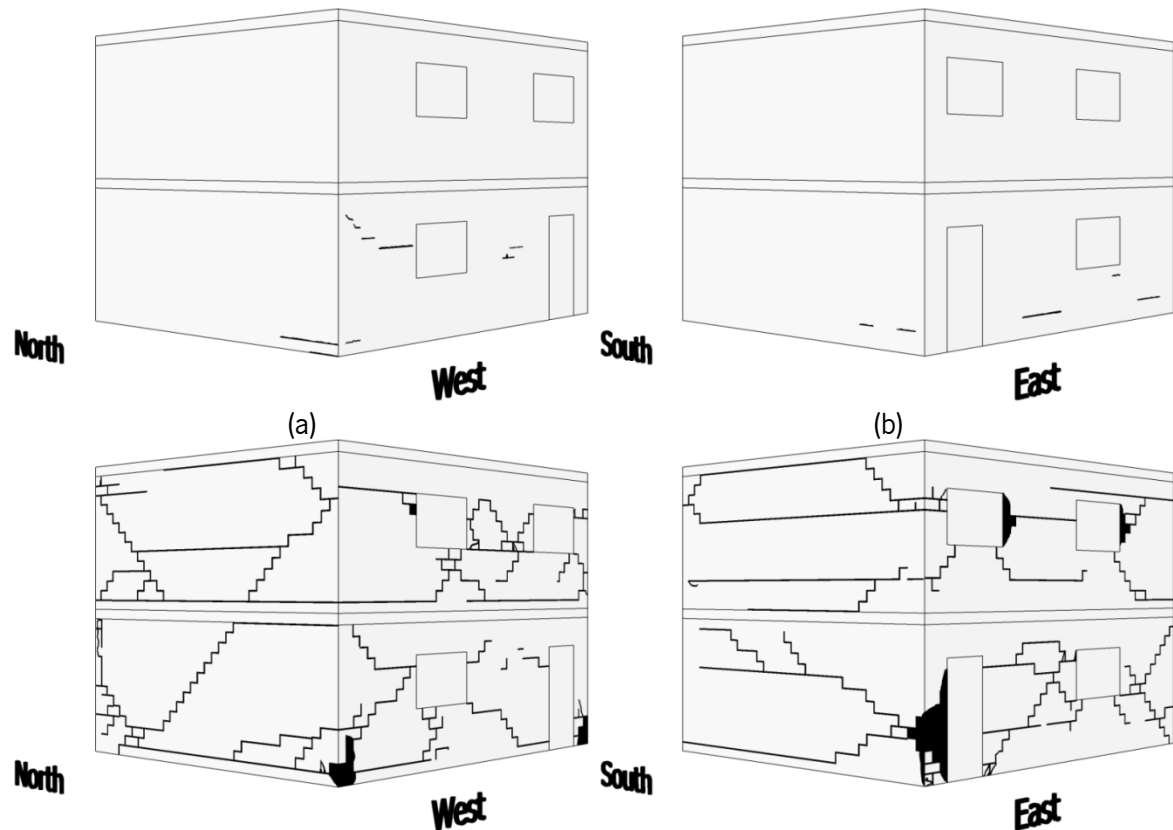


Figure 3.17 - Crack patterns after the seismic input of 250%: (a, b) RM building and (c, d) UM building

3.5.4 Variation of the frequency and damping along the seismic inputs

The trend of variation of the stiffness and damping of any structure subjected to dynamic loads is one of the main objectives of designers. These properties are important for the prediction of the seismic structural behavior. Besides, the trend of variation of these properties along the seismic inputs in the experimental campaign can serve as an indicator for damage characterization. The continuous ageing and subsequent structural deterioration of a large number of existing structures have made that structural engineers pay more attention and interest in the modal identification based on vibrations, which allow the assessment of damage detection. Nowadays, this is a common technique called structural health monitoring. Structural dynamic testing is vital to understand and optimize the actual behavior and inherent dynamic properties of structures, to ensure reliable and safe operation, leading to better seismic performance.

It is intended in this section, to determine the dynamic properties of the buildings to complement the characterization of damage of the buildings through all the seismic input tests and thus to correlate them to the damage and stiffness degradation of the masonry buildings. With this respect, it is well known that the evolution of the natural frequencies can be related to the progress of damage, associated to the increasing of the seismic actions imposed to the models by the shaking table. Indeed, a reduction of the natural frequencies can be explained by the reduction on the stiffness of the models, which is associated to the existence of damage. In addition, a relation between the stiffness and the energy dissipation (damping) properties of the structure can also be found. Over

the past decades, the equivalent viscous damping has been used as a key parameter in the predictions of the maximum nonlinear response. However, due to the uncertainty in its experimental estimation and the difficulty in its appropriate modeling method (that includes it in the design process), is that damping constitutes nowadays an open parameter to experimental and analytical research. Therefore, for the present work it was decided to obtain the natural frequencies and damping coefficients for the initial condition of the buildings and after each seismic test corresponding to the imposition of increased level of seismic loading. The dynamic properties found for each dynamic characterization are summarized in Table 3.3. It is observed that in the RM building there is a decreasing trend of the frequencies as the seismic input loading increases, at the decreasing rate of 1Hz and 0.3 Hz per test in the longitudinal and transverse directions, respectively. From the observed damage after each test and at the end of the seismic inputs, it was clearly seen a higher density of cracks in the longitudinal walls, mainly starting from the corners of the windows and following a diagonal path to an opposite corner. The transversal walls only presented damage at the bottom of them up to the two first courses of blocks, caused by the low shear resistance of the bed joint mortar. In this building, no any relevant damage affected any block unit.

Table 3.3 - Evolution of the frequency and damping coefficient

			Test run									
			Initial	50%	75%	100%	150%	200%	250%	300%	400% 1	400% 2
F (Hz)	RM	Trans	11.90	11.66	11.66	11.35	11.11	11.11	11.05	10.99	10.99	10.74
		Long	20.02	19.17	18.19	17.21	15.69	15.32	14.40	14.40	13.18	12.57
	UM	Trans	11.11	11.14	-	11.02	11.73	12.09	11.85	-	-	-
		Long	16.12	15.05	-	13.98	15.40	14.69	13.63	-	-	-
ζ (%)	RM	Trans	2.62	2.75	3.06	3.18	3.40	4.70	4.73	4.81	3.73	3.90
		Long	1.34	1.52	2.65	3.20	3.30	5.32	6.45	7.63	5.84	6.24
	UM	Trans	3.85	4.06	-	4.62	5.04	4.90	5.47	-	-	-
		Long	3.52	4.76	-	5.34	5.52	6.06	7.68	-	-	-

The damage observed in the UM model developed with a considerable higher rate than the one observed in the RM and this is confirmed by the evolution of the frequency values. Similarly, to the RM building, higher rate of decrease is observed in the longitudinal direction. This tendency reveals the influence of openings in the resistance capacity of the masonry walls in which the resistant mechanism is concentrated in the piers between openings. As previously discussed, the damage on the UM building was considerable at earlier stages, so that severe cracks were observed after the second tests performed, corresponding to 100% of the reference signal and with a PGA of 0.43g – 0.51g. However, after test of 100% no logical trend was obtained in the frequency values. In both direction, from test of 150% to 250% values increasing, achieving values with only a slight difference in relation to the ones obtained for the seismic input of 100%. This behavior is explained for the loss of connection in the walls in which continuous horizontal and diagonal cracks were presented through the bed and head joint forming a sliding mechanism that divide the building horizontally in almost independent structures. As discussed, it started from test run of 150% with a PGA of 0.68g –

0.80g, in which large horizontal cracks developed around the UM model, extending to different walls. It appears that this crack path modified the vibration properties of the structure. A comparison between the highest and lower frequency obtained shows a reduction in the frequencies of 37% in the RM model and a 13% for UM model, both of them obtained in the longitudinal direction.

In conjunction with the frequency behavior, it is also observed a change in the damping ratio, but contrary to what was described for the frequency and as expected, damping values increased after each incremental seismic test. This is observed partly because damping is also a parameters that controls the peak amplitude of the structural response to dynamic loads. The trend observed in the damping values suggests that more energy dissipation mechanisms developed along the loading history of the buildings. From the results, it is seen that that initial damping ratios found for RM building are about half of the ones obtained in the UM model. At the end of the seismic inputs damping ratio increase about 6 times for RM and 3 times for UM in the longitudinal direction. It was observed, that the maximum damping value in the RM building occurred in the longitudinal direction for the test of 300%, being in agreement with the higher quantity of damage found on the walls in this direction in comparison with the transverse walls. For the UM building, the higher damping value was obtained during the last input test in the longitudinal direction. The damping coefficient increases through all the input tests, except for the input of 200% in the transverse direction. The increment is in agreement with the damage observed in this building, which affected all the structure, being the reduction in the transverse direction a consequence of loss in connection.

3.5.4.1 Damage indicator

It has been very well established, by several research investigations, and confirmed in this study that loss of structural integrity is reflected by variations in modal characteristics such frequencies and damping ratios. This means that these properties can be related directly with the progress of the damage observed in the buildings. With the obtained data from the experimental shaking table tests, it is possible to relate the progress of damage with the stiffness degradation, meaning that a relation between the damage and frequency reduction can be defined. As discussed from Table 3.3, the frequency evolution for the UM building was not clear for high seismic inputs, justifying that the damage indicator was only obtained for the RM building.

Considering that there is no loss of mass during each of the i test inputs, a simplified damage indicator (DiPasquale and Cakmak 1987) $d_{k,i}$ for the mode shape k of the masonry building can be estimated by means of Equation 3.1:

$$d_{k,i} = 1 - \left(\frac{f_{k,i}}{f_{k,0}} \right)^2 \quad 3.1$$

Where $f_{k,i}$ is the frequency obtained after each input loading series and $f_{k,0}$ is the initial first natural frequency, determined before the series of shaking table tests. Similar methodology has been implemented by Coelho et al. (2000) in reinforced concrete buildings and by Mendes et al. (2014) in masonry buildings to correlate the evolution of damage of structures tested through incremental

inputs on shaking table. Figure 3.18 summarizes the relation between this damage indicator and the imposed PGA for the RM building. It is important to stress that the damage indicator refers to the cumulative damage.

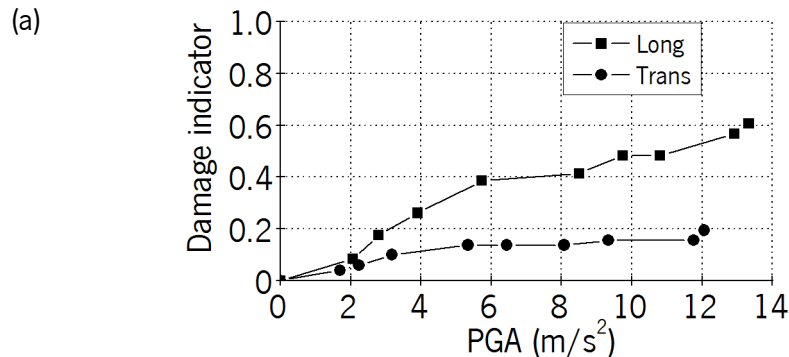


Figure 3.18 - Simplified damage indicator for RM building

As already discussed, for this building the frequency degradation in the transversal direction is lesser significant than in the longitudinal direction for all the inputs, which results from rough diagonal cracking developed on the longitudinal walls with openings. The damage indicator appears to be largely related to the higher damage observed in the longitudinal walls, when compared with the transversal walls. It should be mentioned that the longitudinal walls present higher concentration of reinforcements than the transversal walls due to the presence of openings, which improved the distribution of damage on these walls avoiding for instance its concentration on specific locations. On the contrary, the transversal walls for this model show a general concentration of horizontal cracks mainly at the bottom of the first floor, leading an almost stabilization of the damage indicator.

3.6 Seismic performance

Complementary to the qualitative characterization of damage, it is necessary to evaluate the quantitative parameters of the masonry buildings that include for example their in-plane and out-of-plane walls' behavior in terms of accelerations and displacements. It is also important to assess the interaction between in-plane and out-of-plane behavior, as earthquakes induce both responses. Indeed, the development of in-plane resisting mechanisms, which provide basic resistance and stability for masonry buildings subjected to seismic actions, depends on the out-of-plane resistance of the walls. On the other hand, the out-of-plane resistance of masonry walls depends on the tensile bond strength at the unit-mortar interfaces and on the boundary conditions. Then, it is essential that good connections exist between intersecting walls and between walls and slabs so that good seismic global behavior is attained. Another aspect to be considered is the influence of the out-of-plane cracking on the in-plane crack pattern. Parameters like the accelerations and displacements will give information that is not perceptible to the human eye and that helps considerably in the statistical quantitative analysis of any structure.

3.6.1 Amplification factors from the accelerations

The acceleration time histories are the first and main direct results obtained from the accelerometers placed on the masonry buildings. From them, important parameters as the velocities and displacements are indirectly obtained. Among others, its analysis and study can give a good idea of the forces developed on the model due to the seismic inputs. On the masonry buildings, as the main parameter for the evaluation of the seismic input was the Peak Ground Acceleration (PGA), it was considered to be relevant to analyze the influence of the seismic induced accelerations through the height of the buildings by using a similar parameter of comparison, i.e. the peak accelerations from the accelerometers.

The amplification factors were obtained from the ratio between the peak accelerations recorded at the floor levels and the peak acceleration recorded at the base of the models. The acceleration histories measured at each floor and at the base of the models for the seismic inputs of 100% and 250%, which were used for the calculation of the acceleration amplification factors are displayed in Figure 3.19.

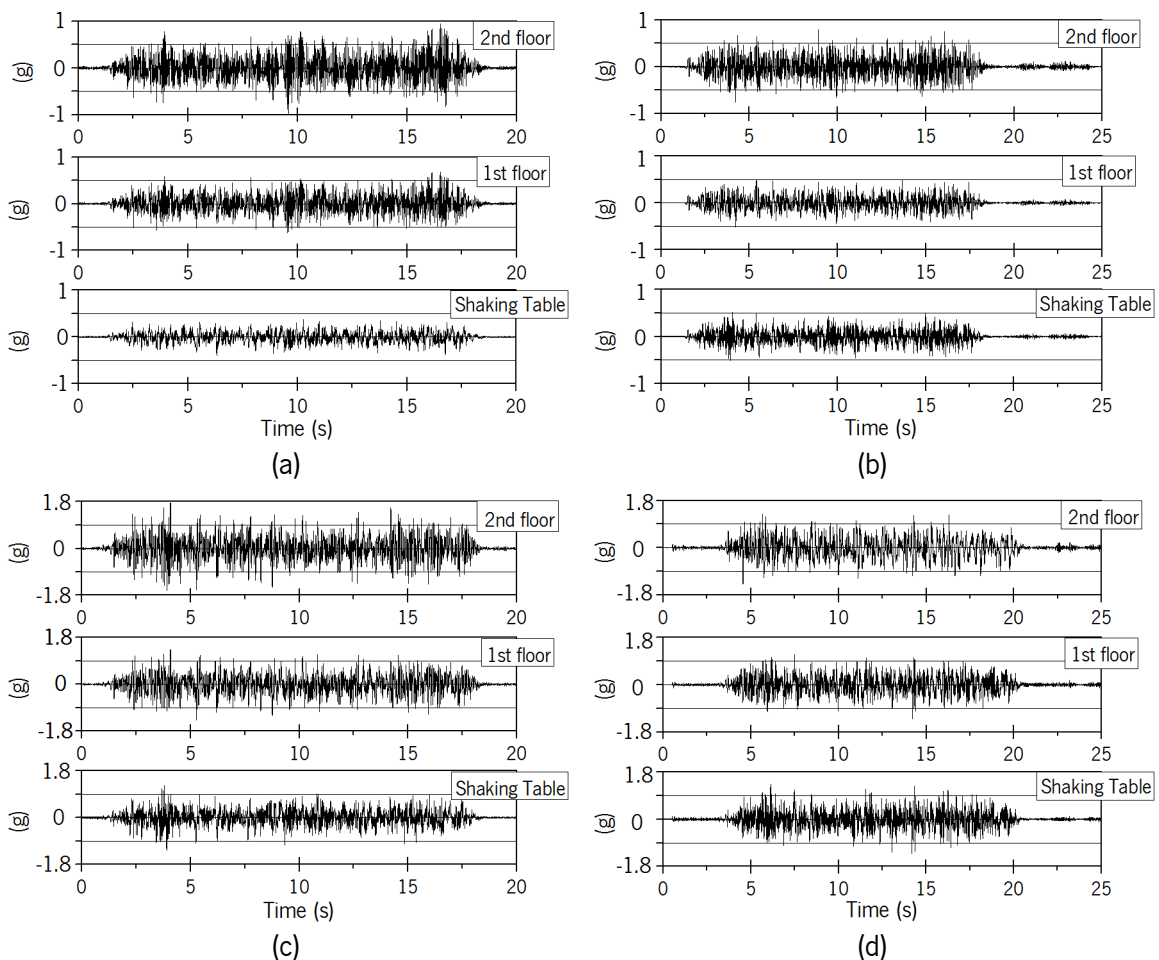


Figure 3.19 - Measured accelerations for each level: (a) RM model 100%-long; (b) UM model 100%-long; (c) RM model 250%-long and (d) UM model 250%-long

The acceleration and dynamic acceleration amplification factors for the different input PGAs are presented in Figure 3.20 and Figure 3.21 for the RM and UM buildings, respectively. To make the analysis easier, the exact PGA value for each seismic input is displayed in vertical dot lines, in which the respective accelerations and amplifications for each floor level are plotted. On the left side of every graph is found the peak acceleration and on the right the amplification factor. The registered peak acceleration at floor levels increased with the PGA in both models and for each direction of analysis, as expected. The only exception occurs for the seismic input of 250% in case of the heavily damaged UM model, which is due to the predominant shear sliding mechanism developing at the unit-mortar interfaces along the bed joints. In general, it was found that the acceleration amplification factors decrease as the imposed PGA increases, which is due to the accumulation of damage during the successive tests. The plots also show that the structural response in the longitudinal direction (walls with openings) experienced higher amplification than the transverse one. Besides, higher amplifications were recorded in the RM model due to the low damage experienced by this building.

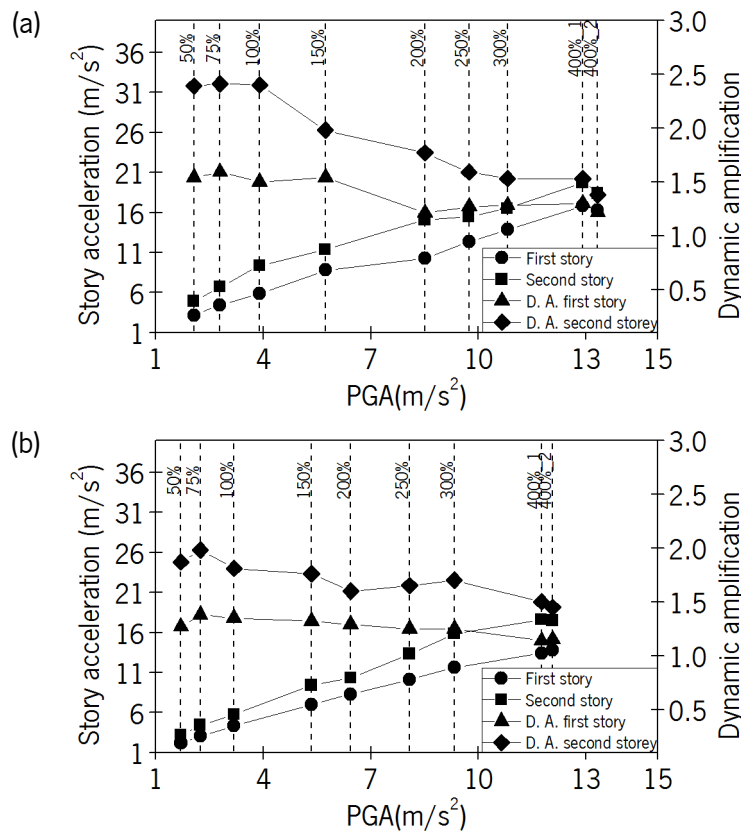


Figure 3.20 - Story accelerations and dynamic amplification factors versus PGA of RM model: (a) longitudinal direction and (b) transverse direction

The largest amplification reduction in this model is presented at the second story in the longitudinal direction, reducing more than 40% from 2.40 to 1.38. The first story showed always less reduction than the second story, for both directions.

In the UM model the largest amplification reduction measured between the first test input and the input of 250% occurs in the transversal direction for the second story with a degradation of 35% and

of 28% in the longitudinal direction. For the same seismic input, the degradation of the amplification factor of 12% was observed in the transverse direction for the RM model and of 33% in the UM model. As aforementioned, the UM building presented severe damage with horizontal masonry blocks that moved almost independently. The transverse direction seems to have more sliding movements during the tests, thus explaining the behavior found.

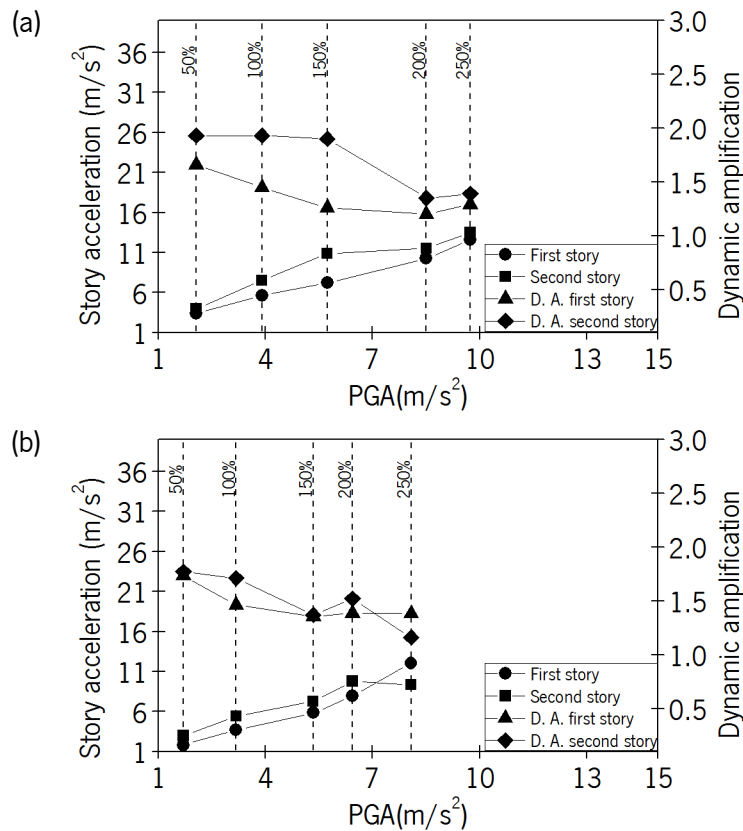


Figure 3.21 - Story accelerations and dynamic amplification versus PGA of UM model: (a) longitudinal direction and (b) transverse direction

3.6.2 Analysis of deformation of the buildings

Modern design procedures for buildings are based on structural displacement response. It is then important to perform an analysis and study of this parameter from the experimental campaign developed on the two masonry buildings aiming at obtaining their deformation capacities.

The deformation of a building gives an accurate idea of its ductility, which in combination with its resistance determines its ability to ensure its stability and robustness during earthquake events, preserving human lives. Deformation is the first energy dissipation mechanism most structures used for dissipate the induced energy by dynamic loads. The analysis encompasses, among others, the in-plane and out-of-plane deformations in individual structural walls as well as in the buildings as global structures.

3.6.2.1 In-plane displacements and interstory drifts

Concerning the deformation of the buildings, firstly the in-plane displacement profiles along the height of the walls are presented, and then the relative displacements (inter-story drifts) at the floor levels are calculated. Figure 3.22 and Figure 3.23 show the in-plane displacement profiles found for longitudinal and transversal walls for the RM and UM models, respectively.

The displacements presented are the maximum values obtained for each seismic input. Figure 3.24 and Figure 3.25 present the inter-story drifts, which are calculated based on the total displacements measured at the levels of the slabs.

The displacement profiles and drifts obtained in reinforced and unreinforced masonry models differ considerably. In the RM model, there are small differences between north and south façades as well as between west and east façades, meaning that the behavior of the walls was homogeneous. These results occur because there is double symmetry of the model, thus small torsion, and the reinforcement provides tensile resistance. Furthermore, in this model the maximum lateral drifts are higher in the first floor, particularly in case of longitudinal walls, which is associated to the higher level of damage developed at this story.

Only in the south façade, higher interstory drifts are found at the second level, with a maximum value corresponding to 0.37%. As mentioned before, the damage in this model is concentrated in the first floor with a maximum interstory drift of 0.34%, which is in accordance with the fast increase on the in-plane displacements at this level. In this model, the first crack appeared during the test input of 100% (0.39g) with an interstory drift of 0.05%. The evolution of displacements in the second floor is much slower, which reflects the minor damage developed at this story, which behaves almost as a rigid block by the end of the test. Globally, the displacements are rather small (maximum displacements attained values of 5mm in both directions for the final input test), as the result of the low level of damage. It is also noted that the repetition of the last seismic input increased the maximum displacement marginally (less than 10%).

On the contrary, in the UM model all façades exhibit distinct profiles close to collapse due to the asymmetric damage distributed in the building. The increase in the displacements and lateral drifts are moderate up to the seismic input loading corresponding to 200% (1.11g), with previous maximum drift values of 0.25%. For this test input, extensive diagonal cracks occur together with sliding along the bed joints. Up to this stage, the displacement profile is almost linear in elevation, and the maximum drift values reach 0.5%. The significant increase on the displacements of the walls occurs for the first 250% seismic input (1.33g) and, then, during its repetition. The increase on the displacement occurs at both floor levels, with no uniform displacement increase in height. The maximum drifts were recorded at the second floor and reached a maximum value of 2.5% with similar values for the first floor. The large displacements are associated to the increase of the opening of the diagonal shear cracks that became clearly visible for the last seismic inputs. It is also noted that the repetition of the last seismic input increased the maximum displacement significantly (about 100%). Figure 3.26 shows the final damage in south and east façades for the UM building after test inputs of 200% (1.11g) and 250% (1.33g).

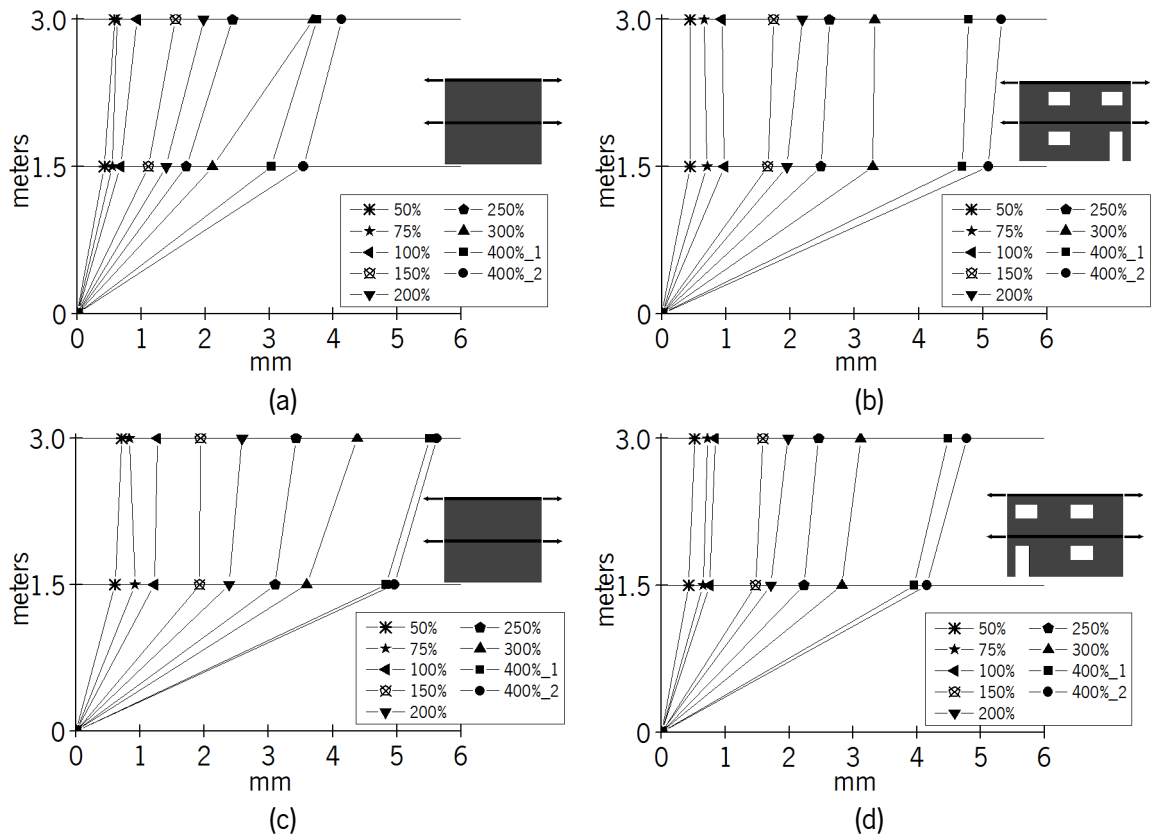


Figure 3.22 - In-plane displacements in walls of RM building: (a) north façade, (b) west façade, (c) south façade and (d) east façade

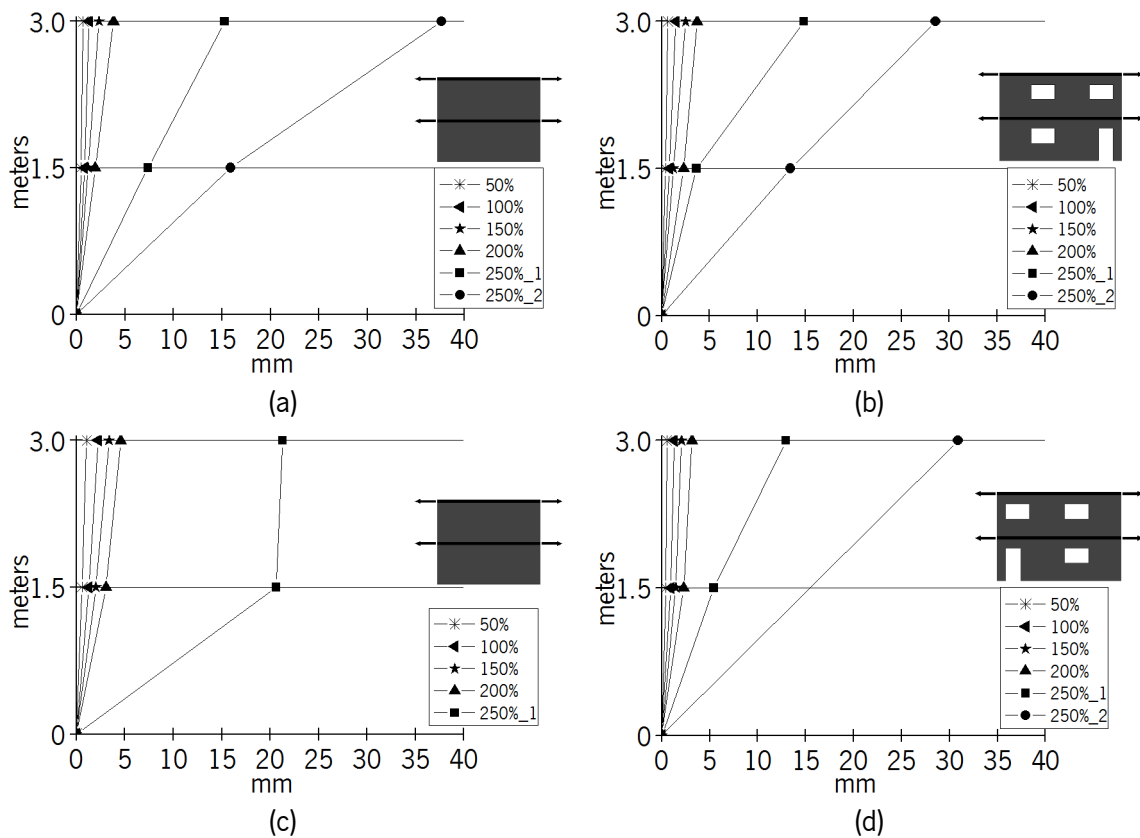


Figure 3.23 - In-plane displacements in walls of UM building: (a) north façade, (b) west façade, (c) south façade and (d) east façade

It is possible to observe that the shear failure developed at the lower part of the south façade with a crack progressing around the building. This crack exhibited openings over 10mm during test input of 250%. Additionally, a longitudinal crack appears at 3/4 height of the first level in the south façade and further diagonal cracking appears at the right part of the window in the east façade.

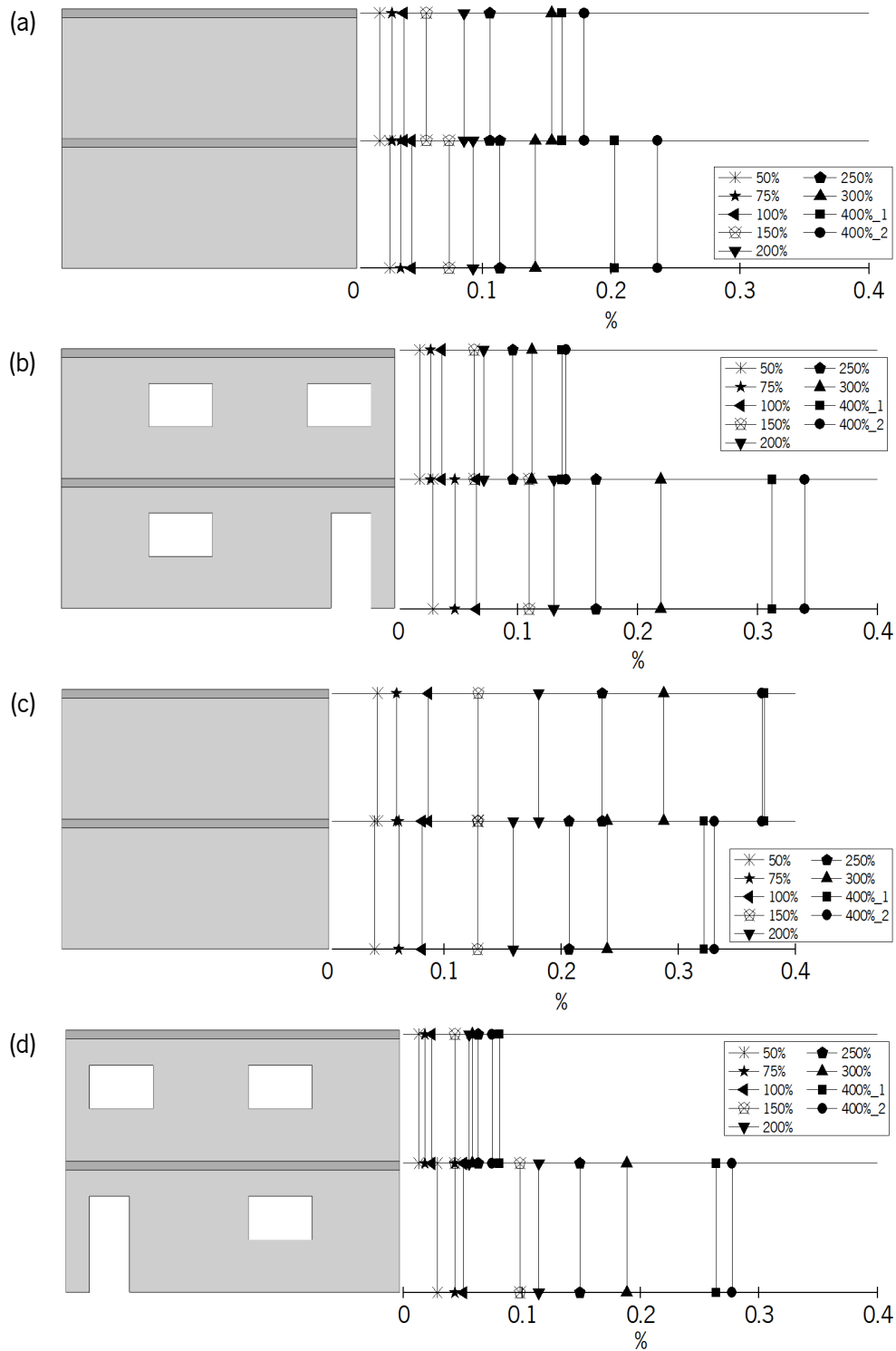


Figure 3.24 - Interstory drifts for RM model: (a) north façade, (b) west façade, (c) south façade and (d) east façade

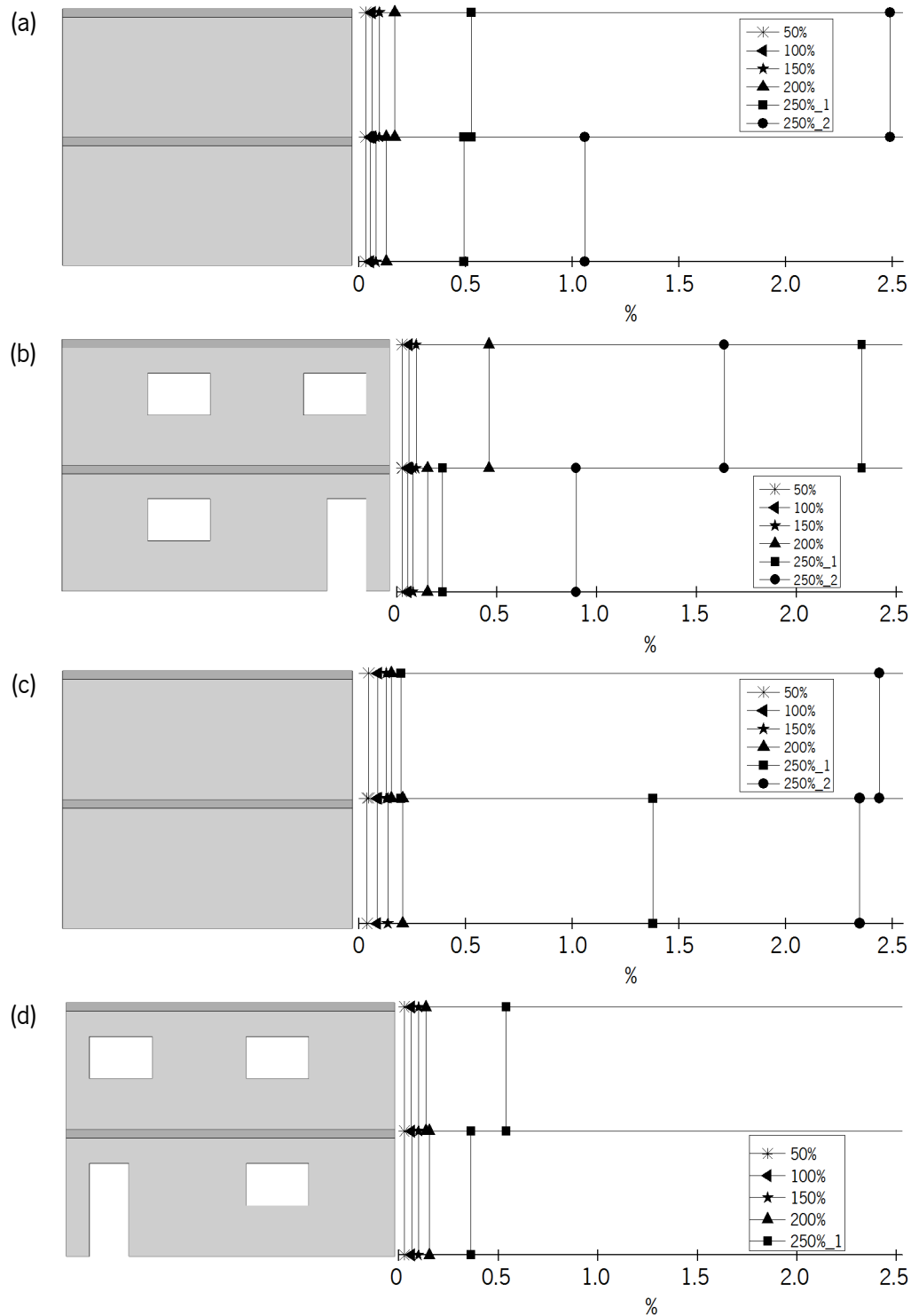


Figure 3.25 - Interstory drifts for UM model: (a) north façade, (b) west façade, (c) south façade and (d) east façade

The south-east corner exhibits severe damage, leading to a maximum displacement of 20mm at first floor level. The continuous crack around the building also developed in the second level, at approximately 3/4 height of the wall, similarly to the first level, promoting a sliding mechanism and increasing the maximum displacements up to 30mm. The repetition of the 250% input results in the important progress of damage and displacements discussed. The sliding mechanism that developed

along the unit-mortar interface cracks affects the upper and lower story and provides a weak connection through the height of the model. Still, the shear sliding mechanisms provides good capacity of the model to dissipate energy during the seismic input, as observed.

The results also show that the lateral drifts found for test run of 100% (0.51g) are of 0.085% in the first floor and of 0.089% in the second floor. These values, and the low damage in the UM model for this level of seismic input, confirm the suitability of modern unreinforced masonry regular buildings to withstand moderate seismic loading. As a conclusion, the lateral drifts recorded in the RM model for test run of 400% (1.61g) are associated to minor and controlled damage. In case of the UM model, the damage and lateral drifts are very low for a PGA of 0.51g but increase considerably for a PGA of 1.33g, due to the progressive, severe and extensive damage. As stated before, no collapse of this structure was observed, even after the repetition of the last input seismic loading.

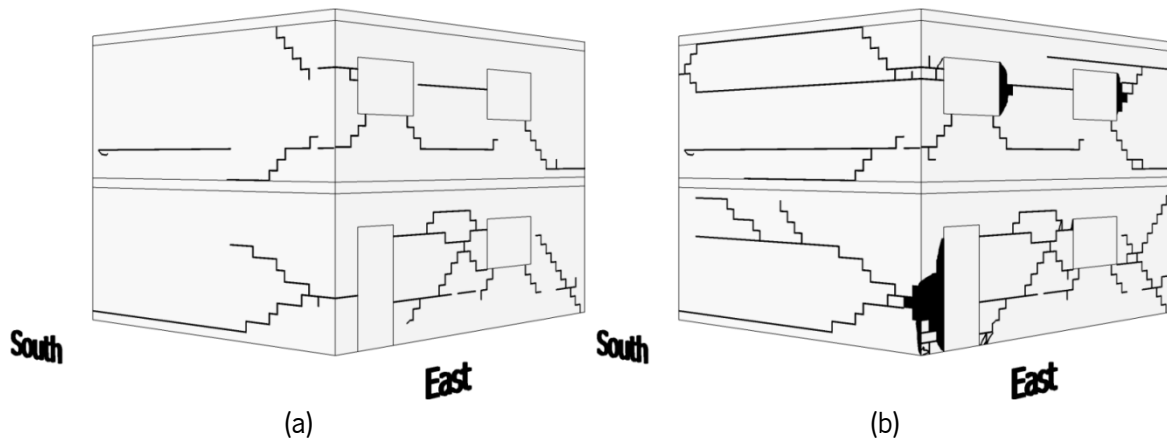


Figure 3.26 - Damage of the UM model in south and east façades after: (a) test run of 200% (PGA=1.11g) and (b) test run of 250% (1.33g)

3.6.2.2 Out-of-plane displacements

The vulnerability of masonry to out-of-plane loads can result in the early collapse of structural masonry walls, precluding the development of the in-plane resisting mechanism of the masonry walls and adequate stability of masonry buildings. For the masonry models under analysis, in spite of the out-of-plane effects in the masonry walls, the connections of the intersecting walls and the connections with the slabs revealed themselves to be adequate enough to avoid detachment and excessive out-of-plane rotation of the masonry façades.

The out-of-plane displacements of the masonry façades are shown in Figure 3.27 and Figure 3.28 for the RM and UM models, respectively. In these plots, the total out-of-plane displacements in height (left column of plots) and the relative ones are shown (right columns of plots).

The total displacements were calculated from the accelerometers placed along the height of the façades. In the transverse direction (east and west walls), it was planned to measure the out-of-plane displacements at three different sections, aligned with the windows corners at the two story levels as well as window and door corners. The accelerometers were glued with epoxy resin to the masonry

units and some of them felt during the tests, providing incomplete displacement profiles. Alignment West B in the UM model was the most affected and the results could not be analyzed. Still, the data allows a better understanding at the central part of the walls, away from the corners, where the out-of-plane behavior affects more severely the response.

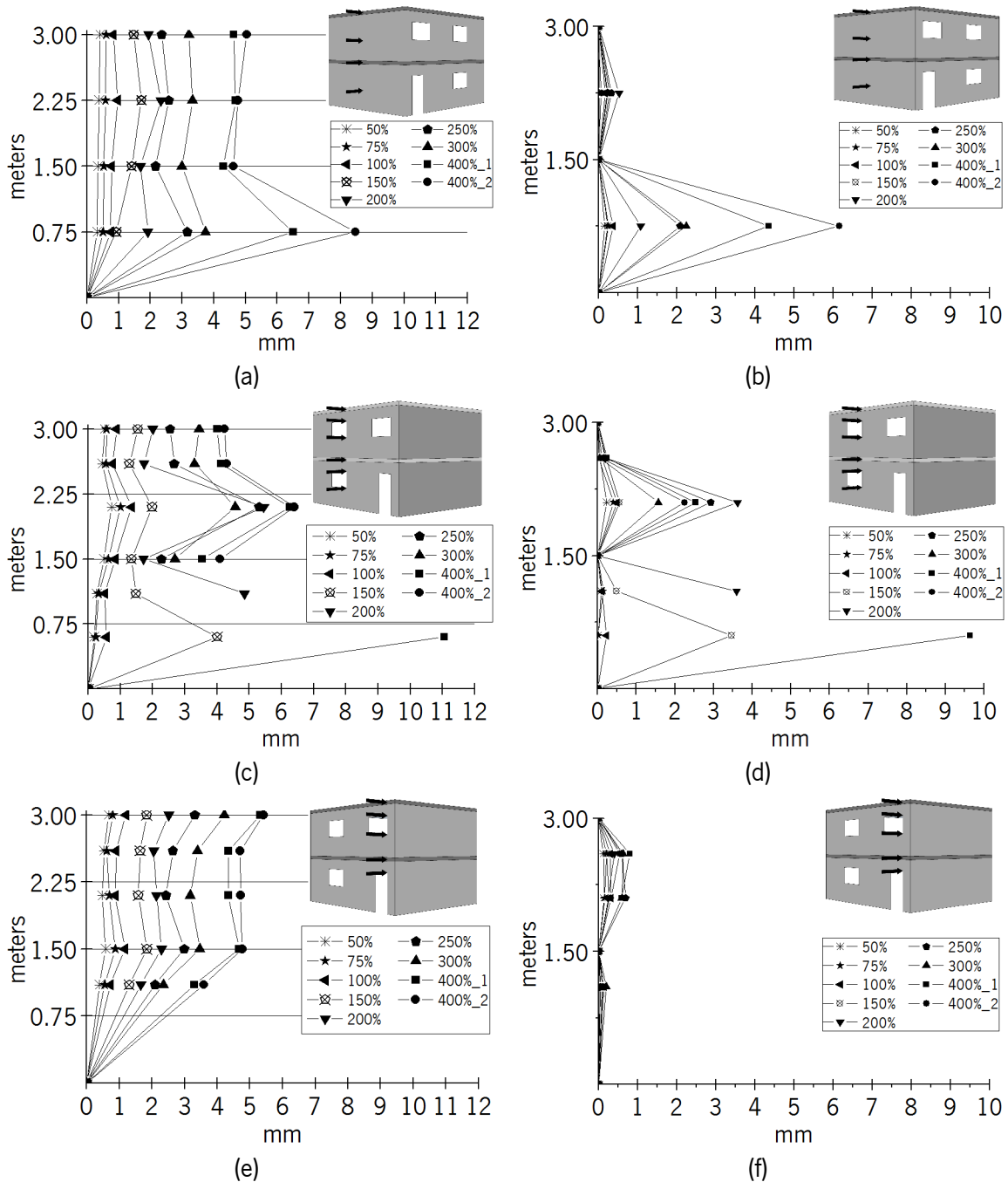


Figure 3.27 - Global and relative out-of-plane displacements for RM model: (a, b) south façade, (c, d) west B and (e, f) west C

The relative displacements were calculated by subtracting from the total out-of-plane displacements the linear component of the displacement profiles defined between the base of the buildings and the first floor and between the first and the second floors. This procedure makes the analysis easier as it

isolate the pure out-of-plane displacements of the selected points of the façades. Note that a comparison with Figure 3.22 and Figure 3.23 indicates that, in general, similar values are found at the floor levels, indicating a good correspondence between the different measures.

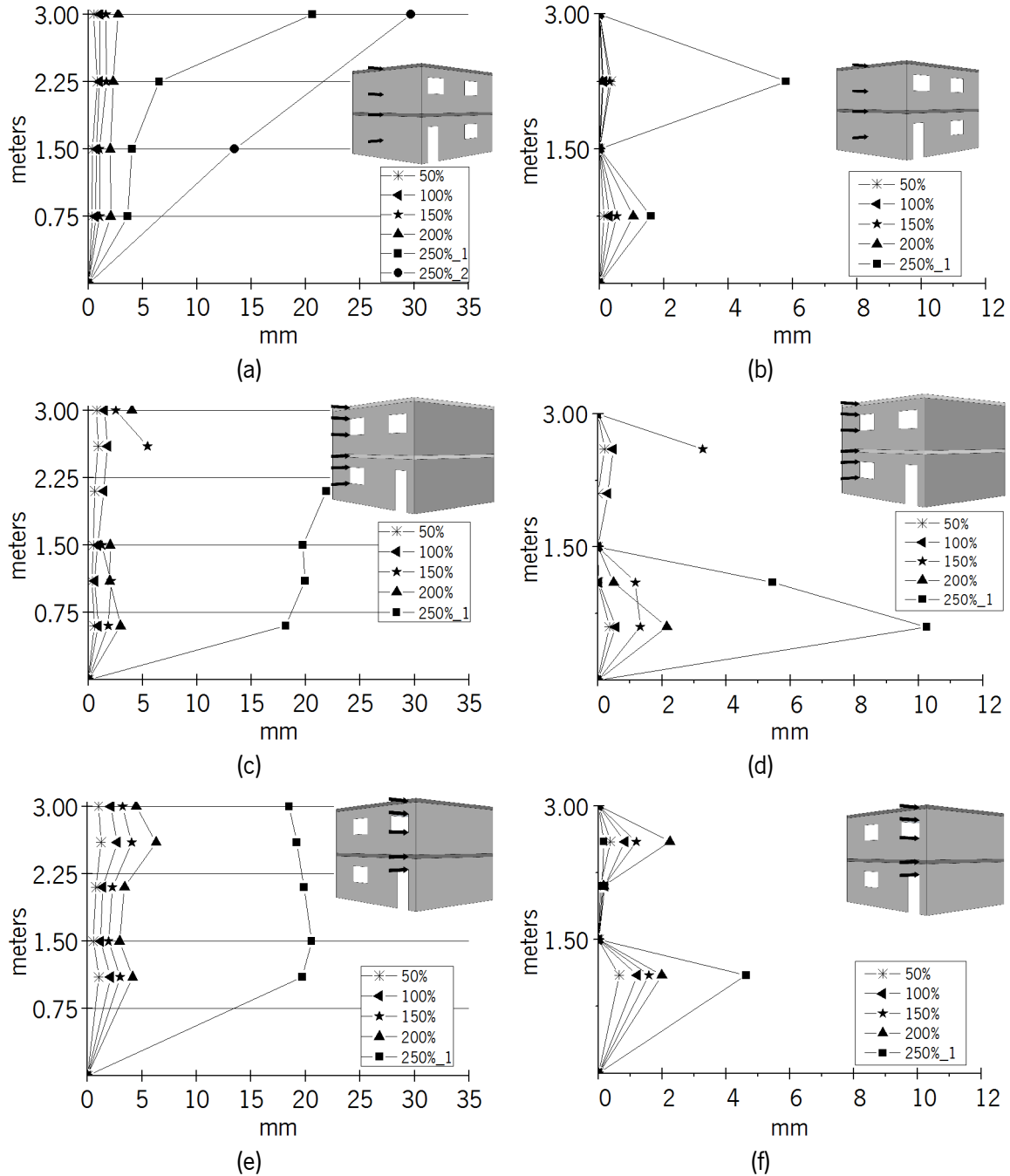


Figure 3.28 - Global and relative out-of-plane displacements for UM model: (a, b) south façade, (c, d) west A and (e, f) west C

In the analysis of the RM model, it is observed that for each façade and vertical alignment the out-of-plane deformation does not vary significantly until test input of 100% (0.39g). Until this loading stage, the maximum relative out-of-plane displacements are lower than 0.5 mm. The out-of-plane displacements are more visible after the test input of 150% (0.64g). It is seen that there is a

considerable difference on the out-of-plane displacements between south and west façades. In the south façade, the highest out-of-plane displacements occurs at the first level and only minor out-of-plane displacements were found at the second level (see Figure 3.27b). In fact, almost no damage was recorded in the second floor of the south façade. In case of the central profile of the west façade (alignment west B), see Figure 3.27c,d, the highest out-of-plane displacements occurred at first floor, but the displacements recorded at the second floor are also considerable. This behavior can be justified by the presence of the openings. In this wall, there is also a tendency for the out-of-plane displacements to reduce in the proximity of the corners, as would be expected if the connections of the walls are adequate. Therefore, to this behavior, also contributes the placement of vertical reinforcements, improving the connection at the corners due to the combination with the horizontal reinforcement. In all cases, only minor differences on the displacements of the slabs were recorded between the first and the second floors, which confirms the predominance of relative deformation at the first floor, in correspondence with the higher damage developed at this level in case of the RM building.

It was noted that there is no logical evolution of the out-of-plane displacements, mainly at the second floor, according to the seismic loading imposed to the shaking table. This behavior holds for the south and west façades, due to a high nonlinear behavior of the model. In general, it is possible to conclude that significant cracks developed in all façades when relative out-of-plane displacements are over 4mm.

The out-of-plane deformation of the masonry walls in the UM model is more regular in terms of evolution of increasing out-of-plane displacements with increasing seismic loading. In both directions, the out-of-plane displacements follow an almost incremental trend up to the test input of 200% (1.11g). After this loading stage, there is a remarkable increase of the out-of-plane displacements. Similarly to the RM model, the maximum out-of-plane displacement occurred in the transversal direction; i.e. in the west wall, at the first floor (over 10mm) at the test input of 250% (1.33g). Before this, the out-of-plane displacements are very moderate (about 2.15mm). The final out-of-plane displacement in west A for UM model is similar to the one in west B of RM model, in which a maximum displacement of 9.6mm was recorded after test run of 400% (1.61g).

Small displacement values are found in the proximity of the corners as seen in Figure 3.28e and f, meaning that the traditional bond pattern adopted for the UM model corners presents an adequate behavior even for large values of seismic loading. In the south façade, the maximum out-of-plane displacement is registered during the last test input at the second floor with a value about 6mm. Before this loading stage, the relative out-of-plane displacements are of 0.35mm.

The damage in UM model started to develop since test input of 100% (0.51g) for all the façades, but contrarily to RM model, the first cracks appear in both stories and with considerable length. These cracks are mainly associated with shear behavior, being the reason for having small out-of-plane displacements at low input tests. Complementary to the diagonal cracks, are the shear sliding cracks developed along the perimeter of the building, which contribute to important global out-of-plane displacements (slabs level).

3.6.2.3 Biaxial displacements

Another interesting measurement was made with the Position Sensitive Detectors (PSDs) or Hamamatsu cameras, which measure the global displacement path at one specific point. These devices were located at the north-east and south-west corners of the two slabs in addition to the one located at the base foundation of the models. Figure 3.29 shows an example of the recorded signals made with the Hamamatsu units for the slabs displacements during test run of 250% for both buildings.

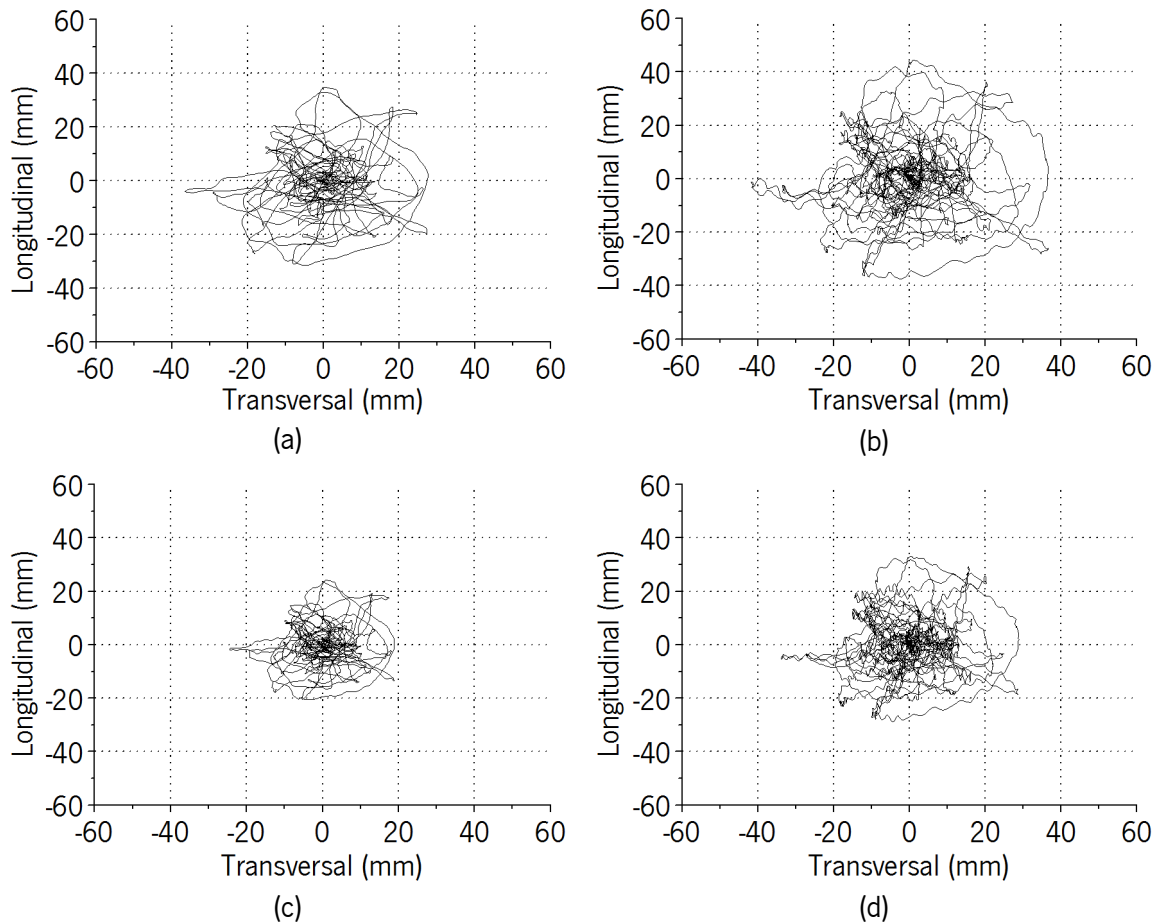


Figure 3.29 - Biaxial displacement trajectories in the horizontal plane at north-east corner for test run of 250% in: (a) RM model at second story, (b) UM model at second story, (c) RM model at first story and (d) UM model at first story

The displacement trajectories are plotted in terms of North-South displacement vs East-West displacement (longitudinal vs transversal directions). With this type of graph, it is possible to observe what was the path followed by the buildings corners second by second, during all the seismic inputs. Furthermore, the actual displacements amplitude developed on the buildings due to the signal imposed can be easily appreciated. In addition, one PSD was placed at the base so that amplitude parameters and correlations with previous displacement can be validated. These graphs can also be used to observe the phase relationship between signals. Then, if the two orthogonal signals were in phase, the trajectories will be a diagonal line inclined 45° , when they are not in phase the line opens

into an ellipse as phase difference increases. If the ellipse becomes into a circle it means that the phase difference is 90° and so on.

On the plots, it is possible to verify that the use of the two uncorrelated artificial seismic inputs provides a response that covers all directions with a smooth envelope and a few preferential directions not aligned with the model axes. This behavior is desirable, as it represents what happened during real seismic events. The differences of the responses of the buildings when are subjected to the same seismic input is also clear (the RM model attained a $PGA=1.26g$ and UM model a $PGA=1.33g$). The results show a stiff RM model with lower displacement amplification of the input signal in well define curves and a UM model with higher displacement amplification in both levels, as already discussed, but with weak curves.

3.6.2.4 Amplification factors from the displacements

Similarly to the acceleration amplification factors, the displacement amplification factors were obtained from the ratio between the peak displacements recorded at the floor levels and the peak displacements recorded at the base of the models. For this analysis, the PSDs records were used, taking advantage of the accuracy of these devices regarding global displacement measurement method. Then, the biaxial displacements (discussed in 3.6.2.3) of every corner at each floor were analyzed. The evaluation of this parameter was made in terms of the opening range from those biaxial displacement trajectories. The evolution of the amplification displacement factors can be observe in Figure 3.30 for both RM and UM models. Here, the first letter (N or S) refer to a north or south directions, the second (T or B) refer to the second (top) or first (bottom) slab and the last one (R or U) for RM or UM buildings, respectively. The PGA for each seismic input is presented in dotted vertical lines on which the amplification factors for each level and each building are plotted.

In terms of displacement amplification factors, the trend is quite different from the one obtained for the acceleration amplification factors. In case of the RM model, the displacement amplification factors only slightly increase up to the test run of 200% in both directions, followed by a sharp decrease for the test run of 250%, after which slower reduction occurs up to end of the test. In this building, there is no difference on the displacement amplification between the first and second floor before the onset of damage. On the other hand, after the onset of the damage, it is observed that the amplification of displacement at second floor remind similar but the ones at first floor are rather low, mainly at north corner, when compared to the values obtained in the second floor. This behavior is associated to the predominant propagation of damage at the first floor level on this building. In case of the UM model, it is observed a remarkable difference between the north and south corner in both longitudinal and transversal directions. At north corner are registered important differences between the first and second floors, whereas at south corner almost not differences were found.

Contrarily to the RM model, there is not much variation of the amplification factors until the seismic input of 200%, after which there is a generalized increase. This increase is associated to the characteristic sliding mechanism occurring in the UM model. The large difference in the

amplification factors between the first and second floor levels of north and east walls, contrarily to what happened in south and west walls indicates that the UM model experimented rotation.

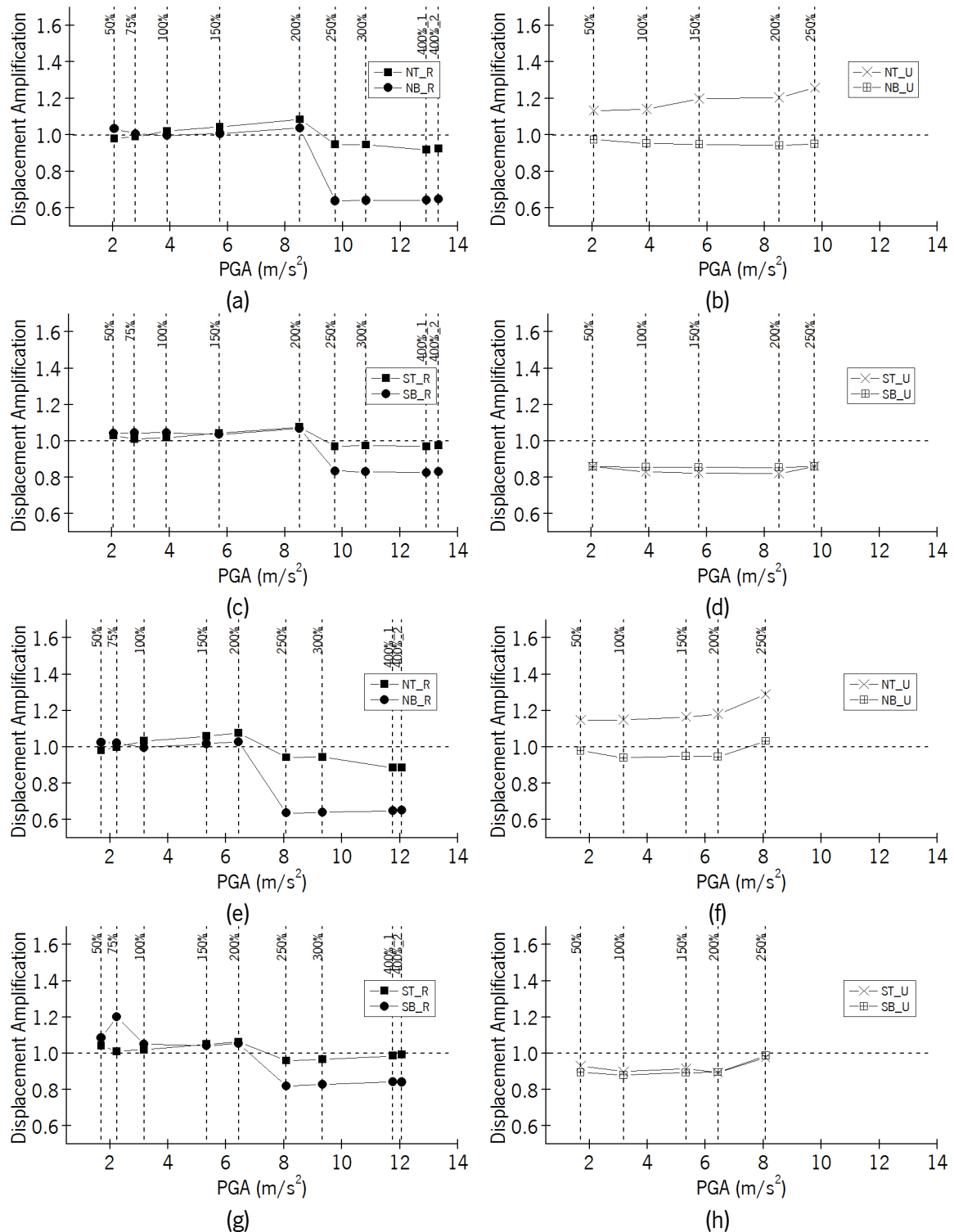


Figure 3.30 - Displacement amplification versus PGA: (a, b, c, d) longitudinal direction and (e, f, g, h) transverse direction

3.6.2.5 Local displacements

Local displacements are measured through linear variable differential transducers (LVDTs) according to the configuration shown in Figure 2.21a, which allows for the discussion of diagonal crack opening occurring in the masonry piers as well as in the north wall. Selected results for the RM and UM models are summarized in Table 3.4 (one per pier). Similarly, to the Hamamatsu devices, the LVDTs recorded positive and negative displacements, corresponding to tensile and compressive diagonal fields. The results obtained refer only to in-plane deformation and mainly measure the diagonal crack opening.

Table 3.4 - Maximum values of the displacements measured by LVDTs (in mm)

	LVDT 1		LVDT 4		LVDT 5		LVDT 9	
	RM	UM	RM	UM	RM	UM	RM	UM
50%	1.12	0.93	0.43	0.11	0.38	0.53	0.85	1.58
75%	1.98	-	0.86	-	1.03	-	1.05	-
100%	1.42	1.92	1.22	0.28	0.39	0.79	0.80	3.47
150%	3.75	3.91	2.61	0.70	1.84	1.21	1.93	9.06
200%	-	5.22	-	2.42	-	2.13	2.62	30.17
250%	3.68	7.19	2.97	4.00	1.83	7.35	2.19	52.12
300%	4.29	-	3.19	-	2.76	-	2.39	-
400%_1	5.32	-	4.42	-	3.62	-	2.98	-
400%_2	5.94	-	5.30	-	3.73	-	3.34	-

The analysis of the results reveals that in accordance to the failure patterns found, the maximum diagonal displacements of the model were recorded in the UM model, particularly if one compares the values for the same seismic input loading. The maximum elongation of a given wall at low seismic input levels can be larger for the RM model, possibly due to existing cracking occurring while anchoring the model to the shaking table or early (non-visible) minor cracking induced in the joints by the reinforcement. For each pier the value at which the first visible crack appears are highlighted. An inverse relation between the width of the panel and the displacement needed to generate a crack is found (see LVDTs 1 and 4), while a direct relation is found with the pre-compression of the pier (see LVDTs 1 and 5).

On the other hand, it can be observed that the crack localization in masonry piers of the walls with openings in UM building occurs especially for the seismic input of 200%, corresponding to an increase on the displacements measured by the LVDTs, even if some piers cracked at a lower 150% seismic input (e.g. LVDT 4). This is confirmed by the crack patterns given before. The major diagonal crack was measured in the north wall of the UM model (LVDT 9), in which a central crack developed with some crushing at the wall toe. The displacements measured by LVDT 5 are not associated to diagonal cracking but to shear sliding along concrete block-mortar interface developed at the left top of the window opening of the west wall.

Finally, maximum values for RM building in the west façade; i.e. LVDTs 1, 4 and 5, are about 6mm while for UM building, are about 7.35mm. The damage on both buildings has been already

discussed in which RM presents much less cracking in comparison with UM. These results validate the implementation of steel reinforcement as solution, not only for the improvement in ductility, which directly improves the seismic energy dissipation, but also for the better distribution of cracks and even for the prevention of them at low seismic loads.

3.6.3 Base shear vs. displacement diagrams

The experimental base shear is given in terms of a base shear coefficient (BSC), calculated as the ratio between the base shear developed in the model during shaking (BS) and the weight of the model above the base W , as described in Equation 3.2. The base shear has been calculated as the sum of the inertial forces developed at each story. The typical base shear coefficient versus total drift hysteresis loops, corresponding to the test input of 100%, are presented in Figure 3.31 both for RM and UM building.

$$BSC = \frac{BS}{W} \quad 3.2$$

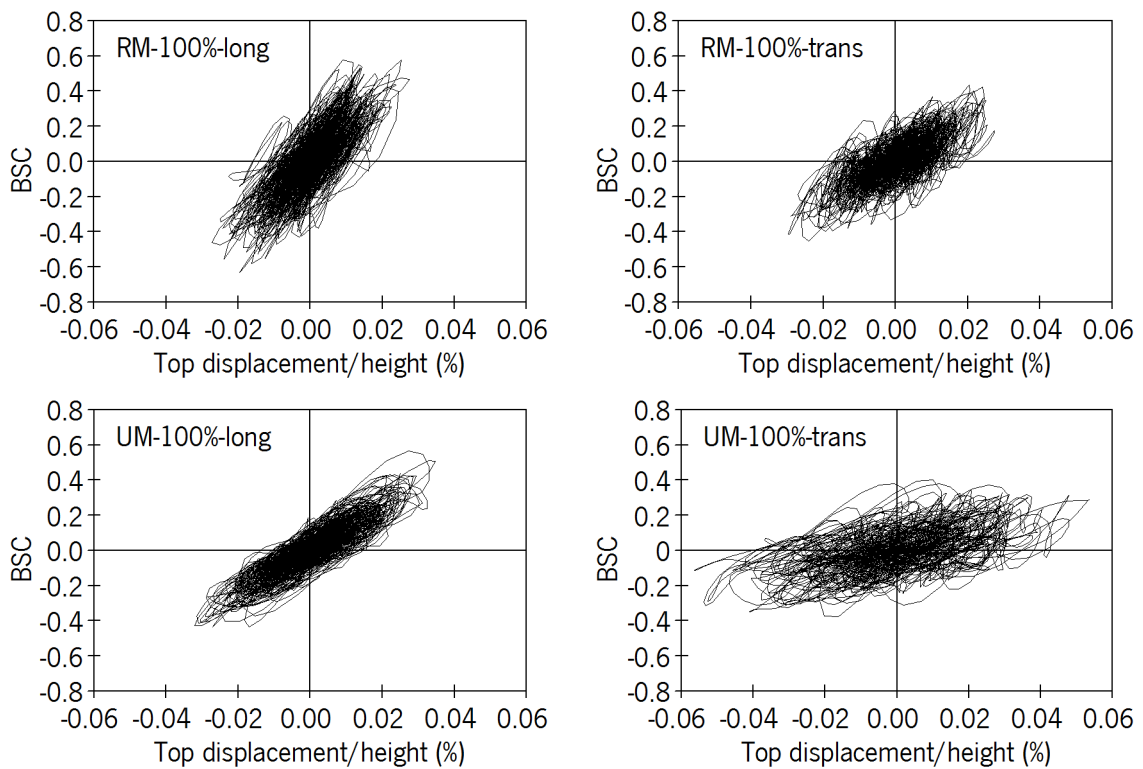


Figure 3.31 - Base shear coefficient versus top displacement/height in percentage for 100% seismic input

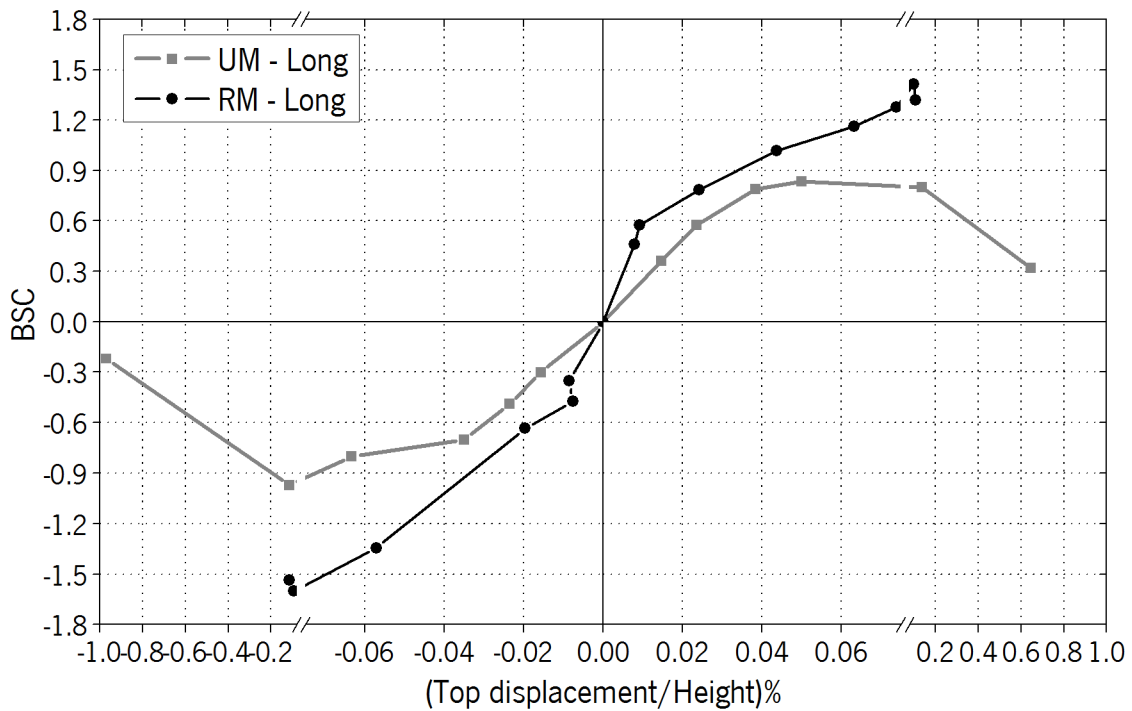
From these diagrams it is possible to observe that for the 100% loading stage the stiffness of the RM model is higher than the stiffness of the UM building, both in the longitudinal and transversal directions, due to the higher level of damage in the UM model. This results also in larger displacements of the UM model. The behavior of the models in the longitudinal and transversal direction is rather distinct, being both models stiffer in longitudinal direction than in the transversal direction. The displacements obtained in the transversal direction for the UM model are considerably

higher than the ones found in RM model, which can be to a certain extent attributed to the shear sliding mechanism occurring along continuous bed joints. According to Vasconcelos et al. (2012) the shear modulus increases if vertical reinforcement is added to the model. For this loading stage, the hysteresis loops found for the UM model involves more energy dissipation, particularly in case of the transversal direction, due to the predominance of a sliding mechanism.

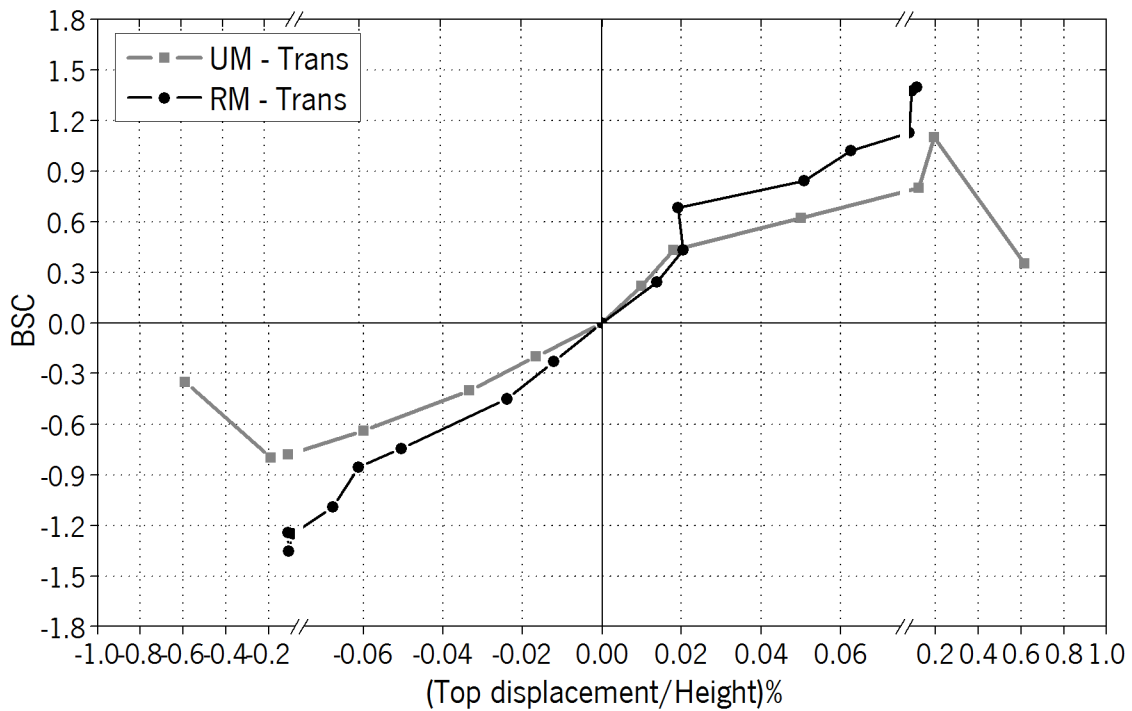
To summarize all the capacity behavior of the buildings a hysteresis envelopes covering the results for all the input tests was made. Figure 3.32 presents these hysteresees for both buildings in the two main directions. It should be noted that the horizontal scale of both graphs has a break in order to make easier the representation of all the complete curves in one single plot. The curves validated all the discussed results until now. It is observed the stiffer behavior of RM building in all directions and even in the positive and negative buildings' positions.

At the same time, it is observed the less displacement maximum values obtained in comparison with the UM building. The RM model presents a well-defined initial linear stiffness, which after the input of 100% started to decrease. This is in concordance with the onset of cracks in this model. The first two seismic inputs induced few changes in the displacement behavior. However, after the crack initiation, the loading imposed to the model influenced considerably the displacement response. In the longitudinal direction, it seems that the curve starts to behave in the nonlinear regime, seeming that the maximum BSC capacity corresponding to input of 400%₂ was smaller than the previous ones of 400%₁. On the transversal directions is not clear the onset of the nonlinear regime. From the diagrams, it can be also observed that the UM building presents less load capacity in comparison with RM building, as expected, but higher displacement behavior for much less seismic input (250%). On this model, it was clear that the maximum capacity load was attained for both directions and in all positions; i.e. positive and negative, with maximum capacity load for the last test lower that previous test.

In general, the behavior presented in longitudinal and transversal direction is quite similar in terms of both BSC capacity and displacements. This building presented considerable damage at early stages distributed around all walls and levels, which increased remarkably through the tests progression. As observed, in the last test of 250%, besides the loss on resistance capacity, the building presented a considerable increment in its displacement response. These values suggested that another input of the same magnitude or higher would cause an imminent collapse of the structure.



(a)



(b)

Figure 3.32 – Experimental hysteresis envelopes curves for RM and UM buildings: (a) longitudinal direction and (b) transversal direction

3.7 Conclusions

Two reduced 1:2 scaled models with symmetric geometry in plan and in elevation were built, one in reinforced masonry and the other in unreinforced masonry. The models were subjected to increasing seismic input loading induced in a shaking table, from which it was possible to study their dynamic

properties and to record the crack patterns, accelerations and deformation features. From the results obtained, the following conclusions can be pointed out:

- The RM and UM models exhibited a very distinct behavior concerning the crack and deformation patterns. The use of horizontal and vertical truss type reinforcements clearly improves the seismic response of concrete block masonry, leading to adequate structural robustness for very high seismic loading. The combination of vertical and horizontal reinforcement, about the minimum required by Eurocode 8 (2004), increased the capacity of the masonry building to, at least, about the double. Still, the UM model provided very good capacity for moderate to high seismic loading, together with a ductile failure mode with enough capacity for vertical loading even after major damage. The results confirm the adequacy of modern unreinforced masonry, with robust units, to withstand seismic loading.
- Cracking of the RM model is concentrated at the first floor and is composed of smeared diagonal cracking on the masonry piers between window and door openings. Almost no damage is observed at the second floor. The addition of steel reinforcement led to this distribution, avoiding concentration in specific locations of cracks.
- In case of UM model, cracking develops at first and second floors as long horizontal and diagonal stepped cracks in the masonry piers and in the north and south walls at the concrete block-mortar interfaces. Damage in the units occurs at the corners (compressed toes), where crushing was found. Sliding movements developed along the continuous bed joint cracks but also along the diagonal cracks. Considerable collapse of units occurred for a load of 2.5 times the reference PGA value for Lisbon, Portugal, and in spite of the extreme damage developed with large lateral drifts, failure for a PGA associated to moderate to high seismicity was rather controlled.
- The proposed constructive solution, when applied for the constructions of medium residential symmetric buildings, with concrete block unreinforced masonry, performed rather well and can be a competitive solution for medium size and regular buildings in regions of moderate to high seismicity, or regions where mistrust about the seismic performance of modern unreinforced masonry holds.

Chapter 4

Experimental investigation of asymmetric masonry buildings

Abstract

This chapter continues with the experimental validation of the masonry building system in analysis. The study of the symmetric geometrical configuration in plan and in elevation for reinforced and unreinforced masonry buildings revealed valuable information regarding its seismic performance. Now, an asymmetric geometrical building's plan configuration is considered. Similar test procedures and methods carried out for the symmetric buildings have been adopted on the asymmetric ones. Thus, dynamic tests of two identical two-story concrete block masonry buildings with asymmetric plan geometry configuration were performed on a shaking table in reduced scale 1:2, with focus on the global behavior. Both models were tested by imposing uncorrelated artificial accelerograms compatible with the elastic response spectrum defined by the Eurocode 8 (2004) in the two orthogonal horizontal components, and the inputs were applied incrementally to the buildings. The first model was tested in reinforced conditions (RM), while the second building was tested as an unreinforced solution (UM).

From the experimental campaign, the analysis of buildings' dynamic properties together with their seismic performance in terms of accelerations and displacements will be discussed. Additionally, damage patterns and correlation with stiffness degradation will be studied. Finally, conclusions relating their structural capacity with the global dynamic behavior and comparisons between the results of the two buildings will be presented.

4.1 Introduction

Nowadays, modern concepts for open spaces and free areas are present in buildings architecture, resulting in geometrical setbacks (re-entrant corners or edge recesses) and uneven distribution of openings (doors and windows), mainly for residential buildings. This results in asymmetric configurations of the current residential building constructions. Codes like Eurocode 8 (2004) and Eurocode 6 (2005) impose limitations in terms of geometry plan layouts in order to maintain structural simplicity and bi-directional resistance together with stiffness, including the resistance capacity to rotational movements caused by torsion.

Few recent studies are available in the literature related to the analysis of the asymmetry of masonry buildings subjected to seismic loading. Juhásová et al. (2008) performed shaking table tests on an asymmetric one story stone masonry building reinforced with polymer grids in order to assess the performance of the reinforcing technique in the increase on the seismic resistance, ductility and control of damage. The seismic response of the original building included the contribution of large out-of-plane deformation of walls. It was found that the response of the repaired model exhibit smaller increments of absolute accelerations and relative deflections in comparison with the response of the original model. Bairrão and Falcão Silva (2009) carried out experimental shaking table tests on an asymmetric limestone masonry building. The structure presented considerable damage at the bottom of the walls and at the corners of the openings with random distribution at the joints. More recently Tomažević and Gams (2012) studied the seismic behavior of asymmetric confined masonry buildings by using the shaking table. Two buildings, one of three stories and one of four stories were tested. In all cases, typical shear behavior was observed, with diagonally oriented cracks in the walls of the first story, determining the failure mechanism. All models exhibit good seismic behavior, with adequate resistance and energy dissipation. The authors proposed typical design values for displacement capacity and structural behavior factor.

Based on the limited studies regarding the effect of the torsional movements induced by the complexity of geometry in plan on masonry buildings, it is important to have a better insight on their influence in the seismic performance of masonry buildings. This is an issue, particularly in case of new masonry systems, for which stronger architectural demands can be required.

4.2 Objectives and methodology

As discussed in the previous chapter, modern regular geometry masonry buildings seem to behave well in low to moderate seismic hazard zones. In particular, the maximum resistance of the reinforced concrete block masonry building tested in the shaking table was not achieved due to limitations of the table. As the previous buildings were symmetric, the torsional effects were only the result of the non-symmetric distribution of damage. In general, buildings have to resist large intensity ground motions, which induce inelastic deformations. In particular, asymmetric buildings undergo coupled inelastic lateral and torsional deformations that could be the governing factors for their design. Then, the effects and combination of in-plane and out-of-plane displacements can

excessively accelerate the damage in this type of buildings and considerably reduce the time of evacuation for occupants.

The main objective here is to obtain the seismic performance of asymmetric masonry buildings built with the construction system under study. Thus, this chapter is focused on the analysis of the seismic response and performance assessment of residential masonry buildings with non-symmetric in plan geometry. From the results, it is expected to get a better insight on the influence of in plan eccentricities on the resistance and deformation parameters of the masonry buildings.

To accomplish these objectives, two two-story concrete block masonry buildings were planned. Similarly, to the symmetric buildings, one of the buildings is made with unreinforced masonry and another one has the same reinforcing system composed of truss type reinforcements at the horizontal and vertical continuous joints. It was intended that the buildings presented asymmetric plan configuration, from which torsional behavior is expected. Additionally, the buildings have irregular distribution of openings at both levels.

The methodology followed in the shaking table testing of the symmetric buildings is the same as the used for the asymmetric buildings (see Chapter 3). The seismic inputs are imposed to the models in two directions (longitudinal and transverse). Through the incremental seismic inputs, the identification of the dynamic parameters is carried out aiming at defining indicators that characterize the damage patterns of the buildings. The damage patterns and the main parameters characterizing the seismic behavior of the masonry buildings are provided. Finally, it should be mentioned that, identically to the symmetric buildings, all results discussed in this chapter are related to the scaled models. Therefore, Cauchy similitude law presented in Table 2.1 can be implemented in order to obtain the prototype 's values.

4.3 Validation of the seismic input - Theoretical input vs. real input

4.3.1 Signal processing

The quantitative analysis of the seismic behavior of the asymmetric buildings includes the records obtained by the accelerometers, the Position-Sensitive Detectors (PSDs) and the Linear Variable Differential Transformers (LVDTs) during each seismic input (Figure 2.21 c and d). Additionally, the response of accelerometers is also taken into consideration during the dynamic identifications. The signals processing was carried out through the software LNEC-SPA (2007) following the same strategy adopted in the symmetric buildings.

For the analysis of the present asymmetric buildings, a band pass Fourier filter between 0.6Hz and 40Hz was applied for the removal of the quasi-static components and noise to all the acceleration signals after each seismic input. The procedures for the other parameters of scale, noise reduction and offset correction were similar to the ones performed for the signals recorded from the symmetric buildings.

A favorable observation, after the signal processing performed on the data acquired in the asymmetric buildings, was the considerably reduction in the signals failure, mainly from the

accelerometers. The loss of signals dropped almost to zero, resulting in better signals profiles and allowing more confidence on the analysis. On the asymmetric buildings, the accelerometers were fixed with screws to the models instead of glue (as done in the symmetric models), obtaining reliable results and the final positive increment in the quality of plots.

4.3.2 Analysis of the seismic inputs

Following the procedure adopted in the symmetric buildings, the seismic input was applied by phases, considering increasing percentages of the reference seismic input corresponding to the seismic input in the region of Lisbon, for rock. Table 4.1 summarizes the input tests sequence for both models (RM and UM models), characterized by the peak ground acceleration (in SI units) in both longitudinal (NS) and transverse (EW) directions.

Table 4.1 - Input series and corresponding PGA for the asymmetric buildings

Test	Reinforced model		Unreinforced model	
	PGA NS (m/s ²)	PGA EW (m/s ²)	PGA NS (m/s ²)	PGA EW (m/s ²)
25%	-	-	1.16 (0.12g)	0.89 (0.09g)
50%	2.57 (0.26g)	1.63 (0.17g)	2.50 (0.26g)	2.31 (0.24g)
75%	3.83 (0.39g)	2.91 (0.30g)	3.25 (0.33g)	2.79 (0.28g)
100%	4.72 (0.48g)	3.90 (0.40g)	4.57 (0.47g)	4.05 (0.41g)
150%	6.51 (0.66)	5.53 (0.56g)	6.45 (0.66g)	10.46 (1.07g)
150% 2	-	-	6.44 (0.66g)	12.19 (1.24g)
200%	7.80 (0.79g)	7.59 (0.77g)		
250%	10.42 (1.06g)	9.32 (0.95g)		
300%	11.92 (1.21g)	9.33 (0.95g)		
300% 2	12.80 (1.30g)	9.77 (1.00g)		

On the reinforced masonry building, a second test of 300% was imposed to the model to evaluate the progress of damage of the building, taking into account that considerable damage was obtained for the first test of 300%. However, this test of 300%² was stopped at about 50% of the input signal due to the imminent collapse of the structure. On the unreinforced masonry building, a test of 200% was planned but due to a mistake, the same seismic level was introduced (150%). This seismic input corresponded to a damage level close to the collapse and it was decided to stop the experimental campaign.

The reliability of the shaking table to represent the artificial inputs introduced is validated through the comparison of the theoretical input, given by the artificial accelerograms (Figure 2.22), and the output signals obtained at the base of the masonry buildings. This analysis is mandatory before any further analysis of results, so that it is possible to consider the seismic behavior of the buildings tested at the shaking table accurate. With this respect, it should be mentioned that the mechanisms and control system of the shaking table should attain an accurate representation of the given input, even if hardly, the same as the theoretical one. The analysis of the seismic response of the masonry buildings must be based on the real seismic inputs, which are the input signals registered at the

base of their foundations. The comparisons between imposed and recorded seismic inputs at the base of the models are made in terms of accelerations and displacements for each step of the loading history (Figure 4.1 and Figure 4.2). In the plots, AL and AT means acceleration in the longitudinal and transverse direction, respectively, and similarly, DL and DT refer to longitudinal and transverse displacements. RM and UM corresponds to reinforced and unreinforced masonry buildings, respectively.

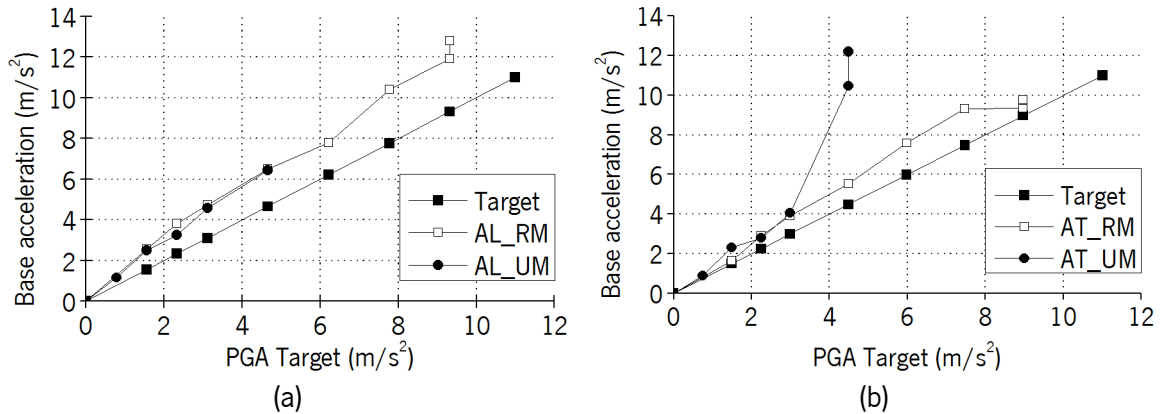


Figure 4.1 - Diagrams correlating the peak accelerations at the base of buildings and PGA targets: (a) longitudinal direction and (b) transverse direction

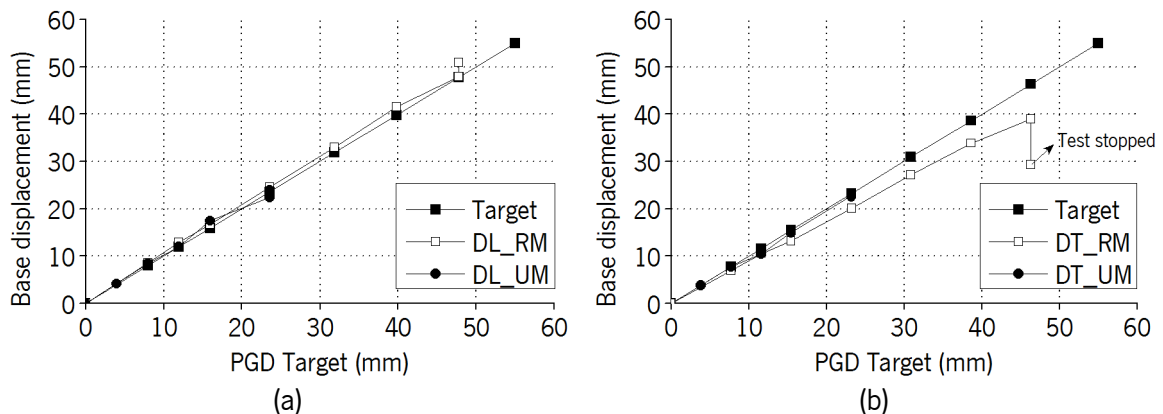


Figure 4.2 - Diagrams correlating the peak displacements at the base of buildings and PGD targets: (a) longitudinal direction and (b) transverse direction

The signals introduced in the shaking table correspond to the displacement time histories of the artificial inputs. Thus, most of the control performed by the system is based on displacements, however is not the only one. The system of the shaking table controls several variables like accelerations, velocities, frequencies and displacements, but as understandable, it is not possible to have the same grade of accuracy in all of them. The displacements are most of the time very well controlled by the system, being possible to obtain an excellent fitting with the expected inputs, which is also confirmed by the present results in terms of displacements, see Figure 4.2. This behavior is in correspondence to the results found in the symmetric buildings. For the present case, the displacements recorded in the longitudinal direction exhibit the best correlation with maximum differences of +8% for the RM building and +10% on the UM building. On the transverse direction, it

is found a maximum difference of -16% for RM building, if the last value obtained in input of 300%_2 is not considered, given that the test was stopped. Moreover, in the UM model a maximum difference of -10% was recorded in the same direction.

Regarding the accelerations, during the first four tests the input and recorded acceleration presented a good fitting. As observed, the recorded values are close to the target objectives. After the fourth test, the fitting of the input and recorded accelerations was not so good, being the recorded values always higher than the target accelerations. For the longitudinal direction, a difference of about +60% in both buildings was found. For the transverse direction, the RM model presented a maximum difference of +30%. The UM building presented abnormal peaks for the test of 150% and its repetition, corresponding to differences of about +133% and +172% for each test respectively. It should be mentioned that the good correlation on the displacements suggest that the shaking table's actuators attained the desirable displacements but with higher velocity rate than expected, generating a sudden change that produce the observed peaks in the accelerations. Finally, it is important to stress that a previous input calibration was performed on the shaking table with inert masses, representing the same weight of the buildings to be tested. However, those masses cannot represent the behavior of the models. Therefore, the actual inertial forces and real distribution of stiffness are not fully represented. As observed, the main differences were obtained during the final tests, in which the response of the table is largely influenced by these components, and their swift change due to damage.

4.4 Dynamic Properties

The dynamic characteristics of structures, namely natural frequencies, damping ratios and mode shapes are fundamental properties for the earthquake resistance design. These values are useful, among other, for future numerical model validation. The damping value gives an idea of how much the kinetic and strain energy of the vibrating system is dissipated. This dissipation is achieved by various mechanisms, which in most cases are difficult to be identified and evaluated, as many of them may be present at the same time. In a masonry building, for instance, these mechanisms can include the opening and closing of micro cracks and friction between unit blocks (head joints without mortar).

Similar modal identification process performed to the symmetric buildings was followed in the asymmetric buildings. Thus, input-output techniques were also used in these experimental models. The identification was done after each of the models were placed and fixed to the shaking table before any input seismic test. For it, the artificial white noise signals presented in Figure 2.23 (Chapter 3) were used as input. The data collected from the accelerometers placed on the models was analyzed by using the software LNEC-SPA (2007) to derive both the natural frequencies and damping ratios. Parameters like the type of window function and percentage of overlap were controlled in this process.

From the peaks of the frequency response function, the Half-Power bandwidth method has been used for identification of the damping ratios. The values found for the natural frequencies and

damping ratios are presented in Table 4.2. Here, again note that the directions are: transversal / East-West; longitudinal / North-South.

Table 4.2 – Dynamic properties

Model	Direction	F (Hz)	ζ (%)
RM	Trans	11.68	2.70
	Long	19.40	1.18
	Rota	22.32	0.93
UM	Trans	11.50	5.50
	Long	13.47	5.00
	Rota	21.77	1.65

From the analysis of results, it is possible to observe that both buildings presented very similar natural frequencies for the first and third directions (transversal and rotational modes shapes) even if the RM model present always slightly higher values. The most important difference is related to the second frequency, corresponding to a second translational mode shape in the longitudinal direction. These differences cannot be easily explained, as steel reinforcement has a low contribution to the elastic stiffness and the effect of filling of the vertical joints is not likely to be so large. Given the existence of many openings in the longitudinal walls, the difference can be due to execution aspects, the presence of micro-cracking around the openings in the UM model, with some effect of the additional vertical reinforcement at the opening borders and higher quantity of mortar at vertical joints.

The same data processed for the obtainment of the frequencies (43 accelerometers placed on each model) was used for the identification of the mode shapes. This identification was performed for each masonry building and was focused in global structural modes. The mode shapes found for RM building are presented in Figure 4.3, being also similar in case of UM model. It should be noticed that the first and the second mode shapes are practically pure translational modes, in the transversal and longitudinal directions. Nevertheless, for the second mode shape, it was observed a small local component at the windows of the second floor in the longitudinal walls. Here, some corners of the windows move in the transversal direction. Those movements were relatively small in comparison with the longitudinal global mode. The third mode shape corresponds to a torsional motion of the structure. During this mode, the building presented clockwise and anti-clockwise turning movements in which opposite walls in both directions move in anti-phase.

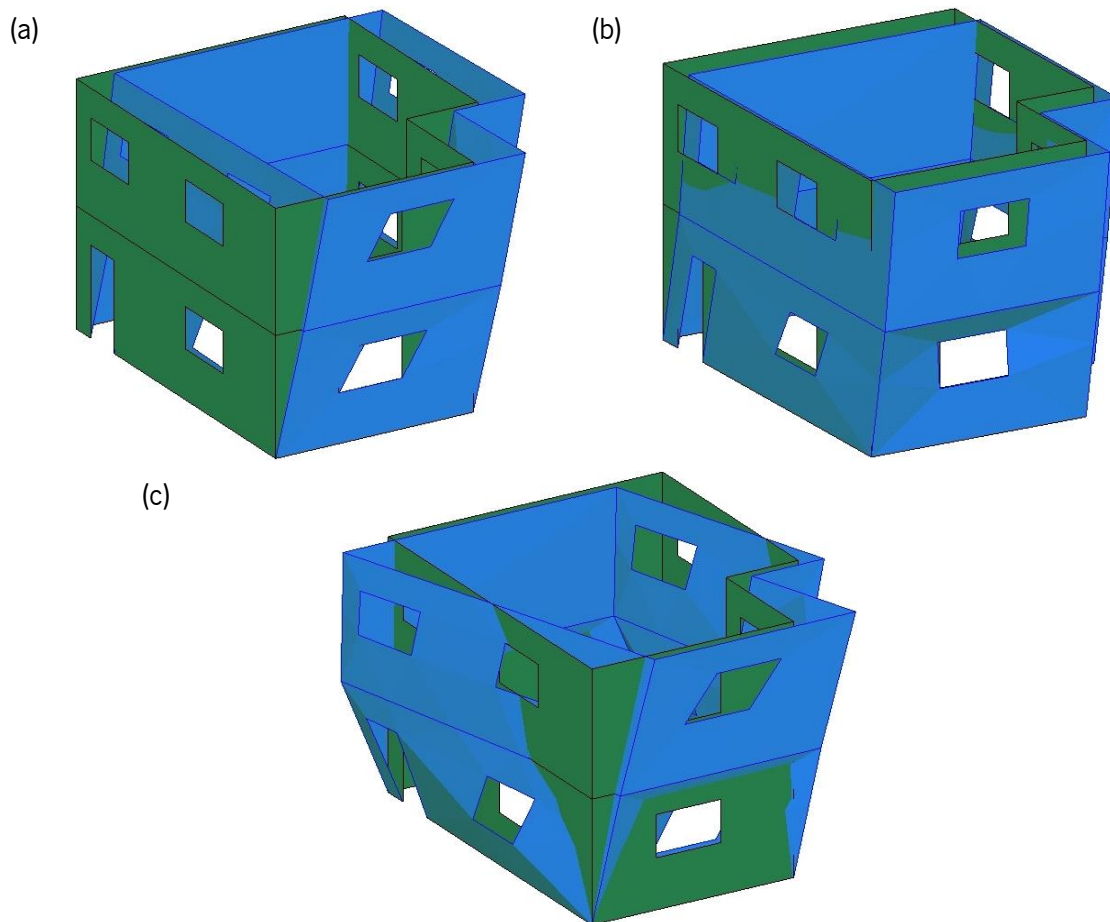


Figure 4.3 - Global mode shapes for both asymmetric masonry buildings: (a) first: transversal, (b) second: longitudinal and (c) third: torsional

4.5 Damage patterns and failure modes

This section aims at presenting and discussing the major features of the crack patterns that develop in both RM and UM models tested at the shaking table for the distinct seismic inputs. This discussion is based on a detailed visual inspection of the cracks, which were labeled with colors on the models. It should be noticed that cracks with different widths developed, being important to determine its relevance. Some cracks opened since early stages of the test and increased in length and width progressively in accordance with the increasing seismic inputs. At the end of the experimental tests, it was seen that cracks with many ranges of widths and lengths developed. Figure 4.4 shows an example of two different size cracks located in the same region (RM model). In some other cases, cracks exhibited an opening-close mechanism during tests, making their evaluations and final labeling more complex. Even if the maps with cracks for both models were defined after each seismic input, it is stressed that mainly cracks with widths higher than 0.3 cm were highlighted in the final stage of the loading.

Both buildings presented micro cracks during their transportation and fixation to the shaking table, mainly at the first rows of the first level. Those fissures were registered, labeled and followed during the experimental tests. At the end of the experimental campaign, it was concluded that there was no influence of the previous fissures on the final patterns and damage.

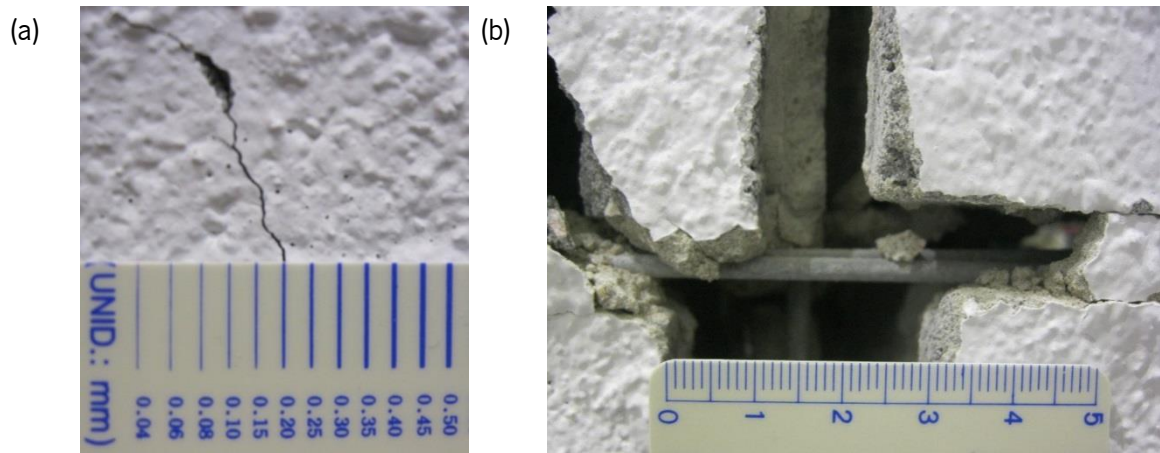


Figure 4.4 – Different crack widths developed in the RM model

4.5.1 RM model

In order to make the detailed description of cracks easily identified the north façade that contains the windows is called “north 1”, the north façade without any opening is called “north 2”. Similarly, the west façade, that contains only windows, is called “west 1” and the west façade that contains the door at the first floor is called “west 2”.

Even if a first shaking table test with a seismic input of 50% (0.26g) was carried out in the RM model, the first visible damage occurred only for the test of 75% (0.39g) at the first floor. Very few, small (maximum 10 cm length) and thin horizontal cracks opened at the first floor (all walls, except for wall north 2) together with small stepped cracks along the vertical and horizontal mortar joints in the façades with openings, see Figure 4.5. The additional damage found for the test of 100% (0.48g) is composed of a horizontal crack at the intersection corner of walls west 1 and north 2 connecting two small stepped cracks. The damage progressed for the test of 150% (0.66g) with the increase on the size of the previous developed cracks at the first floor and new other cracks developing mainly in the west 2 wall. New stair stepped cracks developed at the bottom of the pier between the door and window openings together with three horizontal cracks in the left pier of the door. In the east wall, a new diagonal crack develops in the pier in the right side of the window (between the window and the wall’s corner) at the first floor. No damage was recorded in the second floor. The input test of 200% (0.79g) considerably increases the damage at the first level, but no damage was seen in the second floor. Several stepped cracks develop in the piers between openings, particularly in the north wall (north 1) and east wall and at a minor extent in the west wall. The diagonal cracking along the block-unit interfaces results from lateral loading and its amount should be associated to the redistribution of forces promoted by the presence of reinforcements.

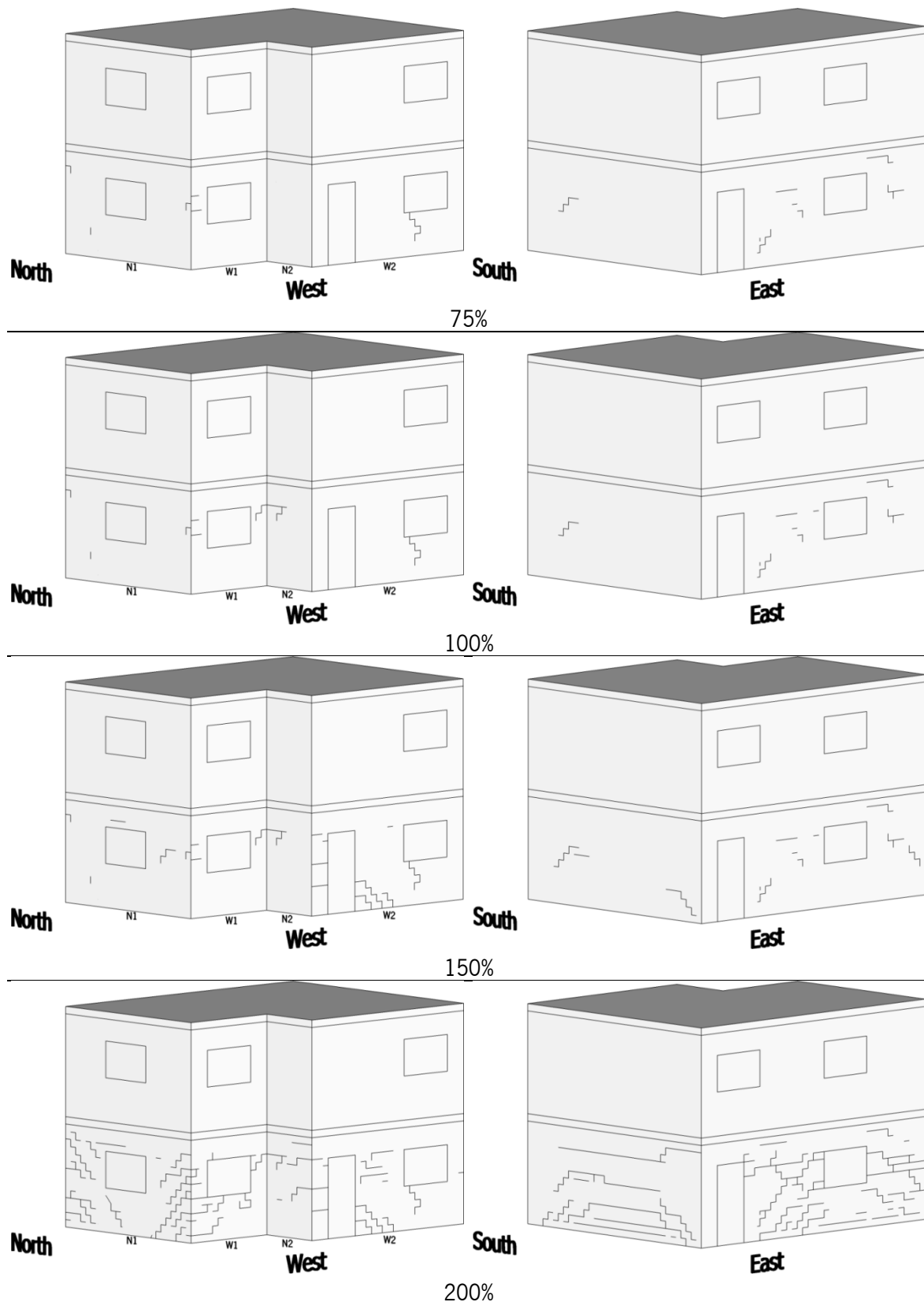


Figure 4.5 – Damage observed after each seismic input test for the RM model (from 75% to 200%)

Besides the diagonal cracks, important horizontal cracks at the bed joints developed, namely: (1) five long cracks at the south wall (first floor) at different levels: three bed joint cracks in the first third of the wall, one crack at mid height (length of 160cm) and another one at three courses from the

slab of the first floor (length of 210cm); (2) in the east wall at the piers between the door and window and between the window and the right corner. The top horizontal crack developed in the previous test in the left side of the door opening in the west wall, connects to the horizontal crack developed in the wall west 1, reaching the top right corner of the window. Another horizontal crack develops in this wall connecting the left corner of the window and the left corner of the wall. Even if not properly relevant, the first cracks at the second floor developed for the seismic input of 250% (1.06g), see Figure 4.6. Additionally, an extension of the previous damage was observed at the first floor for all walls.

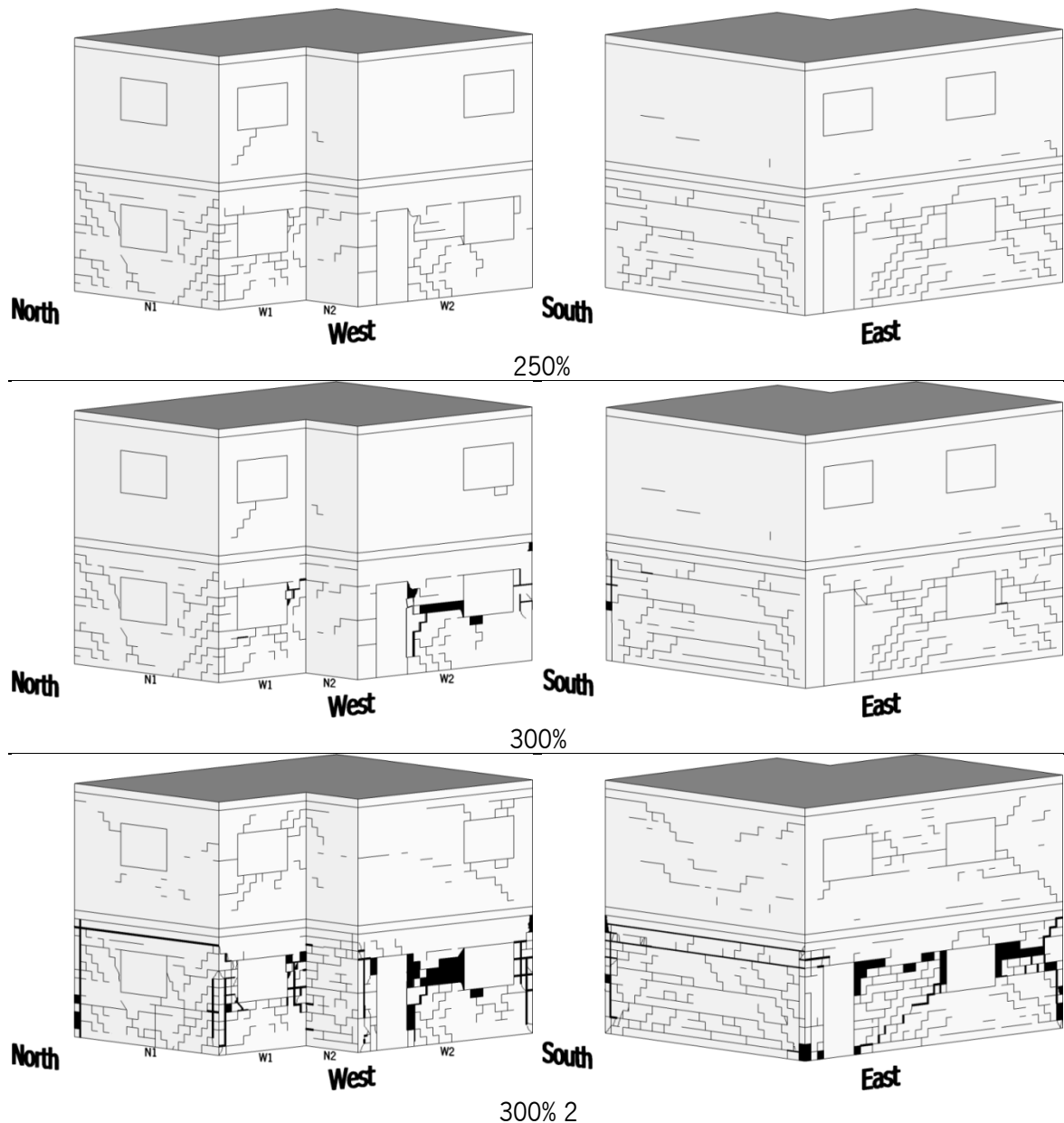


Figure 4.6 – Damage observed after each seismic input test for the RM model (from 250% to 300%)

At the this loading stage it was observed the increase on the opening of previously formed cracks and the development of new diagonal cracks, particularly at the west, east and south walls. In the latter wall, the stepped cracks developed from the previous bed joint long cracks. Besides, the length

of the horizontal cracks increased. Additional horizontal cracks develop in the east walls, being the cracks developed one course from the slab and coming from the right corner. A vertical crack developed in the wall west 1 in the bottom left corner that connects with the north wall, in correspondence with the continuous reinforced vertical joint. The first cracks affecting unit blocks were found for this loading stage at the east wall at the borders of the openings and in particular at the upper right corner of the door and at the bottom left corner of the window.

The RM building suffered an important extension of damage for the input of 300% (1.21g), with increasing openings of the previous cracks, particularly at the first floor, as in the second floor the progression of damage was not so significant in relation to the previous input. The west wall presented crushing and loss of blocks in the masonry piers. The wall west 1 shows crushing of units at the upper right corner of the window at the first level and severe deterioration of horizontal mortar joints in the surrounded area. The detachment of masonry units was more severe in the wall west 2 in the pier between the door and the window, see Figure 4.7. The detachments of the masonry units in the central part of the pier resulted also in the increase on the opening of the crack at the vertical continuous joint in the border of the door. It was observed that the piers slide along the horizontal joints, which together with the out-of-plane movements of the wall pulled away the unit blocks. In the South façade an important vertical crack opened at the reinforced vertical joint of the corner with wall West 2.

The repetition of the seismic input of 300% (1.30g) was decided to evaluate the progress of damage in the second floor, even if the first floor was already with important damage. However, the seismic input was stopped at about 50% of its original total duration due to the eminent collapse shown by the building. According to Figure 4.6, an important increase on the damage was observed at first floor with crushing and detachment of masonry units mainly at the walls with openings (east and west walls). A view of the crushing of the concrete blocks in the right border of the window of west wall is presented in Figure 4.8. At this stage of loading, the openings of crack reached great values, particularly in case of walls with openings as can be seen from Figure 4.9, where the final state of diagonal cracks is shown, with loss of mortar at the bed joints.

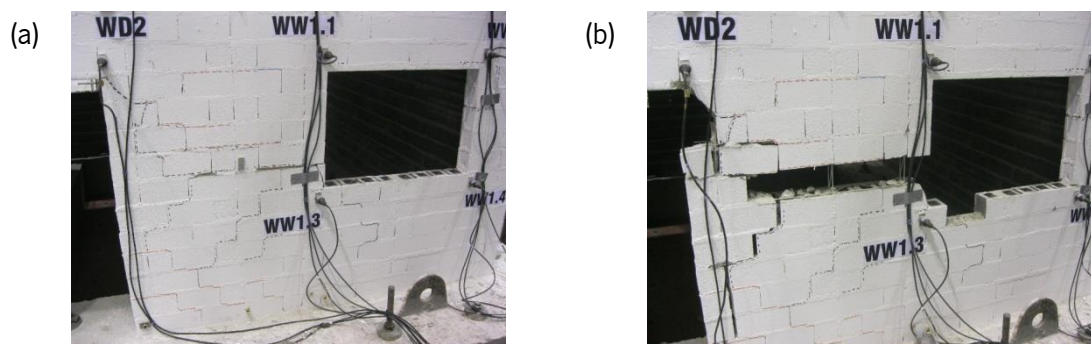


Figure 4.7 – Wall west 2 at first level after seismic input of: (a) 250% and (b) 300%

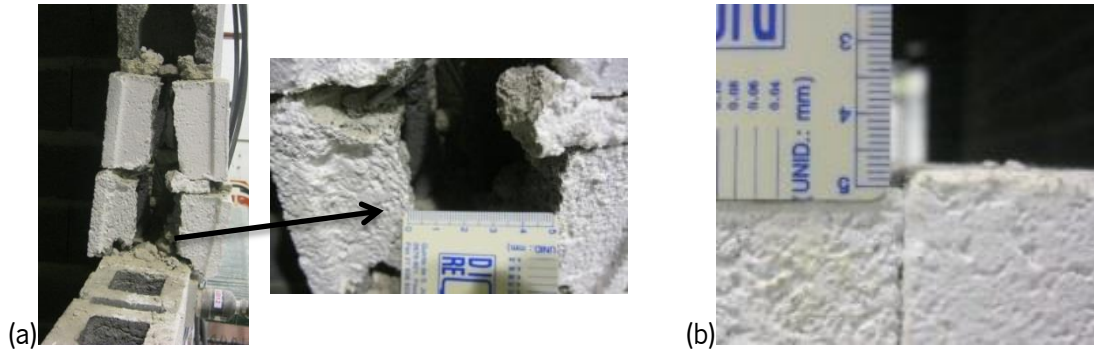


Figure 4.8 – Crush failure (west wall) during seismic input of 300% 2

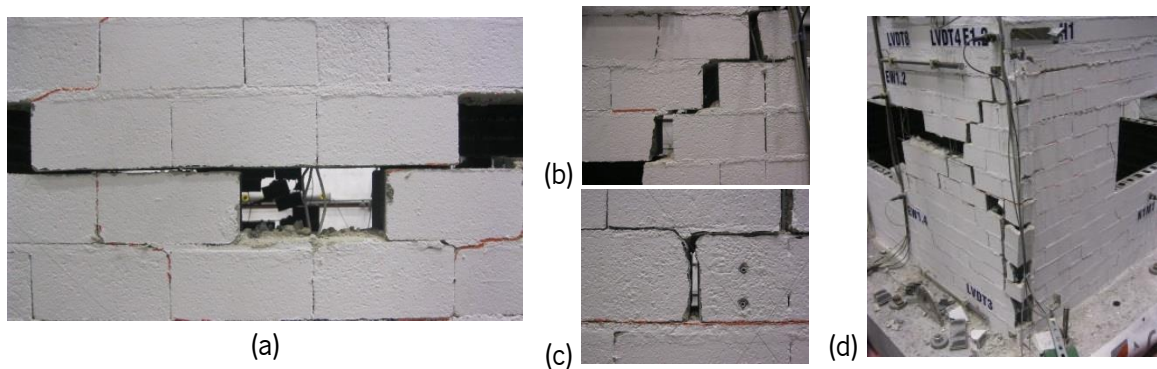


Figure 4.9 – Lost of mortar joints at the first floor of the east wall: (a) left pier of the window; (b, c and d) right pier of the window

The extreme loading condition of the building in the longitudinal direction resulted in the predominance of the out-of-plane resisting mechanism of the south and north transverse walls, leading to the increase on the openings of the horizontal cracks and to its instability. The combination of those mechanisms motivated to stop the test from the control room, avoiding the total collapse of the structure and protecting all the equipment. In Figure 4.10, some deformation and cracking developed on the south and north walls after the repetition of the seismic input of 300% (1.30g) can be observed. In both cases, there is a trend for the out-of-plane detachment of the masonry units and separation of the intersecting walls at the connections. The complete separation between the north and south walls in relation to the west and east walls was avoided by the existing vertical reinforcement and particularly to the horizontal reinforcement that was anchored at the corners. In Figure 4.11, some images of the deformation of the vertical and horizontal reinforcement are shown. It was common to observe lateral instability of the vertical reinforcements related to the shear resisting mechanisms developed in the walls, resulting in the dowel effect of these reinforcements. Furthermore, the contribution of the reinforcements for the resistance is also seen by the yielding of the horizontal reinforcements, resulting in the failure of the welding, these types of failures were also common in the tests carried out by Haach et al. (2010) in shear walls under static-cyclic in-plane loading.

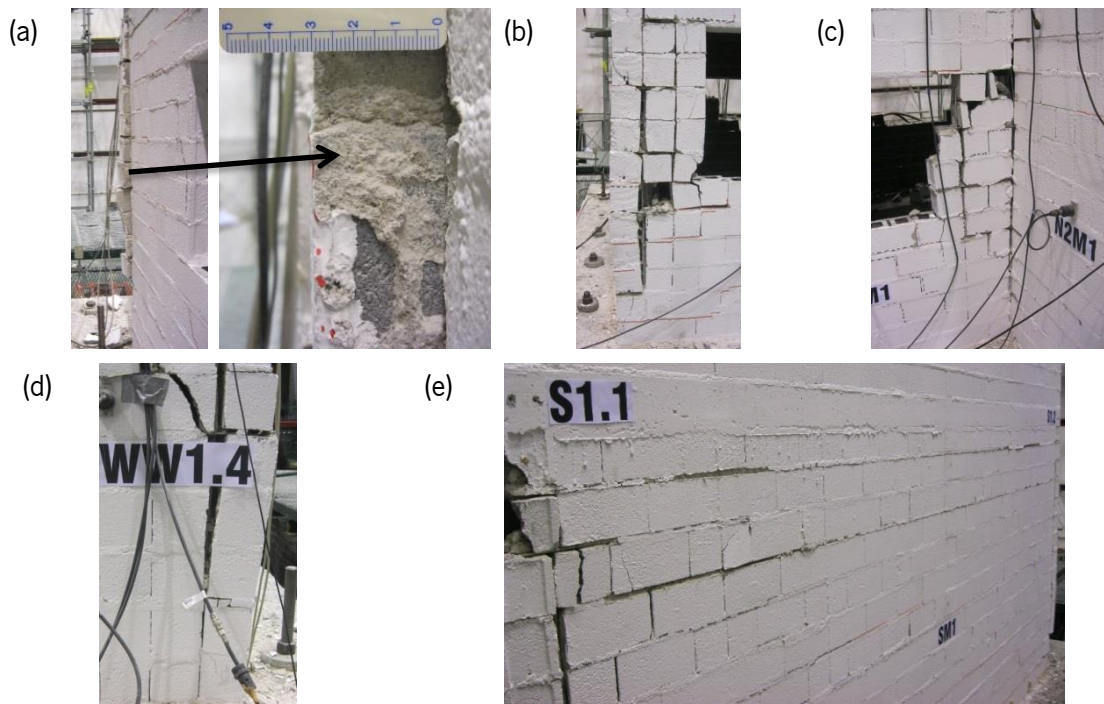


Figure 4.10 – Out-of-plane failures; (a) separation of the north wall at the corner with the east wall; (b) left pier of west 1 wall (c) out-of-plane detachment and separation of the west 1 and north 2 walls; (d) separation between west and south wall; (e) out-of-plane cracking at the south wall

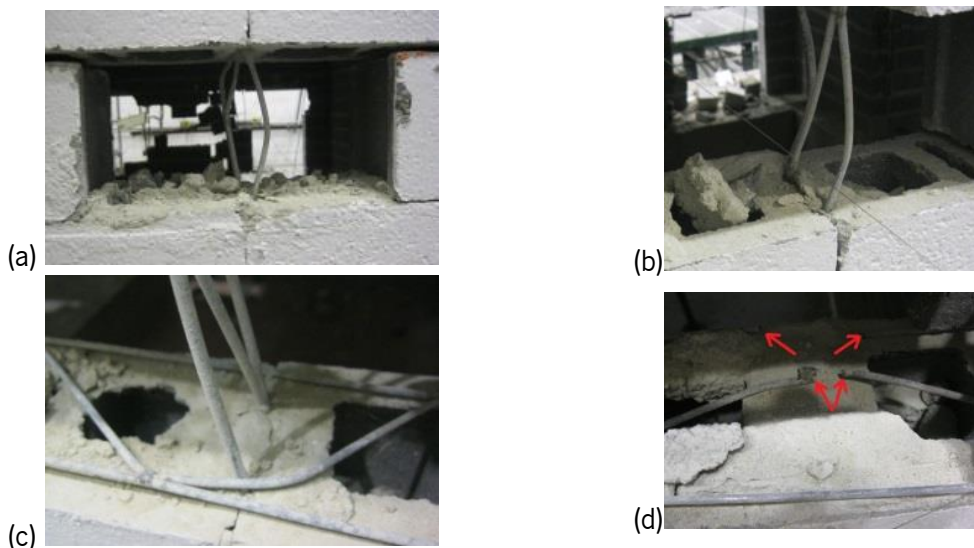


Figure 4.11 – Damage on steel; (a and b) dowel effect in vertical reinforcement; (c) deformation on horizontal reinforcement due to cycle movements; (d) failure of horizontal reinforcement at welding connection

After a detailed visual inspection of all the structure, it was also found that this input test caused considerable damage at the second level, characterized by many stepped diagonal cracks in all the walls (with and without openings) and some horizontal cracks, mainly in the west and south walls. It should be noticed that the opening of these cracks is considerably smaller than the opening of the majority of cracks developed in the first floor, being only visible at short distance. Figure 4.12 gives a view of the state of the building after the final seismic input, showing that the second floor appears

rather intact. The important of a system that allows the slab to redistribute loads to increase the robustness of the building is clearly demonstrated. In this case, an embedded ring beam combined with a solid concrete slab was used.

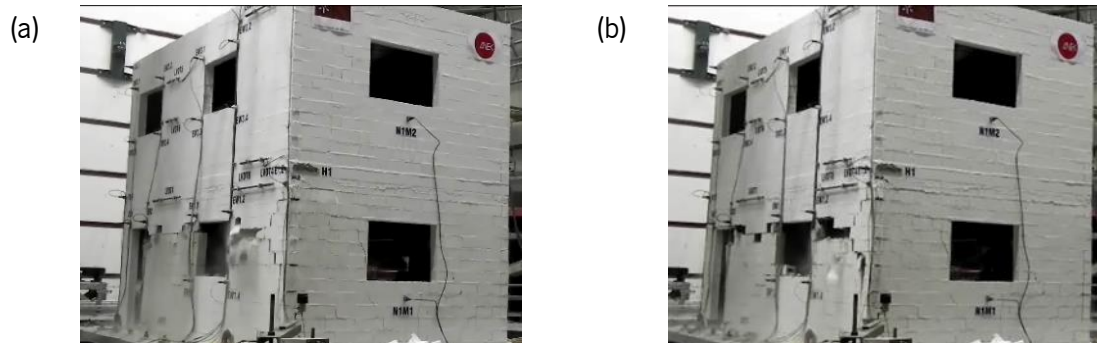


Figure 4.12 – Damage on RM model during shaking table test of 300%_2

4.5.2 UM model

The evolution of the damage and crack patterns of UM building obtained in the experimental campaign is shown in Figure 4.13 since seismic input of 50% (0.26g) until the seismic input of 150% (1.07g). The final state of damage, corresponding to the repetition of the seismic input of 150% (1.24g) is presented in Figure 4.14.

It should be mentioned that the UM model did not exhibit any sign of damage for the seismic input of 25% (0.12g), and only minor damage composed of two stepped cracks around the window openings in the east and west walls (west 2) were recorded for the seismic input of 50% (0.26g). The damage occurred in the sequence of the seismic input of 75% (0.33g) is more relevant, and develops at first and second floors but the higher level of damage is concentrated at first floor. The damage at the second floor consists of a horizontal crack along 2/3 of the wall west 2, which extends to the walls north 2 and to the wall west 1 connecting a stepped crack starting from the right bottom corner of the window. Important horizontal cracks developed also at the first floor starting from the left side of the door opening, progressing to the wall north 2 and to the wall west 1 at the level of the bottom border of the opening, connection to a stair stepped crack that develops in the walls north 1 up to the foundation. Additional horizontal cracks develop also in the wall west 1, close to the foundation, and progress to the walls north 1, and in the wall west 2 from the right side of the door close to the base of the walls. For the east façade, a horizontal 1m long crack was observed at the bottom of the left pier of the window and a diagonal one at the right pier. The cracks formed during this test were longest in comparison with the same stage for the RM building. Besides, this seismic input affected the second level, whereas in the RM model only until the seismic input test of 250% (1.06g) was found slight damage of the second floor.

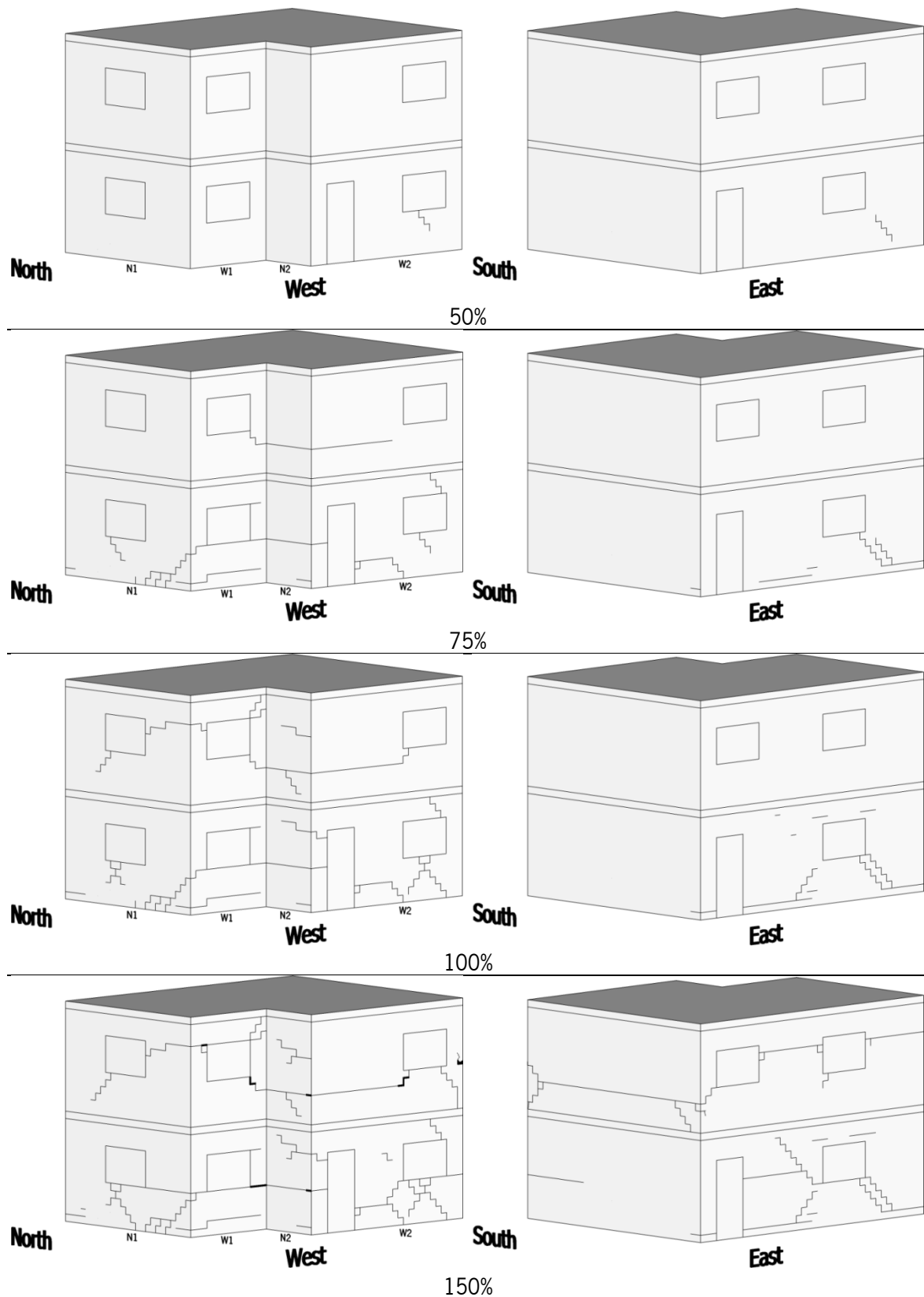


Figure 4.13 - Damage observed after each seismic input test for the UM model (50% to 150%)

The seismic input test of 100% (0.47g) increased the damage of the structure at both levels. At the second floor, the horizontal crack developed in the previous loading step extends and connect until a stepped crack starting from the bottom left corner of the window. Additional horizontal and diagonal

cracks developed in the walls north 1 and west 1 at the level of the top border of the windows. It should be noticed that the damage was mainly concentrated in the north and west walls and no damage occurred in the south both at first and second floors until this loading state. No damage developed also in the east wall at the second floor and the damage at the first level was much controlled. The loading state corresponding to the seismic input of 150% (1.07g) results in the extension of the previous damage and in the onset of damage in the south walls and east wall at the second floor. It was recorded the opening of a long and continuous horizontal crack at south wall at the second floor at approximately 1/3 of the height, being connected to a stepped crack connecting the left bottom corner of the window of east wall. An important horizontal crack appeared on the masonry piers at top border of the window openings of the east wall at the second floor. Additional horizontal and diagonal cracks develop in the east floor at the first floor. It should be stressed a predominance of horizontal long and continuous cracks at the different levels of the walls in both levels, being even connected in some perpendicular walls and more localized diagonal cracks.

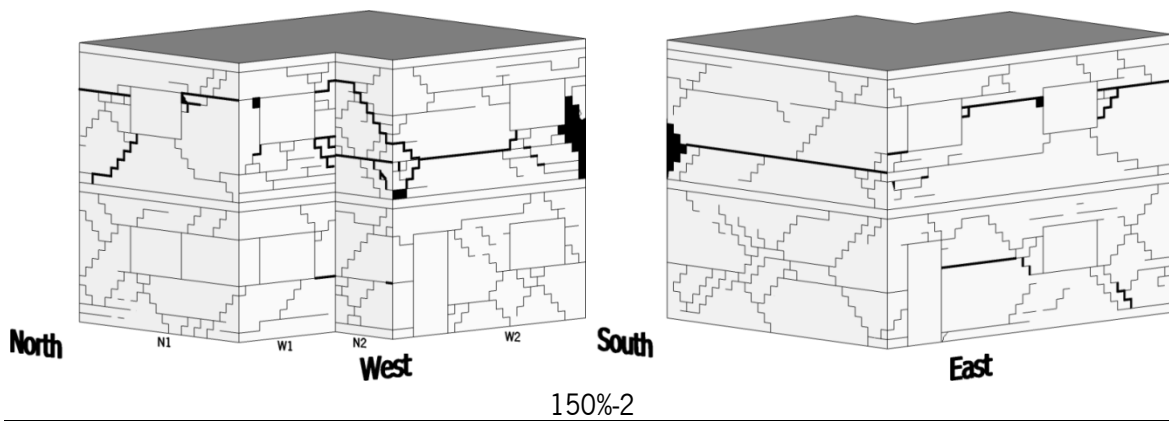


Figure 4.14 - Damage observed after repetition of the seismic input of 150%

The repetition of the seismic input of 150% (1.24g) (Figure 4.14) induced severe damage to the building, resulting from the extension of the previous one and the onset of other, namely: (1) Opening of additional long horizontal cracks, crossing the length of the south wall at first and second floors. These horizontal cracks connected to existing and novel horizontal cracks developed in the east and west walls; (2) Progress of the horizontal crack at the second floor in the north wall to the left pier and connection with the existing one in the east wall; (3) Connection of the horizontal cracks developed in the east and west walls to the ones existing in the north and south walls, mainly at the level of the openings. An important diagonal crack developed in wall north 2 at the second floor connecting the existing horizontal crack at 1/3 height of the wall; (4) Opening of higher amount of diagonal cracks on all walls at both levels. At this stage, all walls are severely damaged, but the detachment of masonry blocks only occurred at the second floor in the corners connecting south and west walls. Additionally, it was seen that the horizontal cracks at the second level present larger openings. Some cracks developed along the concrete blocks. Figure 4.15 illustrates some of the cracks already described that developed at both levels of the building for the final stage of loading.

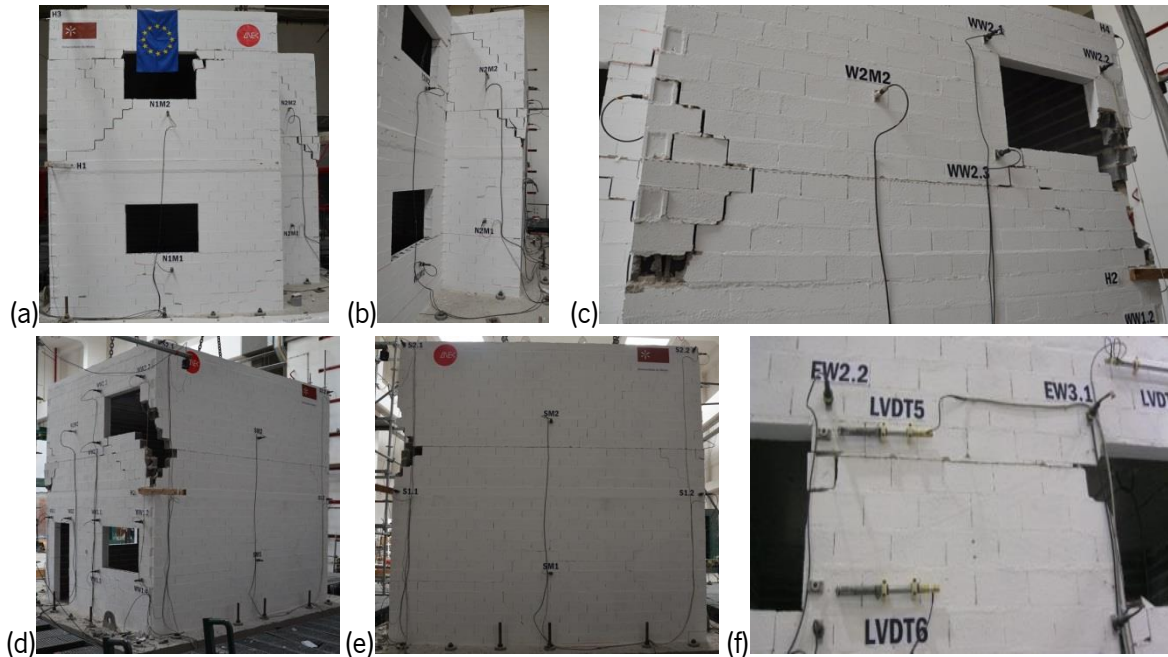


Figure 4.15 – Final damage in the asymmetric unreinforced masonry building: (a) north 1, (b) north 2, (c) west 2 at second level, (d) corner between west 2 and south walls, (e) south wall and (f) east wall at second floor

This building presented a clear shear sliding mechanism at the second level along the continuous horizontal joints crossing almost all perimeter of the building. The upper part of the structure was totally separated from the rest of the building by a horizontal crack in the perimeter, see Figure 4.16. During the last test, the movements of the upper part in all directions were evident, and should be related to some distortion of the building. This deformation mechanism is particularly evident from Figure 4.16d. It was possible to observe final displacements of about 1cm in different locations of the structure.

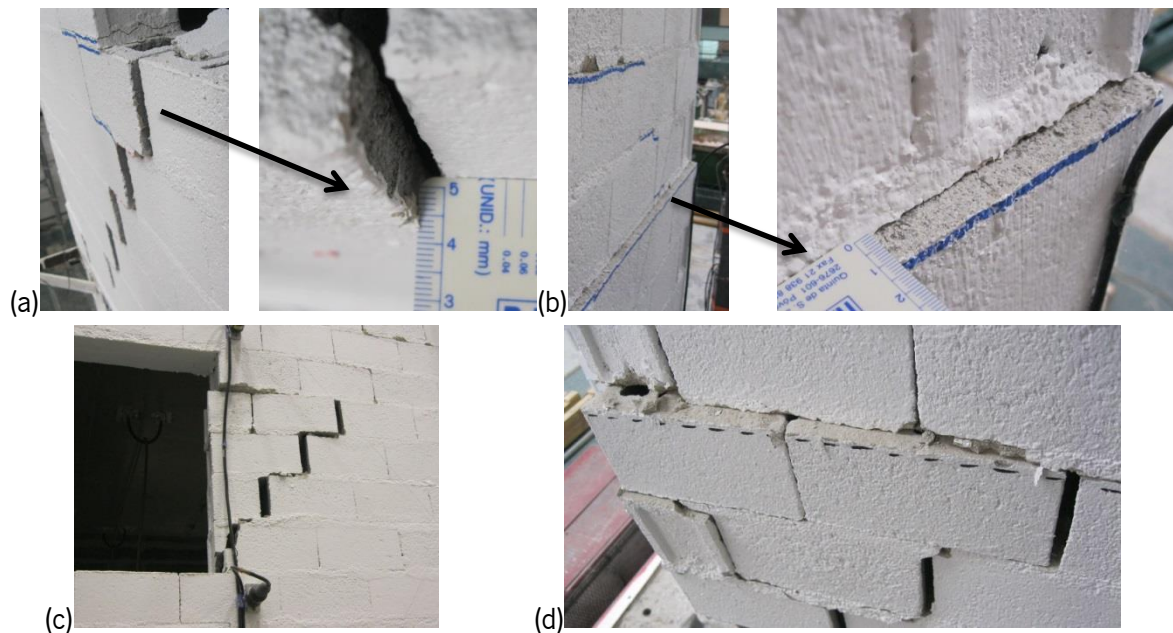


Figure 4.16 – Sliding mechanism evidence at second floor after final input test on UM model: (a) north 1, (b and c) east and (d) west 2 walls

4.5.3 Comparison of damage between UM and RM models

For a better comparison of the final damage on the UM and RM models, the final damage obtained in both buildings is summarized in Figure 4.17.

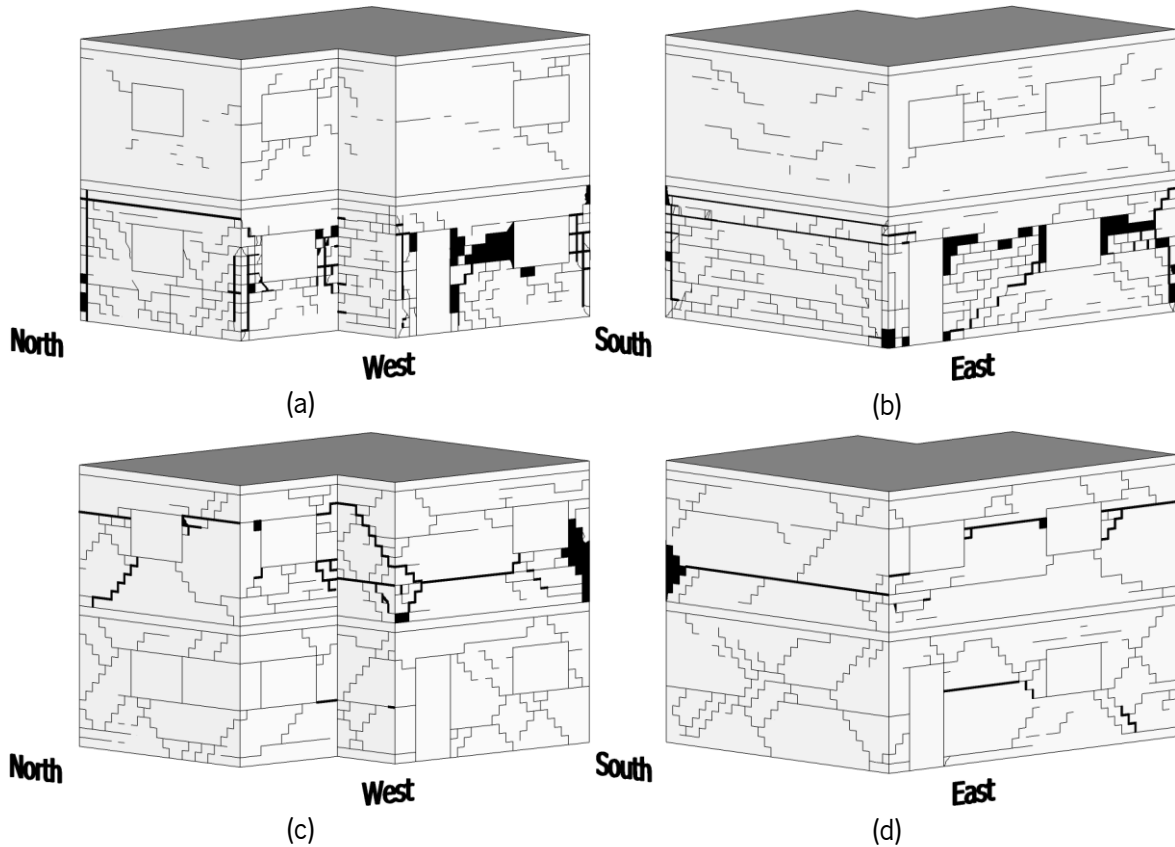


Figure 4.17 - Final damage patterns for the asymmetric: (a, b) reinforced building and (c, d) unreinforced building. Note that different seismic input applies

The final state of the building after the tests on the shaking table was characterized by severe damage, in spite of the models afforded distinct seismic input levels. In RM building, the state of imminent collapse (pre-collapse of the building taking into account that it would present minor or no capacity to withstand another seismic input) occurred to a seismic input of 300%, with a maximum PGA of 12.80m/s^2 or $1.30g$. The same state was observed in the UM building for an input test of 150%, with a PGA of 12.19m/s^2 or $1.24g$. From a general overview, RM model presented the severest damage at first level with loss of units and significant crack openings and only minor cracks developed at the second floor. On the contrary, UM model presented the more severe damage with loss of units and remarkable cracks openings at second floor. In spite of important amount of cracks developed in the first floor, it appears that the major sliding mechanisms and major cracks openings were at the second level. The opening of vertical cracks at the corners in the RM model indicates that care should be taken to the anchorage of the horizontal reinforcements as they can help in avoiding the separation of the corner.

Aiming at analyzing the influence of reinforcement, the damage in the RM model for a seismic input of 150% ($0.66g$) is shown in Figure 4.18 for a direct comparison with UM model for the same

loading stage. It is seen that the level of damage of RM model for seismic input of 150% (1.07g) is very controlled as the reinforced building only presented smeared cracks with no significant opening at the first level without any sign of damage for the second floor. Contrarily, the unreinforced masonry building presented considerable damage at both levels, with important long horizontal cracks and more localized diagonal cracks. At this stage, the UM model exhibited important opening of cracks but no signs of sliding mechanism developed. It is considered that the UM building presented an acceptable behavior for medium seismic levels. For a seismic input, with a PGA about 1g the UM building did not present a well-defined failure mechanism.

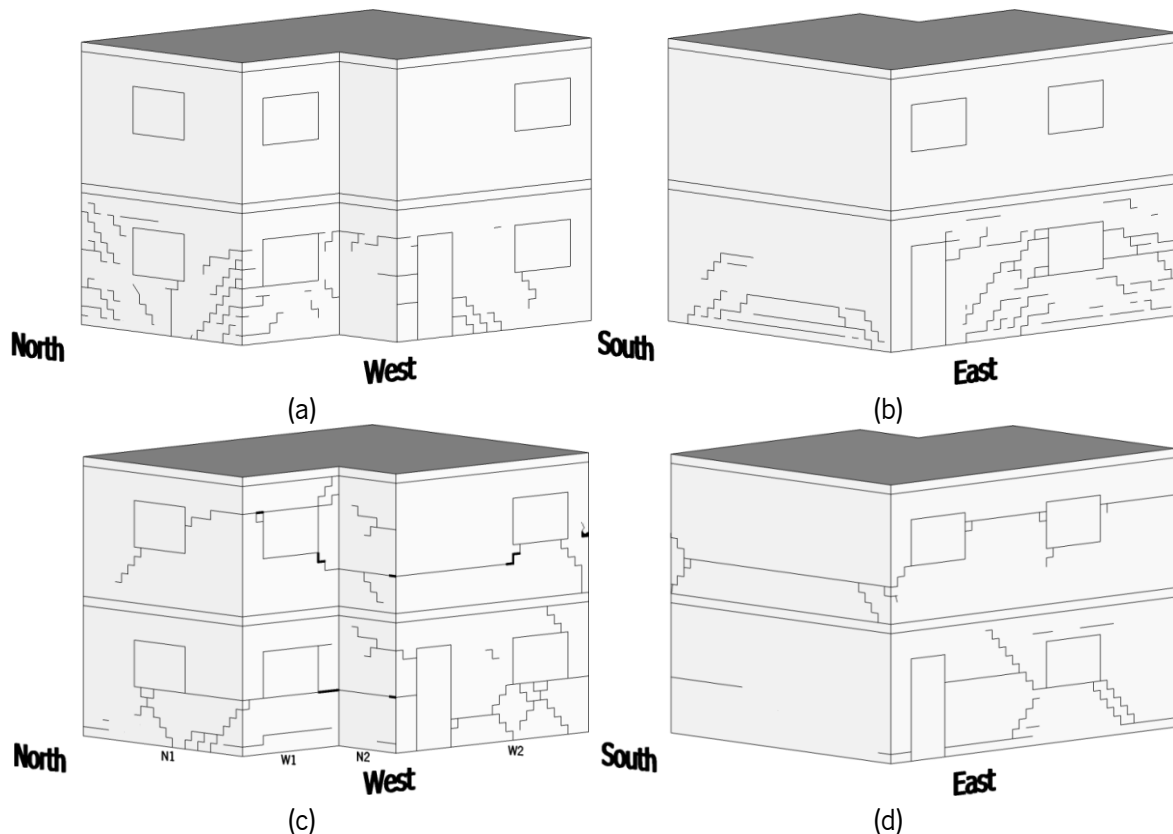


Figure 4.18 - Crack patterns of the RM and UM models at 150%: (a, b) RM model; (c, d) UM model

As observed, the main roles of the reinforcement are the control of damage, the localization of damage at the first floor and, as will be discussed later, the improvement in resistance. As a result of the better distribution of cracks, the RM building should present better energy dissipation during the shaking table tests than the unreinforced masonry building, in which the absence of vertical and horizontal reinforcements should be responsible of the long horizontal cracks at the second floor.

4.5.4 Variation of the frequency and damping along the seismic inputs

As a complement for the characterization of the damage evolution, the building models were characterized at the shaking table after each individual seismic input to obtain the frequency and damping coefficient by using a white noise input. The evolution of the frequency and damping coefficients found after each seismic input for each masonry building is summarized in Table 4.3.

The evolution of damping for each seismic input gives an idea on dissipation of the kinetic and strain energy of the vibrating system.

Table 4.3 - Evolution of the frequency and damping coefficient

			Test run										
			Initial	25%	50%	75%	100%	150%	150%2	200%	250%	300%	300%2
F (Hz)	RM	Trans	11.68	-	11.26	11.20	11.16	10.85	-	10.22	7.41	4.90	3.44
		Long	19.40	-	18.77	18.53	18.36	17.52	-	15.23	12.93	11.89	3.96
		Rota	22.32	-	22.01	21.66	21.28	20.55	-	19.29	18.67	8.66	6.15
	UM	Trans	11.50	11.09	10.47	10.05	9.74	7.46	6.12				
		Long	13.47	13.47	13.16	11.71	12.03	10.47	10.16				
		Rota	21.77	21.66	19.28	18.45	17.83	17.10	-				
ζ (%)	RM	Trans	2.70	-	4.65	5.94	7.23	6.61	-	7.00	10.92	16.96	20.44
		Long	1.18	-	1.37	1.59	1.97	2.38	-	2.07	2.41	3.06	4.00
		Rota	0.93	-	3.35	3.61	4.57	5.05	-	8.93	6.75	9.19	11.5
	UM	Trans	5.50	5.11	7.69	8.63	9.84	12.60	13.27				
		Long	5.00	4.75	5.22	6.83	9.09	9.80	11.92				
		Rota	1.65	2.14	2.70	3.10	2.39	2.12	-				

The analysis of results allow to conclude that for both models the frequencies present decreasing values and the damping coefficient increases for each increasing seismic input. This is directly related to the progress of damage along the phases of testing. In the RM model, the decrease of the frequencies is very moderate until the seismic input of 150% (0.66g) in the three main directions considered (decrease of about 7.1%, 9.7% and 7.9% in the transversal, longitudinal and rotational directions respectively in relation to the initial reference values). On the other hand, the damping ratios recorded in the seismic input of 150% were 2.4, 2.0 and 5.9 times greater than the initial reference values in the transversal, longitudinal and torsional directions respectively. The moderate reduction of the frequencies is associated to the moderate damage recorded until this seismic input, which is accompanied by important increase of the dissipation of energy. The most abrupt reduction of frequency occurs: (1) In the transverse direction for seismic inputs of 250% (1.06g) and 300% (1.21g), associated to the development of important horizontal cracks and connection of these with diagonal cracks in the transverse walls (north and south walls); (2) in the rotational direction for the seismic input of 300% (1.21g) (reduction was about 10Hz), appearing to be related with the highest levels of damage found at the corners of the building. In the repetition of the seismic input of 300% (1.30g) there was a generalized decrease on the values of frequency and an increase on the damping coefficient resulting from the severe degradation of the stability conditions of the building and severe damage observed. Here, the longitudinal direction was more affected, which appears to be the result of the crushing and breakage of masonry around the openings and corners at the first floor (west and east walls). Total reductions of 71% for the first transversal mode, 80% for the second longitudinal mode and 72% for the third torsional mode were recorded in the RM model. Comparing to the initial reference values, the highest increase on the damping coefficient was recorded in the transverse and torsional directions.

It is interesting to notice that the decrease of the frequencies in the UM building recorded for each seismic input was different for the three mode shapes. The maximum reduction attains values of 46.8% in the transversal direction, 24.5% in the longitudinal direction and 21.5% for the rotation direction (first seismic input of 150% (1.07g)). This behavior should be associated to the fact that in case of the UM model the progression of damage is more uniform for increasing seismic inputs. However, it should be mentioned that the reduction of the frequency between the first and second seismic inputs of 150% is considerably more relevant in case of transverse direction. This is related to the remarkable increase of cracks in the north and south walls from the first seismic input of 150% (1.07g) to its repetition (150%² (1.24g)). The damping coefficient increased progressively in the transverse and longitudinal directions, achieving values of approximately 2.4 times greater than the initial reference values. The increase of the damping coefficient was not so uniform in case of the rotational mode. It presented increasing values until the seismic input of 100% (0.47g), after which a reduction was recorded (from 3.1 up to 2.12) for the last seismic input, even if keeping greater values regarding the initial reference value. The lowest increase on the damping coefficient in relation to the RM model is attributed to the lowest ability to dissipate energy, resulting from the more localized cracking instead of the more intense smeared cracking recorded in the RM model.

If the frequency and damping coefficients obtained in the RM and UM models for the first input of 150% are compared, it is seen that the reduction of frequencies and increase on the damping coefficients in relation to the initial reference values (linear regime) is considerably higher in case of UM model for both transverse and longitudinal directions. This result reflects the higher levels of damage recorded in the UM model for this seismic input. It is possible that the lower value of the damping coefficient measured in the UM model is a consequence of the predominant sliding mechanisms developed in the transversal and longitudinal directions along the long horizontal cracks dividing the model in blocks sliding among them. In this case, dissipation of energy appears to results from this predominant sliding mechanism.

4.5.4.1 Damage indicator

The dynamic characterization of the masonry buildings after each seismic input revealed the decrease of the frequencies both for longitudinal and transverse directions. This behavior can be associated with the decrease in the structural stiffness. The degradation of stiffness is here represented by the damage indicator already used in Chapter 3 for the characterization of the damage of the symmetric buildings (see Equation 3.1.). Each mode has associated a damage indicator. The damage indicator ranges from zero (no damage) to one (collapse).

The evolution of the damage indicator found for the two masonry buildings is presented in Figure 4.19. Following the template of previous graphs in this work, the damage indicator is plotted against the PGA obtained during each seismic test. Here, the first mode (transverse) is presented with reference to the PGAs of the transverse direction, the second mode (longitudinal) with reference to the longitudinal direction and the third mode (rotation) use again the transverse direction as reference.

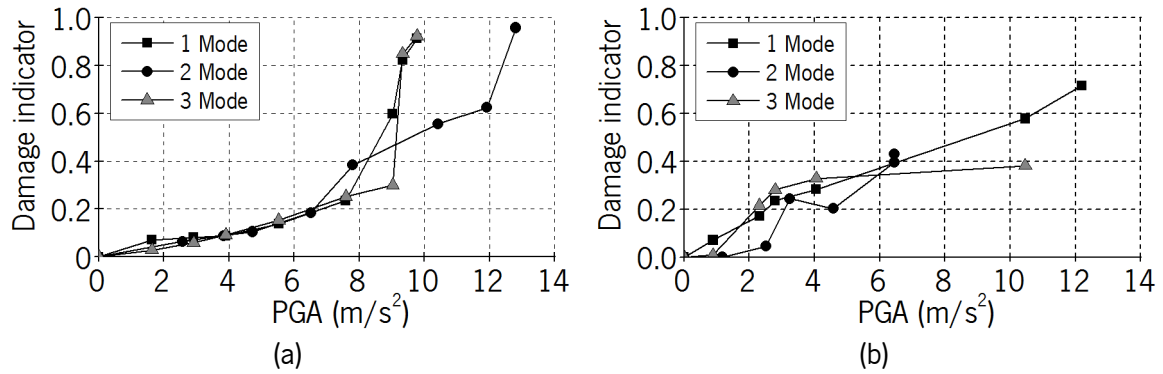


Figure 4.19 – Damage indicator for: (a) RM and (b) UM

In the RM model, the evolution of the damage indicator on the three modes is practically coincident until the seismic input of 150% ($6.51 m/s^2$), achieving a value lower than 0.2 (20%). After this seismic input, the damage indicators progressively increase in accordance with the progression of damage and reduction on the stiffness. The first test of 300% ($9.33 m/s^2$ – 1st and 3th mode) led to a significant increase of the damage indicators, particularly the first and third mode, achieving values of 0.82 and 0.85. The final seismic input induce severe reduction on stiffness due to the remarkable increase on the damage indicators, attaining values close to 1 (values above 0.90 for all modes, with a maximum of 0.96 for the second mode). These damage indicators reflect the compromised structural condition of the building, which justified the stop of the test for 50% time duration of the seismic input.

In case of UM model, it is seen that the damage indicator corresponding to the third mode present a distinct trend from the transverse and longitudinal damage indicators (roughly linear trend). For the seismic input of 50% ($2.31 m/s^2$), the third mode already registered a damage indicator over 0.2. Until the input test of 100% ($4.05 - 4.57 m/s^2$), the damage indicator was quite similar for all the modes. Nevertheless, the last two inputs led to the considerably increase for the damage indicator in the transverse direction (first mode). Due to the absence of identification of the third mode (rotation) during the final input of 150%, it was not possible to obtain the damage indicator. Only the value found for the first seismic input of 150% ($10.46 m/s^2$) is available (0.38). For the first mode (transverse), a value of damage indicator of 0.71 was obtained and for the second mode (longitudinal), the damage indicator reached a value of 0.43. This means that the first mode (transverse) contributed more for the degradation of the stiffness of the building, which was associated to the more severe damage developed in this direction (south and north walls).

The comparative analysis of results enables to conclude that: (1) the evolution of the damage indicator is different for RM and UM model. This should be associated to the distinct progress of damage observed in both buildings; (2) the damage indicators characterizing the damage of the RM model follow an exponential trend, being rather close. On the other hand, the UM model presents a rough linear trend for the damage indicators of transverse and longitudinal direction and nonlinear evolution in case of the rotation direction; (3) in spite of both masonry buildings were close to the collapse for the final imposed seismic inputs imposed, it was seen that the damage indicators found for the RM model are considerably higher, when compared to the values found for the UM model. This should be attributed to the distinct typology of damage developed in both buildings. In the RM

model predominated the smeared diagonal cracking, reflecting the presence of reinforcements promoting the stress redistribution. In this case, the horizontal cracking is considerably more controlled than in case of UM model. This different behavior should be attributed to the existence of vertical reinforcement in the RM model. On the contrary, an extensive horizontal crack (almost in the total perimeter) developed at the second floor of the UM, dividing the building in rigid blocks. This crack patterns appears not to be so important for the reduction of the stiffness of the building.

4.6 Seismic performance

The quantitative evaluation of the seismic performance of the masonry buildings was carried out in terms of: (1) amplification of the accelerations; (2) displacement profiles along the height of the buildings in the in-plane and out-of-plane direction to the walls; (3) lateral drifts; (4) hysteresis loops and capacity diagrams. The global displacements were obtained by the PSDs and the relative displacements were obtained by double integration of the accelerations measure in the accelerometers. Additionally, local displacements were taken from the LVDTs placed in the piers between openings (east wall). A comparison was made between the buildings with reinforced and unreinforced concrete block masonry in terms of deformation and loading capacity. Furthermore, a discussion about the relation between the stiffness degradation and the evolution of the frequencies is presented.

4.6.1 Amplification factors from the accelerations

The accelerations can give an indirect idea of the inertial forces developed on the model due to the seismic inputs. The seismic response of the buildings in terms of acceleration was focused on their global behavior rather than in their local behavior. Therefore, only the accelerometers placed at the foundation and at levels of the slabs levels were considered (i.e. the accelerometers at openings' corners were not taken into account in this section). The idea is to evaluate the global response of the buildings in each orthogonal direction and assess the evolution of accelerations for each input motion. Figure 4.20 presents an example of the time history records for the RM and UM models in the longitudinal direction for the seismic input of 100% and 150%. It is observed that each building presents different amplification for the same input at each level (first and second levels).

In order to quantify such amplification, the PGA at the base of the buildings and the absolute Peak Acceleration for each level were calculated for each input. The amplifications found for the accelerations are presented in Figure 4.21 and Figure 4.22 for the RM and UM models, respectively. Each plot has four lines: (1) two lower lines corresponding to the peak acceleration values (PA) for the first and second slab levels. These values can be read at the left scale of the plots (in m/s^2); (2) two upper lines corresponding to the amplification ratio (DA) between the PGA and the peak acceleration recorded at each level. These values can be read at the right side of the plots.

As expected, the story acceleration for each level in both directions increased for increasing seismic inputs. For the last test, the accelerations decreased as consequence of the important damage developed in the building. For this damage state, the building was not able to amplify the

acceleration at the same rate and the dynamic amplification reduced, after a peak of about 2.5 for the seismic input of 200%. As expected the dynamic amplification is higher in the second floor but the difference of the dynamic amplification between both levels is higher in the transverse direction.

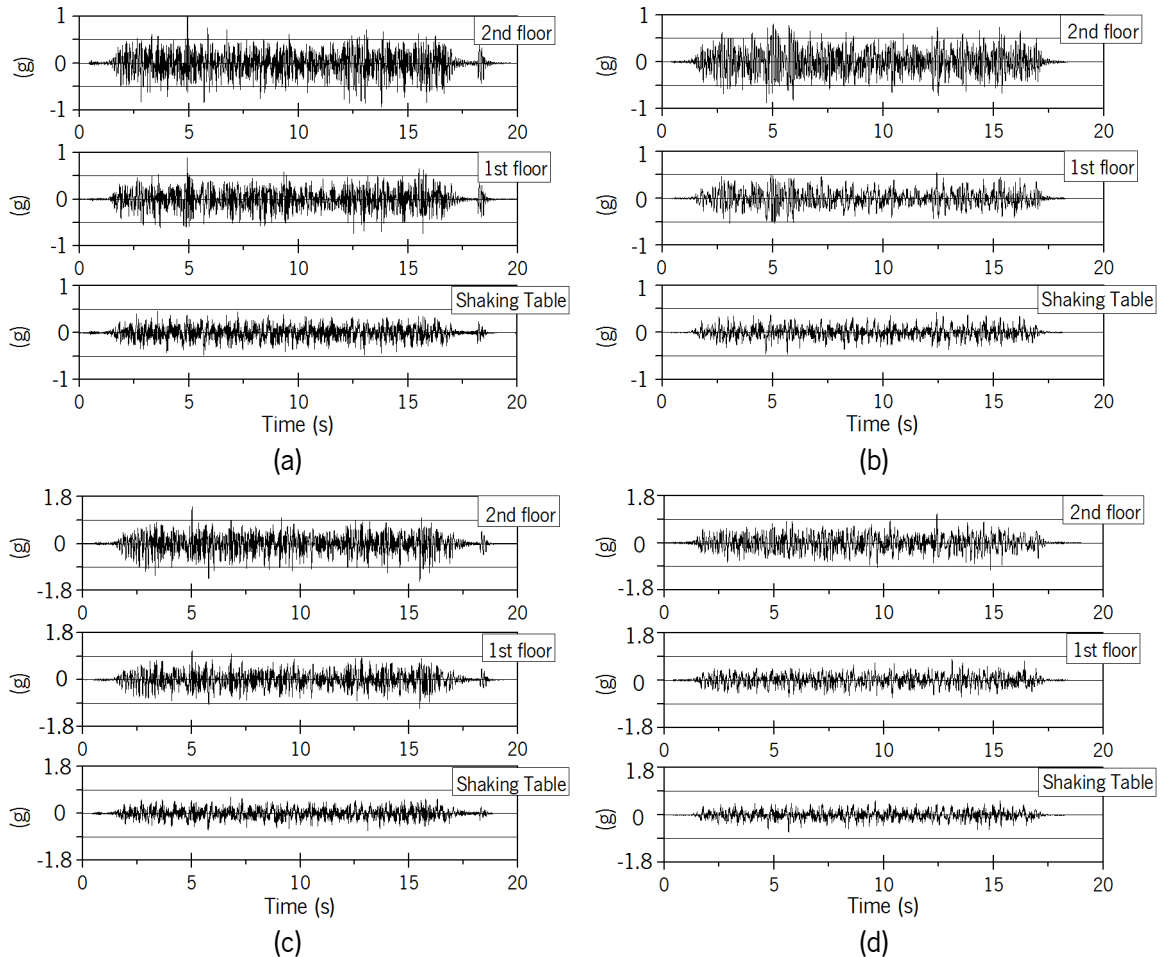


Figure 4.20 - Measured accelerations in the longitudinal direction: (a) RM model at 100%; (b) UM model at 100%; (c) RM model at 150% and (d) UM model at 150%

In case of UM model, the evolution of the PGA for both directions presented similar values until the seismic test of 100%. For the final input of 150%, the transverse direction presented a considerable increment on the PGA in relation with the longitudinal one, which is in agreement with the values found and discussed in Figure 4.1. The almost monotonic increasing of the dynamic amplification obtained in RM does not happen in the UM model. In fact, in spite of the peak acceleration increase for all seismic inputs, the dynamic amplification decreased after the seismic input of 50% in the longitudinal direction and from the seismic input of 75% in transverse direction. This drop coincides with the observation of the first crack at the second level of the structure.

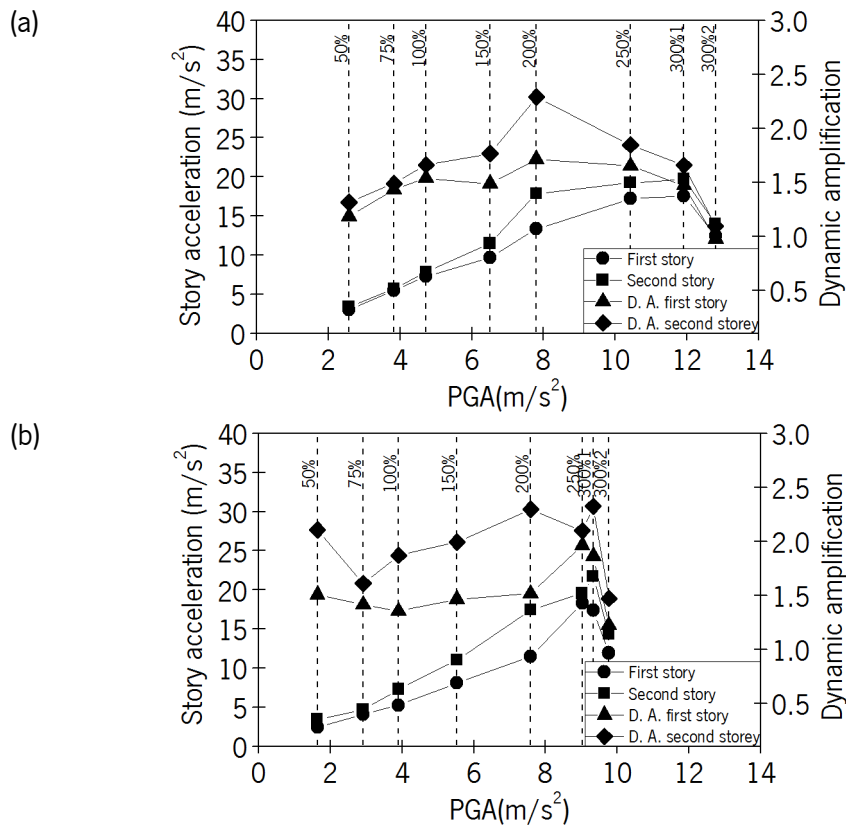


Figure 4.21 - Story accelerations and dynamic amplification factors versus PGA of RM model: (a) longitudinal direction and (b) transverse direction

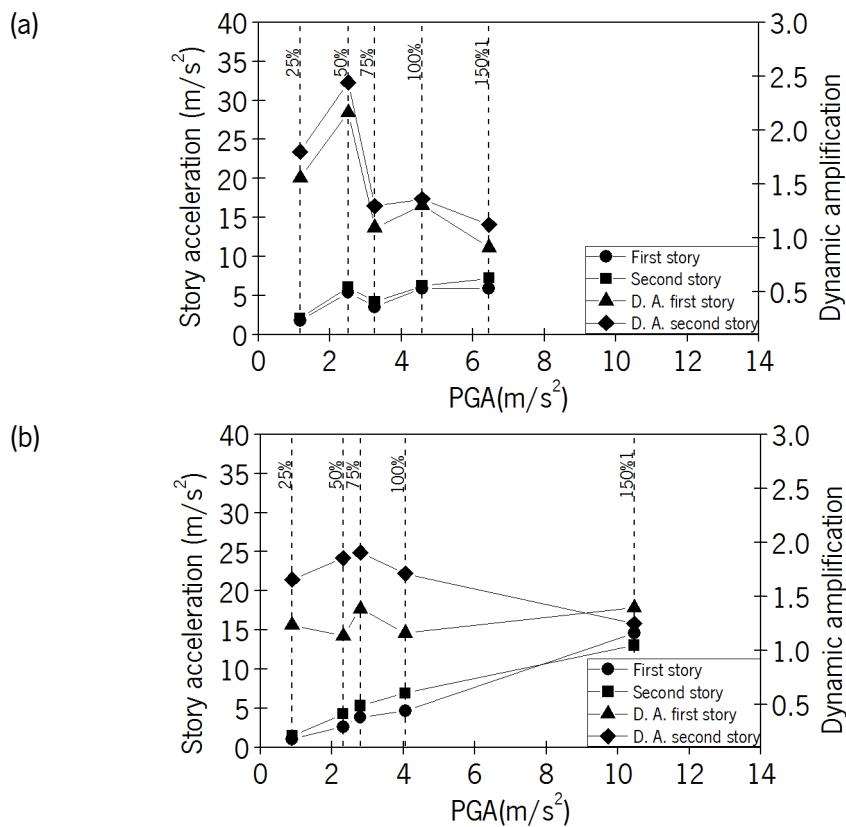


Figure 4.22 - Story accelerations and dynamic amplification versus PGA of UM model: (a) longitudinal direction and (b) transverse direction

This crack affected horizontally three walls including two longitudinal ones (west 1 and west 2). The maximum value of the dynamic amplification reached a maximum value close to 2.5 but presented a steep reduction for the seismic input of 75% to approximately 1.5 for both floor levels. The reduction of the dynamic amplification in the transverse direction is smoother and the maximum dynamic amplification is close to 2 for the seismic input of 75%.

The reduction on the dynamic amplification is associated to the progressive damage observed in the UM model from the seismic input of 75%. The test of 150% was the most destructive, affecting considerably all the walls at both levels. As discussed in the previous section, the unreinforced building presented more damage and finally failure at the second floor. This is also related to the highest amplification observed in the first floor at the final of the seismic inputs.

For both buildings and directions, the story peak acceleration presented a clear trend to increase for increasing loading inputs, as expected, apart from the case where the building was near collapse as in the seismic input of 300%. On the other hand, the amplification of the accelerations presented important reductions at the end of the tests campaign, presenting value close to 1.0, which indicate that there is no ability for acceleration amplification for severe damage.

4.6.2 Analysis of deformation of the buildings

This section aims at describing and analyzing the main features of the deformation of the asymmetric masonry buildings. As already discussed, the asymmetric masonry buildings presented displacements that involve in-plane, out-of-plane and torsional movements that affect the walls of the buildings at different stages. In detail, in this section an overview is provided encompassing the in-plane and corresponding interstory drifts, out-of-plane displacements and biaxial displacements. Additionally, a discussion on the amplification factor found for the displacements and the local displacements is presented.

4.6.2.1 In-plane displacements and interstory drifts

The analysis of the in-plane deformation behavior of the masonry structural walls of both buildings is made for each wall, taking advantage of the position of the accelerometers at slab levels, from which the global in-plane displacements were obtained. The relative displacements were obtained by subtracting displacement time history of the slab position to the displacement time history of the base. Besides, the interstory drift is an important deformation index used for the assessment of the seismic structural performance of civil engineering structures. The interstory drift is defined as the relative displacement between two consecutive floors and is calculated by subtracting the displacements between two consecutive levels divided by the height of each floor (1.5m) and presented in percentage.

The relative in-plane displacement profiles along the height of the buildings corresponding to the different seismic inputs are presented in Figure 4.23 and Figure 4.24 for RM and UM models respectively (two walls for each direction). The interstory drifts found for the RM and UM models are presented in Figure 4.25 and Figure 4.26, respectively.

In the reinforced masonry building, the displacements increased for the subsequent seismic inputs with different rates: (1) the increase in the displacements is very moderate from test of 50% (0.26g) to 150% (0.66g), attaining values lower than 5mm, corresponding to maximum lateral drifts of 0.25% and 0.26% for west and east walls respectively (longitudinal walls). These inputs caused considerable cracking at the first floor but without important openings; (2) for the test of 200% (0.79g) all the walls presented a higher increase on the displacements, being over 5mm (lateral drifts of 0.27% and 0.37% in the north and south walls, and of 0.37% and 0.36% in the east and west walls respectively). This seismic input led to the spread of the cracks at the first level affecting considerably all the walls and in particular affecting the south wall, in which a large horizontal crack appeared at the top of the first level; (3) the increase in the displacements is considerably higher after the seismic input of 200% (0.79g), particularly in the walls with openings (west and east walls) and in the south wall. The test of 250% (1.06g) presented relative displacements higher than 8mm in all the structure (maximum lateral drift of approximately 0.57% in the first floor of west, east and south walls and 0.33% for the north wall). For the first input of 300% (1.21g), the most important displacement's increase occurred in the west2 wall with a maximum value of about 20mm at the second floor, corresponding to a drift of approximately 1.0%. The east wall presented maximum lateral displacement of 12mm at first floor, corresponding to a drift of 0.80%, as the result of the increase in the damage but without loss of units. Finally, the walls in the transverse direction (north and south) registered lower values, for instance the north wall presented displacements of 7mm and 9.6mm for each floor.

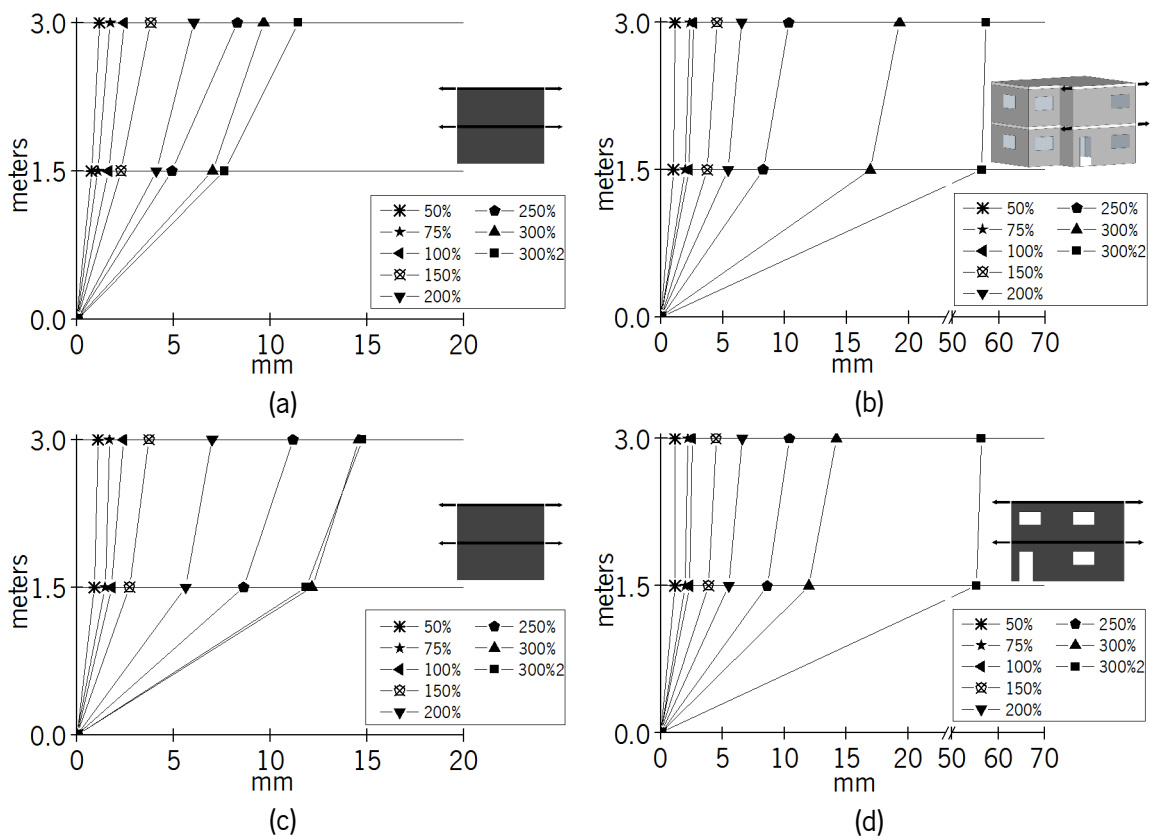


Figure 4.23 - In-plane displacements for RM in façade: (a) north, (b) west2, (c) south and (d) east

The second input of 300% (1.30g) considerably increases the in-plane displacements in the longitudinal walls, in which values near the 60mm were obtained, corresponding to lateral drifts of 3.76% and 3.68% in the west and east walls respectively. These displacements are related with the high level of damage in the longitudinal walls with important diagonal cracking and with detachment of masonry blocks from the walls at the first floor. However, at this stage the increase on the displacements at the second floor is very small, which is related to the moderate progress of damage at the second floor. It should be stressed that the longitudinal walls play a central role in the resistance of the RM masonry building.

On the other hand, the displacements for the transverse walls did not show an important increase from the first test of 300% to the repetition of this seismic input, with a maximum increase of 19% recorded in this direction (lateral drifts below 0.8%). The main resisting mechanism developed in the final seismic input in the transverse walls was the out-of-plane resistance, resulting from the severe damage in the longitudinal walls, achieving a state close to the collapse. The combination of these two mechanisms can suggest an important contribution of the second mode (longitudinal) of the structure for its final capacity.

The unreinforced masonry building presented very moderate increase on the displacements until the seismic input of 100% (0.47g), even if cracking started after the test of 50% (0.26g) at the first floor. The test of 100% presented maximum displacements in the north and west 2 façades with 2.73mm and 2.65mm, respectively.

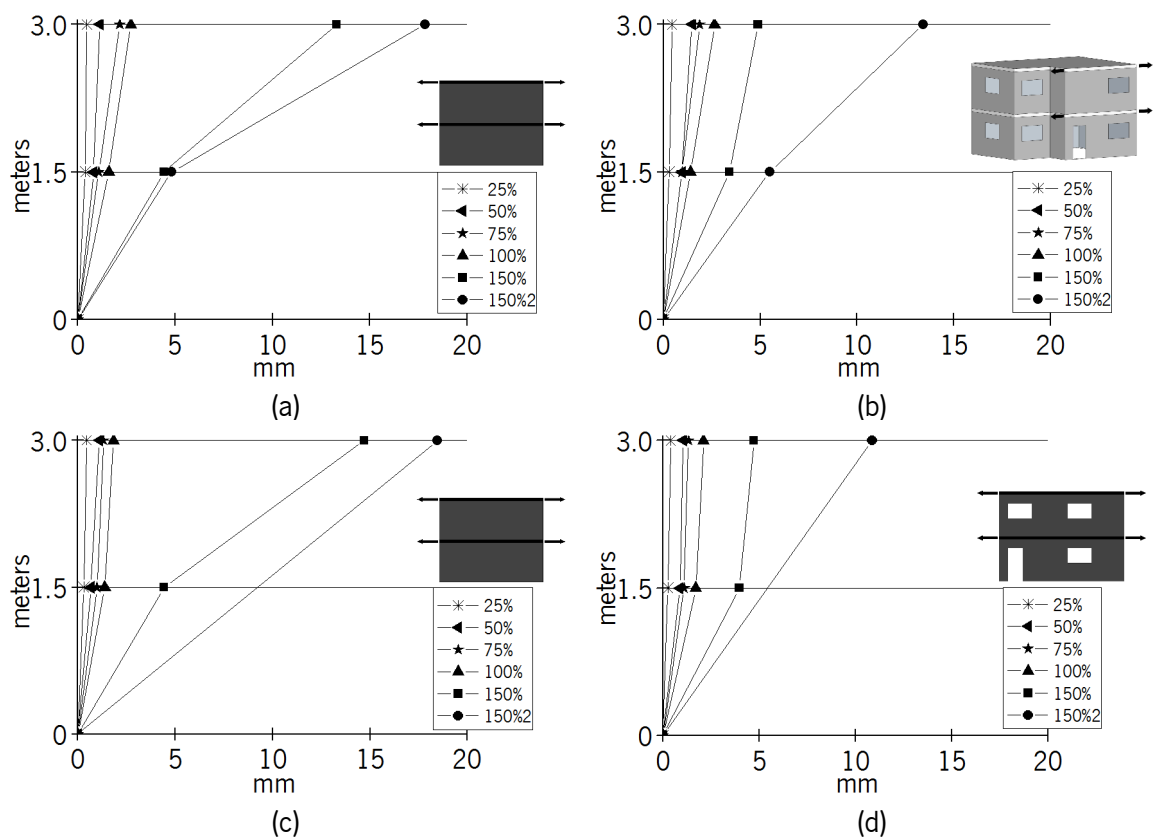


Figure 4.24 - In-plane displacements for UM model in façade: (a) north, (b) west2, (c) south and (d) east

The first test of 150% (1.07g) increased considerably the displacements for all walls but in particular for the transverse walls. Maximum displacements of 14.70mm and 13.30mm were found for the south and north walls at the second floor (lateral drifts of 0.85% and of 0.71%). These values are significantly higher than the values 4.88mm and 4.73mm found in west and east walls (lateral drifts below 0.18%). Besides, there is a clear difference in the displacement profile between the longitudinal and transverse walls: (1) the transverse walls present very high displacements at the second floor, increasing at higher rate in relation to the displacement at their first floor; (2) the longitudinal walls present much lower displacements at the second floor in relation to their first floor. This behavior is associated with the development of damage at the second floor, which is particularly relevant in case of transverse walls with the opening of long horizontal cracks crossing the entire south wall at the second level. The repetition of the seismic input of 150% (1.24g) resulted in the increase of the in-plane displacements for all walls due to the generalized extension of damage, particularly at the second level, reflecting the higher damage observed at this input, with important sliding along the joints predominantly in the transverse direction (lateral drifts of 1.25% in the north wall). Contrary to the damage observed in the reinforced building, the failure mechanism observed in the unreinforced model, suggests an important contribution of the first transverse mode to this final state.

From a comparison of the two asymmetric buildings, it is possible to observe very different behaviors for the same imposed seismic input: (1) the relative displacement profiles of the RM model and corresponding lateral drifts are typical of a behavior with a first story mechanism, with concentration of the damage at the first floor (maximum lateral drift of 3.8% in the west wall at the first floor). In case of the UM model, the damage is more distributed between the first and second floors. However, the damage presented a trend to concentrate more at the second floor for the last seismic input (maximum drift at the second floor of 1.25%); (2) the in-plane displacements corresponding to the seismic input of 150% are considerably higher in case of the UM model, when compared to the RM model. This is associated to a completely different damage state of both buildings for the same seismic input. For this stage, the UM model is very close to the maximum deformation capacity (lateral drifts at the second floor of 1.25% in the north wall); (3) the RM model is able to exhibit considerable higher deformations (lateral drifts) in comparison with the transverse walls, for the last seismic input of 300% (1.30g) in the longitudinal direction, associated to the severe damage developed in the walls with openings. It is interesting to notice that the displacements in the transverse walls of the RM model are in same order of the displacements measured in the UM model, but in the latter case, the seismic input is half of the seismic input imposed to the RM model.

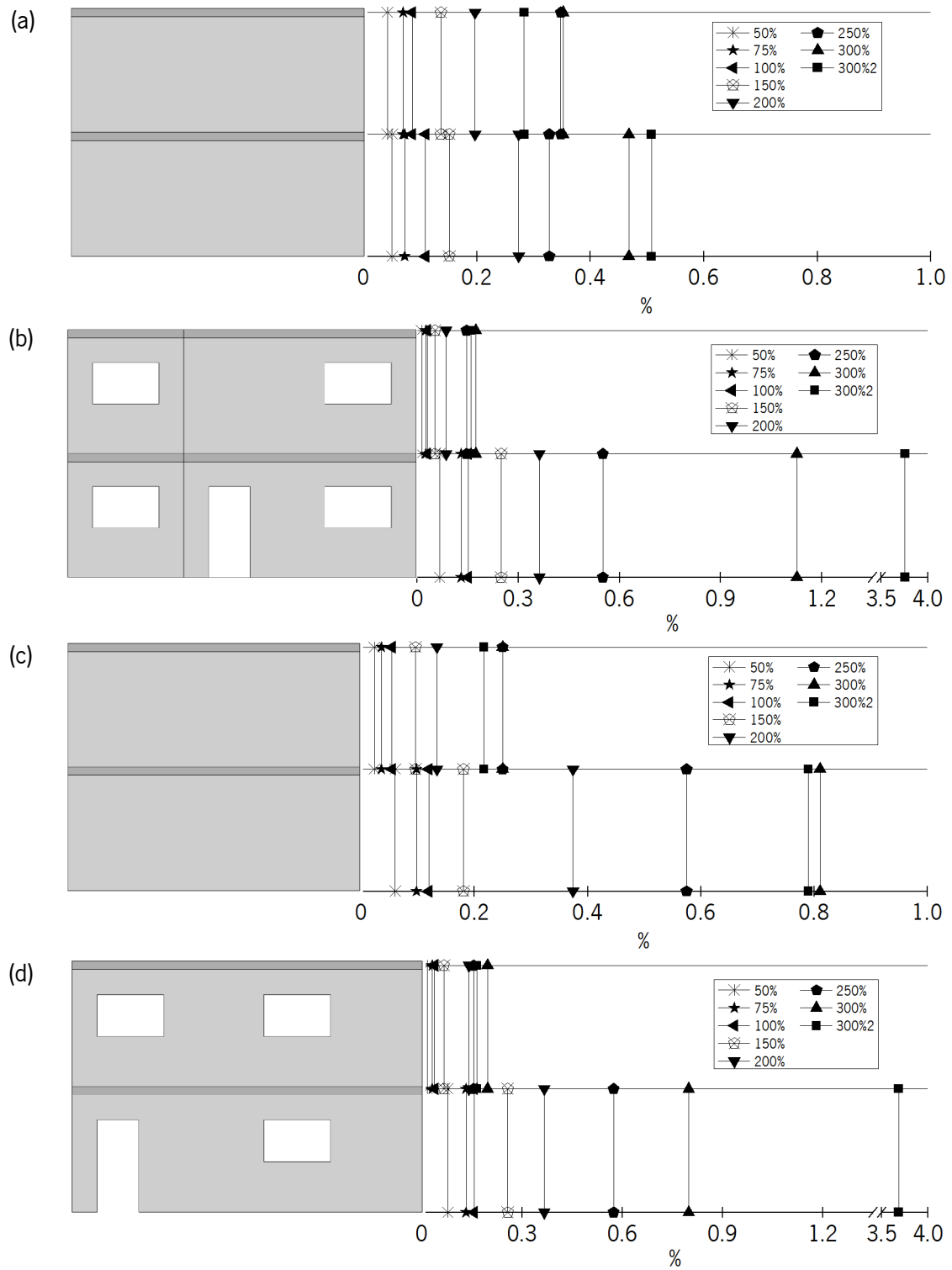


Figure 4.25 - Interstory drifts for RM in façade: (a) north, (b) west2, (c) south and (d) east

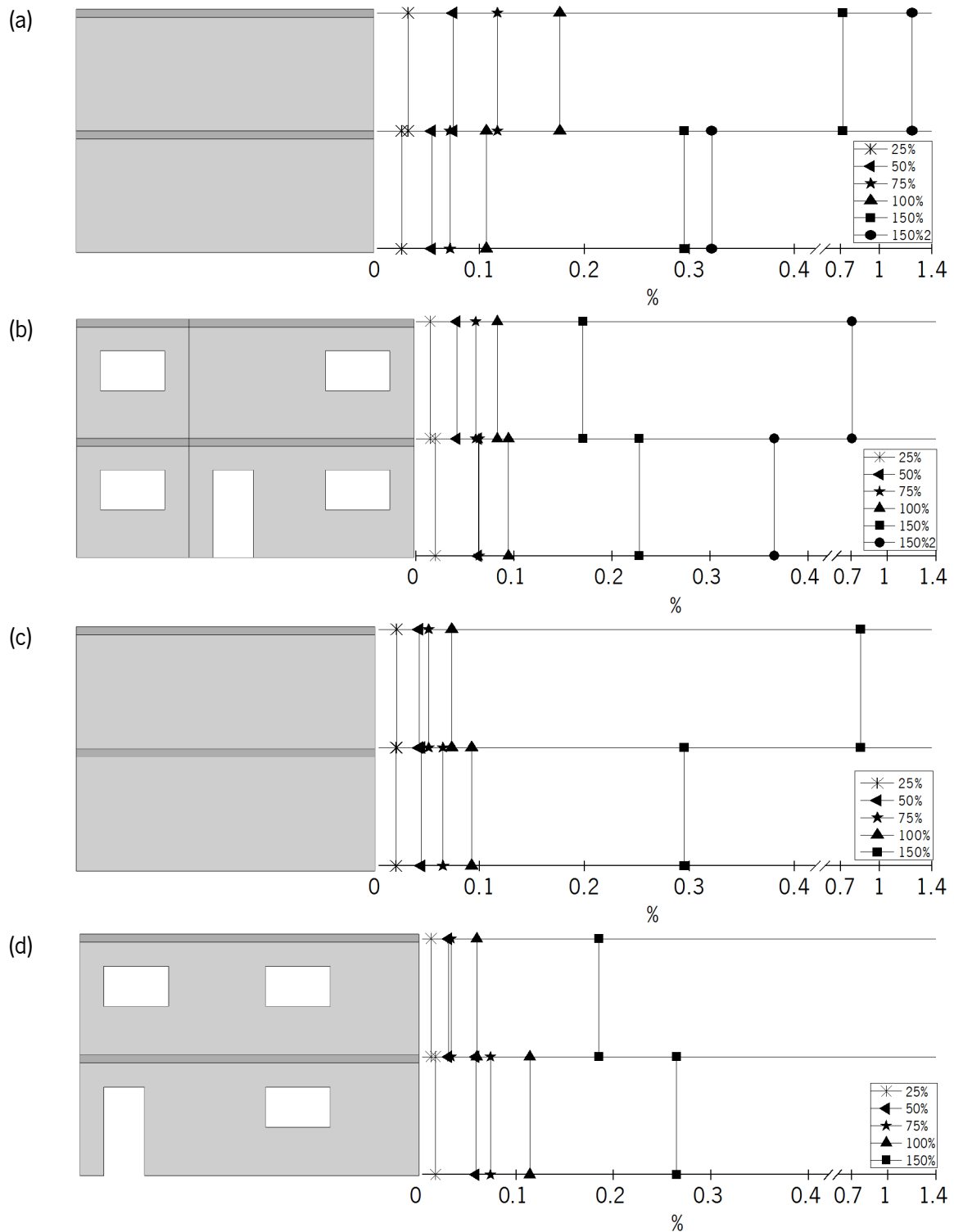


Figure 4.26 - Interstory drifts for UM in façade: (a) north, (b) west2, (c) south and (d) east

The asymmetric RM model presented higher in-plane displacements than the symmetric RM model (maximum values were about 5mm in both directions), for a final seismic input (PGA of 1.30g) corresponding to 75% of the final seismic input imposed to the symmetric building. This is related to the higher damage observed in the asymmetric building near collapse. The symmetric RM model presented only smeared and very thin cracks at the first level for the final seismic input (1.61g).

In case of the symmetric and asymmetric UM models, some considerations can be made: (1) the asymmetric building presented higher in-plane displacements but more severe damage for a seismic input of 150%; (2) the symmetric building presented higher in-plane displacements for all the walls for the last seismic input of 250% and consequently higher lateral drifts; (3) the symmetric UM building attained an input of 250% with a PGA of 1.33g, whereas in the asymmetric building a maximum input of 150% with a PGA of 1.24g was registered; (4) both buildings presented similar shear sliding mechanism at the second floor (long horizontal cracks), similar weak direction (transverse) and severe damages in all the structural walls at both levels, leaving the buildings near the collapse.

4.6.2.2 Out-of-plane displacements

Under dynamic seismic loading, the in-plane and out-of-plane deformations develop simultaneously. However, if adequate connections between structural elements (intersecting walls or walls / floors) are ensured, out-of-plane deformations of structural elements are minimized and in-plane resisting mechanisms develop predominantly. This is the reason by which several post-earthquake research and experimental investigation have revealed that if out-of-plane failure is prevented, the resistance under seismic actions in masonry buildings is insured by the in-plane resistance of the structural masonry walls.

The out-of-plane displacements of the walls are calculated in two steps: (1) calculation of the relative out-of-plane displacements (subtraction between the displacements calculated from second derivative of accelerations measured at the walls and at the base); (2) subtraction of the displacements of the slabs (linear profile in height between each two consecutive floors) to the displacements calculated in the previous phase to obtain the actual relative displacements of the walls. Figure 4.27 and Figure 4.28 show the out-of-plane displacements for the RM and UM models, respectively. On the plots, the diagram in the left side presents the relative out-of-plane displacements to the base and the diagram in the right side, represents the actual out-of-plane displacements of the walls.

Similarly to the in-plane displacements there are clear differences on the out-of-plane displacements of the walls belonging to the RM and UM models. In the RM model, very small out-of-plane displacements were found until the seismic input of 200% (0.79g) (out-of-plane displacements lower 3.5mm). The major out-of-plane displacements were found at the first floor, being the highest value found at the first floor of the south wall (9mm) for the seismic input of 300% (1.30g). An increasing on displacements was evident from seismic inputs of 250% (1.06) to the seismic input of 300% (1.21g) and even more from the 300% (1.21g) to 300% (1.30g), as at this stage the transverse walls (with out-of-plane resisting mechanism) guaranteed the stability of the building in the longitudinal direction. At this stage, the severe in-plane damage of the longitudinal walls reduced significantly its in-plane resistance. The out-of-plane displacements in the longitudinal walls were relatively modest, achieving maximum values of 5.9mm in the first floor and of 3.4mm in the second floor in the east wall.

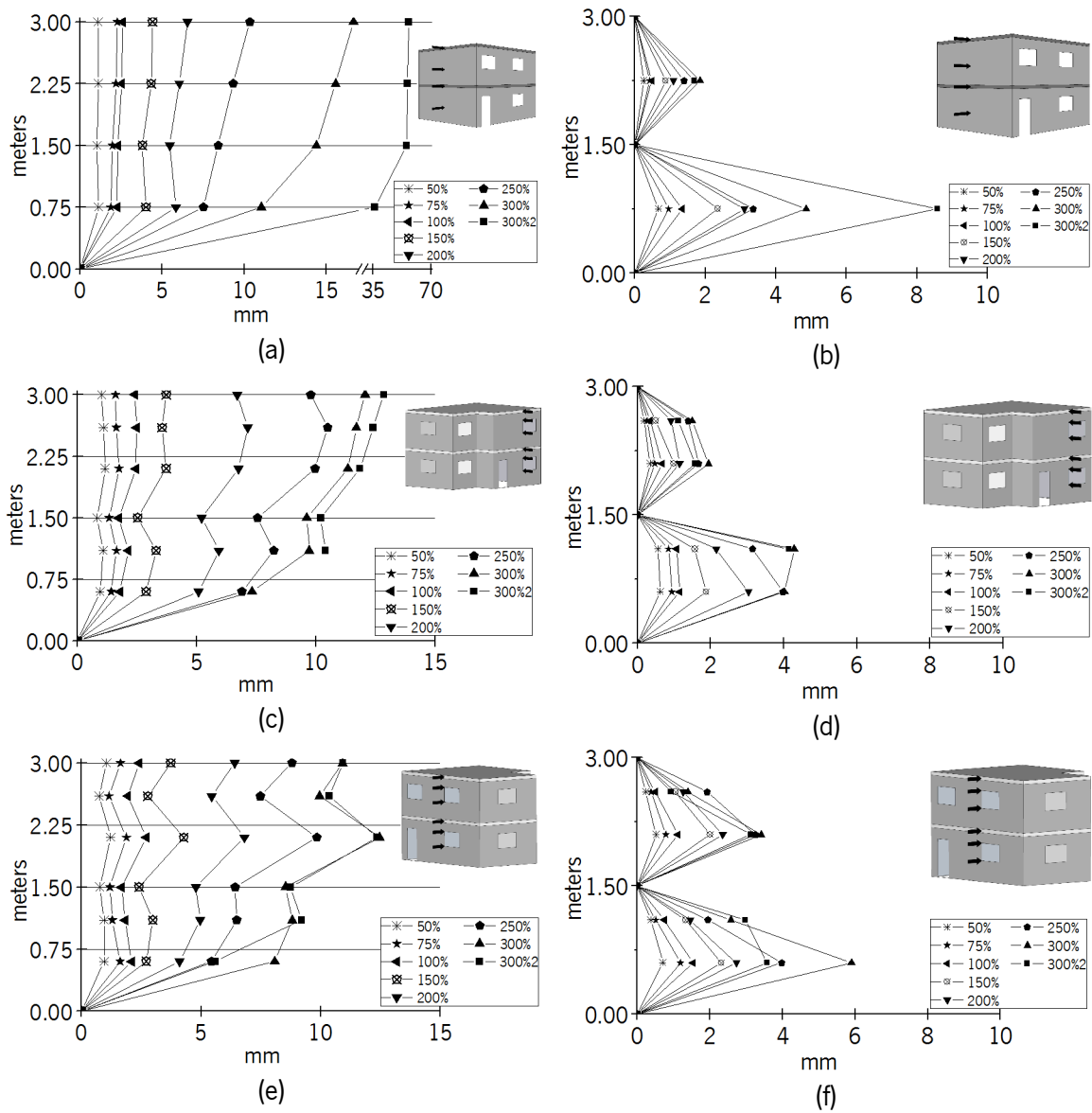


Figure 4.27 - Global and relative out-of-plane displacements for RM in façade: (a, b) south, (c, d) west2 and (e, f) east

In the UM building, the out-of-plane displacements increased for increasing seismic inputs, but kept very modest until the seismic input of 75% (0.33g) (values lower than 1.0mm). The input test of 100% (0.47g) presented an out-of-plane of 2.90mm at the second level of the west wall. Then, an abrupt increase on the out-of-plane displacements were recorded in all walls for the seismic input of 150% (1.07g) and 150%2 (1.24g), particularly in the west wall, whose maximum displacements were measured around the openings. The maximum displacement was recorded at the second floor and was of 4.0mm. In all walls, the higher out-of-plane displacements were measured at the second floor, confirming that the major in-plane and out-of-plane deformations of the UM building developed at this floor.

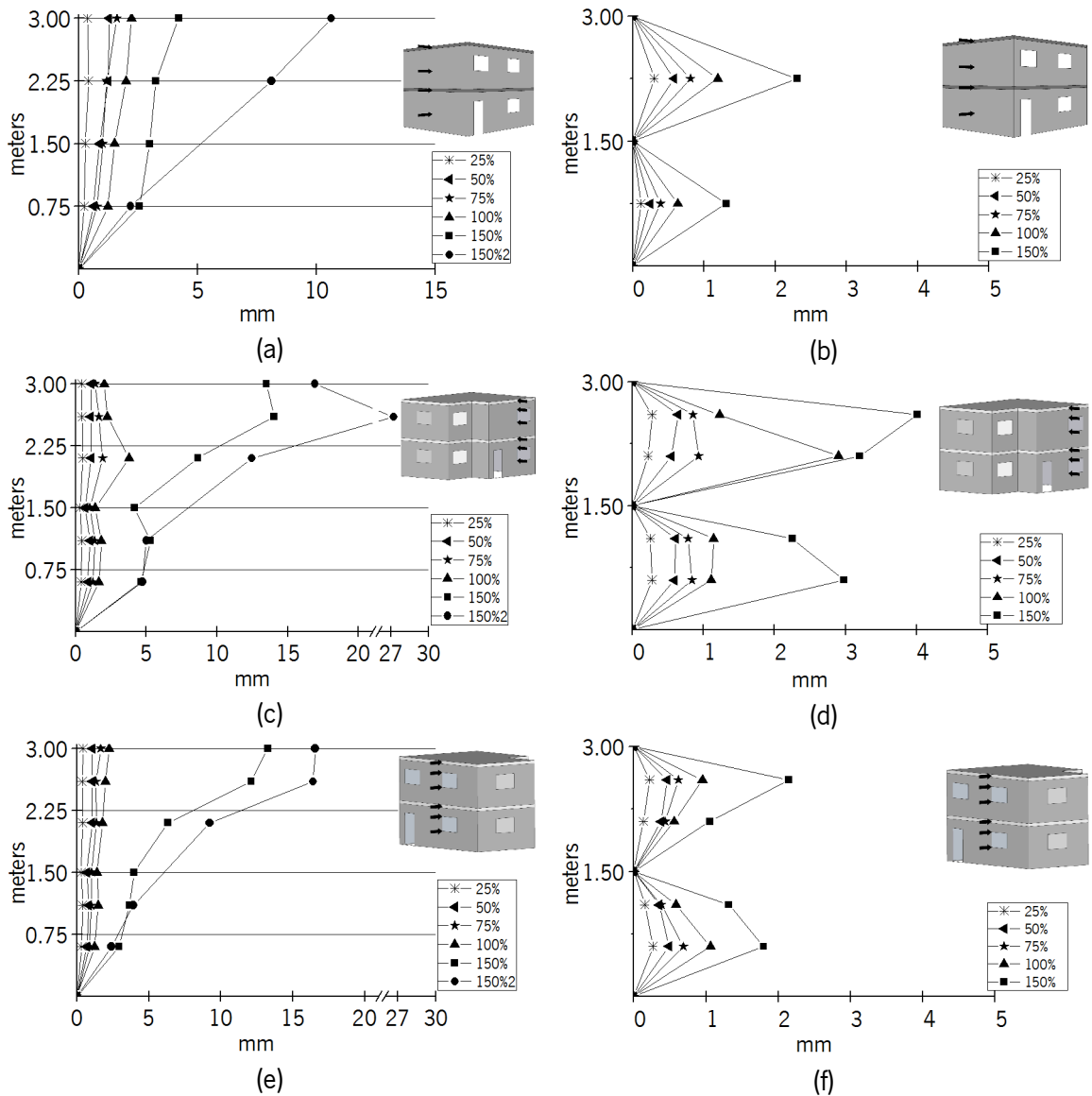


Figure 4.28 - Global and relative out-of-plane displacements for UM in façade: (a, b) south, (c, d) west2 and (e, f) east

Comparing the two asymmetric buildings is observed that the actual out-of-plane displacements in the reinforced structure are higher than the maximum values of the unreinforced building. Additionally, it should be said that this result is associated to very different global behavior of both buildings.

From the comparison between the symmetric and asymmetric buildings, it is concluded that the out-of-plane displacements measured in the RM asymmetric building are higher, which resulted from the more severe damage developed. On the other hand, the out-of-plane displacements measure in the symmetric UM model are slightly higher than the ones measured in the asymmetric building, which is attributed to the higher seismic input reached by this building.

4.6.2.3 Biaxial displacements

The biaxial displacements recorded by the PSDs are the true trajectories in the horizontal plane made by specific points of the structure where the sensors are located. Both asymmetric buildings were instrumented with these devices at two opposite corners of each floor and at the base foundation. Because the camera is mounted on an external frame, the trajectories described the real global movements experienced for the structure or at least for the part of the structure in which the sensor is placed. The biaxial displacements at the south-west corner of the buildings for the final seismic inputs are presented in Figure 4.29.

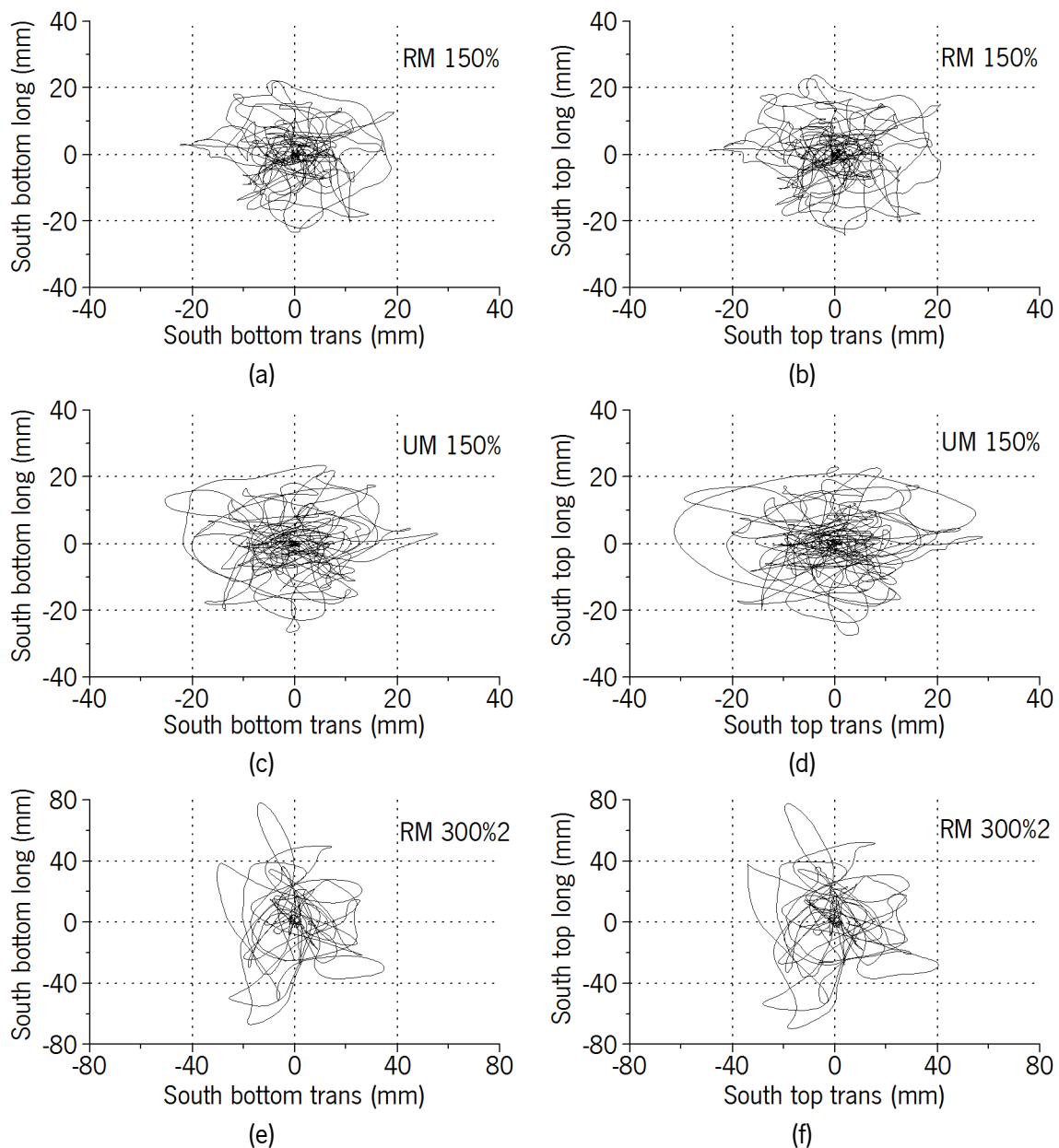


Figure 4.29 - Biaxial displacement trajectories in the horizontal plane at south-west corner in: (a, b) RM building at first and second story for input of 150%, (c, d) UM model at first and second story for input of 150% and (e, f) RM model at first and second story for input of 300%2. Note the different scale for the last plots

The plot presents the results of the input of 150% (0.66g) for the RM building and the first input of 150% (1.07g) for the UM building for comparison purposes and, additionally, the trajectories recorded during the final input of 300% (1.30g) for the RM building.

From the comparison of diagrams, the following conclusions are obtained: (1) as expected, the UM model present higher displacement trajectories in the final seismic input (seismic input of 150%), when compared to the RM model. At this stage, the RM model has only minor damage, whereas the UM model was deformed and developed severe damage; (2) the predominant deformation of the UM model was in the transverse direction, suggesting that the transverse walls are main resisting elements; (3) in the UM model, there is a clear difference on the biaxial displacements from the first to the second floor, which is associated to the major damage at the second floor associated to sliding mechanism along the cracks formed; (4) in case of the RM, the major displacements for the last seismic input are in the longitudinal direction, which resulted from the severe damage on the longitudinal walls; (5) in the RM model, there are no major differences from the first to the second floors, which is associated to the first story resisting mechanism. In fact, the lateral drifts observed in the last stage of loading are very modest. As the damages were concentrated at the first floor, the second slab moves almost the same as the slab at first floor; (6) in the RM model the transverse movements are practically the double of the transverse displacements seen in the UM model, considering the last loading stage for both of them. In the longitudinal direction, the RM model presented almost 4 times higher amplitude than the UM building.

4.6.2.4 Amplification factors from the displacements

The analysis of the amplification of the displacements was based on the displacement trajectories registered by the PSDs located at the South-West and North-East corners, and at the base. The displacement amplification of the slabs was subtracted to the amplification calculated at the base foundation for both longitudinal and transverse directions.

Figure 4.30 presents the displacement amplifications vs PGA for the two asymmetric buildings. The plots are separated by direction and the abbreviations labels are N, for north; S, for south; T, for top or second slab; B, for bottom or first slab and R or U for reinforced or unreinforced, respectively.

By comparing both buildings, it is seen that the displacement amplification factors are usually above 1.0 and present a trend for increasing with increasing PGA. This means that the structure always amplified the given input.

RM building presents amplification factors very close for the first and second floors in the longitudinal and transverse directions, when the displacements measured corners north-east are analyzed. It is observed that from the displacements measured at the south-west corner, in general, the longitudinal and transverse directions are slightly higher at the second floor. These behaviors can be explained as follow: (1) the damage concentrate at the first floor and as already discussed, the second slab exhibits very close total displacements to the displacements measured at the first floor. This behavior is in agreement with the final failure mechanism presented in this building, which considerably affected the longitudinal walls at first level. The second level was almost not affected by

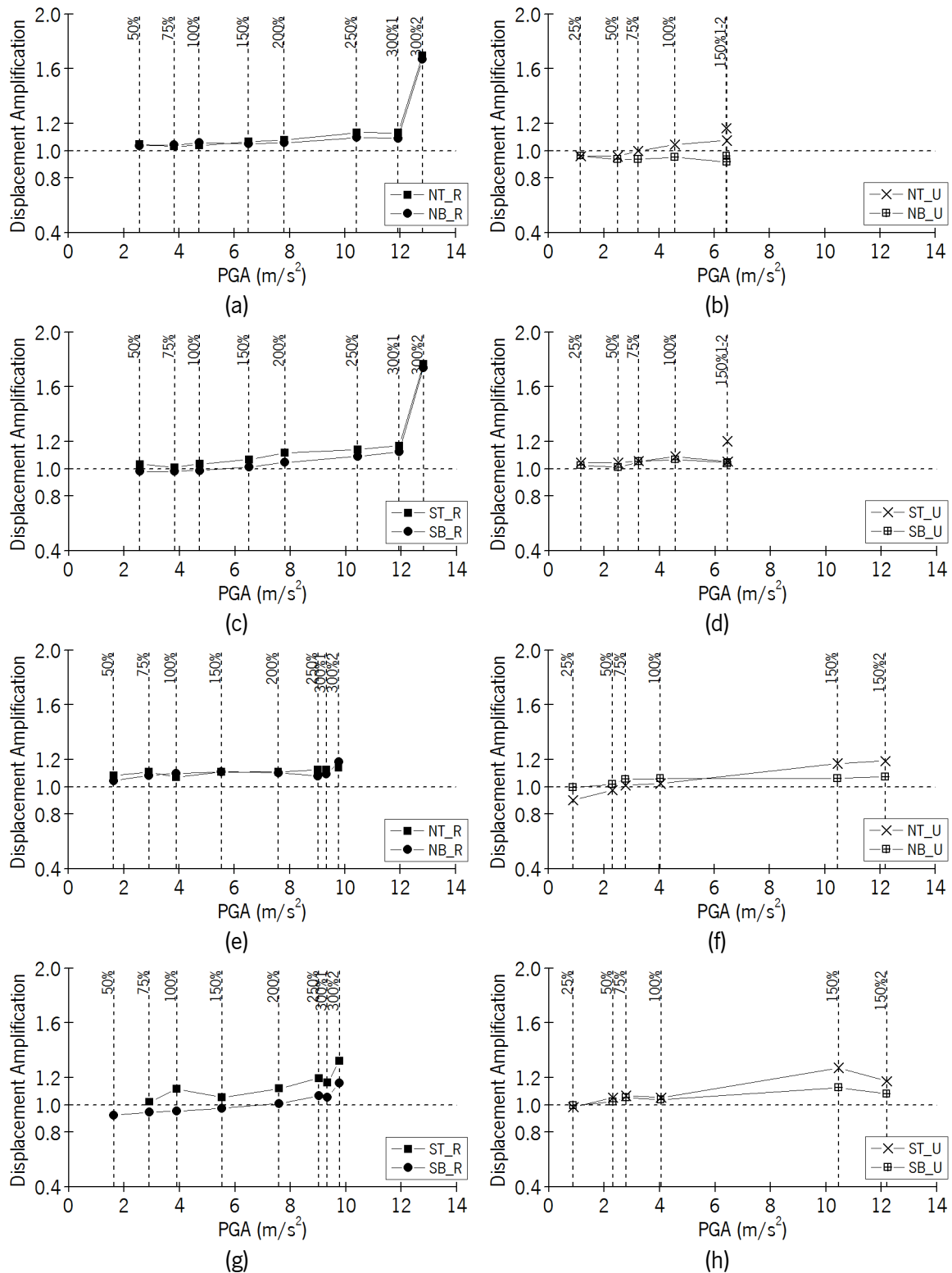


Figure 4.30 - Displacement amplification versus PGA for: (a, b, c, d) longitudinal direction and (e, f, g, h) transverse direction

the seismic inputs and then it moves according with the first slab; (2) on the other hand, it appears that some distortion occurred, leading to the differences at the south-west corner. This can be also justified by the slightly different amplification factors of the displacements in the transverse direction,

as can be seen when north-east and south-west corners are compared. On the other hand, it is seen that the abrupt increase on the displacement amplification factor measure in the longitudinal direction (from both south-west and north-east corners), is associated to the severe damage observed in the longitudinal walls for the seismic input of 300%2 (1.30g).

In case of UM model, the differences of the displacement amplification factors between the first and second floors are higher than in case of the RM model. As already discussed, this can be explained by the predominance of the damage at the second floor. When the amplification factors of the longitudinal displacements are analyzed, it is seen that there is a distinct trend in the displacements measured at south-west and north-east corners (Figure 4.30 b, d). In fact, the amplification factors are practically coincident at the first and second floor in case of the longitudinal displacement is measured in the south-west corner. However, the different is considerably higher in case of the longitudinal displacements measured at the north-east corner, where a distinct increasing and decreasing trends were observed for the first and second floors, respectively (Figure 5.29b). This behavior confirms that: (1) the different behavior presented for each level and (2) the rotational movements presented in this model. When the transverse direction is analyzed, it is observed that the displacement amplification factors present an increasing trend, either if the transverse displacement is measured at the south-west or at north-east corners. In this direction, it is seen that the displacement amplification factor presents lower values at the second floor up to a PGA of 4.0m/s^2 .

In any case, it is also observed an important increment in the amplification for the transverse direction, which has relation with the high PGA presented in this direction (about twice the PGA in the longitudinal direction). The high PGA for the last inputs was also discussed in Figure 4.1b. For this building, it was clear that the transverse direction was the weakest one, decreasing its capacity and leading to a failure mode that boosts the forces and displacements on it.

4.6.2.5 Local displacements

The local displacements are the displacements measured by the LVDTs located in the piers between openings in the east wall to obtain their in-plane deformations at both levels (Figure 4.31).

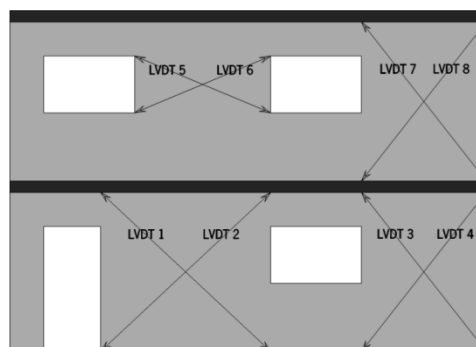


Figure 4.31 – LVDTs position on asymmetric buildings at east wall

During the seismic input tests, the LVDTs registered positive and negative displacements according to the cyclic (dynamic) displacements induced in the piers. The maximum positive and the minimum

negative values were obtained, after a sum of absolute values it was obtained the range or total length of displacement performed. Table 4.4 presents the total length obtained for each LVDT through all the input tests for both masonry buildings.

Table 4.4 - Maximum values of the displacements measured by LVDTs (in mm)

	LVDT 1		LVDT 2		LVDT 3		LVDT 4	
	RM	UM	RM	UM	RM	UM	RM	UM
25%	-	0.41	-	0.19	-	0.35	-	0.21
50%	0.83	0.76	0.26	0.83	0.16	1.19	0.82	0.64
75%	2.09	0.43	0.43	0.65	0.79	1.03	1.48	0.91
100%	3.09	1.27	0.63	1.24	1.28	3.28	2.17	1.21
150%	4.05	3.47	1.08	3.55	3.01	5.67	3.35	4.65
150%2	-	4.10	-	3.03	-	8.90	-	3.28
200%	4.60		1.62		4.23		3.64	
250%	9.01		2.53		6.51		5.76	
300%	12.88		4.18		11.78		8.86	
300%2	77.90		62.31		120.68		63.29	
	LVDT 5		LVDT 6		LVDT 7		LVDT 8	
	RM	UM	RM	UM	RM	UM	RM	UM
25%	-	0.06	-	0.13	-	0.06	-	0.20
50%	0.50	0.15	0.10	0.16	0.06	0.23	0.02	0.45
75%	1.08	0.14	0.13	0.18	0.24	0.28	0.05	0.33
100%	1.53	0.27	0.29	0.23	0.43	0.36	0.07	0.56
150%	2.56	3.64	0.54	3.54	0.89	4.14	0.08	5.94
150%2	-	17.99	-	18.21	-	6.68	-	12.72
200%	4.26		0.63		1.14		0.14	
250%	5.89		0.90		1.78		0.23	
300%	6.16		1.06		1.57		0.28	
300%2	5.82		0.69		1.44		0.23	

The analysis of displacements of LVDTs revealed very interesting results as they confirm the damage levels at the eastern masonry piers for each seismic input level. Thus, it is possible to observe that: (1) the values of displacements of the diagonals in the UM model are relatively small until the last input of 150% (1.07g), both at first and second levels. The displacements have an abrupt increase for the seismic input of 150%2 (1.24g) in the masonry piers at the second floor, resulting from the increase on the opening of horizontal cracks and sliding along the horizontal cracks that develop in these piers; (2) in the RM model, the displacements generally increased for the increasing seismic inputs. The diagonal displacements are much higher at the first floor than in the second floor as the results of the more extensive cracking at this floor. The abrupt increase on the displacements for the seismic input of 300%2 (1.30g) at the first floor is associated to the crushing and consequent detachment of masonry blocks from the masonry piers. The final displacements at the second floor are much reduced, which is associated to low level of damage and thin crack openings, as discussed previously; (3) the results of local displacements are very well related with the damage

observed in the masonry piers, revealing to be a good indication on the deformation features of the masonry piers of both masonry buildings.

4.6.3 Base shear vs. displacement diagrams

The seismic capacity of the asymmetric buildings submitted to seismic loading is evaluated through the base shear vs lateral displacement diagrams. The base shear was calculated as a base shear coefficient (BSC) defined by Equation 3.2, already used in Chapter 3. It is calculated as the ratio between the base shear at the base of the model and its total weight. The displacement considered in the diagram is normalized by the height of the building, being given by the ratio between the top displacement and the height of the building (in percentage). This procedure was also followed in Chapter 3 and aims at avoiding the influence of the geometrical scale both on the base shear and on the top displacement.

For the calculation of the experimental base shear, each building was divided in several bodies according with the distribution of the accelerometers, for which the mass was obtained. Then, together with the accelerations of each accelerometer, the inertial forces were calculated for every time step. At the same time, the displacements at the top of the building were recorded. Figure 4.32 presents the hysteresis loops obtained for the input test of 100% for the two asymmetric masonry buildings. The seismic capacity of the buildings was studied for each direction individually. From the comparative analysis of the hysteresis loops, it is stressed the considerable larger loops obtained for the RM model, indicating a higher capacity to dissipate energy. This is notable, as for the seismic input of 100%; the RM model only presented few cracks at the first floor. However, it is possible that micro cracking developed, even if it is not visible, contributing to the dissipation of energy. On the other hand, it is clear that the UM model evidenced much lesser dissipative nature, even if the damage is more developed. It is seen that it appears that the dissipation is also higher in the longitudinal direction, which can be attributed to the higher diagonal crack density. The displacement capacity appears to be similar for both models, but the base shear coefficient is higher in case of RM model in both longitudinal and transverse directions. It should be noticed that the RM model is able to reach a higher resistance with much more controlled damage than the UM model.

The monotonic envelopes defined through the maximum base shear and maximum displacement of hysteresis loops obtained for each seismic input are presented in Figure 4.33. The reinforced masonry building presented considerably higher seismic resistance when compared with the UM model in both directions. In the RM building, the BSC is 60% higher in the longitudinal direction and 35% in the longitudinal direction in average.

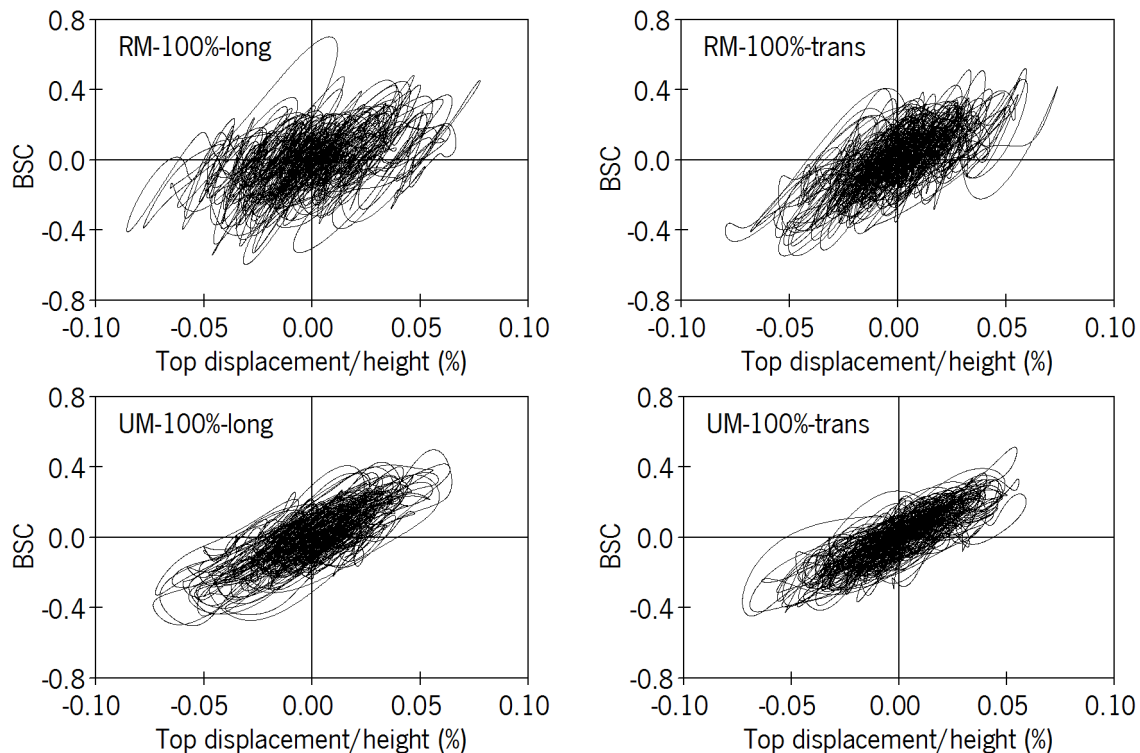
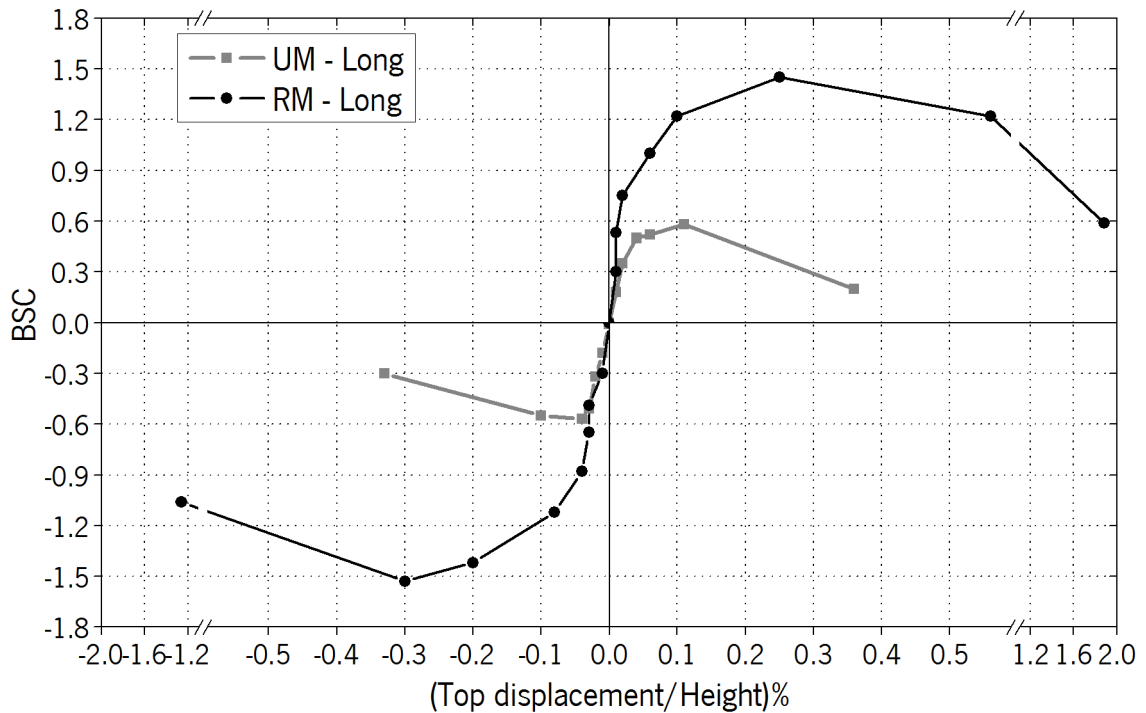


Figure 4.32 - Base shear coefficient versus top displacement/height in percentage, for the asymmetric buildings during the seismic input of 100%

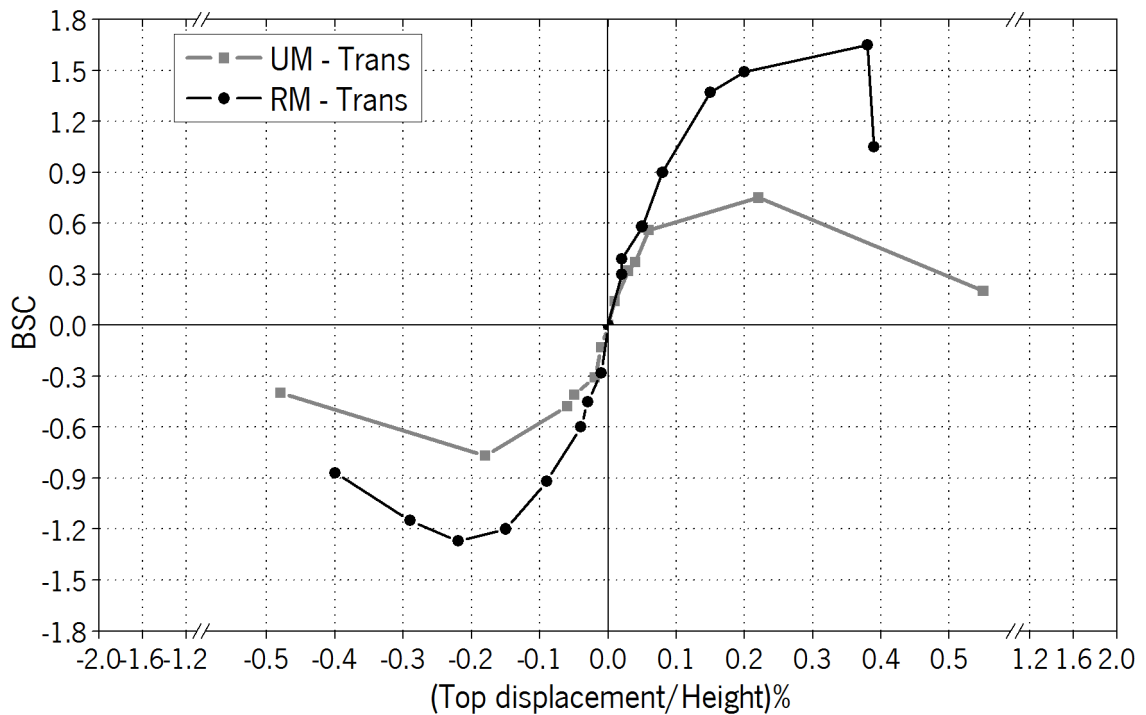
The RM model presented also a much higher ability for the nonlinear deformation in the longitudinal direction, being the deformation in the transverse direction slightly lower than the deformation measured in the UM model. This behavior is associated to the severe damage induced in the longitudinal walls, particularly in the last seismic input of 300%. Besides, the more controlled damage observed in the RM model resulted, even for higher levels of seismic input, in lower values of the deformation than in the UM model. As already mentioned, the RM model is much controlled by the behavior of the longitudinal walls, whereas the UM building is more controlled by the behavior of the transversal walls.

The RM building presents similar base shear coefficients in both directions. However, the degradation of the resistance is faster in the transverse direction, in which out-of-plane resisting mechanism developed, particularly for the last seismic input due to the severe degradation of the longitudinal walls. The addition of the minimum vertical and horizontal steel reinforcement is responsible for the remarkable improvement of the seismic performance of the RM building, both in terms of resistance and deformation ability.

In case of UM building, the resistance was considerably higher in case of the transverse walls, justifying in this way the major role of these walls in its global resistance. With this respect, it should be noticed that the rotational mode appears to be more important in case of UM building, contributing to a higher loading action in the transverse walls without openings. In addition, the displacements were also higher in the transverse direction due to the predominant sliding movements in this direction.



(a)



(b)

Figure 4.33 - Experimental hysteresis envelopes curves for the asymmetric RM and UM buildings: (a) longitudinal direction and (b) transversal direction

In the symmetric reinforced building, the maximum seismic input was controlled by the maximum capacity of the shaking table, whereas in case of the asymmetric reinforced building, the maximum seismic input was controlled by the resistance and damage condition of the building. This means that the resistance of the RM symmetric building was not completely explored and thus the displacement capacity was not exhausted, as well. From the comparison between the symmetric

and asymmetric UM building, it is seen that the symmetric building presents higher resistance and deformation, particularly in the longitudinal direction. This must be related to the additional forces imposed to the walls, particularly the north, east and west wall, by more important torsional effects of the asymmetric building, when compared to the symmetric building. In both cases, it is stressed that UM model can withstand low to moderate seismic inputs without losing the stability, being the damage reparable, if the reference seismic input for Lisbon area is considered.

4.7 Conclusions

In the present chapter, the most important results obtained from the shaking table tests on two concrete block masonry buildings (one reinforced and one unreinforced) were presented and discussed. The buildings exhibit asymmetric plan geometry and can replicate a residential typology with two stories. According to what was made for the symmetric buildings, the models of the buildings were built at a scale 1:2 in relation with their original prototype. Incremental seismic input motions in two orthogonal directions were considered to each building; additionally dynamic identification after each test was performed. From the analysis of results given in terms of damage, accelerations and displacements is possible to conclude that:

1. The dynamic identification of the buildings revealed that the first three frequencies are associated to transverse and longitudinal mode shapes and to a third torsional mode shape. The frequencies of the first and third mode shapes are very close between models, but the frequency found for the second mode is higher in case of RM model. This might be associated with some cracking around the windows for the UM model, combined with the higher percentage of vertical reinforcement and the filling of the vertical continuous joints with mortar, mainly in the walls with openings, for the RM model.
2. The behavior of the concrete block masonry buildings was rather different. The RM building developed a failure mechanism at the first floor, being the behavior ruled by the resisting mechanisms developed in the longitudinal walls (second mode). In this way, the major damage was concentrated at the first floor and the major deformation occurred in the longitudinal direction. In terms of interstory drifts, they were considerably higher at the first floor than at the second floor. On the other hand, the seismic behavior of the UM building was characterized by damage distributed at both floors, even if it was more severe at the second floor. Long horizontal cracks, particularly at the second floor, divided the building in macro-blocks that exhibit relative sliding for the last seismic input of 150%. From the results, it was possible to assess the clear influence of the first transverse and the third torsional modes in the final failure mechanism.
3. As consequence of the damage, it was seen that frequencies and damping ratios exhibit a reduction and an increase respectively as the damage increases. Besides, the evolution of damage indicators is rather distinct for the RM and UM models, which is believed to be associated to the distinct typology of damage developed in each buildings.
4. The RM model is naturally more dissipative than the UM model. This is seen from the hysteresis loops and is a consequence of the typology of damage and deformation capacity

of the buildings. A more distributed diagonal cracking along the unit mortar interfaces, sometimes along concrete block units, is more dissipative than long horizontal joints. The responsibility for more dissipative behavior of the RM building is attributed to the vertical and horizontal reinforcements.

5. The contribution of the torsional mode in the seismic behavior of the masonry buildings resulted in the limitation of the maximum seismic input imposed to the models, due to the development of severe damage, mainly in case of UM model. In fact, when compared with the symmetric buildings, the input reduced from 400% to 300% in case of RM model and from 250% to 150% in case of the UM building. The torsion is a consequence not only of the geometric irregularity but also of the irregular distribution of openings. With this respect, it is stressed that the RM model is able to withstand a seismic input considerably higher than the reference input of Lisbon. On the other hand, the UM building was able to withstand the reference input of Lisbon, even if with lower safety level.

Chapter 5

Numerical modeling of the seismic behavior of masonry buildings

Abstract

Numerical simulation provides the structural engineering community with means to represent reality outside the laboratory. It gives the possibility of simulating real performance, and quickly assessing multiple design alternatives towards design optimization before the first block is placed. This saves time and money, and gives confidence to the designers and constructors. Additionally, this engineering environment allows the representation of different scenarios, hence becoming a tremendous tool that easily handles structural synthesis and refinements based on experimental data and code regulations, aiming at the optimization of the design process and the future performance of the structure.

5.1 Introduction

Complementary to the experimental research on the dynamic behavior of masonry buildings, numerical simulation is important to help the full understanding of the major resisting mechanisms of structural elements and their interaction when submitted to seismic action, namely interaction between in-plane and out-of-plane effects. When seismic loading is addressed in masonry buildings, both non-linear static and nonlinear dynamic analysis can be envisaged. In general, the non-linear static analysis (pushover) can be viewed as a simplification of the dynamic non-linear analysis as the seismic loading is represented in a simpler way, namely with a loading configuration proportional to the mass or proportional to the fundamental mode shape found for the building. Alternatively, nonlinear dynamic approach is more realistic as seismic signals can be given as input to the numerical models.

At the level of numerical simulation based on finite element modeling, two main possible numerical approaches for masonry structures can be followed, namely macro modeling and micro modeling both for static and dynamic loading (Chaimoon and Attard 2009; Haach et al. 2011; Lourenço et al. 1998; Penna et al. 2014; Rota et al. 2008). Micro modeling is more suitable for a detailed analysis of masonry elements, where it is important to describe the local resisting mechanisms. The macro modeling allows an evaluation of large size masonry structures, where the global behavior, including the interaction among the distinct structural elements, is the real concern. Both approaches can be useful for the understanding of the behavior of masonry and they should be selected based on the final aim of the analysis.

In the particular case of numerical simulation of the dynamic behavior of masonry buildings tested in a shaking table, nonlinear dynamic analysis could provide a more complete analysis as it is possible to assess the time history accelerations and displacements along the seismic input. On the other hand, the nonlinear static analysis is a more straightforward method and can give an idea about the stiffness, global resistance and ultimate displacement capacity, if compared with the monotonic experimental envelop.

The numerical simulation of shaking table tests has been carried by several authors (Rezaifar et al. 2008; Tomažević and Gams 2012; Xuwei et al. 2008). Nakagawa et al. (2012) carried out a numerical simulation of a brick masonry building tested on a shaking table, where the bricks were modeled as rigid bodies and the mortar as springs. Similar dynamic inputs to the ones implemented in the shaking table tests were imposed to the numerical model. Good correlation was found in terms of damage but the numerical results differ from those of the shaking table test regarding the collapse mode. Tomažević and Gams (2012) studied the response of three masonry buildings with the same distribution of walls but different number of floors by shaking table tests. From the tests, a numerical model with concentrate masses and building story hysteretic rules was used to simulate the behavior. The results of the simulation presented good correlation with the experimental observations including the nonlinear behavior. From the model, resistance curves were obtained representing accurately their hysteretic behavior. Juhásová et al. (2002) developed a numerical finite element model of a masonry building which was calibrated based on shaking table tests. The emphasis of the model was given to the boundary conditions as it included boundary elements that

represent the interaction model-shaking table that appeared during the experimental tests. For this simulation, vertical and horizontal springs were used at the base of the model. Artificial signals were imposed to the model from which important information was obtained. Retrofitting and specific reparations of the structure were also evaluated with good results. Here, a contribution to the simulation of soil-structure interaction by using shaking tables was presented, as well.

Besides finite elements models, the global behavior of masonry buildings can be also analyzed using other numerical approaches. Different commercial software solutions can be used for this purpose, as AEDES (www.aedes.it), FEDRA (www.runet-software.com), POR 2000 (www.newsoft-eng.it), ANDILWall/SAM (www.crsoft.it) and 3Muri (www.stadata.com), among others. Most of them use macro-elements, as its application in practical situations is more straightforward. Penna et al. (2014) presented a nonlinear macro-element model for the seismic analysis of masonry buildings which has been widely accepted due to its versatility. The model is able to represent the flexural-rocking and shear damage modes as well as the interaction of shear and flexural damage. Marques and Lourenço (2008) performed a comparative study between SAM and 3Muri software solutions. The seismic response of two masonry buildings was predicted using macro-elements and pushover analysis. The results show good performance of the macro-elements, which provide realistic predictions of the structures response to earthquakes.

Most of the available software solutions based on macro-elements do not allow the application of dynamic loads and present limitations for the detailed simulation of connections and boundary conditions. Thus, in the present work it was decided to use a macro modeling finite element approach in which seismic inputs can be given and wide options for the simulation of the nonlinear material behavior of masonry are possible.

5.2 Objectives and methodology

The main objective of the present chapter is to provide a numerical model that represents accurately the seismic behavior of unreinforced masonry. For this, the quantitative and qualitative experimental results obtained in Chapter 3 for the unreinforced symmetric concrete block masonry building are taken into account. It is expected that after a detailed calibration process, the numerical model will represent mathematically, as accurate as possible, what happened during the experimental campaign.

A detailed numerical finite element model should be defined based on full 3D representation of the actual experimental unreinforced masonry building in which all its structural components will be considered. The material properties previously obtained from experimental investigation in section 2.6 are used in the numerical simulation. Besides, phase structural analysis is planned for the simulation of the incremental seismic input motion. In this way, damage produced by previous inputs is considered as initial conditions for the next inputs, identical to what happened in testing. Nonlinear dynamic analysis with time integration is performed for every stage of seismic inputs, considering also the phased increasing seismic loading. Finally, similar data as the one obtained for the experimental building regarding accelerations, displacements and strains (damage) are provided.

5.3 Construction of the numerical model

The finite element method is adopted in this study for the numerical simulation of the structural seismic behavior of the unreinforced masonry building studied in Chapter 3. Due to the available time for the elaboration of the present thesis and aiming to obtain useful information for unreinforced masonry behavior, it was decided to focus only in one model (from the four experimental models tested). The first tested building, i.e. the symmetric unreinforced masonry building, was selected for this purpose.

The computer program TNO DIANA (DIANA 2010), which is a 3D software package that integrates parameterized CAD models with powerful structural analysis solvers, was adopted. DIANA can evaluate properly the nonlinear tensile behavior of masonry, which is a key parameter for its study as a structural material.

Prior the construction of the numerical model it is mandatory to select the modeling strategy. As discussed previously in section 1.1.2, the micro and macro modeling approaches can be used for masonry. As the structural analysis in the present study is focused on the global dynamic behavior of a concrete block masonry building (masonry walls will interact with other structural elements, subjected to simultaneous in-plane and out-of-plane forces) and taking into account the time and computational capacity costs, a macro modeling approach was adopted.

Additionally, it is also necessary to define which types of elements should be used in 3D. In general, it is possible to use solid elements or simplified elements (beam, plane, shell elements, etc.). Solid elements represent directly the real volume of objects. Instead, other elements have the geometry embedded and only the axis or middle plane are considered. For example, a beam can be represented by a line, to which geometry properties like height and width are assigned. In solid elements, the geometry of the masonry unit blocks and therefore walls are drawn with their real dimensions, representing their volume and mass. With shell elements, unit blocks must be drawn based on its middle plane. Then, attention is needed when defining the intersection between structural elements like the wall to wall and wall to slab connections.

The structural components of the unreinforced masonry building are the masonry walls, the reinforced concrete slabs and the reinforced concrete beam foundation. Because the reinforced concrete beam foundation was attached to the shaking table and no displacements are expected from it, the numerical model firstly considered only the masonry walls and the rigid concrete slabs. The size of the model, the objective of the analysis, the large systems of equations generated, the available time and the accessible computational capacity, suggest that shell elements should be selected. Thus, the dimensions of the numerical model correspond to the dimensions of the midline of the walls and slabs from the experimental model.

For the present model, both the walls and the slabs will share the same type of element, namely a quadrilateral eight nodes curved shell element. This element is designated by the software as CQ40S; see Figure 5.1a. Curved shell elements are isoparametric elements that include transverse shear deformation according to the *Mindling-Reissner* theory. Five degrees of freedom were defined in every element's node, namely three translations and two rotations. Further characteristics of the

curve shells are that they must be thin, i.e. their thickness must be small in relation to the in-plane area dimensions, which is in agreement with the walls and slabs geometries. Moreover, force loads may act in any direction, namely in-plane and out-of-plane directions to the element. This confirms them as excellent candidates for the study of model behavior under dynamic loads. The basic variables of regular curved shell elements are the translations u and the rotations ϕ . The derived variables are the strains, the Cauchy stresses and the generalized moments and forces. In particular, the interpolation polynomials for the translations u and the rotations ϕ for the CQ40S curve shell element are expressed in Equation 5.1 and Equation 5.2

$$u_i(\xi, \eta) = a_0 + a_1\xi + a_2\eta + a_3\xi\eta + a_4\xi^2 + a_5\eta^2 + a_6\xi^2\eta + a_7\xi\eta^2 \quad 5.1$$

$$\phi_i(\xi, \eta) = b_0 + b_1\xi + b_2\eta + b_3\xi\eta + b_4\xi^2 + b_5\eta^2 + b_6\xi^2\eta + b_7\xi\eta^2 \quad 5.2$$

Typically, for a rectangular element, these polynomials yield approximately the following strain and stress distribution along the element area in the ζ thickness: The strain ϵ_{xx} , the curvature κ_{xx} , the moment m_{xx} , the membrane force n_{xx} and the shear force q_{xz} (DIANA 2010).

A Gauss integration over the ξ and η element area should be selected. The integration in the thickness (ζ axis) may be Gauss or Simpson. Then, following the order of $n_\xi \times n_\eta \times n_\zeta$ the slabs present an integration scheme of $2 \times 2 \times 2$ and the walls of $2 \times 2 \times 9$. Thus, in the in-plane element area both slabs and walls have the same integration rule i.e. Gauss integration, see Figure 5.1b. Along the thickness, the slabs have 2 integration points according with Gauss integration rule, as they will remain elastic, and the walls have 9 integration points according with Simpson rule, as they will behave inelastic. The decision of using this quantity of integration points seeks for better accuracy of the numerical model, in the through-thickness integration in the presence of non-linearities. Figure 5.2 shows the enumeration of the integration points in the thickness direction for the various schemes and an example of slabs' integration points.

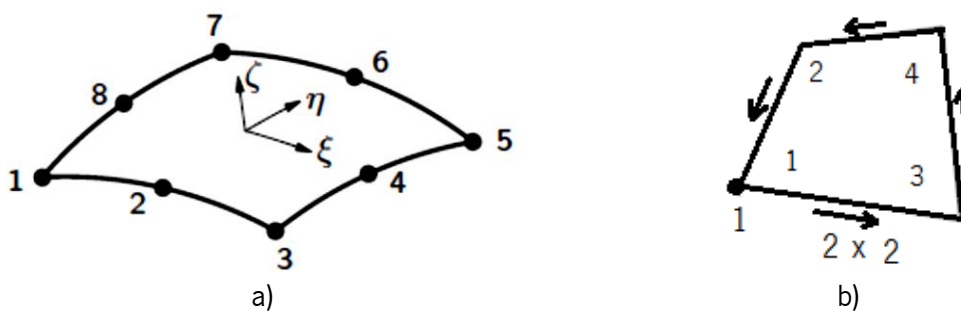


Figure 5.1 – Curved shell element (CQ40S): a) Example of element implemented for walls and slabs, b) in-plane Gauss integration for quadrilateral elements

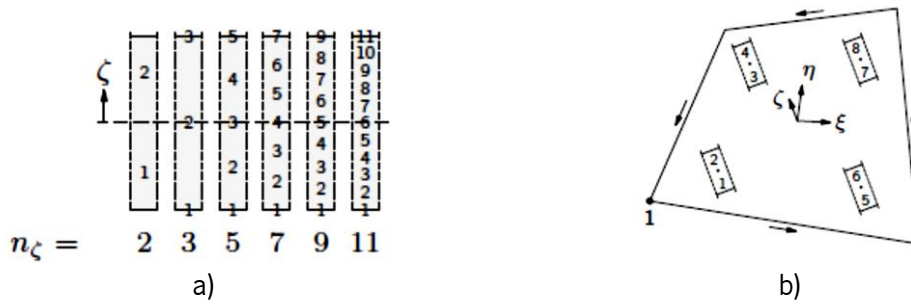


Figure 5.2 – Thickness integration schemes for quadrilaterals: a) Gauss (2-point) and Simpson (more than 2 points) integration, b) example for slabs' integration $2 \times 2 \times 2$

The meshing process was performed by using paving algorithm with a density value of one (ranging from 0.1 to 2). This algorithm creates a quadrilateral free mesh on any type of surface. Special care was taken with the dimensions of the elements, as the idea was to evaluate the main structural components with acceptable computer effort and adequate element quality. Figure 5.3 presents the final mesh distribution of the model. Note the difference between elements' size in walls with and without openings.

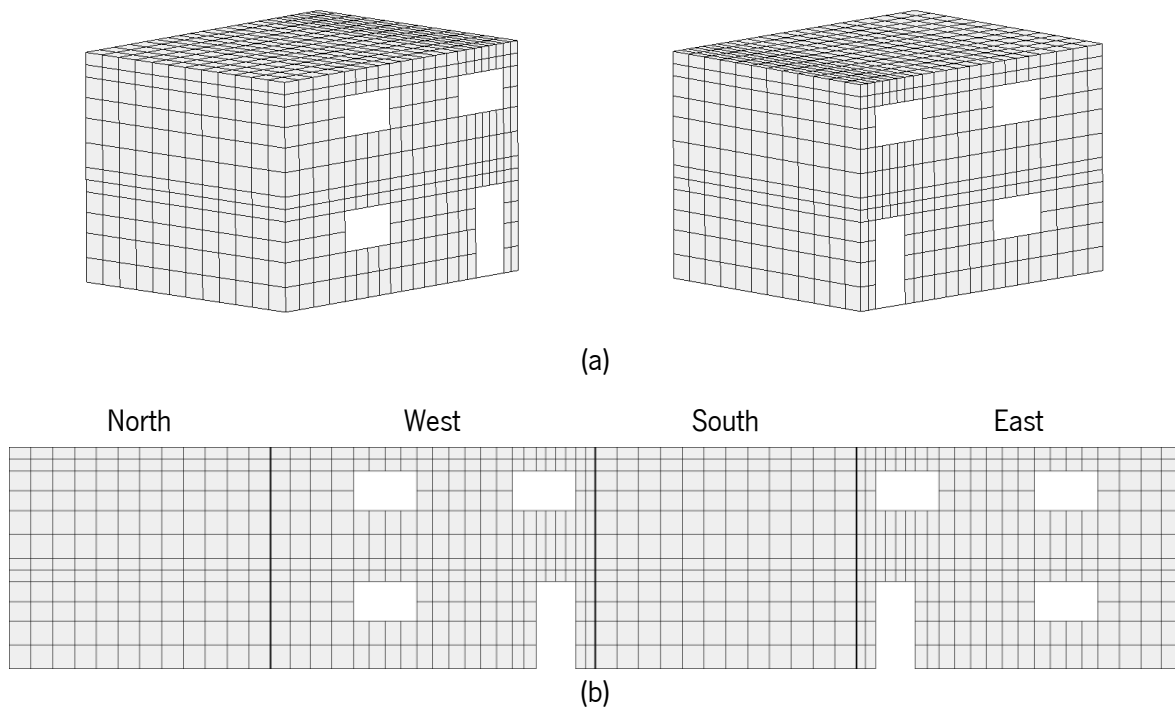


Figure 5.3 – Mesh of the numerical model: (a) 3D view and (b) detailed view

The boundary conditions correspond to total fixed constraints. It should be reminded that the physical concrete beam foundation was not considered in the model, as it was considered that is fully and adequately attached to the shaking table and no displacement occurs at the base of the beam. Thus, fixed constraints were applied at the base of the perimeter of the walls. The final model is composed by 1256 curved shell elements and 136 fixed constraints.

The thickness for either the walls or the slabs was 10cm, as in the experimental model. With regard to the material properties, at the stage of the calibration of the model, only linear properties are

required. They were taken from the materials characterization, discussed in section 2.6. The values for the elastic properties are summarized in Table 5.1.

Table 5.1 – Linear elastic material properties

Element	Material	Young 's Modulus E (GPa)	Poisson 's Ratio ν	Specific mass ρ (kg/m ³)
Walls	Masonry	5.3	0.2	1200
Slabs	Reinforced concrete	30	0.2	2500

For the completion of numerical model 's construction, it is needed to define the loads. At the stage of the calibration of the numerical model, only the application of the dead weight load is required.

Finally, it is important to note that, as aforementioned, both walls and slabs were implemented with curved shell elements, which imply that their geometry have to be drawn according to the middle line of the thickness of the corresponding experimental structural elements. Consequently (and in particular), the slabs does not have the real perimeter of the experimental model and the final total mass of the numerical model is slightly lower than the real one. To overcome this, the density of the slabs was modified in order to obtain the real mass.

5.4 Calibration of the numerical model

After the construction of the numerical model and specification to the software of the physical and material properties, boundary conditions and loads, the calibration of the model, based on the experimental results of the natural frequencies and mode shapes, was carried out. The calibration is a process in which the numerical modal parameters (in the linear range of the structure) are compared with the experimental ones. The calibration is the first validation of the numerical model and a guarantee that the numerical model behaves according to the experimental one, at least in the linear range.

For the calibration process, the methodology used by Teughels (2004) and Ramos (2007) was implemented. It consists of a nonlinear least square method that minimizes an objective function π , involving the numerical and experimental results of the natural frequencies and modal shapes ' displacements. In detail, the function considers the relative error between the numerical and experimental natural frequencies and the difference between the numerical and experimental mode shapes, as defined in Equation 5.3:

$$\pi = \frac{1}{2} \left[\sum_{i=1}^{m_{\omega}} W_{\omega,i} \left(\frac{\omega_{i,N}^2 - \omega_{i,E}^2}{\omega_{i,E}^2} \right)^2 + \sum_{i=1}^{m_{\phi}} W_{\phi,i} (\phi_{i,N} - \phi_{i,E})^2 \right] \quad 5.3$$

where m_{ω} and m_{ϕ} are the number of eigen frequencies and mode shapes respectively used for the calibration, $W_{\omega,i}$ and $W_{\phi,i}$ are the global weighting diagonal matrices for the frequency values and

mode shapes' displacements, $\omega_{i,N}$ and $\omega_{i,E}$ denotes the numerical and experimental eigen frequencies values and finally $\phi_{i,N}$ and $\phi_{i,E}$ are the numerical and experimental mode shapes' displacements. Here, the experimental and numerical mode shapes are normalized so that the maximum real value of the modal displacement is equal to one. Thus, the numerical and experimental values can be compared.

The calibration was carried out using the software MATLAB (2006) (function *lsqnonlin*) to minimize the objective function and the software DIANA (2010) to obtain the numerical natural frequencies and mode shapes' displacements. The experimental values of the natural frequencies and mode shapes for the unreinforced symmetric building discussed in the section 3.4 were used as experimental targets. The tolerance given for the updating algorithm was 10^{-6} after which the iterative process was stopped.

The calibration process is complex as: (1) the iteration process always consumes a large quantity of time; (2) it is necessary to adopt different hypotheses to find the final calibrated parameters. Next, the procedures considered for each option until arrive to the final calibrated model are detailed.

1. Variation of the elastic modulus of materials

As a first attempt, the numerical model described before is used considering the same elastic modulus of elasticity for all walls, taken as the variable for the optimization process (step 1). In this step, the elastic modulus of reinforced concrete slabs was not considered as variable for calibration. The initial value of the elastic modulus corresponds to the value discussed in section 2.6.5, with a variation range of 10% of the reference value. No acceptable results were obtained after 20 iterations.

The second step corresponds to the variation of the elastic modulus of the walls with openings (transverse east and west walls) and without openings (longitudinal north and south walls). This is justified by the possible variation on the workmanship that could influence the global behavior of the building. Here also, variations up to 10% of the reference value were adopted. The obtained calibrations did not minimize adequately the objective function. Both the frequency values and mode shapes were far from the target objectives, but a better correlation that the one in the previous option was found.

As a third step, it was decided to assess the influence of the variation of the elastic properties of specific parts of the masonry model, namely of the corners. Thus, the elastic modulus of the masonry at the corners was used as the variable. For the construction of the unreinforced masonry building it was used the traditional bond pattern (see Figure 2.8). This pattern develops an interlock connection at the corners between walls, which could suggest an increasing of the stiffness at this area. Once again, the calibration process did not provide satisfactory results. However, options 2 and 3 indicated that the influence in the final behavior given by only variations of 10% from the reference value was significant.

Finally, it was decided to combine the three variables, namely the elastic modulus of the transversal and longitudinal walls and the elastic modulus at the corners (step 4). The same range for the variation previous defined was used. After more than 40 combinations, the optimization process was

not able to arrive to an optimal and acceptable correlation. As a last attempt, it was decided to proceed with the optimization process beyond 10% of variation from the reference modulus of elasticity for all combinations. The results show that the optimal solution is far away from the original, see Table 5.3

Table 5.2 – Parameters for calibration in option 1

Step 1	Material	Geometry part
E1	Masonry	Walls
Step 2		
E1	Masonry	Walls north and south
E2	Masonry	Walls East and West
Step 3		
E1	Masonry	Corners
Step 4		
E1	Masonry	Walls north and south
E2	Masonry	Walls East and West
E3	Masonry	Corners

Table 5.3 – Percentage (from reference value) needed for optimal solution using option 4

Parameter	Material	Geometry part	% from the reference value
E_1	Masonry	Walls north and south	91.9%
E_2	Masonry	Walls East and West	39.8%
E_3	Masonry	Corners	91.9%

All the parameters need to be below of the reference values to satisfy the iteration process. In fact, extremely low values for the modulus of elasticity were required for the East and West walls. As a conclusion, it was assumed that something, beyond just the walls and slabs, was influencing the global behavior of the building.

2. Consideration of the variable boundary constraint

In this second procedure, it was decided to consider the reinforced concrete beam foundation in the numerical model. Thus, the total structural components of the experimental building are: (a) Reinforced concrete beam foundation; (b) Masonry walls and (c) Reinforced concrete slabs.

As described in section 2.5.2, the construction of the experimental model was carried out outside of the shaking table, about 10m far from the shaking table. During the construction of the beam foundation, special care was taken in the leveling of its base. However, after transportation to the shaking table and fixation with post-tensioned steel rods, it was observed that this process was not totally perfect due to problems of leveling of the beam foundation.

It is believed that the system of beam foundation and steel rods are affecting the frequency of the model, altering the behavior of the experimental model, influencing the results at the level of the calibration. Alternatively, this can be due to the system of the shaking table itself and actuators. It was decided to include the concrete beam foundation in the numerical simulation and to assume vertical constraints at the corners as a parameter for calibration, to replicate the lack of perfection connection to the table. For this, two possibilities were envisaged, namely: (1) the vertical constraint was modified along 1.0m in each direction from every corner. The evaluation of this parameter permits values of zero or one, corresponding to rigid to loose respectively, see Table 5.4; (2) the vertical constraint was modified at the center of the foundation beam, being completely fixed 1.0m in each direction from each corner.

A three-node, three dimensional beam element designated by DIANA (2010) as CL18B was used for representing the beam foundation (see Figure 5.1a). Geometrically it possesses the same dimensions of the experimental foundation and a density $\rho = 2500\text{kg/m}^3$ similar to the reinforced concrete slabs.

Table 5.4 – Parameter for calibration in option 5

Parameter	Geometry part
K_1	Corner constraint
K_2	Middle foundation constraint

The results obtained in the first option above did not provide a substantial improvement for the calibration process. Natural frequencies and mode shapes present a similar behavior to the one obtained with the original model. The second option appears closer to the experimental model. The allowed movement from the foundation clearly improves the calibration process. These results confirm the importance of the boundary conditions. However, an accepted final calibration could not be obtained.

3. Consideration of vertical movement of concrete beam foundation

Based on the results of the previous calibration model, it was decided to place interface elements in the lower part of the foundation along each beam. The zero-thickness interface elements were a CL24I, between two lines in a curve shell configuration. Their shear stiffness was considered to be infinite as no shear sliding was admissible, while an assigned normal stiffness is present. From the corners to the middle of the beams on each direction, they have identical stiffness value every 50cm length (coinciding with the steel rods in the foundation). The numerical model has 9 interfaces (5 parameters to be calibrated – D1 to D5) for the foundation beams in the longitudinal direction and 6 interfaces (3 parameters to be calibrated - D6 to D8) for the beams in the transverse direction, see Figure 5.4 and Table 5.5. With this procedure, only the interfaces at the base of the model appear as parameters for calibration. The letter D is the linear stiffness of the interfaces in the vertical direction. The modulus of elasticity of the masonry remains as the reference value found in the material characterization.

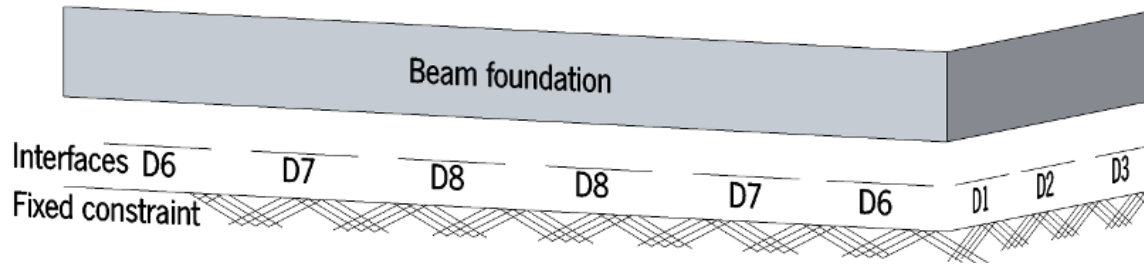


Figure 5.4 – Location and distribution of interfaces elements

Table 5.5 – Normal stiffness for the interfaces

Parameter	Geometry part
D_1	Interface longitudinal beam first segments
D_2	Interface longitudinal beam second segments
D_3	Interface longitudinal beam third segments
D_4	Interface longitudinal beam fourth segments
D_5	Interface longitudinal beam fifth segments
D_6	Interface transverse beam first segments
D_7	Interface transverse beam second segments
D_8	Interface transverse beam third segments

After several attempts of calibration, this procedure finally shows an acceptable solution and Table 5.6 presents the final parameters' values for the calibrated model.

Table 5.6 – Normal stiffness for the interfaces at the base of the numerical model

Parameter	Calibrated value (N/m ³)
D_1	2.56340E+07
D_2	2.19475E+07
D_3	3.37408E+07
D_4	7.50879E+07
D_5	1.26999E+09
D_6	6.16945E+07
D_7	3.86157E+08
D_8	8.54571E+08

It can be observed that D_5 and D_8 present the highest values in correspondence with the middle of the longitudinal and the transversal beams, respectively. In fact, the normal stiffness increases from the corners (D_1 and D_6) to the middle of the beams. Table 5.7 presents a comparison of the experimental and numerical values for the final calibrated numerical model. All the calibrations were based on seven digit values.

Table 5.7 – Experimental and numerical frequency values

Mode	Experimental Fq (Hz)	Numerical Fq (Hz)
1 - Transverse	11.11	11.11
2 - Longitudinal	16.12	16.21

Additionally, in Figure 5.5 the graphical comparison of the two global mode shapes for the transverse and longitudinal directions, between the experimental building and numerical model, is presented.

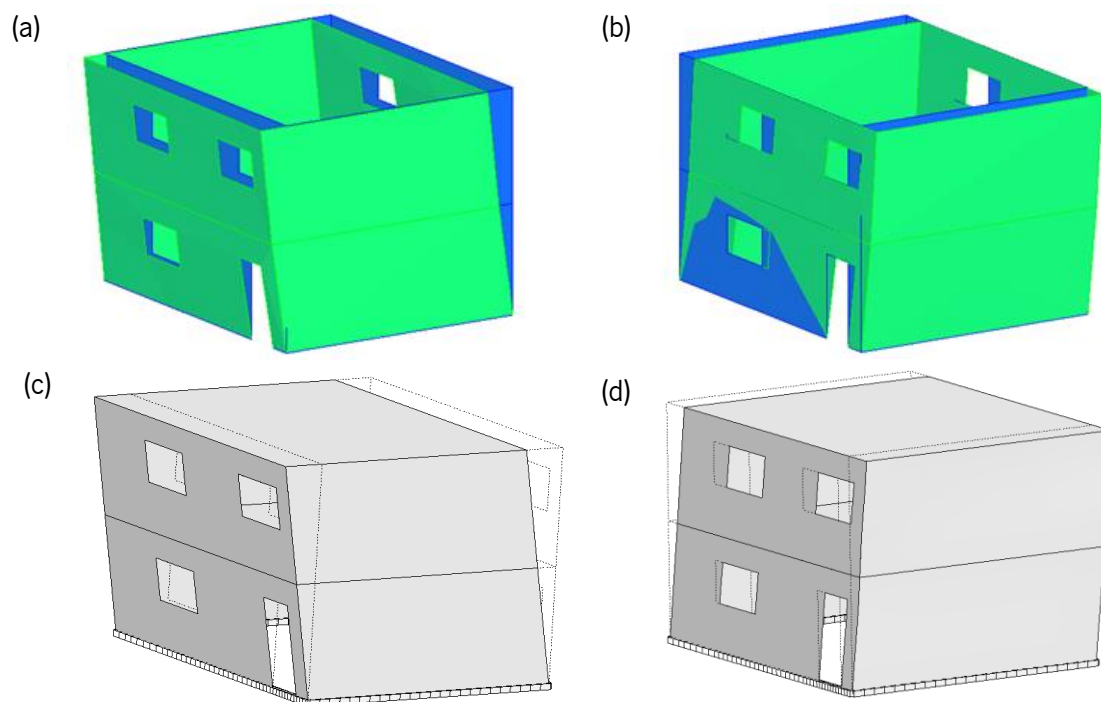


Figure 5.5 – Mode shapes of: (a, b) experimental results, (c, d) numerical results

Figure 5.6a shows the percentage of the frequency errors for the two natural frequencies. For the modes' shapes validation, the MAC (Modal Assurance Criterion) matrix was used. The MAC value is a statistical indicator for the comparison of two scenarios of the same variable. The function provides a measure of consistency between vectors. It is defined as follows:

$$MAC_{E,N} = \frac{\left| \sum_{i=1}^m \varphi_i^E \varphi_i^N \right|^2}{\sum_{i=1}^m (\varphi_i^E)^2 \sum_{i=1}^m (\varphi_i^N)^2} \quad 5.4$$

Here φ^E and φ^N are the experimental and numerical mode shapes' vectors and m indicates the numbers of degrees of freedom. The MAC expression leads to a scalar that ranges from values of

zero to one, associated to no correspondence to a consistent correspondence, respectively. Figure 5.6b presents the MAC matrix between the calibrated numerical model and the experimental one.

These results validate the final numerical representation of the experimental building in the linear regime. With frequency errors under 0.6% and MAC values above 0.99, the numerical model is taken as fully acceptable and as a truthful representation of the actual unreinforced masonry building.

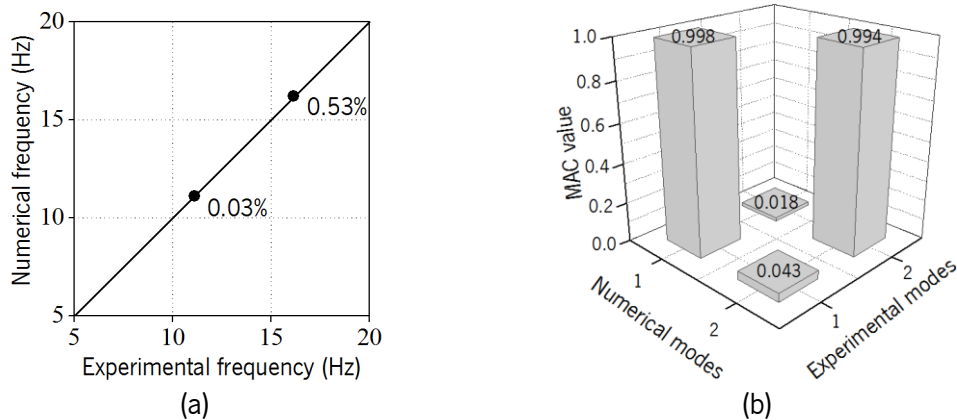


Figure 5.6 – Optimization 's results: (a) frequency errors between experimental and numerical values, (b) MAC matrix for the mode shapes

5.5 Phased nonlinear dynamic simulation

5.5.1 A brief introduction

The best option to evaluate the vulnerability of a building to earthquakes is the combination of both the nonlinear material behavior and dynamic loading, simulating the effect of the seismic loading (nonlinear dynamic analysis). This analysis method is considered the most difficult to carry out, as it is a very time consuming approach and expert knowledge is required. On the other hand, with a reliable numerical model, different scenarios of loading for the same structure, geometry changes or even different material properties in both local or global structural components can be analyzed,

In a detailed micro modeling approach, such as the one presented in Figure 5.7, nonlinear properties for tension and compression are given for both the bed joints and the head joints. On the other hand, the implementation of the macro modeling approach requires simplifications in the material data. In Figure 5.8, a brief overview of the general behavior described for the two types of modeling is presented for different loading combinations.

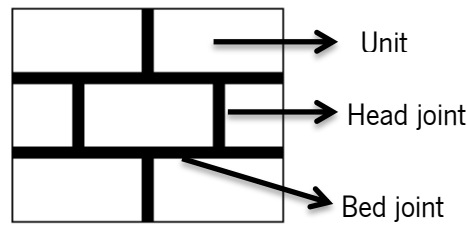


Figure 5.7 – Micro modeling approach

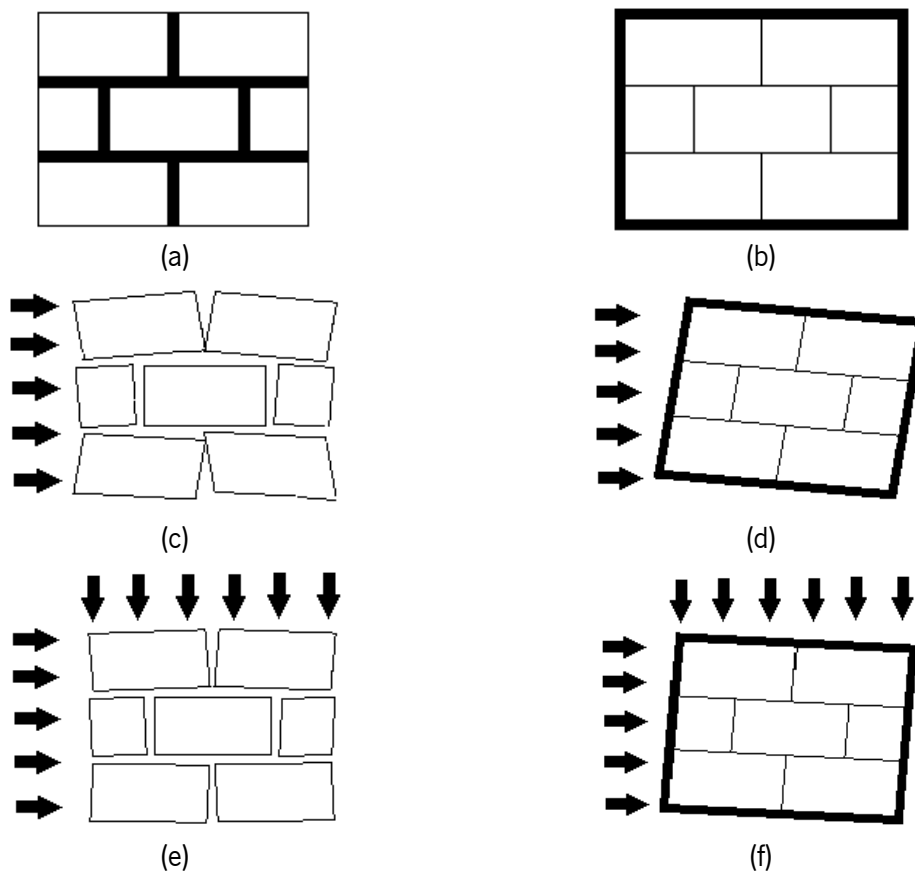


Figure 5.8 – Modeling behaviors of masonry when subjected to a force or combination of forces: (a, c, d) micro modeling and (b, d, f) macro modeling approach

Numerically, cracking is represented by degradation of material strength in different planes, which can become active or inactive during the process. Each of these planes has a dedicated set of state variables (Weihe et al. 1998). In Figure 5.8c and d, it is seen that in case of micro modeling of masonry under lateral loading it is possible to represent not only the opening of the bed joint but also the opening of the head joint, being simulated in detail the different planes of degradations for masonry. These detailed deformation mechanisms are not possible in the macro modeling approach in which masonry is represented as a homogeneous material. Similar situation is observed with a combination of vertical and lateral forces, like in Figure 5.8e and f. The macro modeling approach has evolved into a great tool for describing the behavior of solids, even if the representation of stronger localized phenomena remains a challenge (Weihe et al. 1998). In the particular case of the masonry building to be analyzed, it was decided to model the tensile behavior of masonry by considering different values of the tensile strength in the first and second floors to take into account

the influence of the self-weight on the tensile resistance of masonry. This solution is a simplification that allows take into account the increase weight on the first floor generated by the added masses of the floors (after the construction of the buildings), resulting in a more accurate representation of the nonlinear behavior.

5.5.2 Constitutive model for the simulation of masonry

A major issue for the simulation of the nonlinear material behavior of masonry is the selection of the constitutive material model. In this numerical analysis, the total strain crack model was chosen as the best option for representing masonry behavior. The model represents random and smeared cracks over structural materials. It has been used successfully in masonry materials by several authors (Carpinteri et al. 2005; Haach et al. 2011; Mendes and Lourenço 2009).

The total strain crack model describes the tensile and compressive behavior of masonry with a stress-strain relationship that is suitable for nonlinear analysis predominantly governed by cracking or crushing. The behavior in loading and unloading can be modeled in a different way, by considering linear or secant unloading paths, see Figure 5.9a. Within the total stress-strain relationships, two approaches are possible, namely, fixed and rotating stress-strain crack models. In the fixed crack model (FCM), the stress-strain relationships are evaluated in a fixed coordinate system, even upon cracking. Here, failure is initiated in the direction perpendicular to the maximum tensile (principal) stress when the principal stress exceeds the uniaxial tensile strength, f_t , of the material. The main characteristic of this method, in the process of further loading, is that the initial orientation of the plane of degradation remains fixed. In the rotating crack model (RCM), also known as the coaxial stress-strain concept, the crack direction rotates continuously with the principal directions of the strain (principal) vector. The model assumes that the initiation of the damage is controlled by the maximum tensile stress as well. However, in this case, the orientation of the cracking path is adjusted to remain orthogonal to the direction of the current major principal stress (Rots 1988). Thus, the degradation mechanism is controlled by the maximum principal stress.

For the model under analysis, both total and rotating crack models were tested with different range of values. Approximately 50 nonlinear simulations and comparison with the experimental results were carried out. In this analysis, it was found that the rotating crack model represents more accurately the results from the experimental campaign. Theoretically, if the axes of principal stress do not change during the total analysis process, there will be no difference between the FCM and the RCM, but if the axes change after the crack is initiated, the response of both models is different. From the physical point of view, the RCM seems to be more reasonable than the FCM (De Borst and Nauta 1985; Li and Zimmerman 1998). Furthermore, in the FCM a shear retention factor β has to be chosen to decide the shear stiffness, which sometimes is quite delicate. In addition, shear strains may arise along the crack plane and, consequently, the residual normal stress may exceed the tensile strength in a direction inclined with respect to the defined crack plane. These two inconveniences do not exist in the RCM, in which the tangential shear stiffness automatically arises from the requirement of coaxiality between principal stress and principal strain and, therefore, the normal stress will never infringe the crack criterion in a direction inclined to the crack plane. The

rotating crack model has been used widely in concrete structures (Feenstra and De Borst 1995; Foster et al. 1996; Rots 1988; Sasani et al. 2011; Vecchio and McQuade 2011), but few information is found regarding its implementation in masonry, as well as in relation to comparison studies among crack models (da Porto et al. 2010; Lotfi and Shing 1991).

5.5.3 Material properties

Besides the elastic properties obtained from the calibration of the numerical model (section 5.4), the nonlinear properties of the materials need to be provided. For the total strain crack model implemented in this work, a tension-softening curve and a compressive parabolic diagram have been used, see Figure 5.9b and c respectively. Besides the tensile and compression behavior, one of the most important features of the cracking behavior of masonry is the opening and closing of the cracks, which is directly associated to the unloading and reloading process inherent to seismic loading. Here, two options can be followed, namely the elastic and the secant unloading, see Figure 5.9a. For the elastic unloading, the crack closes immediately upon a strain reversal. Thereafter further strain-decomposition (in plasticity concepts, it is the assumption of strain decomposition into an elastic part and an irreversible, or plastic part) is canceled and a rigorous return is made to the elastic behavior. One of its advantages is that after “crack’s closing” the incremental strain of the crack disappears, saving computing time (De Borst and Nauta 1985). However, this unloading method always provides the same unloading stiffness, even beyond the strain corresponding to the crack initiation, ε_c . Instead, for secant unloading, the crack normal strain is reversible and upon reaching the origin of the stress-strain diagram the crack truly closes ($\varepsilon = 0$). Thereafter elastic behavior is recovered. With this method, the unloading stiffness decreases with the increasing of the crack opening and therefore implies more computational effort. In the present work, unloading and reloading of the stress-strain relationship was modeled using a secant approach.

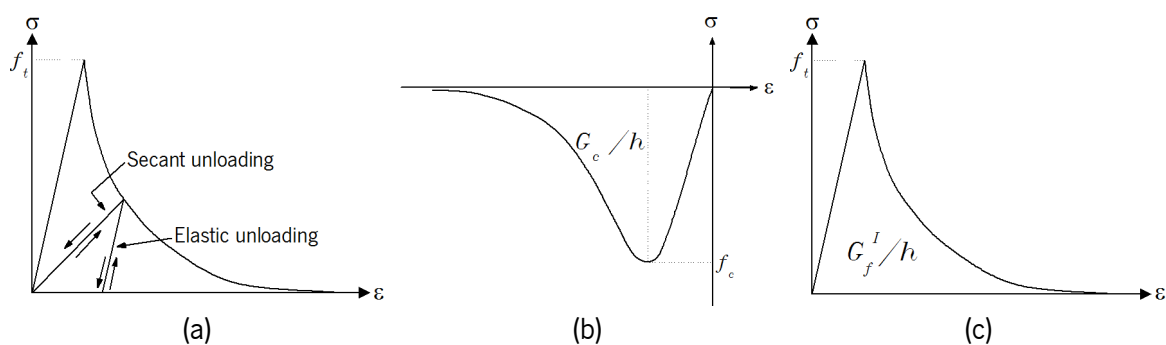


Figure 5.9 – Stress-strain curves: (a) Secant and elastic unloading in a tension-softening curve, (b) Parabolic compressive behavior (c) Exponential tensile behavior

The nonlinear properties defining the softening behavior under tension and compression are the mode-I fracture energy, G_f^I , and the compressive fracture energy, G_c . In both cases, the fracture energy is divided (normalized) by the crack bandwidth of the element, h . The value of h is related to the area of the shell elements, A . The value of the crack bandwidth, h , is defined as follows:

$$h = \sqrt{A}$$

5.5

Then, this relation is made to the particular finite element dimension and its geometrical configuration.

A general overview of the full stress-strain relationship implemented for the simulation of masonry's behavior in the numerical model can be observed in Figure 5.10.

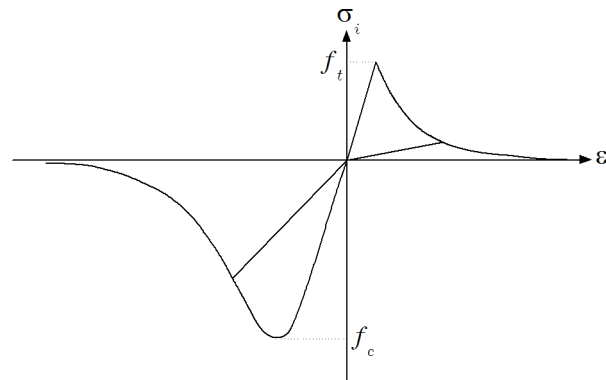


Figure 5.10 – Stress-strain curve with loading-unloading relationship

The material properties defining the tensile and compressive behavior of masonry were obtained from the experimental campaign for the material characterization (section 2.6.5), and in recommendations provided by Lourenço (2008) and by the Eurocode 6 (2005). The values are summarized in Table 5.8 and Table 5.9. As mentioned previously, it was decided to attribute different properties for masonry localized in the first and second floors to take into account the influence of the added masses in the tensile and shear resistance.

Table 5.8 – Tensile material properties

		Tensile strength f_t (MPa)	Mode I fracture energy G_f (N/mm)
Tension	2 nd floor	0.12	0.0075
	1 st floor	0.16	0.0375

Table 5.9 – Compressive material properties

	Compressive Strength f_c (MPa)	Compressive fracture energy G_c (N/mm)
Compression	5.95	9.52

5.5.4 Analysis procedures

In agreement with the experimental tests and the objectives of this thesis, a numerical nonlinear dynamic analysis with time integration is performed, combining the nonlinear behavior of the

masonry and dynamic loading (seismic inputs). Following the experimental testing procedures, successive nonlinear dynamic analyses were carried out in a procedure called phased analysis. For this, the incremental input loadings implemented on the shaking table were simulated (see section 2.5.4) in the dynamic numerical analysis. This procedure enables also to have a better basis for the comparison between experimental and numerical results.

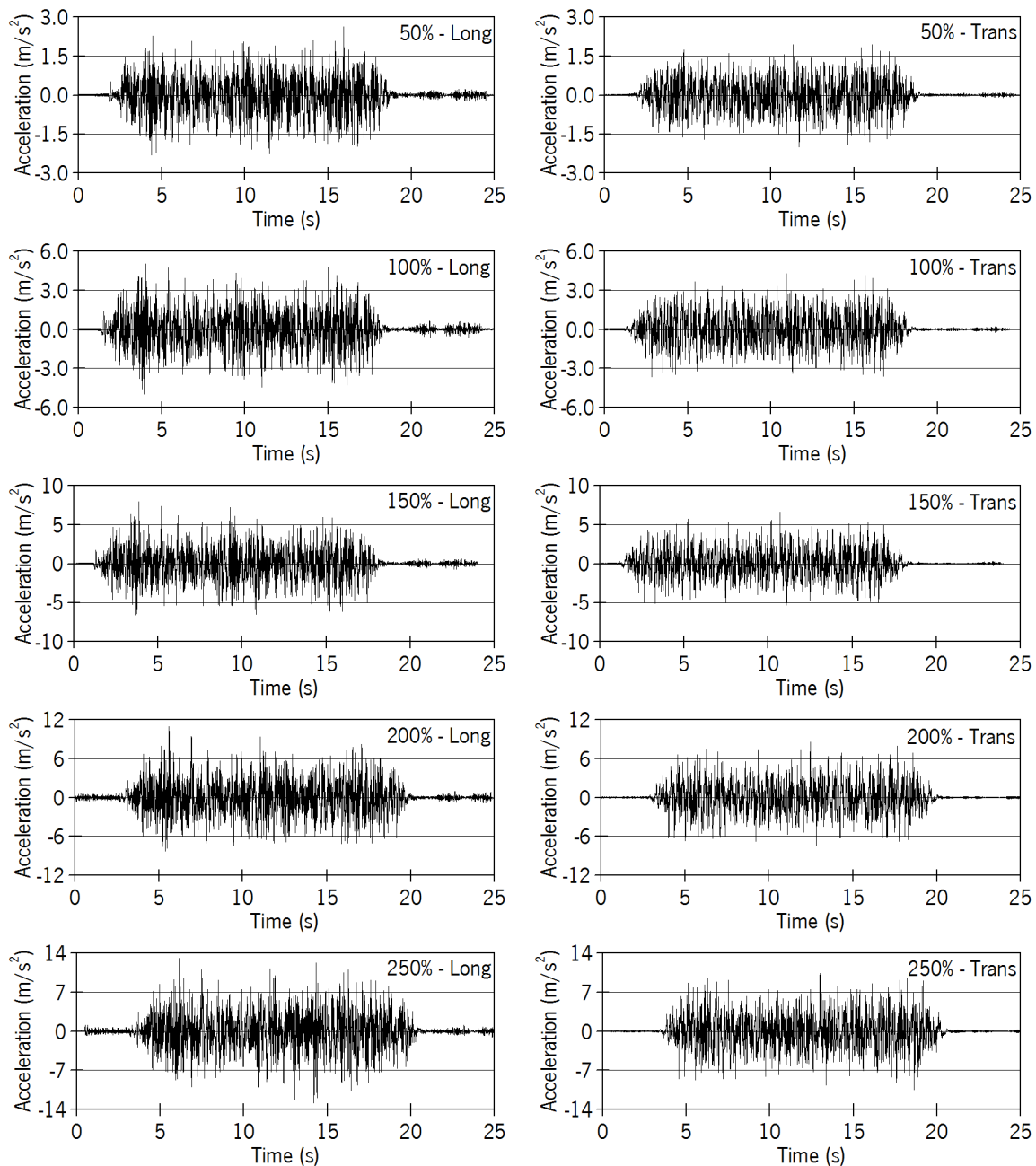


Figure 5.11 – Signals inputs implemented in the numerical simulation

The analysis comprises several calculation phases, and in each phase, the results of the previous phases (stresses, strains, accelerations, velocities, displacements, etc.) are automatically used as initial values. Besides, between each phase, the finite element model can be modified by adding or removing elements and/or constraints.

For the present numerical phased analysis, each seismic experimental stage performed in the shaking table campaign was considered in the numerical model. In fact, the same time history accelerations recorded at the base of the models in the two orthogonal directions for each seismic input were used. In this way, the actual signals that the buildings faced, instead of the theoretical inputs introduced to the shaking table's control, are used. The input signals implemented in the numerical simulation are presented in Figure 5.11. It should be mentioned that both signals (longitudinal and transversal) were introduced at the base of the numerical model acting simultaneously, representing in this way, similar test conditions as the ones implemented during the experimental tests.

The system of governing equations for a time integration dynamic problem at time t is generally written as:

$$M\ddot{u}(t) + C\dot{u}(t) + F_{int}(u, \dot{u}, \epsilon, \sigma, t, \dots) = F_{ext}(t) \quad 5.6$$

Where M is the mass matrix, C is the damping matrix and F_{ext} is the external force vector or right-hand-side vector of forcing functions. Additionally, \ddot{u} , \dot{u} , and u are the resulting acceleration, velocity and displacement vectors respectively, ϵ and σ are the strain and stress fields. The vector F_{int} corresponds to the internal set of forces developed for a certain loading history. For a physical nonlinear analysis, F_{int} must be calculated for the actual stress distribution satisfying all nonlinear conditions, according to:

$$F_{int} = \int B^t \sigma \quad 5.7$$

Where B is the strain-displacement relation. Then, the solution of the second order differential presented in Equation 5.6 is obtained by direct time integration techniques. For the time integration analysis of the present study, the Hilber-Hughes-Taylor (HHT) method (also called the α method) was adopted. The method uses the same finite difference equations scheme as in the Newmark method:

$$\dot{u}^{t+\Delta t} = \dot{u}^t + [(1 - \gamma)\ddot{u}^t + \gamma\ddot{u}^{t+\Delta t}]\Delta t \quad 5.8$$

$$u^{t+\Delta t} = u^t + \dot{u}^t\Delta t + \left[\left(\frac{1}{2} - \beta \right) \ddot{u}^t + \beta\ddot{u}^{t+\Delta t} \right] \Delta t^2 \quad 5.9$$

Where

$$\gamma = \frac{1}{2}(1 - 2\alpha) \quad 5.10$$

$$\beta = \frac{1}{4}(1 - \alpha)^2 \quad 5.11$$

γ and β are parameters associated to the Newmark method, α is the parameter associated to the HHT method, being defined for the present study with a value of -0.1. Here t is the time and Δt is the time step. Thus, the time-discrete equation of motion, Equation 5.6, is modified as follows:

$$M\ddot{u}^{t+\Delta t} + (1 - \alpha)C\dot{u}^{t+\Delta t} - \alpha C\dot{u}^t + (1 + \alpha)F_{int}^{t+\Delta t} - \alpha F_{int}^t = F_{ext}^{t+\Delta t(1+\alpha)} \quad 5.12$$

The time step size was selected by taking into account the contribution of the dominant frequencies and mode shapes obtained in the unreinforced masonry building. Thus, according to the recommendations given by the manual of DIANA (2010):

$$\Delta t \leq \frac{1}{20} T_i \quad 5.13$$

Where Δt is the time step and T_i is the period of the corresponding F_i natural frequency. Then, in order to make sure that the contribution of the high-frequency modes was computed correctly, the period T of the highest mode was used. Following this criterion an error of less than 5% is expected.

In order to account for all energy dissipating mechanisms, the structural modal damping ratios discussed in section 3.4, i.e. the damping ratios from the longitudinal and transversal modes, were introduced in the numerical model as viscous damping. This is a form of damping which is proportional to the velocity. Here, Rayleigh damping coefficients were used according with Equation 5.14 as follows:

$$C = \alpha M + \beta K \quad 5.14$$

Where C , M and K are the damping, mass and stiffness matrix respectively, α is the mass-proportional damping and β is the stiffness-proportional damping, with units of sec^{-1} and sec respectively. The damping ratio for the n^{th} mode of such system is:

$$\zeta_n = \frac{\alpha}{2} \frac{1}{\omega_n} + \frac{\beta}{2} \omega_n \quad 5.15$$

Then, the coefficients α and β can be determined from the specific damping ratios ζ_i and ζ_j for the i^{th} and j^{th} modes, respectively. Because it is assumed that both modes have the same damping ratio ζ , which is reasonable based on experimental data (Chopra 1995), the two parameters can be described as follow:

$$\alpha = \zeta \frac{2\omega_i\omega_j}{\omega_i + \omega_j} \quad 5.16$$

$$\beta = \zeta \frac{2}{\omega_i + \omega_j} \quad 5.17$$

For the unreinforced masonry building the coefficients α and β found were $\alpha = 2.9745$ and $\beta = 0.00042097$. Thus, the graphical representation of the coefficients α and β together with the Rayleigh damping used for the numerical simulation is presented in Figure 5.12.

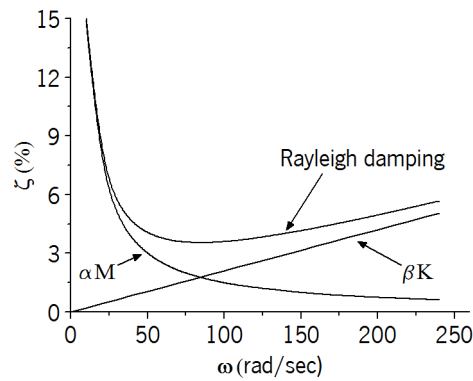


Figure 5.12 – Rayleigh damping implemented in the numerical simulation

The integration scheme adopted for the structural elements used for the numerical simulation is described in Table 5.10. The structural elements implemented in the 3D numerical model are numerically integrated. It is possible to indicate to the software how many integration points and which method of integration should be used for each direction. As an example, the beam elements are not only integrated along their bar axis, but also in their cross-section. Here, it is noted that beam and slab elements remain elastic, which justified the low number of integration points in the cross section.

Table 5.10 – Integration schemes

Structural element	Number of integration points	Geometry direction	Integration rule
Interfaces	3 x 9	Long x Thickness	Newton-Cotes x Simpson
Beam	2 x (3 x 3)	Long x (cross-section)	Gauss x Simpson x Simpson
Walls	(2 x 2) x 9	(Cross-section) x Thickness	Gauss x Gauss x Simpson
Slabs	(2 x 2) x 3	(Cross-section) x Thickness	Gauss x Gauss x Simpson

Finally, in DIANA (2010), it is possible to adopt several iteration procedures to solve the system of nonlinear equations arising from the discretization, like the regular and modified Newton-Raphson method, the Quasi-Newton or Secant method and the linear stiffness method. In the iterative methods the total displacement increment Δu is updated by adding iterative increments δu to previous converged displacement, until equilibrium is reached, up to a prescribed tolerance, see Equation 5.18.

$$\Delta u_{i+1} = \Delta u_i + \delta u_{i+1} \quad 5.18$$

Mendes (2012) performs a comparison between several iterative methods for the nonlinear analysis of an unreinforced masonry building, finding that the linear stiffness method presented the best results in terms of convergence, for nonlinear dynamic simulations. The same method is adopted in this study. The computational effort of the method per iteration is also lower since the stiffness matrix need to be set up only once, even if more iteration steps are needed to obtain convergence. Here, a convergence criteria based only on the internal energy, with a tolerance of $10E-3$ was used.

5.6 Results and validation against experimental data

The phased nonlinear dynamic time history analysis provide results for each seismic intensity used in the experimental shaking table tests and enables their comparison with the experimental results. The validation of the numerical model with the experimental results needs that the mathematical solution proposed, including the numerical approach, constitutive model and mechanical properties, effectively represent the actual behavior of the unreinforced masonry building, not only in the linear range but also in the nonlinear range.

In order to accomplish the validation of the numerical model two general approaches are followed, considering quantitative and qualitative parameters. In the first one, direct values from the accelerations and displacements are analyzed, whereas, parameters like the strains and damage patterns are used in a more qualitative analysis.

5.6.1 Accelerations

The time history for accelerations of specific corners of the model was obtained from the numerical model. Thus, a comparison was made between the numerical and experimental accelerations recorded at the accelerometers placed at the corners of the masonry buildings at first and second floors. In Figure 5.13, a summary of the numerical and experimental maximum accelerations (peak values) recorded for the different phases of the analysis, corresponding to distinct seismic inputs, are presented. It should be mentioned that all results for the experimental and now for the numerical model correspond to relative values; i.e. are the difference between the global values on the model (building and openings' corners) and the global (horizontal) values at the base of the building. The signals from the accelerometers of the north and west walls, N1.1 and W1.2 respectively, were lost during the test of 250%_2 and no registration could be made. As the building is symmetric, it is observed that the behavior at both sides of the walls presents a similar tendency. That is also why only the north and west walls are presented next.

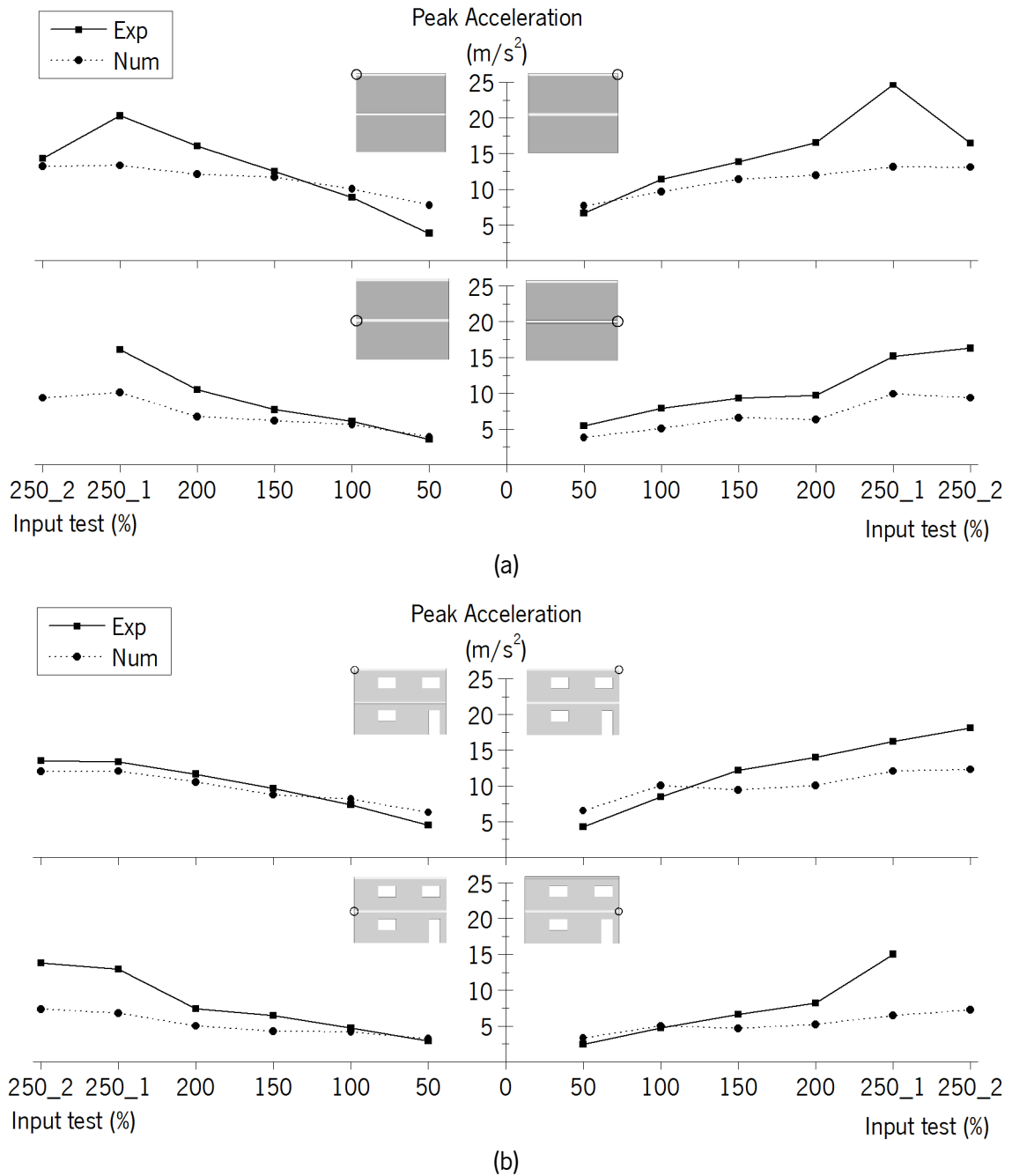


Figure 5.13 – Numerical and experimental peak acceleration values: (a) North façade – longitudinal direction and (b) West façade – transverse direction

In general, the numerical and experimental accelerations in both directions and in both levels presented a good correlation, even if there is a trend for the numerical analysis to presents almost always lower values for the accelerations, see Figure 5.13 This is particularly relevant for the final two stages (test of 250%_1 and 250%_2). It is observed that higher acceleration peak values were obtained in the north façade (longitudinal direction), when compared to the west wall (transverse direction), and as expected, higher accelerations are recorded at the second floors. The highest experimental peak value occurred during the first test of 250% at point N2.2 with a value of 24.70 m/s^2 (2.52g), being compared with the numerical value of 13.11 m/s^2 (1.34g) and representing a

difference of 53%. In terms of numerical response, the highest acceleration was recorded at N2.1 with a value of 13.34 m/s² (1.36g).

It should be mentioned that the reason by which the numerical model gives higher errors after the seismic input of 200% is related to crack pattern along the horizontal and diagonal stair stepped cracks along the joints. In fact, as discussed in Chapter 3, after the development and extension of this localized cracking, the dynamic behavior of the buildings is greatly affected by the discrete macro blocks that moves along the discontinuities forms by the horizontal or diagonal cracks. This behavior is possibly not well represented by the macro modeling approach used in this work.

A complementary study, at the level of the accelerations, can be the consideration of the analysis of the evolution of the acceleration along the time history, corresponding to the total seismic input of each phase. This parameter should provide in a more accurate way the dynamic response and consistency of the numerical model with the experimental one along the entire seismic event and not only related to the peak values recorded. Therefore, aiming to perform an analysis in which all the time history is taken into account, an integral parameter should be analyzed. For this, the Root Mean Square (RMS) was chosen, defined according to Equation 6.19:

$$RMS_X = \sqrt{\frac{1}{t_E} \int_0^{t_E} X^2(t) dt} \quad 5.19$$

Where X is the parameter under analysis (can be acceleration, velocity or displacement) and t_E is the total duration of the signal. In this way, a statistical measure of the acceleration is performed in which its positive and negative variation is taken into account. As an integral parameter, the RMS is, as well, an effective option for the measurement of the energy content. From the RMS values of the acceleration, two important measurements of earthquake destructiveness related to the energy imposed to the model can be derived, namely *Arias intensity* (I_A) and the *Saragoni Factor* (P_D), (Bommer et al. 2004; Tomazevic et al. 1996b).

The values of the calculated RMS acceleration both for the experimental and numerical models are presented in Figure 5.14. When two data sets are compared (numerical and experimental), the RMS can serve also as a measure of how far, in average, all the signal data is from zero (0) in the y axis (giving an indirect measure of the half amplitude of the signal). It is observed that in all the façades, the experimental and numerical results are relatively close and following the same trend throughout the inputs presented. However, it is clear that the numerical model follows the experimental results with less accuracy for the last seismic inputs, which should be related in great extent with the differences found for the peak values. The most remarkable differences are recorded at the north façade (longitudinal direction) at the second floor. As observed in Figure 5.13, the highest accelerations occur also at the same location. At West façade (transverse direction), it is observed a very good fitting for both peaks and particularly RMS accelerations until the last two seismic inputs.

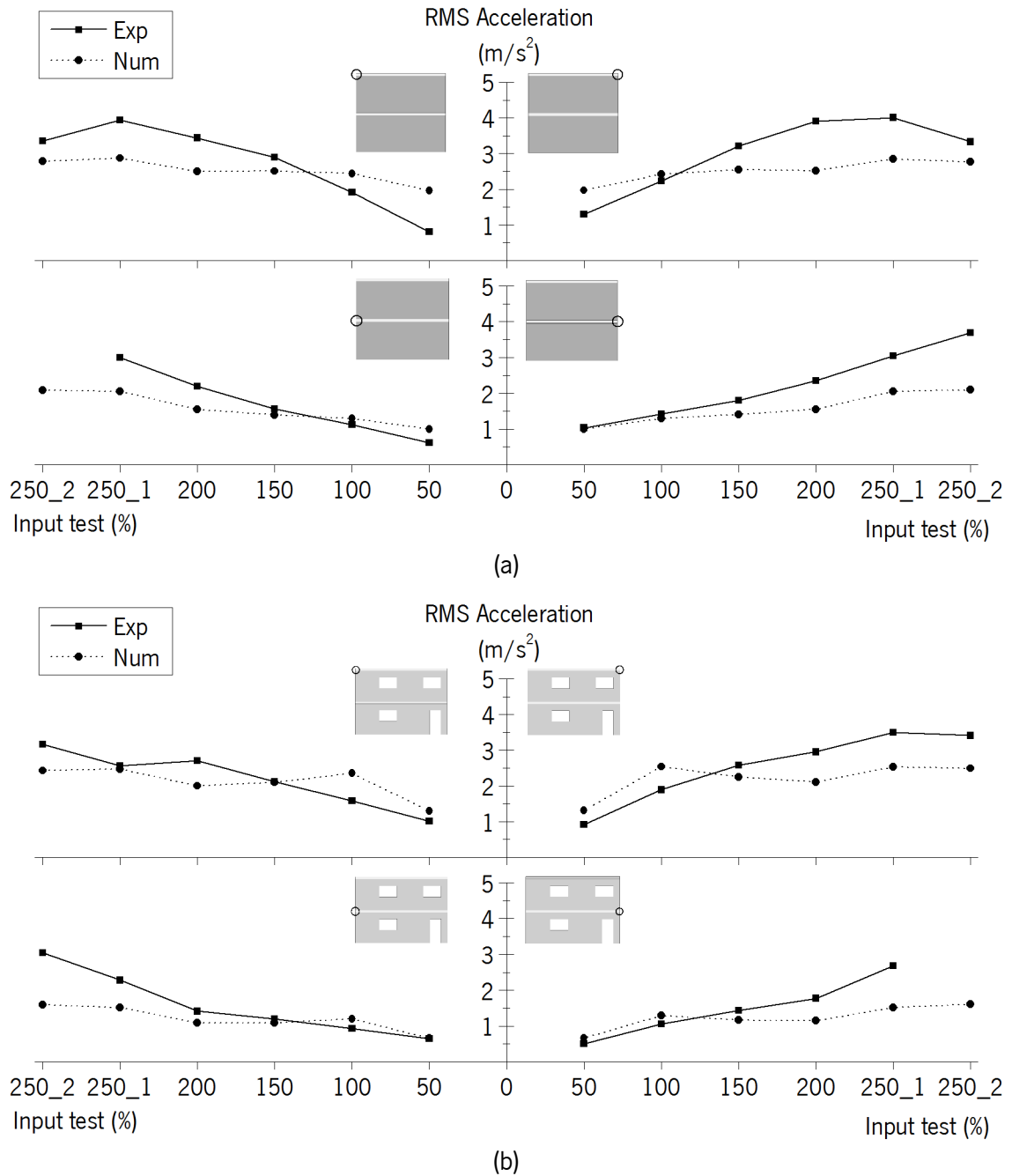
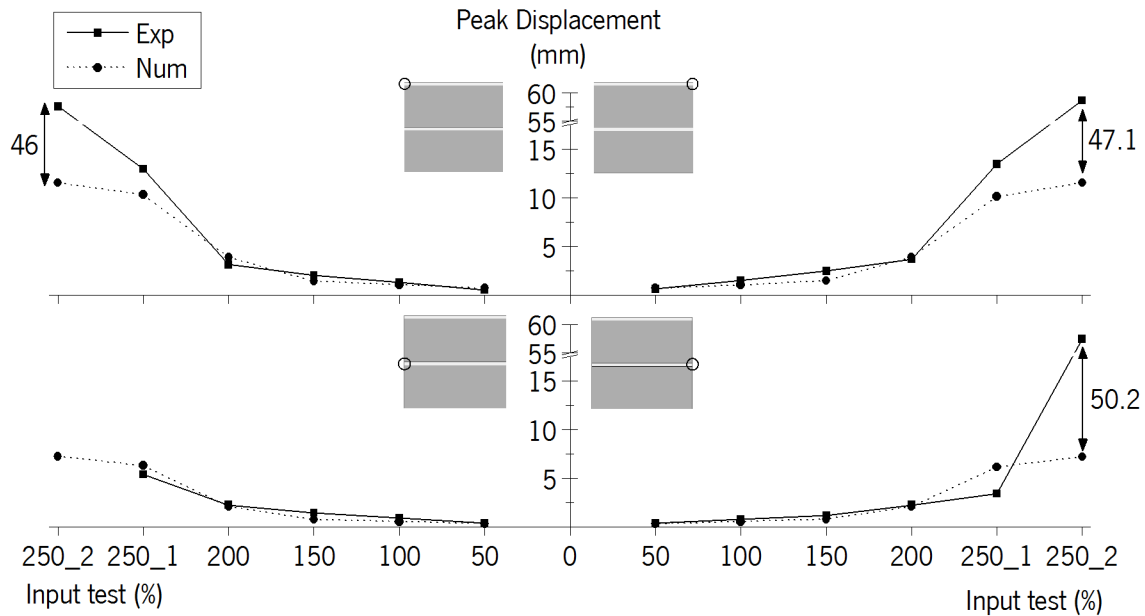


Figure 5.14 - RMS acceleration values comparison: (a) North façade – longitudinal direction and (b) West façade – transverse direction

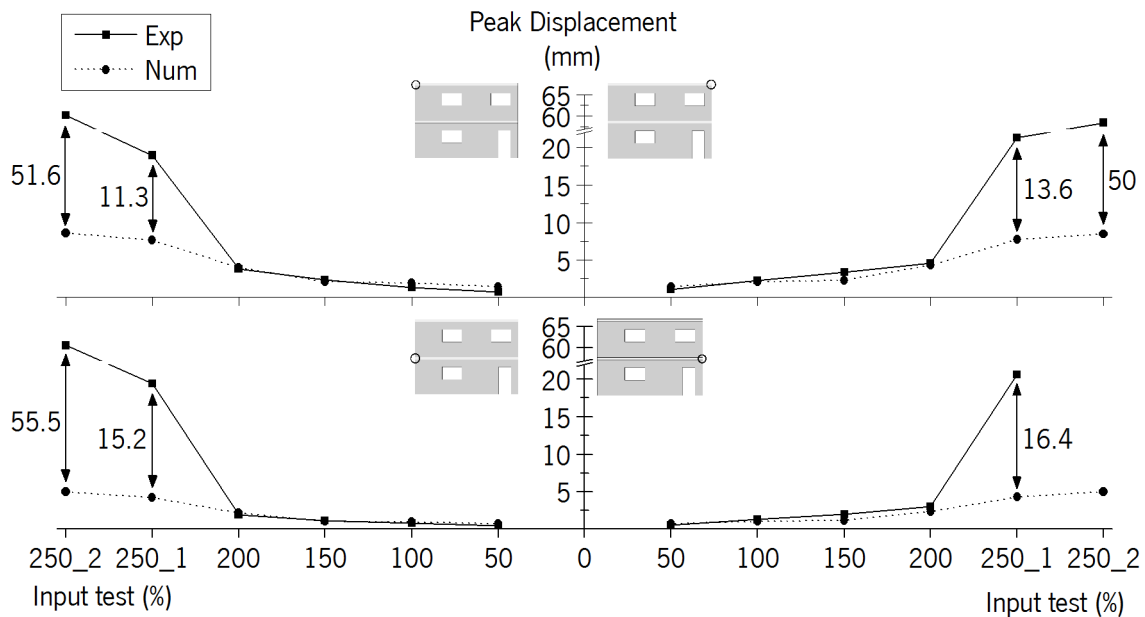
5.6.2 Displacements

The analysis of the relative displacements involves also comparisons of the peaks and RMS displacements between numerical and experimental models. It should be mentioned that the study of the displacements for a dynamic analysis, which includes linear and nonlinear material nature is a challenging and arduous subject that demands a detailed and complete mathematical representation. Being aware of the importance of an accurate validation of the numerical model for the study and design of future constructions, in the present thesis all the displacement comparisons

are made in millimeters (mm). The comparison of the peak and RMS displacements recorded in the experimental and numerical analysis can be made through Figure 5.15 and Figure 5.16, respectively.



(a)



(b)

Figure 5.15 – Comparison between numerical and experimental relative peak displacements: (a) North façade – longitudinal direction and (b) West façade – transverse direction

From the comparison of the peak experimental and numerical values, it is observed that a very good fit is achieved until the input test of 200%. The longitudinal direction presents a good approach between numerical and experimental results in both floor's levels even for the first input of 250%. No similar tendency was observed for the same input tests in the transverse direction, on the west façade, in which at this stage numerical results present values 1cm lower than the ones recorded

during the experimental test. The last simulation of 250% presented, on average, values 5cm lower than the ones obtained in the experimental model in all the points. This means that for this specific input, the numerical model represents only about 10% of the experimental results.

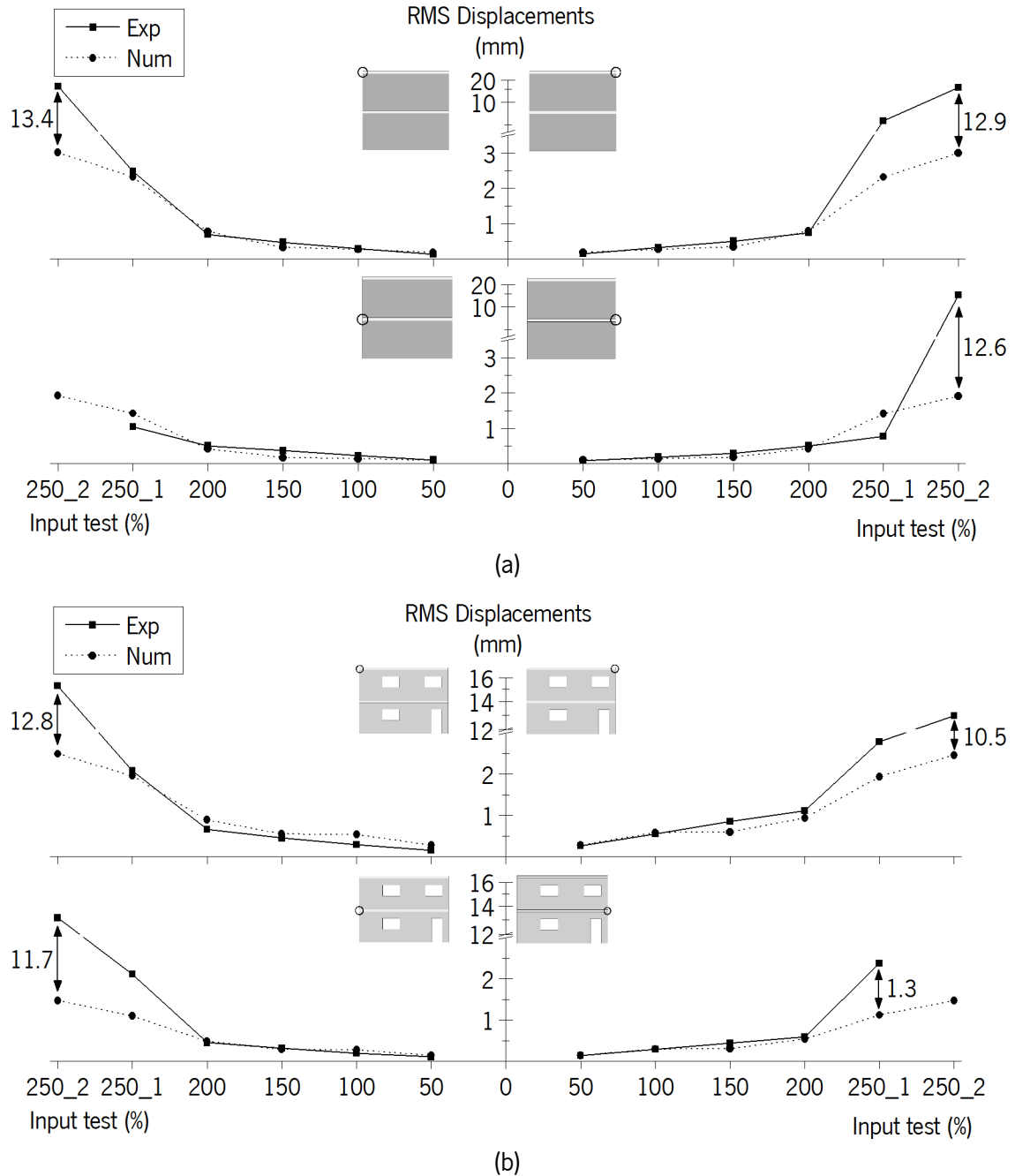


Figure 5.16 - Comparison between numerical and experimental relative RMS displacements: (a) North façade – longitudinal direction and (b) West façade – transverse direction

The RMS displacement results suggest that what happened in the peaks' evaluation for the first test of 250% (Figure 5.15), at least in the transverse direction, is the result of a punctual situation that directly influences the peak values. As observed in Figure 5.17, in which the time history displacement obtained for point W2.1 during the 250%_1 input test is presented, the numerical signal of displacement is very close to the experimental one but at around the 18-second the two

remarkable peaks recorded in the experimental model could not be followed for the numerical simulation. Similar situation was found for all the corners in this wall, affecting this direction (transverse), which is attributed to the sliding mechanism presented in this model and discussed in section 3.5 and section 3.6. As already mentioned, the simulation of sliding movements of the masonry macro block created after the complete localization of the horizontal bed joints cracks and diagonal stair stepped cracks is not possible with the macro modeling approach used to numerically simulate the dynamic behavior of unreinforced masonry building. To achieve a better approximation at the stage, a micro model simulation approach is necessary, in which not only the bed joints but also the head joint are represented in such a way that the localized cracks can clearly develop.

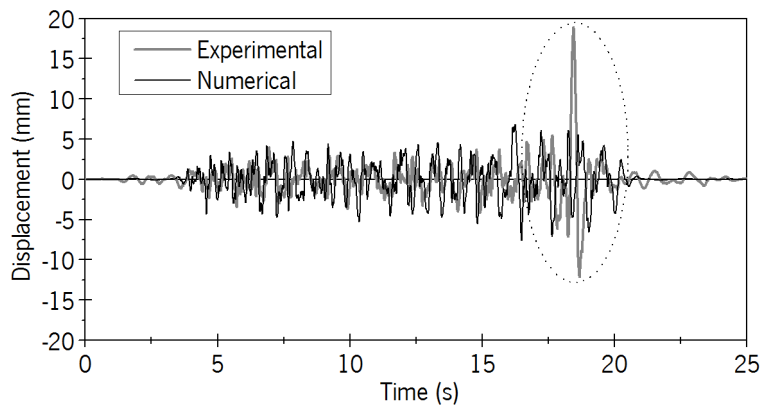


Figure 5.17 – Experimental and numerical time history signals for point W2.1 during test of 250%_1

5.6.3 Capacity curves

The evaluation of the structure's energy dissipation is a key parameter for the seismic design, mainly as related to the lateral resistance and displacement limitations. Masonry's codes around the world demand specific restrictions regarding several limit states, e.g. occupancy, serviceability and collapse, for which the graphical representation (envelope) of the building's energy dissipation evolution plays an important role. The simplified design and assessment of the seismic performance of masonry buildings uses the concept of "capacity curve". According with the Eurocode 8 (2004) the capacity curve of a structure is the relation between the base shear force and a control displacement, usually located at the top of the structure. For a general assessment and further comparison of the numerical capacity curves with the experimental ones and aiming to overcome the influence of the scale dimensions in the final results, it was decided to represent the capacity curves based on normalized parameters. Then, they were defined based on the relation between a factor representing a normalized base shear capacity (BSC: base shear coefficient) and the top displacement normalized by the height of the model. The Base Shear Coefficient (BSC) is defined according to Equation 5.20:

$$BSC = \frac{BS}{W} \quad 5.20$$

Where BS is the base shear and W is the weight of the model. Regarding the displacements, the following ratio is used:

$$\frac{\text{Top displacement}}{\text{Height}} \times 100\%$$

Here, $Height$ refers to the distance from the base to the reference displacement's point, which in this case is equal to the total height of the model. After each numerical phase, the hysteresis of the model for each direction was evaluated. For it, the reactions in X and Y directions for every fixed constraint at the base of the model, were obtained for each time step. All the individual fixed constraint's values were added with a spreadsheet obtained the total reactions or base shear for each step in the two directions. These values were finally normalized by the weight of the model. Similarly, for the displacements, which were obtained after each time step directly from the top of the model and divided by the height of the building from the base. Finally, both results were jointly plotted for each time step. Figure 5.18 presents a comparison of the hysteretic response in the longitudinal direction for the experimental unreinforced masonry building and its numerical simulation during the input signal of 100%.

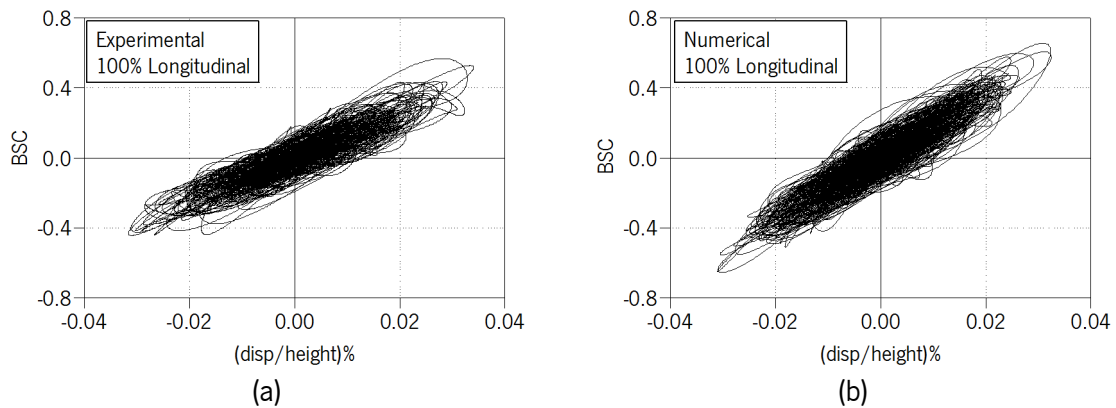
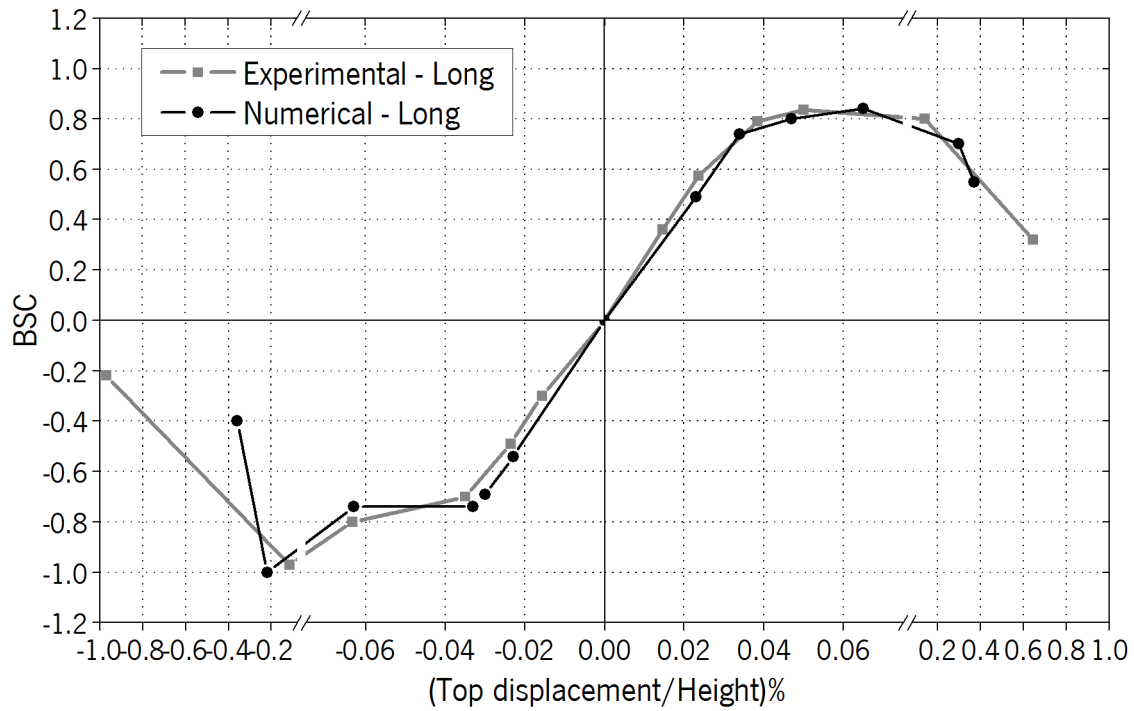


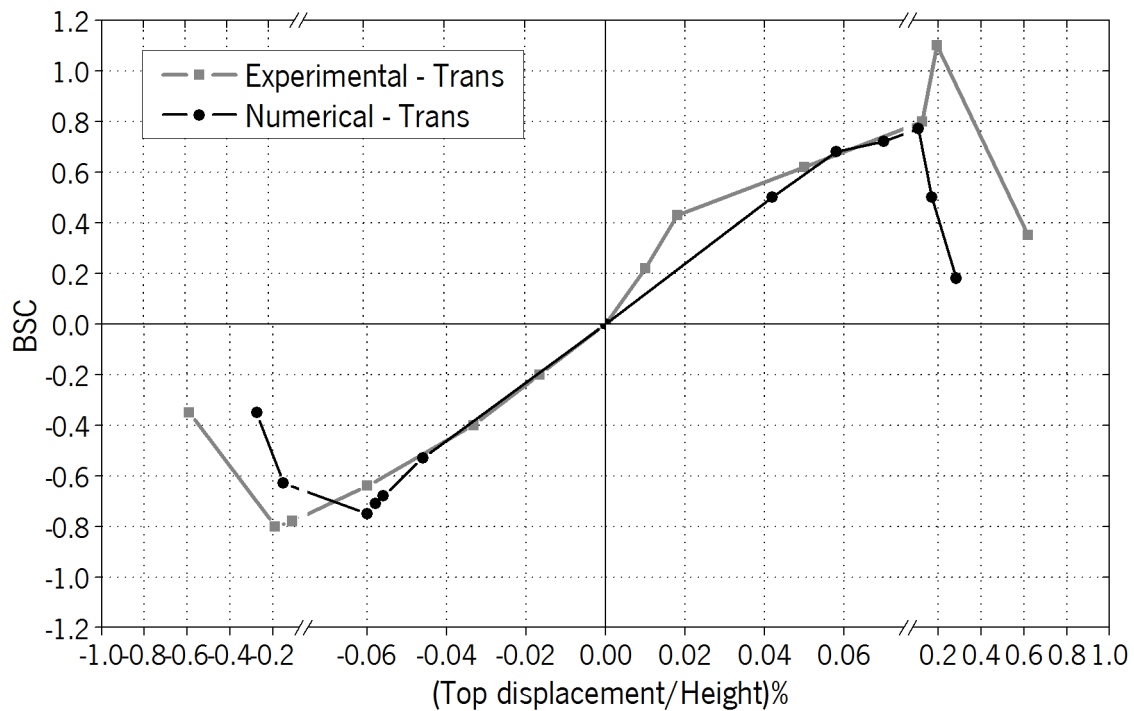
Figure 5.18 – Hysteretic response in longitudinal direction for input signal of 100% in:
(a) experimental building and (b) numerical model

The hysteretic responses in the longitudinal and transverse direction for all the phases (or inputs) were obtained and plotted. Then, in a similar process like the one performed for the experimental results in chapter 4, the envelope composed of the maximum force and corresponding displacement of each seismic input phase was taken into account in each direction. Those envelopes can be seen as the capacity curves of the numerical model.

From Figure 5.19, a comparison between the numerical and experimental capacity curves in the two orthogonal directions is carried out. As the longitudinal and transverse walls have different geometry and configuration (longitudinal walls have a certain percentage of openings), it was needed to evaluate the capacity curves for both longitudinal and transverse directions.



(a)



(b)

Figure 5.19 – Capacity curves relating base shear coefficient and top normalized displacement: (a) longitudinal direction and (b) transverse direction

From a general observation, it is possible to state that the numerical model accurately represent the dynamic response of the studied constructive system, which is based on unreinforced concrete block masonry. The curves presented a good fitting in both positive and negative sides, in which the nonlinear behavior was satisfactory represented. It is important to stress that the experimental

values were obtained with an average mathematical approximation, in which for example the accelerometers of the first and second level were processed together with a handmade theoretical mass distribution. Those mathematical procedures can induce small errors in the final results, which could influence, among others, in the differences found in the transverse direction.

The positive and negative directions were assumed according to the instrumentation's location in the experimental model. Thus, for the longitudinal direction, movements from North to South are positive and for the transverse direction, the positive movements are from the West to East walls. From both directions, an important concern relates the inefficiency of the numerical model to reach the displacements found in the experimental model, as previously discussed. On the other hand, the strength capacity was very well described by numerical simulation in the positive and negative longitudinal direction and in the negative direction of the transverse direction. However, for the positive range of the transverse direction a remarkable peak was obtained during the shaking table test of the seismic input of 250%_1. Apart from this event, it should be said that the numerical model describes in an adequate manner the pre-peak and post-peak dynamic behavior of the masonry building. One of the characteristics of the numerical model, particularly for the transverse direction, is that it presents a conservative behavior for the post-peak regime for both strength and displacements capacities, when compared to the experimental results. This behavior provides an extra confidence in the numerical model, given that the stiffness of the model, the shear strength and the displacement capacity is very close to the experimental one, at least for a seismic input of 200%.

5.6.4 Damage

A major qualitative indicator about the validity of the numerical model is the damage patterns. In fact, it is mandatory that besides the quantitative agreement of the parameters under analysis, the numerical response represent adequately the main features of the damage patterns found in the experimental campaign. Here, in order to obtain an approximate comparison with the crack paths and crack openings presented in the building tested in the shaking table, the maximum numerical principal total tensile strains (elastic + plastic) were evaluated. The strains, are based on the Green-Lagrange theory and are evaluated in the element's integration points, see Table 5.10. To obtain the maximum values of the tensile strains for the different dynamic inputs a post-processing command was implemented, namely a scan load steps. This command performs a scan in every time step looking for the maximum values of every integration point. Figure 5.20 presents the results of the tensile strains for each phase. These tensile strains can be compared with the damage patterns for the unreinforced masonry building presented again in Figure 5.21.

The evolution of the tensile strain in the numerical model presents a good agreement with the damage pattern exhibited by the experimental building. In particular, a good crack mapping is found in the longitudinal direction (West and East walls with openings). As observed for the phase of seismic input of 200%, the longitudinal walls present diagonal cracks between openings at the first floor, and at the second floor maximum tensile strains are concentrated at the base of the walls, exactly in the same place where the horizontal cracks initiates. It is also possible to observe also

peak tensile strain from the corner of the openings in line with the orientation of the stair stepped cracks in the West wall.

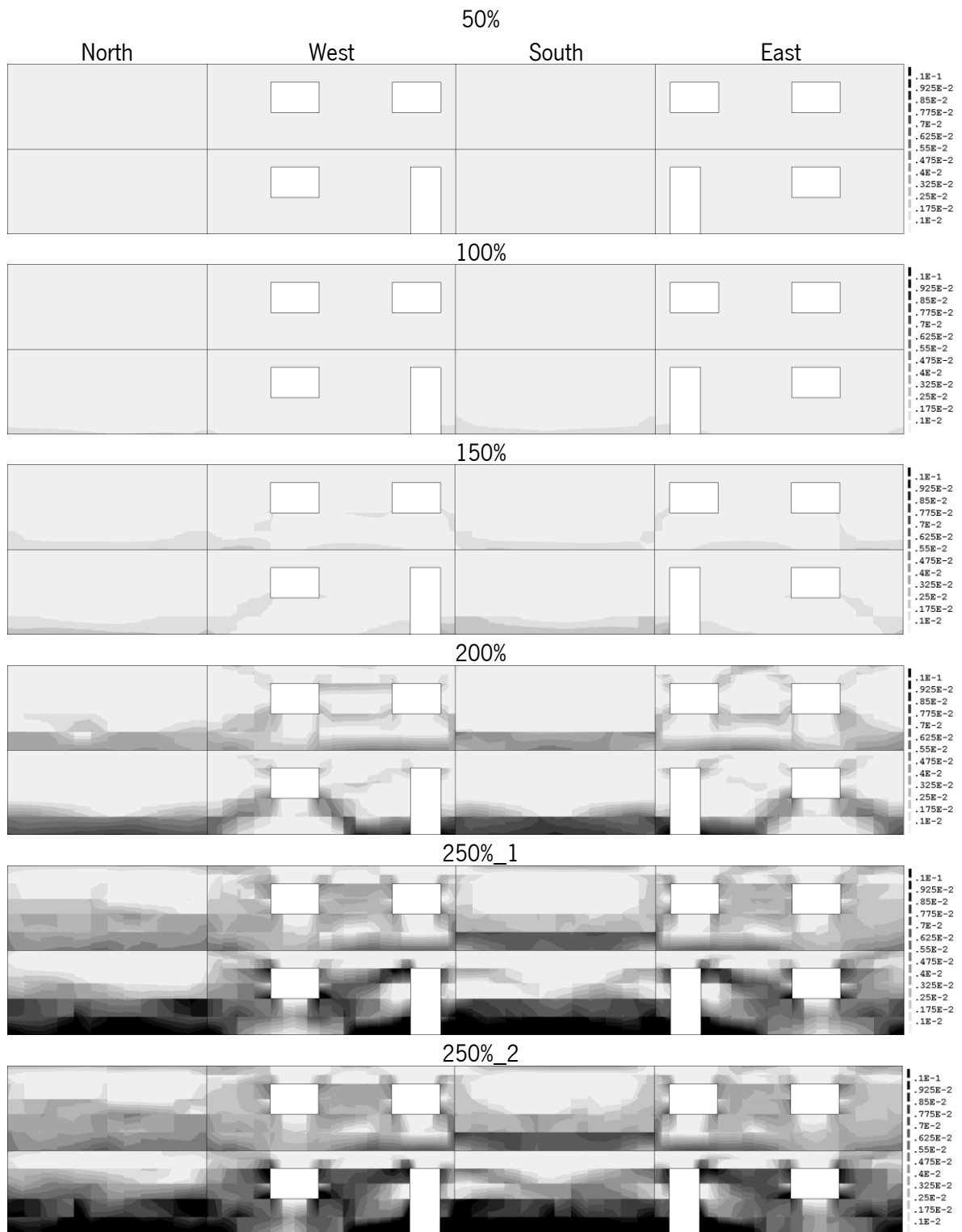


Figure 5.20 – Maximum principal tensile strain for every input

The numerical model was not so effective in the prediction of the diagonal cracks patterns in the transverse direction (north and south walls). The same happens in relation to the top horizontal

cracks. At the final stage of the shaking table testing, the masonry building presented well-defined crack patterns that involve diagonal and horizontal cracks at the top and bottom parts of the North and South walls. These cracks results from a progressive evolution from early cracks initiating in the previous tests and promotes then a clear sliding mechanism. It is considered that the cracks at horizontal bed joints at the base of the wall are well described, both at the first and second floor, but the model is no able to represent so well the diagonal cracks. The numerical model presented considerable strain concentration at the base of those walls. It should be mentioned that even at the top of these walls, the tensile strains appears later in relation to the experimental horizontal cracks at the top of the walls, just at the seismic input of 250%.

At the final stage, both numerical and experimental models present a concentration of damage at the bottom corners of the building and in general higher level of damage at the first floor. The simulation of failing blocks and the failure sliding mechanism are not possible to be described by the numerical approach followed. As previously discussed, those behaviors will be only obtained by implemented a detailed micro model solution. Based on this information and in the quantitative parameters, it is considered that the numerical model is able to represent in general the dynamic behavior of the unreinforced masonry building and thus appears to be reliable and trusty numerical solution in which future studies, regarding unreinforced masonry buildings can be based on.

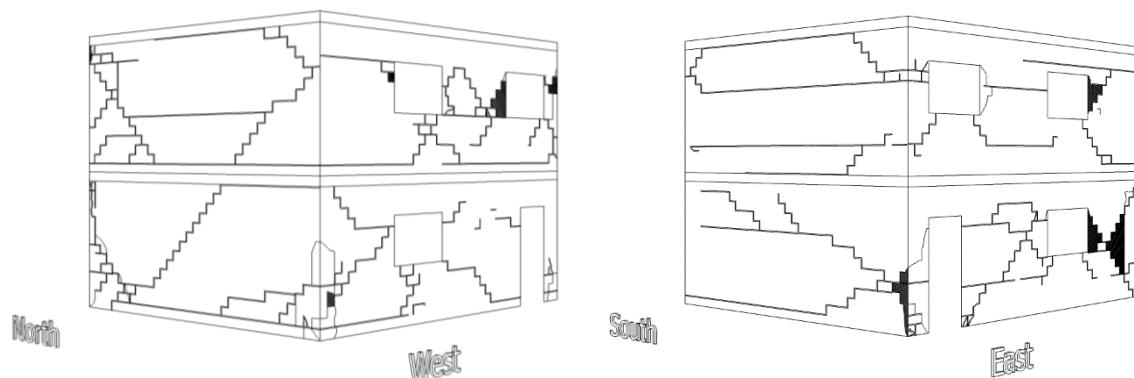


Figure 5.21 – Final damage for the experimental unreinforced masonry building

5.7 Concluding remarks

The elaboration of reliable numerical models based on experimental data constitutes one of the solid bases to further structural studies and designs. In this chapter, all details related to the construction of the numerical models aiming at representing the dynamic behavior of unreinforced concrete block masonry have been presented. A phased nonlinear dynamic time history analysis was performed by using finite element modeling with macro-elements methodology. Results in terms of accelerations, displacements and strains were directly compared with experimental ones. From the process made and results obtained, it is possible to conclude that:

1. The calibration process of a numerical model represents an important role of the subsequent nonlinear analysis, as the nonlinear simulation depends also on the linear mechanical properties considered for masonry material. It must be taken as part of the

whole validation process and considered as one of the most fundamental part of the numerical analysis. With this respect, it is important also to notice that the evaluation of the experimental modal parameters before any seismic input test reveals to be an important tool for the calibration of the numerical model.

2. The macro-model approach implemented in this work, with the rotating total Strain crack constitutive model adopted for masonry demonstrate to be accurate enough for the study and general understanding of the nonlinear dynamic behavior of unreinforced masonry. It simulates the positive and negative pre-peak and post-peak nonlinear behavior with an acceptable approximation. In spite of the few implementations of this modality of the rotating total strain crack model in masonry materials, it is strongly believed that this crack model can represents in a more stable and reliable way the nonlinear masonry behavior than the total fixed crack model, at least in this particular case
3. The nonlinear finite-element incremental analyses by phases have demonstrated to be a useful tool for the description of the dynamic behavior of the unreinforced masonry building tested in the shaking table for increasing seismic inputs. In fact, it enables to describe the pre-peak and the post-peak behavior of the material, given more control to the analyst and identifying not only the ultimate load bearing capacity of the structure but also its displacement capacity and hysteretic response, particularly important in the presence of seismic forces.
4. Comparisons of peaks and RMS presented significant differences for the same parameter. Then, conclusions of quantitative variables in dynamic analysis should be based on at least two different approaches (one should be an integral parameter), as each of them can give different point of view information about the same criterion, completing the analysis and increasing confidence on it.
5. In the numerical simulation of the unreinforced building, the last two seismic inputs (250%) with higher input amplitude were not very well simulated with the numerical model. After this, the developed damage based on very localized horizontal and stair stepped shear cracks promoted relative sliding movements of adjacent macro-blocks, which are quite impossible to be represented with the numerical approach followed in this work.
6. The correct simulation of the experimental boundary conditions has demonstrated to play an important role in the numerical analysis of the structure. Particularly for this study, it was observed through the experimental campaign that to attain a 100% fixed base constraint (with the shaking table) in a building with considerable mass and subjected to seismic motion is a challenging objective. This experimental drawback influenced directly the dynamic behavior of the structure. Then, the assumption of a total fixed constrain for its numerical simulation seems to be debatable.

Chapter 6

Seismic design considerations

Abstract

The main purpose of the design from the structural point of view is to devise a technically and economically efficient system that resist and transmit the forces and/or deformations induced by the excitation imposed to the environment in which the structure is to be built. In codes, the seismic design of residential masonry buildings is generally tackled by simplified methods, which account by less computer cost and analysis time. These methods have proven to be accurately close to the actual structural seismic behavior of buildings. They are normally presented in terms of linear elastic and/or nonlinear static (pushover) analysis. For linear elastic analysis, reduction factors are imposed to account for the nonlinear response of the structure.

In the present chapter, common methods implemented for the design of masonry buildings in present codes are evaluated, namely a linear elastic analysis and a nonlinear static “pushover” analysis. For them, the symmetric unreinforced masonry building will be studied. Results from these methods and comparisons with the nonlinear dynamic analyses developed in the previous chapter will be presented

6.1 Introduction

Bertero (1996) defines the three major objectives of design as (1) safety; (2) good performance and (3) economy. Safety is the most important objective, because structural failure usually endangers human life and always involves economic losses. However, it must be recognized that no structure is unconditionally safe: codes account for some probability of failure due to e.g. human error in design and/or construction or unlikely extreme loading. The design of structures requires the explicit consideration of the problems related to nonlinear structural response and to the nonlinear behavior of materials, members and connections when subjected to cycles of high load reversals. Furthermore, design implies the identification of serviceability conditions and formulations of acceptance criteria with respect to them. Then, it is clear that the achievement of an optimal seismic resistant construction requires both a clear understanding of the role of members and an overall understanding of their relationship in each phase of the design process.

Since the decade of 1960s, based on the limited number of observations of buildings' performance that had been subjected to strong ground motions, researchers knew that if plastic deformations were accepted, it would be possible to design safe buildings for lower strengths than what the observed spectral acceleration would require them to have. Nowadays codes like the ASCE (ASCE/5-02 2002), FEMA (Council 1997) and Eurocodes (Eurocode 8 2004), propose four possible procedures for the seismic analysis of buildings: two linear procedures and two nonlinear procedures. The two linear procedures are termed the Linear Static Procedure (LSP) and the Linear Dynamic Procedure (LDP). The two nonlinear procedures are termed the Nonlinear Static Procedure (NSP), generally known as pushover analysis, and the Nonlinear Dynamic Procedure (NDP). In general, linear procedures are appropriate where the expected level of nonlinearity is low and static procedures are appropriate where higher mode effects are not significant. This is generally true for small and regular buildings. Dynamic procedures are required for tall buildings and for buildings with torsional irregularities or no orthogonal systems. Codes widely accept the NSP for most buildings.

Although an elastic analysis can give a good indication of the elastic capacity of structures and about the most critical stress patterns, it cannot predict failure mechanism and account for redistribution of forces during progressive yielding. The behavior factor q is defined by the Eurocode 8 (2004), shortly EC8, as the factor used for design purposes to reduce the forces obtained from a linear analysis, in order to account for the nonlinear response of a structure, associated with the material. The resistance and energy-dissipation capacity of the building are related to the extent to which its nonlinear response is to be exploited. In operational terms, such balance between resistance and energy-dissipation capacity is characterized by the values of the behavior factor q and the associated ductility classification. Although masonry is considered to be a brittle structural material, the experiments and analysis of earthquake damage show that even plain masonry buildings possess a relatively reasonable dissipation capacity, which makes possible the reduction of elastic seismic forces (Tomažević 1999). Consequently, for the seismic resistance verification of buildings, the balance between the required strength and ductility is specified by this factor, which varies according to different masonry construction systems. Only if the structure is not able to dissipate any energy, it should be designed for strength. In such case, no account is taken of any hysteretic energy dissipation, and the behavior factor is equal to $q=1$.

The last two decades have been characterized by a significant progress in nonlinear methods of analyses of masonry structures to the extent that reliable nonlinear pushover analysis of buildings is a real possibility also for practice. The application of this procedure for the assessment of masonry buildings has been introduced into seismic codes (e.g. EC8, new Italian seismic code OPCM 3274/03) (Galasco et al. 2006). Nonlinear static (pushover) analysis related to the assessment of a structure subjected to an increased lateral load with fixed pattern in which the structural members yield sequentially until a local or global structural failure is achieved. The analysis provides information on the strength and deformation demands. Thus, it permits to identify the critical members that are likely to reach limit states during an earthquake. In the literature, it is possible to find several types of pushover methodologies, namely the conventional: (1) uniform load distribution proportional to the mass; (2) first mode load distribution; and (3) the advanced displacement-based adaptive pushover methods (DAP). The last one takes into account the accumulation damage in the structure. All of them have been implemented in masonry buildings, with symmetric and asymmetric geometrical configuration, in which advantages and limitations have been found (Chopra and Goel 2004; Galasco et al. 2006; Krawinkler and Seneviratna 1998).

The advantage of the nonlinear static (pushover) analysis is its simplicity in comparison to actual nonlinear dynamic response analysis, and its potential to expose weak links in the structure, i.e. give insight on its performance. On the other hand, the principal shortcomings are the questionable validity of a fixed loading pattern. However, with this in mind, the pushover analysis can be viewed as an approximate method for predicting seismic force and deformation demands.

6.2 Objectives and methodology

The main objective of the present chapter is to obtain information about simplified design methods recommended by the codes, and compare them with the experimental and the nonlinear dynamic time history results previously studied in this work.

To accomplish this objective, two design procedures are considered, namely the linear and nonlinear static analysis methods. In relation to the linear elastic analysis, the main issue is related to the behavior factor, q , to be considered in the seismic design of unreinforced masonry. Therefore, the experimental results of the shaking table tests on the symmetric unreinforced masonry building are used to derive the behavior factor. For this, two approaches were used, namely the calculation of the q factor based on force and based on ductility, making also a comparison with the values suggested by the European code. In the second approach, a nonlinear static “pushover” analysis with a lateral load proportional to the mass is carried out. For this, the three-dimensional numerical model calibrated based on the nonlinear dynamic time history analysis was used (Chapter 5). From the nonlinear static “pushover” analysis, the interstory drift, capacity curves and damage patterns for each direction are obtained. These are directly compared with the experimental results from the shaking table tests and with the results of the nonlinear dynamic analysis.

6.3 Seismic resistance verification

As discussed by Bertero (1996) and Pinto (1994), the design process of a civil engineering facility usually involves several phases, of which the following four are the most important: (1) planning; (2) preliminary design, which usually involves approximate analysis; (3) rigorous analysis; and (4) acceptability check of final design. The first and perhaps most difficult technical problem in carrying out this process is the formulation of the design criteria in which engineering experience plays an important role. Most buildings are expected to deform beyond the limit of linearly elastic behavior when subjected to strong ground motion. Thus, the earthquake response of buildings deforming into their inelastic range is of central importance in the design of earthquake resistance buildings.

According to the requirements of Eurocode 6 (2005) and Eurocode 8 (2004), which regulate the design and construction of masonry structures, the structural system should be verified for the required strength and ductility properties. Both of them are related to the capacity of the structure to dissipate the energy and to withstand nonlinear deformations without losing the stability. Then, it is expected, with acceptable probability that the structure will remain in use within the expected life period and under expected maintenance conditions. This means that in addition to withstand all external actions without substantial damage, damage cannot occur disproportionately in cases where accidental events like impacts or human errors might occur. In this regard, the extent of permissible damage occurring to the structure in the nonlinear range should also be carefully evaluated, and consequently, the serviceability limit of the structure should be verified. In practice, due to the structural configuration, there is usually no need for masonry buildings to be verified also for the serviceability limit state (Tomažević 1999). In seismic regions, two basic requirements are considered in the design: (1) no collapse requirement and (2) damage limitation requirement. Here it is intended that the building retain structural integrity and load-bearing capacity after being subjected to an earthquake with expected intensity. With these two objectives defined, the Eurocode 8 (2004) imposes structural design limitations depending of the important class and the masonry type implemented for the construction of buildings that depend mainly of the type of analysis implemented in the design process.

The major uncertainties in the estimation of the potential demands are due to difficulties in predicting: (1) the critical seismic excitation and hazards at the site during the service life of the structure; (2) the state of the entire soil-foundation-superstructure-nonstructural components system when the critical earthquake occurs; (3) the internal forces, deformations, stresses and strains induced in the model; (4) realistic supplies of stiffness, strength, stability, and capacity to absorb and dissipate energy (i.e. realistic hysteretic behavior) of the entire system. In any case, functional requirements must be met if the structural design is satisfactory. Finally, having satisfied damage limitation and no collapse requirement, the structure must be designed for minimum cost.

6.4 Structural behavior factor q for seismic analysis

According to Eurocode 8 (2004), the seismic design of regular masonry structures, which comply with in plane and elevation geometrical regularity requirements, can be carried out considering the

linear elastic behavior of the structure when submitted to design seismic loads. For this, the calculated seismic loads must be based on the elastic response spectrum divided by the behavior factor “q”, which depends on the construction typology. The consideration of the behavior factor assumes that the structure is able to dissipate energy and deform in the nonlinear range.

By definition, according with the Eurocode 8 (2004), the behavior factor q is an approximation of the ratio between the seismic forces that the structure would experience if its response was completely elastic with 5% viscous damping and the minimum seismic forces that may be used in the design considering the non-linear behavior of the structure. Following this definition, the behavior factor can be given as a ratio between base shear coefficients, according to the following equation:

$$q = \frac{BSC_e}{BSC_d} \quad 6.1$$

Where BSC_e is the base shear coefficient developed in a completely elastic structure and BSC_d is the design base shear coefficient.

For seismic resistance verification of unreinforced masonry buildings, a recommended range of q factor values between 1.5 and 2.5 is provided. However, the Portuguese national annex of Eurocode 8 (2004) strictly imposes a maximum value of 1.5. In spite of indicative values of the behavior factor that can be found in different codes, there is not so much information on its verification from experimental analysis based on shaking table tests (Tomažević and Weiss 2010; Zonta et al. 2001). Tomažević (1999) made an attempt to verify the values of q factor proposed by the Eurocode 8 (2004). For it, two three-story plain masonry buildings were tested on a shaking table, as a conclusion the experimental values confirmed the general validity of Eurocode 8 (2004) proposed values of q factor, indicating a possible reserve at the same time. More recent, da Porto et al. (2009) presented values of behavior factor of structural walls based on the data obtained from masonry walls under in-plane cyclic loading with distinct typologies.

Besides the basic calculation of behavior factor, q, in terms of forces, it is possible to calculate the behavior factor based on the global ductility of the structure, μ_μ . This procedure implies the calculation of the idealized bilinear resistance diagrams equivalent to the monotonic envelop of the successive dynamic loops found for each seismic loading step. The bilinear idealization diagram and the definition of the idealized resistance are obtained taking into account the elastic stiffness, corresponding to initial stiffness associated to the linear regime of the building (uncracked stage), and to the equalization of dissipated energies under the experimental envelop and under the idealized bilinear diagram (Figure 6.1) (Tomažević 2007). Once the idealized design seismic resistance and the stiffness are defined, the idealized elastic displacement, $\phi_{e,i}$, is calculated, and the ductility factor, μ_μ , is derived through the Equation 6.2:

$$\mu_\mu = \frac{\phi_{u,i}}{\phi_{e,i}} \quad 6.2$$

Where the $\phi_{u,i}$ is the ultimate displacement. The ultimate displacement, $\phi_{u,i}$, is commonly considered as the displacement corresponding to 80% of the maximum resistance ($\phi_{0.8 Rmax}$). This means that the story drift calculated at 20% of the maximum force degradation is the maximum displacement, which complies with the no collapse requirement.

From the ductility factor, it is possible to derive the behavior factor that takes into account energy dissipation of the system (Tomažević and Weiss 2010):

$$q_{\mu} = (2\mu_{\mu} - 1)^{1/2} \quad 6.3$$

On the other hand, according to what is mentioned by Tomažević and Weiss (2010), an acceptable damage level, to which reasonable deformations and damage limitation are attained, is close to the maximum resistance, corresponding to approximately 3 times the story drift in which occurs the first crack, ϕ_{cr} , as shown in Figure 6.1. The figure presents in a qualitative and simplified way the definition of the behavior factor q , in terms of force and displacement. On the plot, the experimental seismic response envelope curve of an actual structure, idealized as a linear elastic – perfectly plastic envelope, is compared with the response of a perfectly elastic structure having the same initial elastic stiffness characteristics. Then, it is observed how due to the energy dissipation capacity of the actual structure, there is no need for the structure to be designed for strength; i.e. for the expected elastic seismic load $R_{max,ie}$.

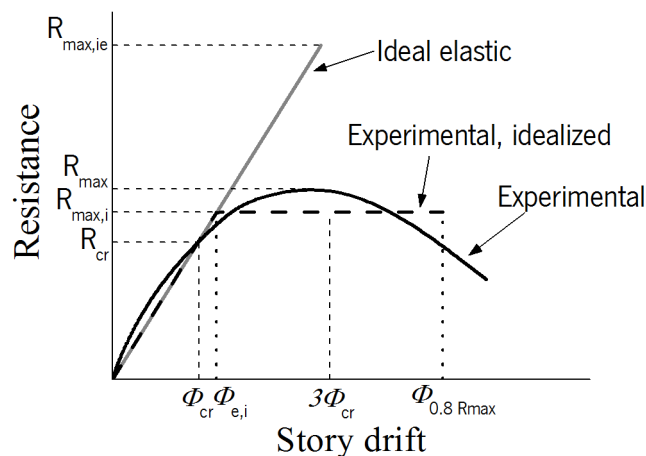


Figure 6.1 – Definition of the structural behavior factor

6.4.1 Experimental behavior factor q for the symmetric UM model

The methodology described previously is used to derive the behavior factor for the symmetric unreinforced masonry buildings tested at the shaking table. For this, the results obtained from the experimental campaign of shaking table tests carried out on the symmetric unreinforced masonry building are used. The reinforced model is not analyzed, as it is considered that the complete response of the reinforced masonry building was not achieved for the level of seismic input imposed to the building. As mentioned by the Eurocode 8 (2004), the value of the behavior factor may be

different in different horizontal directions of the structure. Therefore, the two main orthogonal directions of the building were analyzed separately. As previously mentioned, the experimental base shear is given in terms of a base shear coefficient (BSC), calculated as the ratio between the base shear developed in the model during shaking (BS) and the weight of the model above the base (W) ($BSC = BS/W$). The base shear has been calculated as the sum of the inertial forces developed at each story. Besides, the suggestion given by (Tomažević 2007) to define the resistance curve was used. This author states that in case of unreinforced masonry structures, the resistance curve is adequately represented by the relationship between the resistance of the critical story (usually the first story of the building) and the story drift of the same level. The envelopes of the experimental dynamic behavior (symmetric UM and RM models), in which the relation between the maximum first-story base shear coefficients (developed during each individual input test), and the corresponding values of story drift are given in Figure 6.2. Since inertial forces do not consider the components of damping and stiffness, the final base shear component at the base of the model has been estimated considering only the masses. Consequently, the calculated forces should be considered as an approximation. The comparison of test results indicates clearly the higher resistance of RM model for both directions. Distinct behavior is observed regarding deformation, attaining the UM model maximum values of drift but with lower resistance. This behavior clearly demonstrates the improvement in resistance capacity, stiffness performance and displacement response given by the reinforcement. From the results on a series of diagonal compression tests, Vasconcelos et al. (2012) concluded that the combination of vertical and horizontal reinforcement results in the considerable increase on the shear strength. As discussed in previous chapters, the combination of the reinforcements improves also the distribution of cracking leading to a more distributed pattern. The results also indicate clearly that the UM building reached the maximum capacity. In case of RM model, it is clear that the response obtained in the experimental campaign reflects the low level of damage, with a response predominantly in the linear regime, even if the envelopes seem to present already a very small plateau. As observed in the UM model, the structure resisted seismic loads in the non-linear range without collapse, even if the lateral drifts are quite low (like in the longitudinal direction), meaning that the non-linear regime occurs for low lateral drifts, confirming the more brittle nature of unreinforced masonry structures. The lateral drifts are comparable to the ones obtained for the same masonry typology by Tomažević and Weiss (2010). Figure 6.3 shows the ideal elastic response of the masonry building for each direction and the ideal elastic-plastic curve, from which the behavior factor in terms of force and ductility can be calculated.

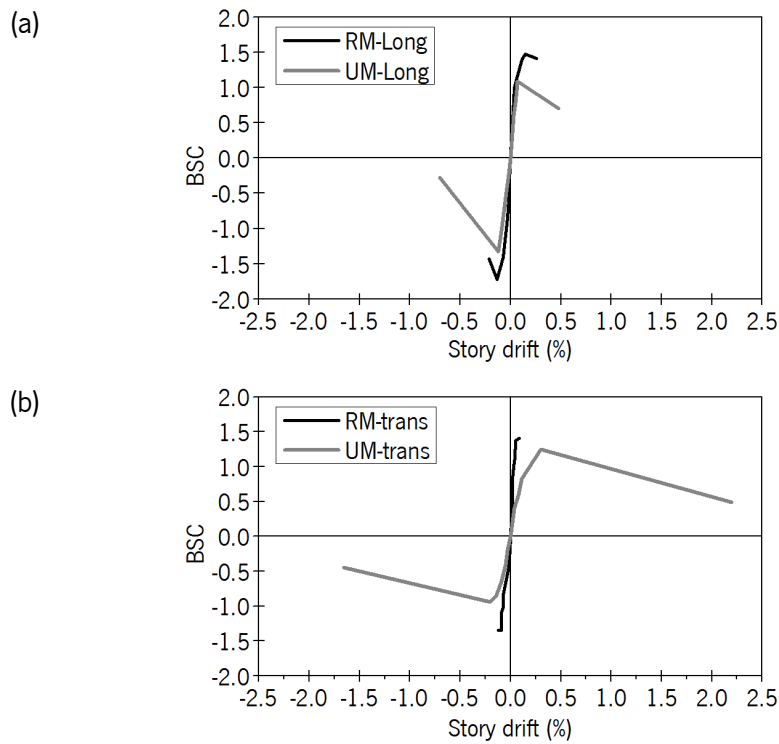


Figure 6.2 – Experimental hysteresis envelopes for the symmetric buildings: (a) longitudinal direction and (b) transverse direction

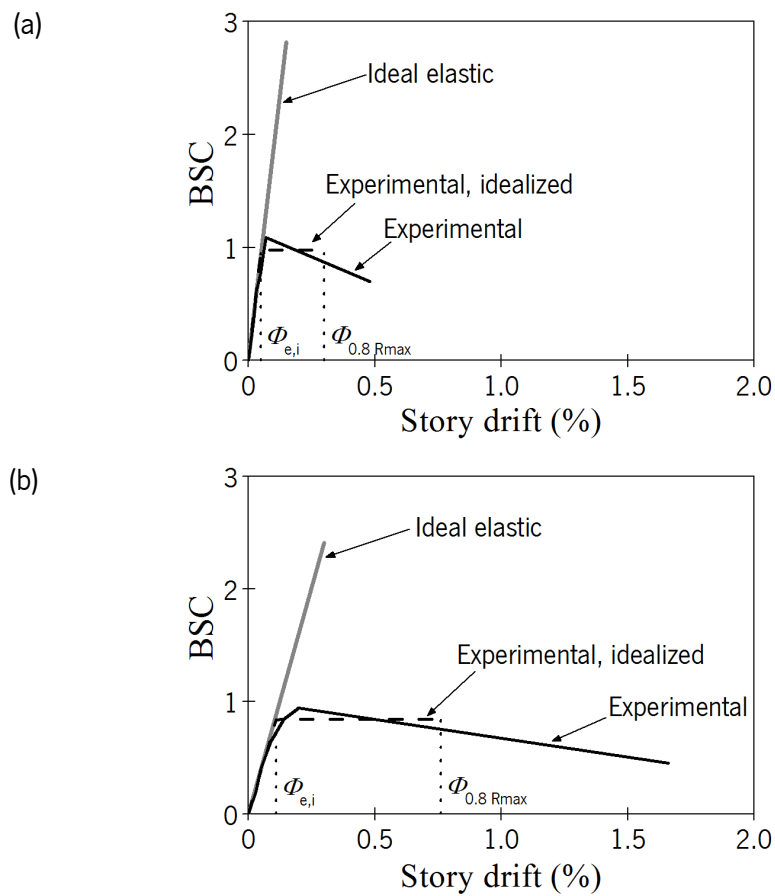


Figure 6.3 – Evaluation of the structural behavior factor for the UM model: (a) longitudinal direction and (b) transverse direction

The calculated maximum ideal elastic base shear coefficient values, $BSC_{ie,max}$, the maximum measured experimental base shear coefficient, BSC_{max} , as well as the design value obtained by the bilinear elasto-plastic curve, BSC_d are summarized in Table 6.1. In this particular case, the BSC_e is the response of an equivalent ideal elastic structure with 5% viscous damping to the input motion, at which the maximum resistance of the experimental model has been attained. Additionally, the values of ductility factor taking into account the maximum, q_{max} , and the design base shear coefficient, q_d , are also provided.

The values of the behavior factor calculated based on ductility, q_u , considering the ultimate displacement corresponding to the degradation of 20% of the maximum resistance, $\phi_{0.8Rmax}$, and a displacement corresponding to a limit damage state, $3\phi_{cr}$, are summarized in Table 6.2.

Table 6.1 – Values of structural behavior factor in terms of force

Direction	$BSC_{ie,max}$	BSC_{max}	BSC_d	q_{max}	q_d
Long	2.82	1.09	0.98	2.58	2.89
Trans	2.41	0.94	0.84	2.56	2.86

Table 6.2 – Values of structural behavior factor in terms of ductility

Direction	ϕ_{ei}	ϕ_{cr}	ϕ_{ui}		μ_μ		q_μ	
			$\phi_{0.8max}$	$3\phi_{cr}$	$\mu_{\mu 0.8max}$	$\mu_{\mu 3\phi_{cr}}$	$q_{\mu 0.8max}$	$q_{\mu 3\phi_{cr}}$
Long	0.054	0.049	0.299	0.147	5.57	2.74	3.19	2.12
Trans	0.105	0.090	0.760	0.270	7.23	2.57	3.67	2.03

It is seen that when the behavior factor is calculated based on force the values are higher than the maximum values given in the interval suggested by Eurocode 8 (2004). When ductility is considered, the values of behavior factor are higher in case the ultimate displacement is taken into account, $q_{\mu 0.8max}$. However, it should be mentioned that for this displacement the building presents considerable damage and is already near collapse. If the damage limitation displacement is considered, corresponding to the drift calculated as three times the drift corresponding to the opening of cracks, the behavior factor decreases considerably and fits in the averaged value in the range 1.5-2.5 suggested by the Eurocode 8 (2004). This means that for this case of unreinforced masonry, it is reasonable to consider the average value of the interval corresponding to limitation of damage in the structure. This result is accordance with other experimental works as referred by Magenes (2006) and Tomažević (1999).

The transversal direction is the predominant direction of vibration (first mode), according to the results obtained in modal identification and corresponds to the direction in which the most severe damage was observed, controlling the behavior factor.

6.5 Nonlinear static “pushover” analysis

The most advanced inelastic analysis method is the complete nonlinear time history analysis (as the one performed in previous chapter for this thesis), which even nowadays is considered overly complex and impractical for general use due to the necessary knowledge required, the time for its preparation and analysis and the computer cost needed. Available simplified nonlinear analysis methods, referred to as nonlinear static analysis procedures are then suggested by codes for the efficient design of residential masonry buildings. The pushover analysis is an alternative method to the analysis based on linear-elastic behavior, which makes use of the behavior factor q to calculate the seismic design loading. In case of masonry buildings, this method can be used if the structure obeys the requirements of geometric complexity limitation (in plan and in height).

The overall capacity of a structure depends on the strength and deformation capacities of the individual components of it. In order to capture the behavior beyond the elastic limits, nonlinear analysis, such as the pushover procedure, is required. The general output of the nonlinear static “pushover” analysis is the generation of the capacity curve. This represents the relation between the strength of a structural element/building and the displacement in a specified point that is considered representative of the lateral displacement of the structure. The capacity curve is generally constructed to represent the first mode response of the structure based on the assumption that the fundamental mode of vibration provides the predominant response.

The pushover analysis is expected to provide more realistic information on the global seismic structural response that cannot be obtained from an elastic static analysis. On the other hand, in relation to non-linear dynamic analysis, it can provide in a more simply way information about the shear resistance and deformation demands, dissipation of energy, damage patterns, which are very important parameters when seismic analysis is carried out. On the other hand, enables to identify the critical regions. In relation to the linear-elastic analysis, the benefits come at the cost of additional analysis effort, with the incorporation of all the structural elements, with modeling their inelastic load-deformation characteristics, and by executing incremental inelastic analysis. According to what has been mentioned by different authors, the linear elastic analysis is generally in the safe side but can provide somewhat unrealistic and too conservative solutions (Marques et al. 2009; Marques and Lourenço 2008).

6.5.1 Capacity curves of the symmetric UM building

For the present study, the same three-dimensional geometrical model used in in the nonlinear dynamic analysis was adopted and the software DIANA (2010) was also chosen for the analysis. The nonlinear material model (total strain crack model) and the material properties were the same as the ones used in the calibrated model (Chapter 5). For the pushover procedure, a uniform load pattern based on lateral forces proportional to the mass of the building was implemented.

The pushover analysis was performed separately for each direction (longitudinal and transverse directions). The orientation (positive – negative) was taken according with the location of the equipment instrumentation in the experimental building: in the longitudinal direction from north to

south and in the transverse direction from west to east it is taken as positive. As the building is symmetric, it would be not necessary to perform such analyses in the transverse direction. In spite of the east and west walls (longitudinal direction) have identical distribution of openings, they are not symmetrically distributed. Therefore, the distribution of stiffness is different and therefore its resistance capacity.

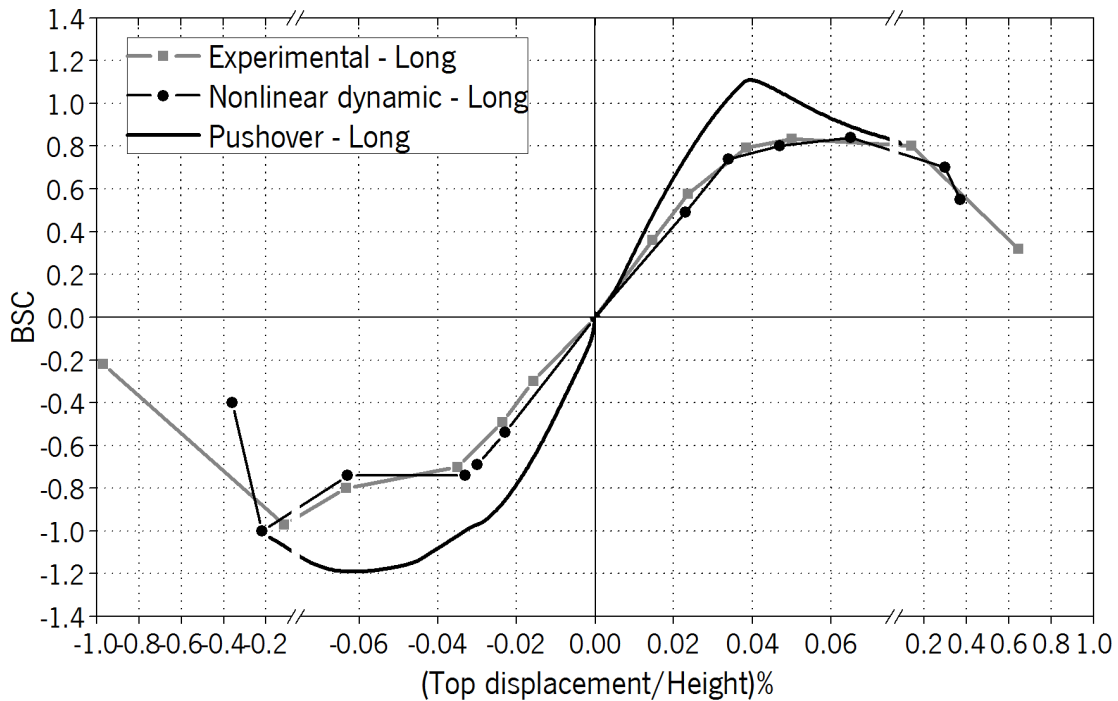
In these analyses, the regular Newton-Raphson iterative method with a convergence criterion based on the internal energy with tolerance of $10E-3$ was used. Furthermore, the Arc Length iteration control method or indirect displacement control was implemented in order to account for the snap-through or snap-back behavior, enabling the record of the response in the post-peak regime. The Line Search Algorithm (DIANA 2010), which scales automatically the incremental displacements in the iteration process and stabilizes the convergence process, was also used.

As already mentioned, the capacity curve gives important information regarding force and displacement capacity of the masonry building. From the pushover analysis, the curve was built through base shear force at the base of the model, and relating it with the lateral displacement at the control node located at the center of the top slab. The capacity curves from the pushover analysis, together with the experimental envelopes of the dynamic hysteresis and with the envelopes obtained in the nonlinear dynamic analysis, for both the longitudinal and transverse directions are presented in Figure 6.4. The pushover analysis provides capacity curves close to the experimental and to the numerical nonlinear dynamic envelopes for both directions. As observed, the curves presented higher base shear capacity and lower displacement capabilities than the experimental and dynamic curves.

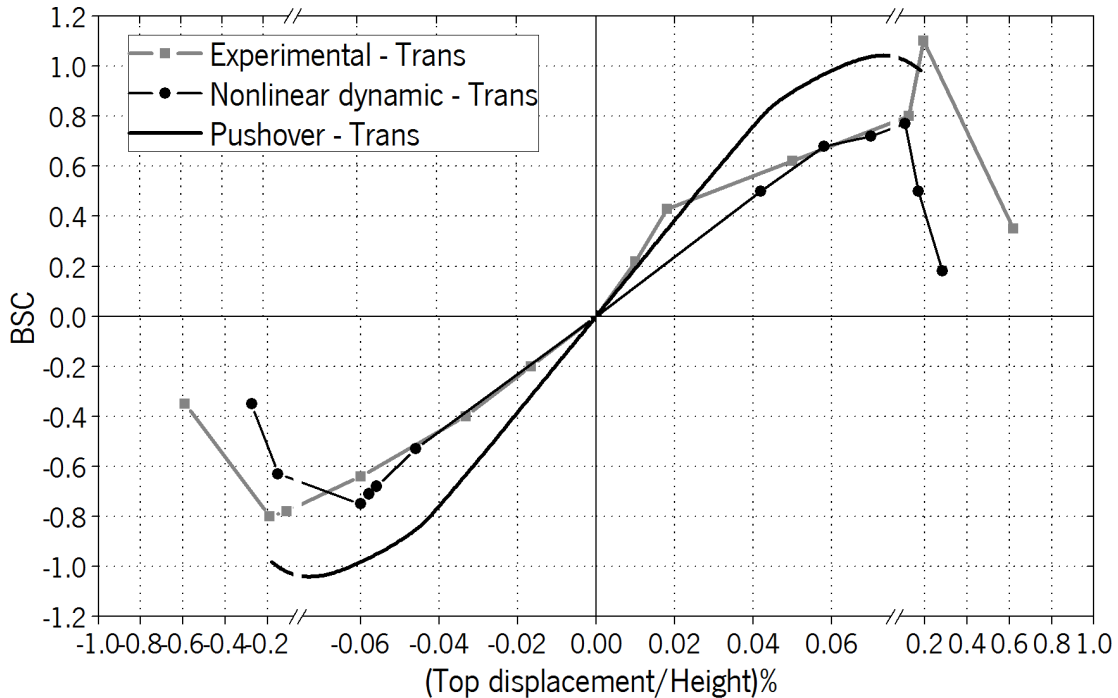
In the longitudinal direction and for both positive and negative orientation, the capacity curve obtained from the pushover analysis presented higher initial stiffness in comparison with the other two curves. Similarly, the base shear capacity presents also higher maximum values in both orientations (1.13 for the positive orientation and 1.20 for the negative orientation). On the other hand, the displacement corresponding to the maximum base shear are lower, which is associated to the more stiff response of the model. The maximum positive base shear capacity of the experimental model was 0.835 with a displacement of 0.05%, whereas for the pushover analysis the capacity curve presented a maximum base shear of 1.13 with a displacement of 0.04%. In the negative orientation, the experimental value was 0.97 with a displacement of 0.115%, for the pushover it was 1.22 with a displacement of 0.067%. This corresponds to differences of 30% for both base shear and corresponding displacement in average.

In the transverse direction, the trend is similar between the experimental and pushover analyses in the negative direction, but in the positive direction there is a higher proximity in terms of stiffness and maximum base shear. A maximum experimental base shear of 1.1 with a displacement of 0.19% compares with a maximum base shear of 1.09 and a displacement of 0.07%. This represents a difference of 0.9% in the maximum force and of 63% difference in displacement. However, it should be mentioned that the maximum experimental force capacity occurred during the test of 250%, in which considerable damage was already presented. This maximum appears outside the trend with a previous force value of 0.8. Furthermore, in the negative orientation the maximum

experimental force is of 0.8, as well. Regarding the negative orientation, the pushover analysis registered a maximum of 1.09 with a displacement of 0.07 (equal to the positive orientation), that is a force 36.25% higher with a displacement 63.2% lower in comparison with the experimental curve.



(a)



(b)

Figure 6.4 – Capacity curve comparison for the experimental, nonlinear dynamic and pushover analyses: (a) longitudinal direction and (b) transverse direction

In terms of maximum displacement, the pushover analysis results present always lower values when compared to the experimental model in both longitudinal and transverse directions.

It is clear that the nonlinear static pushover analysis presented in average 30% higher values of force capacity and displacement values 50% lower than the experimental model. It should be stressed that the pushover analysis did not take into account the progressive damage of the model as considered in the experimental campaign and then in the nonlinear dynamic analysis. This means that the model does not take into consideration the accumulation of damage as it occurs for the loading procedure followed in the experimental testing. Notice that this can be an important factor to take into account, as it could be seen in both the reinforced and unreinforced models, the repetition of the last seismic input (150% in case of UM model and 300% in case of the RM model), lead to a very intensive damage, being necessarily associated to the existing damage.

6.5.2 Analysis of damage

For the characterization of the damage patterns in the nonlinear static “pushover” analysis, similar procedure as the one performed in the nonlinear dynamic analysis was adopted. The maximum principal total (elastic + plastic) tensile and compression strains were evaluated on the numerical model after each push load. The maximum principal tensile strain is commonly adopted as an indicator of the cracking. The maximum principal tensile and compressive total strains obtained for all the walls of the model are presented in Figure 6.5 and Figure 6.6, respectively. The results from the loading applied in the positive orientation are presented in Figure (a) and the results from the loading pattern applied in the negative orientation are presented in Figure (b).

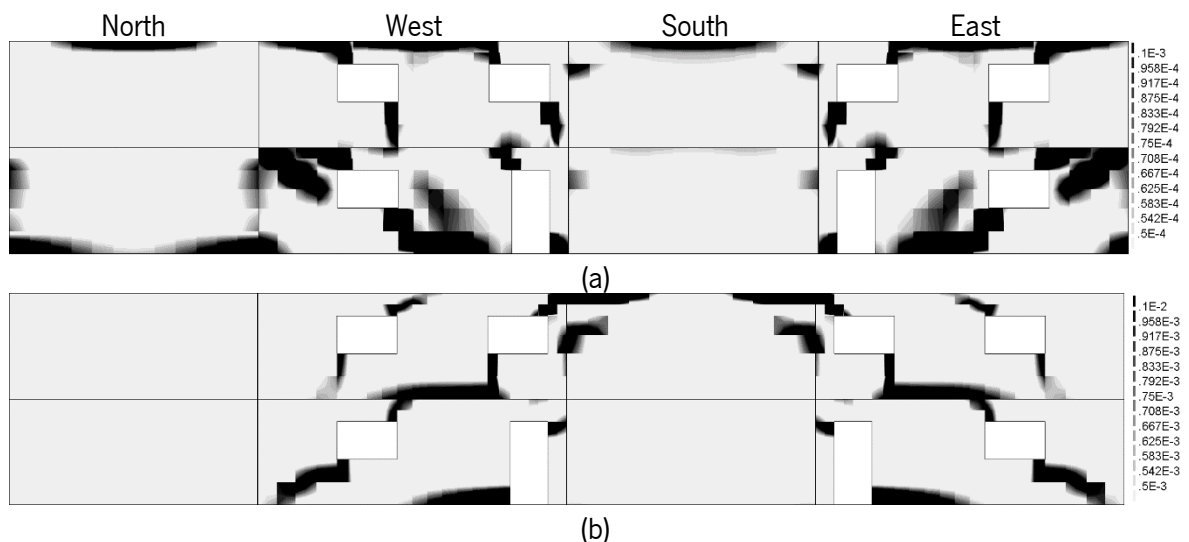


Figure 6.5 - Maximum principal tensile strain: (a) pushover from north to south (positive orientation) and (b) pushover from south to north (negative orientation)

If the total strains of Figure 6.6a) and b) are superposed, it is observed that the highest tensile strains develops in the diagonal direction in the walls with openings. The tensile strains distribution is quite different between the first and second floors, being more remarkable in the first floor. It is observed at the windows of the second level (walls west and east) that the damages from the lower corners have a vertical tendency instead of diagonal. Tensile strains develop also at the corners of the walls.

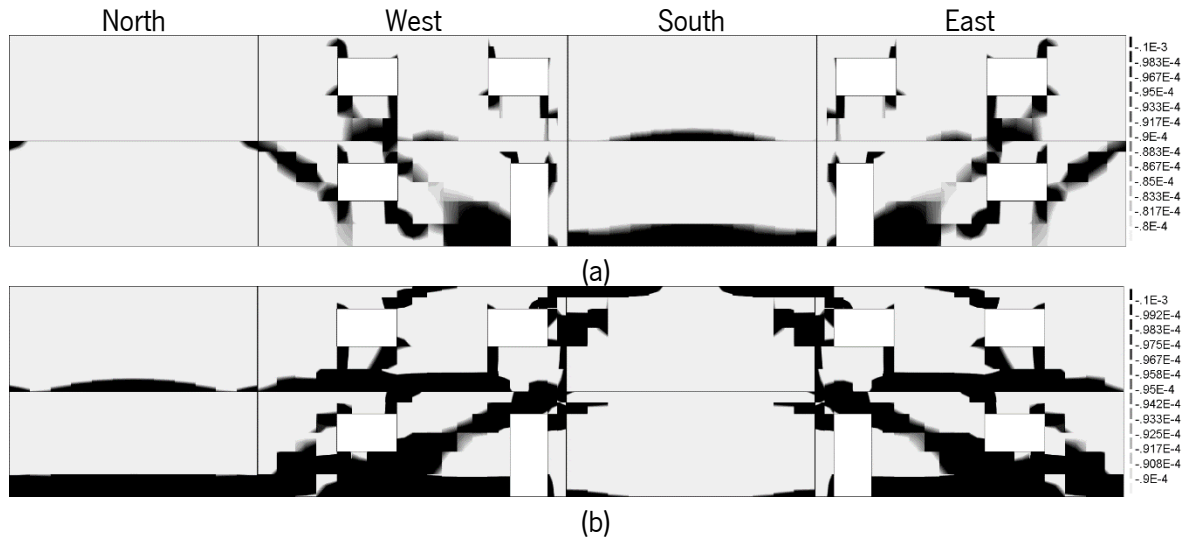


Figure 6.6 - Minimum principal compression strain: (a) pushover from north to south (positive orientation) and (b) pushover from south to north (negative orientation)

The distribution of the compressive total strains is in accordance to the stress concentration at the diagonal direction in the walls with openings, also in correspondence with the total tensile strain distributions. The diagonal compressions in the longitudinal walls (west and east) divided diagonally the first floor in three sections. In addition, here the strain paths are better defined at the first floor level. At the second level, the compression is more concentrate at the corner of the windows and at the lower part of the walls.

When the transverse direction is analyzed, see Figure 6.7 and Figure 6.8, as expected the tensile strain distribution is more effective in the transverse south and north walls, being concentrated at the bottom part of the walls at both first and second floors. The horizontal tensile strains progressed to the walls with openings (east and west walls) until the lower corner of the window and then above the lintel at the second level.

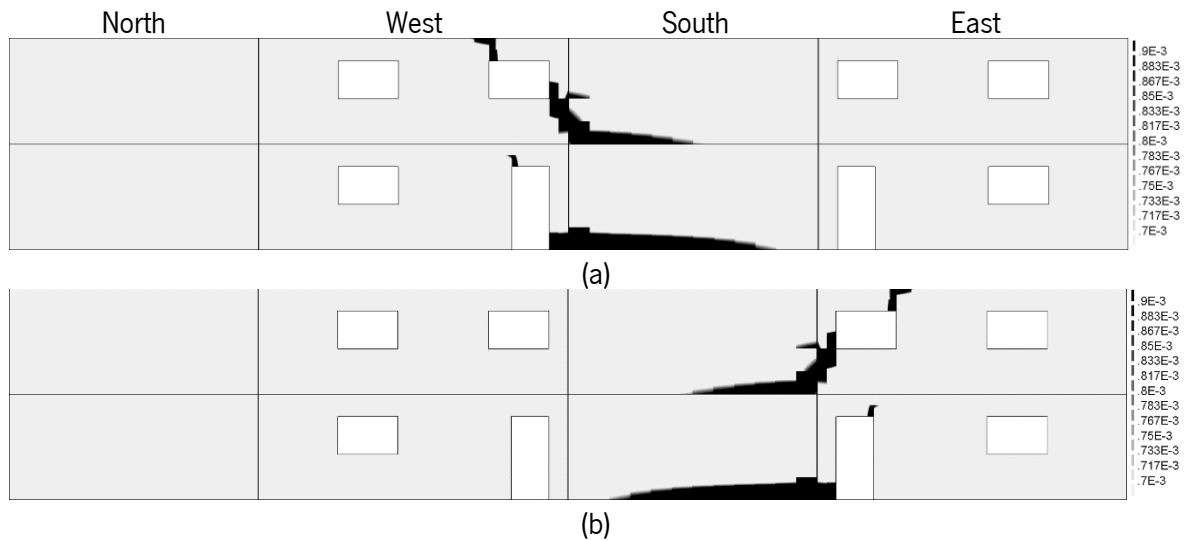


Figure 6.7 - Maximum principal tensile strain: (a) pushover from west to east (positive orientation) and (b) pushover from east to west (negative orientation)

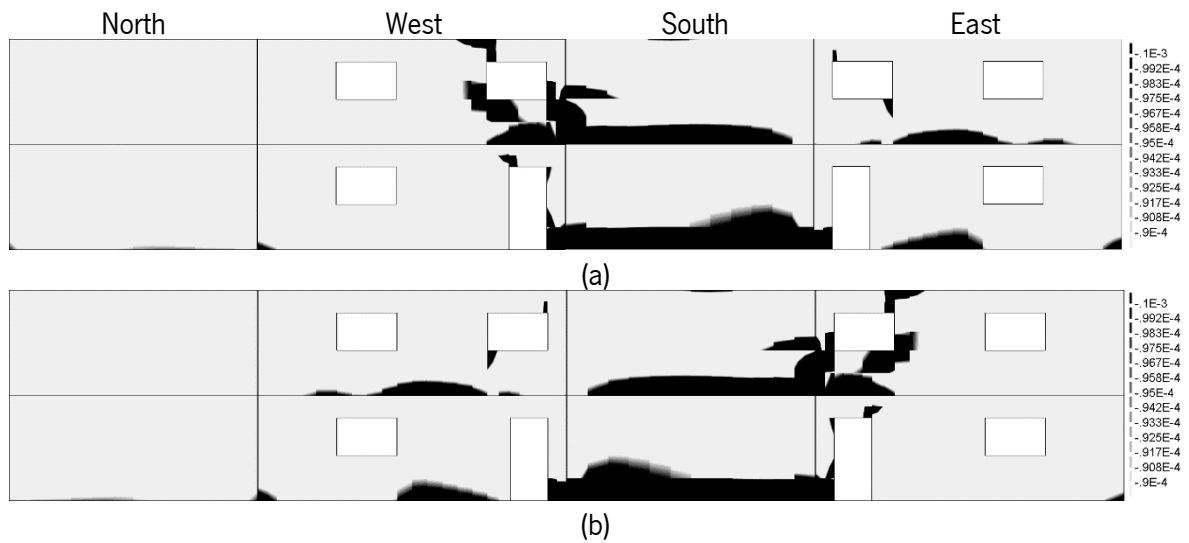


Figure 6.8 - Minimum principal compression strain: (a) pushover from west to east (positive orientation) and (b) pushover from east to west (negative orientation)

In terms of compression strains, the damage once again affected mainly the doors' area of the longitudinal walls and the south wall. In the longitudinal walls, the compression was concentrated at the lower part of both levels and at the corners of the window in the second level. For the south wall, the compression is mainly found at the lower side of both levels' walls. In the south wall, the tension and compression strains affected similar zones, but the compression affected a bigger area.

For comparison purposes, the final damage patterns observed after the final input test of the experimental campaign are presented in Figure 6.9. Besides, the maximum principal tensile strains for the nonlinear dynamic analysis after the input of 200% are presented in Figure 6.10

It should be stressed that the damage observed in the nonlinear static pushover analysis is rather far from the one observed in the experimental testing, and also from the one observed from the nonlinear dynamic analysis. As already discussed in the Chapter 3, the main failure mechanism observed in the experimental model, was the development of a shear sliding mechanism at the second floor, affecting considerably the north and south walls. None of the numerical simulations was able to represent such damage. In particular, for those walls, both simulations only presented damage at the lower part of both levels. In the longitudinal walls, the nonlinear dynamic analysis represented accurately the horizontal crack pattern between windows at the second level of the west wall, but the pushover analysis cannot represent this behavior. However, the diagonal cracks around openings, which are the result of the in-plane resisting mechanism of the structure, are well represented by both numerical simulations, but in the nonlinear static analysis, these are not well represented at the second floor.

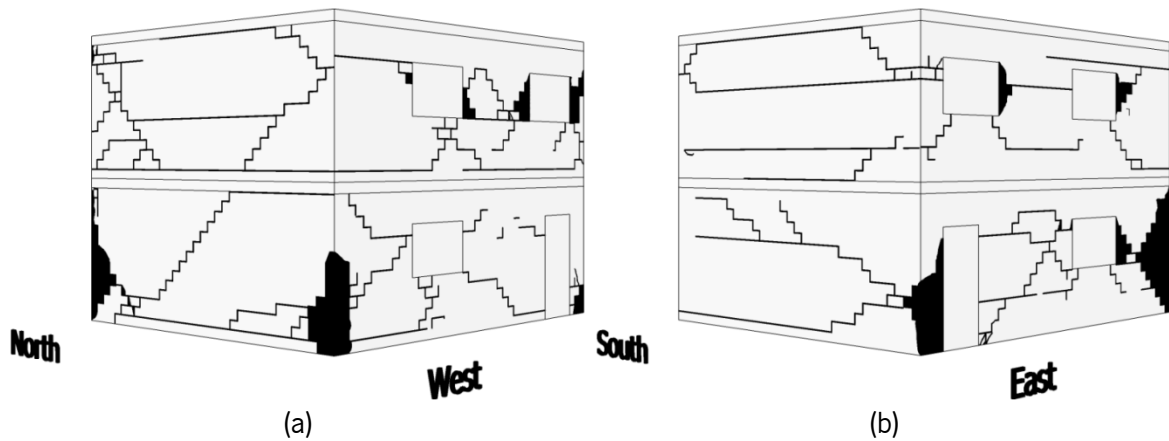


Figure 6.9 - Final damage patterns in symmetric unreinforced masonry building: (a) north – west façades and (b) south – east façades.

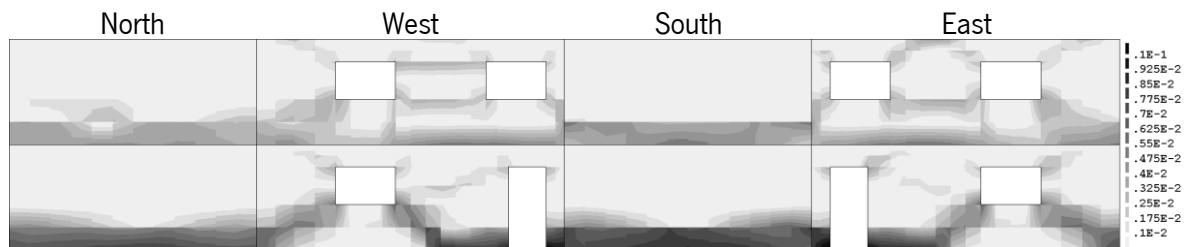


Figure 6.10 - Maximum principal tensile strain for the nonlinear dynamic analysis of 200%

For the pushover analysis, it is possible that the deficient representation of the potential cracking paths can be associated also to the fact that the incremental cumulative damage is not taken into account.

6.5.3 Analysis of in-plane deformation - interstory drifts

In terms of in-plane deformations, it was decided to compare the lateral maximum interstory drifts already selected for the analysis of the deformation performance of the experimental models, as it is a direct damage limitation parameter for the design of buildings in different codes. The results for each direction and comparison with experimental and nonlinear dynamic analysis are presented in Figure 6.11.

As observed, for both directions and both building's levels, the pushover analysis presented the lowest interstory drift values, being followed by the ones provided in the nonlinear dynamic analysis and finally by the ones obtained in the experimental tests. In both directions, for the two numerical analysis (dynamic and static "pushover"), it is found that higher interstory drift values develops at the first level, in opposition to the final drift displacements found experimentally. This is justified by the experimental shear sliding mechanism developed mainly at the second floor in the experimental model.

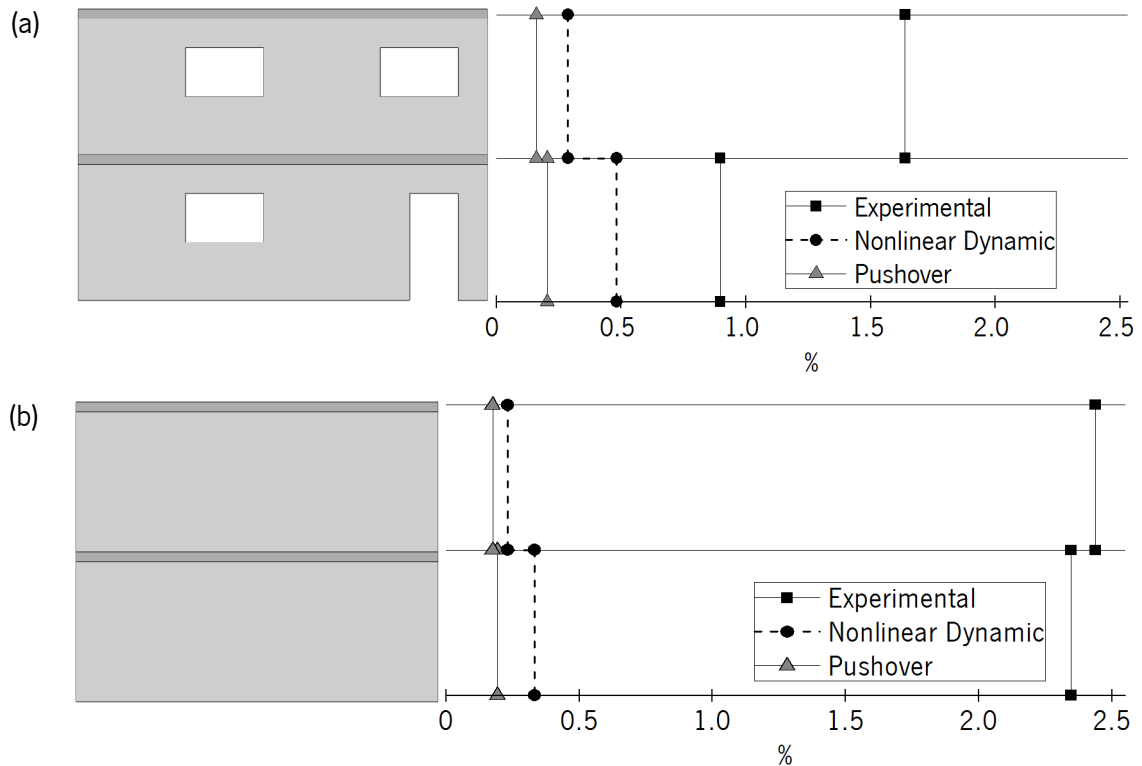


Figure 6.11 – Interstory drifts comparison for the maximum values of experimental, nonlinear dynamic and pushover analyses in the UM model for: (a) longitudinal direction and (b) transverse direction

For the first level, the maximum drift value for the pushover analysis was obtained in the longitudinal direction with a drift of 0.21% and for the nonlinear dynamic analysis, the maximum drift at this floor level also occurred in the longitudinal direction with a value of 0.48%. From the experimental analysis, the actual experimental drift value registered in this direction was 0.90%. However, it is stressed that this value was found for the seismic input of 250% imposed for the second time, for which an extensive damage was observed. In this regard, it should be mentioned that for the first experimental test of 250% a maximum drift in the longitudinal direction of 0.36% was found and for the test of 200% a maximum drift value of 0.15%.

The highest experimental drift at first level occurs in the transverse direction, being of 2.35% during the input test of 250%. For the dynamic and static “pushover” analysis, maximum drift values of 0.33% and 0.19% respectively, were obtained. In particular, this experimental drift presented a huge increment from the value obtained during the test of 200%, for which a value of 0.20% was observed, which is comparable to the value obtained in the nonlinear static analysis. The same behavior is found at the second floor, even with higher lateral drifts measured in the experimental analysis (2.44% in the transverse direction), resulting from the sliding deformation mechanism already discussed. For the same level and direction, the dynamic and static nonlinear analyses presented values of 0.23% and 0.19%, respectively. The experimental maximum interstory drift obtained for input test of 250% at the same floor level and direction was of 0.53% and for the test of 200%, the maximum value was 0.17%. Then, it is found that for this direction, which corresponds with the first natural frequency of the building, and therefore is considered as the most critical, the

dynamic analysis gives a drift value that is higher than the experimental of 200%, but it is far away from the value obtained during the first test of 250%. On the other hand, the static analysis gives a lateral drift value near to the one obtained during the test of 200%. Then, it can be said that in terms of displacements, the nonlinear static “pushover” analysis approximated the lateral drifts developed at the seismic input of 200% (1.11g).

As previously discussed in this thesis, crushing and loss of concrete block units was observed only during the last two inputs of 250%, being the sliding mechanism developed mainly for this seismic inputs, not described by the numerical models (see also Chapter 5).

The Eurocode 8 (2004) imposes an interstory drift limitation of 0.5% for buildings associated to a brittle collapse, as can be considered the case of the unreinforced masonry building. For the design process, both numerical solutions cannot go beyond this value, partly due to the simplifications that aims for practical applications (implementation of macro modeling). In any case, the experimental results validate the code regulation, since the UM model was able to go beyond lateral drifts over 0.5%, without collapse.

6.6 Conclusions

In this Chapter, two design procedures suggested by Eurocode 8 (2004), namely linear elastic and nonlinear static (pushover) analyses were discussed for unreinforced masonry, taking symmetric unreinforced masonry building as the reference. In relation to the linear elastic analysis, the behavior factor q is analyzed and compared to the range suggested in the Eurocode 8 (2004) for unreinforced masonry. Furthermore, a nonlinear static analysis was carried out, and the results compared with the results obtained in the experimental and nonlinear dynamic analysis.

From the analysis of results, it is possible drawn the following conclusions:

1. For the present work, the behavior factor q obtained from the experimental results is 2.56 in terms of force and of 2.86 based on ductility factor. These results are reasonably in line with the values indicated in Eurocode 8 (2004) that suggests a behavior factor, q , for the unreinforced masonry in the range of 1.5 to 2.5, ignoring an overstrength factor considered e.g. in the Italian code.
2. The pushover analysis is a nonlinear static procedure in which displacements, forces, stresses and strains can be obtained. However, it should be emphasized that the pushover analysis is an approximation based on static loads. This means that it represents dynamic phenomena in an approximate way. In this work, some limitations were found in the representation of the damage patterns. In terms of the capacity curve, it was seen that the pushover analysis provides an envelope of the experimental and nonlinear dynamic results, with a reasonable approximate response in terms of both stiffness and maximum resistance. This should be attributed to cumulative damage imposed in the experimental campaign and also represented in the nonlinear dynamic analysis, and not possible to be represented in the pushover analysis. Differences of about 50% were obtained for the real displacements (underestimated).

Chapter 7

Conclusions, final remarks and future works

7.1 Conclusions

The main objective in the research program presented in this thesis was the characterization of the seismic behavior of a new constructive masonry system to be used in residential buildings in Portugal, a country with medium to high seismicity hazard. To accomplish the project main objective, an experimental campaign was designed based on shaking table tests on different types of masonry buildings. Complimentarily, an extended numerical simulation based on a nonlinear dynamic finite element model was performed. Furthermore, seismic design considerations about current codes were discussed.

Four two-story masonry buildings were designed, constructed, tested and analyzed. As a new constructive system, the main idea was to evaluate both the influence of the geometrical configuration and the implementation of steel reinforcement. For it, current design and construction codes were followed for the selection on the geometrical distribution and quantity of reinforcement. For the final design, it was considered an optimum percentage of openings and typical distribution of indoor and outdoor spaces. Furthermore, even the models represent individual residences all of them offer a minimum of one side from which another similar individual building can be added. The buildings have reinforced concrete solid slabs, which work as rigid diaphragms and a reinforced concrete ring beam foundation. The foundation was the base for the construction of the models, which had to be constructed outside the shaking table. In addition, the transportation to the shaking table was made with industrial overhead cranes, which take the models from the ring beam foundation and finally it was the foundation the link structure between the buildings and the shaking table.

On the shaking table, the buildings were submitted to incremental seismic input motions. Between each input, dynamic identifications by input-output methods were carried out. In both cases, the inputs were given simultaneously in the two orthogonal directions. The seismic input motions applied to the models were obtained artificially from the elastic response spectrum proposed by the Eurocode 8 (2004). For the dynamic identifications, low-level uniform white noise signals were given to the table. The experimental seismic behavior of the masonry buildings was studied both quantitatively and qualitatively. Thus, accelerations and analysis of deformations in terms of displacements made part of the quantitative analysis, on the other hand damage and failure modes were part of the qualitative study. Therefore, for each building the amplification of the accelerations, amplification of the displacements, in-plane displacements for each wall, interstory drift for each floor level, out-of-plane displacements, biaxial displacements, local displacements, stiffness degradation and force vs displacement curves were obtained and discussed. Additionally, the progress of the damage through the input tests and the final failure modes, were followed, described, presented and related with the quantitative values obtained from both the dynamic identifications and the seismic performance.

A finite element model of the symmetric unreinforced masonry building was constructed and calibrated based on the experimental results. A simulation of the incremental seismic tests, performed during the experimental campaign, was also performed in the numerical model through nonlinear dynamic time history analyses in a phased procedure. Here, each phase represented each

incremental input test. From each nonlinear dynamic analysis, results in terms of accelerations, displacements, force vs displacement curves and damage were obtained and compared with the experimental ones.

Finally, seismic design considerations for the symmetric unreinforced masonry building were discussed. The current provisions for the design of masonry structures and for the seismic design of structures, given by the Eurocode 6 (2005) and Eurocode 8 (2004) were followed, respectively. Two of the methodologies proposed by the codes were implemented, namely a linear dynamic analysis, in which the behavior factor “q” is evaluated, and a nonlinear static “pushover” analysis, in which a lateral force proportional to the mass of the structure is applied. Values of behavior factors in terms of force and ductility, from the linear analysis were provided. Furthermore, interstory drifts, capacity curves and damage patterns, from the nonlinear “pushover” analysis were presented and compared with the experimental and nonlinear dynamic analyses previously obtained.

From all the previous experimental, numerical and design consideration analyses, the main conclusions and final remarks are presented as follows, taking into account that specific conclusions were already discussed for each particular chapter.

7.1.1 Experimental research

For the construction of the symmetric buildings, the mortar was prepared on site; i.e. specific dosages of its components were followed. The dosage was previously obtained through an extensive characterization of different dosages that intended to find an appropriate consistency and a minimum compressive strength of 10Mpa, necessary for the structures in study. For the asymmetric buildings, the mortar implemented was a premixed product (quality guaranteed) to which only water was added to attain similar consistency properties and the same compression capacity. The use of the premixed product is much faster, clean and straightforward option for the construction process, in comparison with the handmade mortar. However, small variations in water quantities affected considerably both the consistence and the compression strength. Then, it is highly recommended that the mason be aware and take important care in this regard.

Due to its material composition, the unit blocks possess water absorption capabilities. Then, continuing with water as parameter, it is very important that during construction the sides of the unit blocks that will be in contact with the mortar be wet enough before any contact with it. In this way, the units will not absorb the water from the mortar, which as aforementioned can significantly influence in its consistence and final resistance.

One of the first steps in the analysis of the data obtained from the experimental campaign is the processing of the signals. From it, perhaps the most important is the identification of the filter’s limits; i.e. upper and lower. In general, the upper limit affects the accelerations and the lower affects the displacements. Special care must be taken in the identification of such limits. The removal of the noise is in general a demanding but straightforward task, in particular for the shaking table tests, in which the external noise is quite controlled. The identification of the quasi-static components requires more attention as mainly the displacements are the most affected from this process.

However, it must be done, as those quasi-static components are not related with the dynamic behavior of the structure. Therefore, it is highly recommended to use an additional displacement measure device at the base of the models, other than the accelerometers and if possible with an external fixed reference. In this way, not only the actual displacements are validated but also the lower limit of the filter is verified.

The dynamic properties of the structures were not severely affected by the geometrical configuration and the steel reinforcement. Then, it was found that following the code recommendations, regarding geometry plan distribution and percentage of openings, the four buildings presented similar dynamic properties. For instance, the first natural frequency and mode shape were obtained in all buildings for the transverse direction and the second one for the longitudinal direction. Only in the asymmetric buildings, a third torsional mode was obtained. This behavior validates the code restrictions regarding structural regularity for the design of earthquake resistance buildings.

On the unreinforced masonry buildings, the structures (symmetric and asymmetric) were severely affected by the combination of the in-plane and out-of-plane resisting mechanism. In both structures, it was considerable the damage developed at the two floor levels, mainly following "X" shape cracks in piers and long horizontal cracks. Furthermore, local collapse due to the out-of-plane deformation and development of a shear sliding mechanism at the second floor were observed. The experimental damages presented in the walls have been commonly observed in real masonry buildings after earthquake evaluations, which suggest a good representation of masonry behavior. The lack of connection between structural elements both vertically and horizontally played an important role in the degradation capacity of the buildings. Additionally, it can be said that in these buildings in particular, it was considerably important the contribution given by the reinforced concrete diaphragms, to their stability and no collapse.

The reinforced masonry buildings (symmetric and asymmetric), presented concentration of damage at the first floor level. In the symmetric building, it was roughly distributed in the piers, but in the asymmetric one, it was presented loss of unit blocks mainly at the walls with openings, and large out-of-plane behavior. These structures attained higher seismic input and presented higher structural capacity in terms of force, if compared with the unreinforced buildings. The damage however, was appreciably less compromising than the one obtained in the UM models. It was clear from these models, that the addition of vertical and horizontal steel reinforcement improved the resistance capacity and therefore the seismic behavior of the masonry buildings. From the diagonal tests in masonry samples and the experimental buildings, it seems that the horizontal reinforcement avoid vertical and/or stair-step diagonal cracks, whereas the vertical reinforcement provides structural connection between walls and slabs and additional deformation capacity against the lateral loads. Their combination clearly improves the control and distribution of the damage.

During earthquake events, the risk is not only for the occupant of the buildings, but also for the pedestrian near them. In high seismic zones structural failure on these types of structures resulted mainly from wall separation, due to the lack of lateral resistance and use of non-ductile materials. Then, the connections between structural elements on masonry buildings assume high importance for an appropriate global structural performance. The implementation of reinforcement in the two

buildings configurations studied in this work improves the resistance capacity, the energy dissipation and in case of the asymmetric building, the deformation capacity in which the final failure mechanism was more controlled. This improved behavior was partly due to the structural connection generated by both horizontal and vertical reinforcements between all the structural elements that helped to control and to distribute the damage and the energy dissipation.

In general, it was observed that the unreinforced masonry buildings were more affected in the transverse direction (walls without openings) and the reinforced buildings in the longitudinal direction (walls with openings). Then, it is possible to conclude that the unreinforced structures were primarily affected on their first mode (transverse), whereas the inclusion of steel reinforcement move the weak direction of the buildings (improving its seismic performance) to their second mode in the longitudinal direction. In any case, the openings revealed to contribute for the vulnerability of masonry walls, by increasing the crack density and crack opening.

The seismic vulnerability of the unreinforced masonry buildings was governed by global failure mechanisms, typically consisting in sliding shear failure, the structural walls behaved as brittle elements with limited energy dissipation capacity. In the reinforced buildings, the failure mode is more controlled by the combination of the vertical and horizontal steel truss reinforcement, which prevented the separation of the walls, hence improving the resistance and energy dissipation capacity of the structure when subjected to seismic loads. It was observed that a single diagonal or horizontal crack causes severe deterioration in strength and subsequent sliding failure.

Finally, it can be said that residential masonry buildings should behave reasonably well for medium to high seismicity hazard if: (1) an adequate quality of materials is provided; (2) the out-of-plane premature collapse is prevented by adequate connections between the structural elements; (3) local damage and early local failures are avoided; (4) stiff slab diaphragms, which play a significant role in coupling the response of the different walls, are provided. Thus, according with the seismic prone area of construction, unreinforced or reinforced structural masonry can be selected for the construction of residential masonry buildings.

7.1.2 Numerical simulation

The construction process of the numerical model to represent the dynamic performance of a real structure plays an important role in the analysis and in the final results. It is then necessary to:

- Define a detailed and careful geometrical model that represents the structural distribution and connections presented on the actual building.
- Select the appropriate type of finite elements, in order to represent the distinct structural components.
- Accurately describe the material properties. Here, an experimental campaign to characterize those properties is highly suggested.
- Define the distribution of the loads similar to the ones acting in the experimental building.
- Allocate appropriately of the boundary conditions.

All the previous procedures had influence on the numerical simulation of the masonry building. An appropriate distribution of input loads was crucial for the accurate simulation of structural capacity and damage. For the present work, the application of a phase analysis demonstrates to be appropriate and accurate for the simulation of incremental dynamic tests carried out on shaking table. The numerical accumulation of damage is the main advantage of this procedure, as it can represent approximately the actual progress of damage occurred during the experimental campaign.

The definition of the boundary conditions in any structural simulation is a key parameter. On the masonry building studied, it was essential to achieve the accurate results. The non-planarity of the base foundation come up with an additional difficulty in the representation of the model being necessary to make use of interface elements to represent the connection between the model and the shaking table. This situation come out with an important consideration that is in general the numerical simulation of walls and buildings subjected to dynamic loads do not take into account the mass of the foundation, as it is assumed this part is perfectly fixed to the external devices or apparatus and then no movements are expected from them. However, in cases like the one presented during the experimental campaign of this work, the vertical movements of the foundation were not perceptible to the human eye during the shaking process. Those movements of the foundation, introduced to the experimental model additional mass that directly affected its dynamic properties.

The calibration process acts as the first validation of the numerical model with respect to the linear behavior of the experimental building. Positive and precise conclusions were obtained after this process, which even demanding in time increases the confidence and the accuracy of the future nonlinear simulations.

The use of a macro modeling strategy for the simulation of a nonlinear dynamic time history analysis of a 3D model is satisfactory. It reduces the time of numerical model construction and the analysis itself, and produces accurate results when compared to the experimental results. In addition, the rotating crack model (RCM) in which the crack direction continuously rotate with the principal directions of the strain vector, results to be adequate for the simulation of the damage observed.

The comparison of the results between the experimental shaking table tests on the unreinforced masonry building and the numerical nonlinear dynamic analysis shows that the response of the numerical model is good. The accelerations and displacements present an accurate fitting until the test input of 200%, in which the longitudinal direction (walls with openings) presented a better approximation. For the last two inputs of 250%, the damage and mainly the shear sliding failure mechanism developed in the experimental building, resulted in higher differences. This is mainly attributed to the fact that the macro modeling strategy implemented is unable to represent such mechanism. However, in terms of capacity the model is acceptable.

The damage obtained with the numerical simulation, through the maximum principal total tensile strains, was acceptable until the input test of 200%. The damage simulated by the numerical model at this point was even able to represent uncommon horizontal cracks between openings at the second level of the west façade, validating the extent of accuracy provide. Further damage was no

descriptive of what happened in the experimental model, since as aforementioned the numerical modelling strategy implemented is not able to represent such mechanism.

7.1.3 Seismic design considerations

The structural seismic resistance design must balance the realism of the building with the time consuming and cost of the analysis to be performed. Nowadays, current codes suggest several methodologies, with different degrees of complexity and accuracy. In particular, for residential masonry buildings the Eurocodes proposed linear and nonlinear methodologies. On the present work, one linear and one nonlinear approach were discussed for the unreinforced symmetric masonry building.

For modern seismic resistance design, it is necessary the evaluation of the ductile capacity of structure through its nonlinear range. In the linear elastic analysis, the contribution of the energy dissipation and the nonlinear deformation is taken into account in a simple way through the behavior factor “q”. In this work, the two procedures to obtain this factor were tackled, namely in terms of force and displacement based on the experimental results. In terms of force, it was found similar values in both directions (longitudinal and transverse), which are close the maximum value proposed by the code ($q=2.5$). In terms of displacement, the q factor values are higher than 3.0 when obtained from the ultimate displacement (degradation of 20% of the maximum displacement) and 2.0 when obtained from the limit damage state. In the last one, the most affected direction was the transverse one, in which as discussed the damage was more considerable. The reduction factor was then controlled by the displacement capacity instead of the force capacity of the building. The results validated the limits suggested by the code for the linear dynamic design of this typology of construction.

In the nonlinear static “pushover” analysis the structure is already lead to the nonlinear range by applied static loads. The results in both directions were satisfactory but the comparison of force and displacement capacity with the experimental and nonlinear dynamic results presented in average higher force capacity and lower displacement capacity. The higher force capacity should be related to the impossibility of this model of to take into account the damage accumulation as it is made in the experimental and nonlinear dynamic analysis.

On the other hand, the damage from the pushover analysis was acceptable, but in some areas, mainly at the second floor, it was found important divergences in relation to the actual damage. Diagonal tension and compression inside piers were represented at the first floor, but the large horizontal cracks that affected the second level were not described in this model. The drift results from the pushover analysis validated the displacement capacity previously discussed for this model. In a direct comparison with the experimental and nonlinear dynamic analyses, it presents the lowest values for both floor levels, being the first floor the one with higher interstory drift. The nonlinear numerical simulations (dynamic and static), presented higher values of interstory drifts at the first floor, which is in opposition to the experimental results. This, as already discussed, was motivated for the shear sliding mechanism occurred at the second floor, which considerably increase the

displacement at the second level of the experimental building, and that could not be modeled by the numerical models.

7.2 Future works

As a research based investigation, the assessing of the seismic behavior of concrete block masonry buildings is not a completed task. Further research for this typology of structures should proceed. Next, some aspects that deserve future attention are presented:

- During the experimental campaign, the construction process was registered day by day in a “construction book”. Key facts like planning actions, material quantities, workers time, incidentals and mistakes during the construction process are mentioned, together with the actions taken to overcome them. A detailed construction manual for the efficient construction of concrete block masonry buildings is then highly recommended.
- Definition of the design parameters as the limit states and fragility curves with subsequent seismic risk and classification of seismic zones for the symmetric and asymmetric concrete block masonry buildings.
- Study of the influence of different reinforcement schemes in the seismic performance of masonry buildings; e.g. which will be the results if only horizontal reinforcement is added to the joints?
- Actual seismic waves arrive at various instants of time, have different amplitudes and carry different levels of energy. Thus, the most critical direction of incidence of the seismic input, which would produce the largest response, may be different from the direction of the building’s main orthogonal axes. Then, a parametric analysis in which the seismic input play as variable is recommended. Here, it should be study:
 - Artificial signals from both type A and B elastic response spectrums recommended by the Eurocodes,
 - Seismic signals from actual earthquake events,
 - Direction of application,
 - Application of the vertical component,
 - Independent inputs without previous damage.
- A numerical parametrical study, aimed to evaluate the influence of aspects like
 - The steel ratio,
 - The filling of vertical joints,
 - Number of stories,
 - Internal nonstructural walls,
 - Distribution of openings, then study different dimensions for piers and spandrels,
 - Directional slabs, more than bidirectional solid slabs.
- For the nonlinear dynamic simulation of the unreinforced building, a physical nonlinear analysis was implemented, i.e. it was assumed that the model behaved geometrically

linear. In this case, the equilibrium equations were based on the undeformed geometry and the strains are linear function of the nodal displacements. This limited the applicability of the analysis to small displacements, small rotations and small strains, which was in agreement with the behavior of the experimental building until approximately the seismic input of 100%. In particular for this model, the sliding mechanism developed, significantly increases the displacements in all the structural elements. Then, for further nonlinear analyses of unreinforced masonry, a combination of physical and geometrical nonlinearity analysis will be desired.

- A numerical model in which the horizontal bed joints be modeled by means of interface elements would be interesting. By doing this, the computing time and cost will increase but the accuracy simulation of the shear sliding of unreinforced masonry could be controlled and represented by the shear behavior of those interface elements. This suggests a simulation with a “simplified micro modeling” in which neither the head joints nor the individual blocks need to be detailed.
- The implementation of new versions of the nonlinear static analysis by using adaptive pushover methods, which account for the effects of higher modes of vibration and progressive stiffness degradation.

REFERENCES

- Abrams D. P. (1986). Lateral resistance of a two-story block building. *Advances in Analysis of Structural Masonry*, pp 41-57.
- Abrams D. P. (2000). Seismic Response Evaluation for URM Buildings. *Journal of The Masonry Society* Vol. 18, No. 1.
- Abrams D. P. and Costley A. C. (1994). Dynamic response measurements for URM building systems. Technical Report: US National Center for Earthquake Engineering Research, pp 27-39.
- ASCE/5-02(2002). Building Code Requirements for Masonry Structures and Specifications for Masonry Structures. American society of civil engineers. U.S.A.
- Azevedo J. and Sincaian G. (2000). Modelling the seismic behaviour of monumental masonry structures. *Proceedings of Archii 2000*, pp 3 - 8.
- Bairrão R. and Falcão Silva M. (2009). Shaking table tests of two different reinforcement techniques using polymeric grids on an asymmetric limestone full-scaled structure. *Engineering Structures*, Vol. 31, No. 6, pp 1321-1330.
- Bairrao R. and Vaz C. (2000). Shaking table testing of civil engineering structures—the LNEC 3D simulator experience. *Proceedings 12th World Conference on Earthquake Engineering*. Auckland, New Zealand, Vol. 2129
- Bendat J. S. and Piersol A. G. (2011). *Random data: analysis and measurement procedures*. Vol. 729. John Wiley & Sons.
- Benedetti D., Carydis P. and Limongelli M. (2001). Evaluation of the seismic response of masonry buildings based on energy functions. *Earthquake Engineering & Structural Dynamics*, Vol. 30, No. 7, pp 1061-1081.
- Benedetti D., Carydis P. and Pezzoli P. (1998). Shaking table tests on 24 simple masonry buildings. *Earthquake Engineering & Structural Dynamics*, Vol. 27, No. 1, pp 67-90.
- Bertero V. V. (1996). State of the art report on: design criteria. *Proc. of eleventh world conference on earthquake engineering*, p 16. Acapulco, Mexico.
- Berto L., Saetta A., Scotta R. and Vitaliani R. (2004). Shear behaviour of masonry panel: parametric FE analyses. *International journal of solids and structures*, Vol. 41, No. 16, pp 4383-4405.
- Bommer J. J., Magenes G., Hancock J. and Penazzo P. (2004). The influence of strong-motion duration on the seismic response of masonry structures. *Bulletin of Earthquake Engineering*, Vol. 2, No. 1, pp 1-26.

- Bothara J. K., Dhakal R. P. and Mander J. B. (2010). Seismic performance of an unreinforced masonry building: an experimental investigation. *Earthquake Engineering & Structural Dynamics*, Vol. 39, No. 1, pp 45-68.
- Bruneau M. (1994). State-of-the-art report on seismic performance of unreinforced masonry buildings. *Journal of Structural Engineering*, Vol. 120, No. 1, pp 230-251.
- Calderini C. and Lagomarsino S. (2006). A micromechanical inelastic model for historical masonry. *Journal of Earthquake Engineering*, Vol. 10, No. 4, pp 453-479.
- Calvi G. M., Kingsley G. R. and Magenes G. (1996). Testing of masonry structures for seismic assessment. *Earthquake Spectra*, Vol. 12, No. 1, pp 145-162.
- Candeias P., Costa A. C. and Coelho E. (2004). Shaking table tests of 1:3 reduced scale models of four story unreinforced masonry buildings. *Proceedings of the 13th world conference on earthquake engineering*. Vancouver, Canada.
- Carpinteri A., Invernizzi S. and Lacidogna G. (2005). In situ damage assessment and nonlinear modelling of a historical masonry tower. *Engineering Structures*, Vol. 27, No. 3, pp 387-395.
- Carvalho E. (1999). Seismic testing of structures. *Earthquake Engineering-Invited Papers: Proceedings of the eleventh European conference*, Vol. 2, p 53. Paris, France.
- Chaimoon K. and Attard M. M. (2009). Experimental and numerical investigation of masonry under three-point bending (in-plane). *Engineering Structures*, Vol. 31, No. 1, pp 103-112.
- Chopra A. K. (1995). *Dynamics of structures*. Vol. 3. Prentice Hall. New Jersey
- Chopra A. K. and Goel R. K. (2004). A modal pushover analysis procedure to estimate seismic demands for unsymmetric-plan buildings. *Earthquake Engineering & Structural Dynamics*, Vol. 33, No. 8, pp 903-927.
- Coelho E., Campos-Costa A. and Carvalho E. (2000). Assessment of experimental seismic response through damage evaluation. *Proc. 12WCEE*
- Costa A. C., Sousa M., Carvalho A. and Coelho E. (2006). Seismic loss scenarios based on hazard disaggregation. Application to the metropolitan region of Lisbon, Portugal. *Assessing and managing earthquake risk: Springer*, pp 449-462.
- Council B. S. S. (1997) Edition NEHRP Recommended Provisions for the Development of Seismic Regulations for New Buildings, FEMA 302/303.
- da Porto F., Grendene M. and Modena C. (2009). Estimation of load reduction factors for clay masonry walls. *Earthquake Engineering & Structural Dynamics*, Vol. 38, No. 10, pp 1155-1174.
- da Porto F., Guidi G., Garbin E. and Modena C. (2010). In-plane behavior of clay masonry walls: experimental testing and finite-element modeling. *Journal of Structural Engineering*, Vol. 136, No. 11, pp 1379-1392.

-
- Da Porto F., Mosele F. and Modena C. (2011). In-plane cyclic behaviour of a new reinforced masonry system: Experimental results. *Engineering Structures*, Vol. 33, No. 9, pp 2584-2596.
- De Borst R. and Nauta P. (1985). Non-orthogonal cracks in a smeared finite element model. *Engineering Computations*, Vol. 2, No. 1, pp 35-46.
- DIANA (2010). Finite element analysis Ver. 9.4.3. Diana, T.N.O., Delft, The Netherlands.
- DiPasquale E. and Cakmak A. (1987) Detection and assessment of seismic structural damage, Technical report NCEER-87-0015: State University of New York at Buffalo.
- E A. 519-02. (2002). Standard Test Method for Diagonal Tension (Shear) in Masonry Assemblages. ASTM International. United States.
- Elgawady M., Lestuzzi P. and Badoux M. (2004). Dynamic versus static cyclic tests of masonry walls before and after retrofitting with GFRP. the 13th World Conference on Earthquake Engineering, Vancouver, BC, Canada
- EN 1052-1. (1999). Methods of test for masonry - Part1: Determination of compressive strength. European committee for standardization. Brussels.
- EN 1015-3. (2004). Methods of test for mortar for masonry - Part 3: Determination of consistence of fresh mortar (by flow table). European committee for standardization. Brussels.
- Eurocode 2. (2004). EN 1992-1-1 Design of concrete structures - Part 1-1: General rules and rules for buildings. European committee for standardization. Brussels.
- Eurocode 8. (2004). EN 1998-1 Design of structures for earthquake resistance - Part 1: General rules, seismic actions and rules for buildings. European committee for standardization. Brussels.
- Eurocode 6. (2005). EN 1996-1-1 Design of masonry structures - Part 1-1: General rules for reinforced and unreinforced masonry structures. European committee for standardization. Brussels.
- Eurocode 6. (2006). EN 1996-2 Design of masonry structures - Part 2: Design considerations, selection of materials and execution of masonry. European committee for standardization. Brussels.
- Fajfar P. (2000). A nonlinear analysis method for performance-based seismic design. *Earthquake Spectra*, Vol. 16, No. 3, pp 573-592.
- Feenstra P. H. and De Borst R. (1995). A plasticity model and algorithm for mode-I cracking in concrete. *International Journal for Numerical Methods in Engineering*, Vol. 38, No. 15, pp 2509-2529.
- Felice G. d. (2009). Assessment of the load-carrying capacity of multi-span masonry arch bridges using fibre beam elements. *Engineering Structures*, Vol. 31, No. 8, pp 1634-1647.

- Foster S., Budiono B. and Gilbert R. (1996). Rotating crack finite element model for reinforced concrete structures. *Computers & structures*, Vol. 58, No. 1, pp 43-50.
- Galasco A., Lagomarsino S. and Penna A. (2006). On the use of pushover analysis for existing masonry buildings. *Proceedings of the 13th European conference on earthquake engineering*. Geneva (CH), pp 3-8.
- Gardone D., Dolce M., Ponzo F. C. and Coelho E. (2004). Experimental behaviour of R/C frames retrofitted with dissipating and re-centring braces. *Journal of Earthquake Engineering*, Vol. 8, No. 3, pp 361-396.
- Haach V. G. (2009). Development of a design method for reinforced masonry subjected to in-plane loading based on experimental and numerical analysis. PhD dissertation. University of Minho. Guimarães.
- Haach V. G., Vasconcelos G. and Lourenço P. B. (2010). Experimental analysis of reinforced concrete block masonry walls subjected to in-plane cyclic loading. *Journal of Structural Engineering*, Vol. 136, No. 4, pp 452-462.
- Haach V. G., Vasconcelos G. and Lourenço P. B. (2011). Parametrical study of masonry walls subjected to in-plane loading through numerical modeling. *Engineering Structures*, Vol. 33, No. 4, pp 1377-1389.
- Hamamatsu. (2014). www.hamamatsu.com - Product catalog. Optical sensors - PSD, Retrieved 10/Jun 2014.
- Henderson R., Fricke K., Jones W., Beavers J. and Bennett R. (2003). Summary of a large-and small-scale unreinforced masonry infill test program. *Journal of Structural Engineering*, Vol. 129, No. 12, pp 1667-1675.
- Juhásová E., Sofronie R. and Bairrão R. (2008). Stone masonry in historical buildings—Ways to increase their resistance and durability. *Engineering Structures*, Vol. 30, No. 8, pp 2194-2205.
- Juhásová E. I., Hurák M. and Zembaty Z. (2002). Assessment of seismic resistance of masonry structures including boundary conditions. *Soil Dynamics and Earthquake Engineering*, Vol. 22, No. 9, pp 1193-1197.
- Krawinkler H. and Seneviratna G. (1998). Pros and cons of a pushover analysis of seismic performance evaluation. *Engineering Structures*, Vol. 20, No. 4, pp 452-464.
- Krstevska L., Tashkov L., Gramatikov K., Landolfo R., Mammana O., Portioli F. and Mazzolani F. (2010). Large-scale experimental investigation on mustafa pasha mosque. *Journal of Earthquake Engineering*, Vol. 14, No. 6, pp 842-873.
- Lagomarsino S., Penna A. and Galasco A. (2006). TREMURI program: seismic analysis program for 3D masonry buildings. University of Genoa.
- Lang K. (2000). Seismic vulnerability of existing buildings. PhD dissertation. Swiss Federal Institute of Technology. Zurich, Switzerland.

-
- Lee H. S. and Woo S. W. (2002). Effect of masonry infills on seismic performance of a 3-storey R/C frame with non-seismic detailing. *Earthquake Engineering & Structural Dynamics*, Vol. 31, No. 2, pp 353-378.
- Lemos J. V. (2007). Discrete element modeling of masonry structures. *International Journal of Architectural Heritage*, Vol. 1, No. 2, pp 190-213.
- Li Y.-J. and Zimmerman T. (1998). Numerical evaluation of the rotating crack model. *Computers & structures*, Vol. 69, No. 4, pp 487-497.
- LNEC - SPA (2007). Signal processing and analysis tools for civil engineers. *Earthquake Engineering and Structural Dynamic Division (NESDE)*, Lisbon - Portugal.
- Lotfi H. and Shing P. (1991). An appraisal of smeared crack models for masonry shear wall analysis. *Computers & structures*, Vol. 41, No. 3, pp 413-425.
- Lourenço P., Vasconcelos G., Medeiros P. and Gouveia J. (2010). Vertically perforated clay brick masonry for loadbearing and non-loadbearing masonry walls. *Construction and Building Materials*, Vol. 24, No. 11, pp 2317-2330.
- Lourenço P. B. (2004a). Current experimental and numerical issues in masonry research. 6^o Congresso de Sismologia e Engenharia Sísmica, pp 119-136. Guimarães - Portugal.
- Lourenço P. B. (2004b). Design of large size non-loadbearing masonry walls: case studies in Portugal: technical and economical benefits. 13th International Brick and Block Masonry Conference. Amsterdam.
- Lourenço P. B. (2008). Structural masonry analysis: Recent developments and prospects. 14th International Brick and Block Masonry Conference (IBMAC). Sydney, Australia.
- Lourenço P. B. and Roque J. (2006). Simplified indexes for the seismic vulnerability of ancient masonry buildings. *Construction and Building Materials*, Vol. 20, No. 4, pp 200-208.
- Lourenço P. B., Rots J. G. and Blaauwendraad J. (1998). Continuum model for masonry: parameter estimation and validation. *Journal of Structural Engineering*, Vol. 124, No. 6, pp 642-652.
- Lu X.-Z., Ye L.-P., Ma Y.-H. and Tang D.-Y. (2012). Lessons from the collapse of typical RC frames in Xuankou School during the great Wenchuan Earthquake. *Advances in Structural Engineering*, Vol. 15, No. 1, pp 139-154.
- Magenes G. (2006). Masonry building design in seismic areas: Recent experiences and prospects from a European standpoint. First European conference on earthquake engineering and seismology. Geneva, Switzerland.
- Magenes G., Remino M., Manzini C., Morandi P. and Bolognini D. (2006). SAM II, software for the simplified seismic analysis of masonry buildings. University of Pavia and EUCENTRE.
- Marques R. F. P., Gouveia J. P., Lourenço P. B. and Leão C. (2009). Development of design software for plain masonry buildings. Twelfth international conference on civil, structural and environmental engineering computing. Scotland.

- Marques R. F. P. and Lourenço P. B. (2008) Benchmarking of commercial software for the seismic assessment of masonry buildings, International seminar on seismic risk and rehabilitation of stone masonry housing. Azores Islands.
- MATLAB (2006). MATLAB: The language of the technical computing. Ver. 7.2. The MathWorks, USA.
- Mazzon N., Valluzzi M., Aoki T., Garbin E., De Canio G., Ranieri N. and Modena C. (2009). Shaking table tests on two multi-leaf stone masonry buildings. Proceedings of the 11th Canadian Masonry symposium, Toronto
- Mendes N. and Lourenço P. B. (2009). Seismic Assessment of Masonry “Gaioleiro” Buildings in Lisbon, Portugal. *Journal of Earthquake Engineering*, Vol. 14, No. 1, pp 80-101.
- Mendes N., Lourenço P. B. and Campos-Costa A. (2014). Shaking table testing of an existing masonry building: assessment and improvement of the seismic performance. *Earthquake Engineering & Structural Dynamics*, Vol. 43, No. 2, pp 247-266.
- Mendes N. A. L. (2012). Seismic Assessment of Ancient Masonry Buildings: Shaking Table Tests and Numerical Analysis. PhD dissertation. Universidade do Minho. Guimarães, Portugal.
- Moon F. L., Yi T., Leon R. T. and Kahn L. F. (2007). Testing of a full-scale unreinforced masonry building following seismic strengthening. *Journal of Structural Engineering*, Vol. 133, No. 9, pp 1215-1226.
- Nakagawa T., Narafu T., Imai H., Hanazato T., Ali Q. and Minowa C. (2012). Collapse behavior of a brick masonry house using a shaking table and numerical simulation based on the extended distinct element method. *Bulletin of Earthquake Engineering*, Vol. 10, No. 1, pp 269-283.
- Paquette J. and Bruneau M. (2006). Pseudo-dynamic testing of unreinforced masonry building with flexible diaphragm and comparison with existing procedures. *Construction and Building Materials*, Vol. 20, No. 4, pp 220-228.
- PCB. (2014). www.pcb.com - Product catalog. Accelerometers - High sensitivity, Retrieved 10/Jun 2014.
- Pei S. and van de Lindt J. (2011). Seismic numerical modeling of a six-story light-frame wood building: Comparison with experiments. *Journal of Earthquake Engineering*, Vol. 15, No. 6, pp 924-941.
- Penna A., Lagomarsino S. and Galasco A. (2014). A nonlinear macroelement model for the seismic analysis of masonry buildings. *Earthquake Engineering & Structural Dynamics*, Vol. 43, No. 2, pp 159-179.
- Pinto P. E. (1994). Earthquake resistant design: Research developments in basic and in normative research. Proc. of the tenth world conference on earthquake engineering Vol. 11, pp 6597-6611. Madrid, Spain.
- Ramos L. F. (2007). Damage identification on masonry structures based on vibration signatures. PhD dissertation. Universidade do Minho. Guimarães, Portugal.

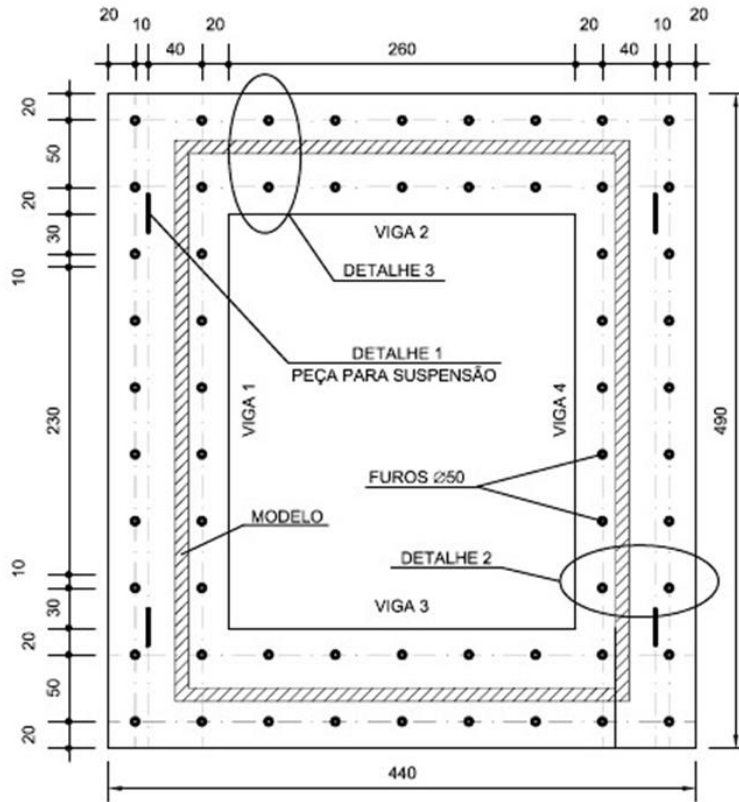
-
- RDP. (2014). www.rdpe.com - Product catalog. Displacement - General industrial, Retrieved 10/Jun 2014.
- Rezaifar O., Kabir M., Taribakhsh M. and Tehranian A. (2008). Dynamic behaviour of 3D-panel single-storey system using shaking table testing. *Engineering Structures*, Vol. 30, No. 2, pp 318-337.
- Rota M., Penna A. and Magenes G. (2008). A procedure for deriving analytical fragility curves for masonry buildings. 14th world conference on earthquake engineering. Beijing, China.
- Rots J. G. (1988). Computational modeling of concrete fracture. PhD dissertation. Technische Hogeschool Delft. The Netherlands.
- Santis S. D. and Felice G. d. (2014). A fibre beam-based approach for the evaluation of the seismic capacity of masonry arches. *Earthquake Engineering & Structural Dynamics*.
- SAP2000 (2009). Integrated Finite Element Analysis and Design of Structures. Ver. 14. Computers & structures, inc (CSI), Berkeley.
- Sasani M., Werner A. and Kazemi A. (2011). Bar fracture modeling in progressive collapse analysis of reinforced concrete structures. *Engineering Structures*, Vol. 33, No. 2, pp 401-409.
- Sucuoglu H. and Erberik A. (1997). Performance evaluation of a three-storey unreinforced masonry building during the 1992 erzincan earthquake. *Earthquake Engineering & Structural Dynamics*, Vol. 26, No. 3, pp 319-336.
- Teughels A. (2004). Inverse modelling of civil engineering structures based on operational modal data. PhD dissertation. Catholic university of Leuven. Belgium.
- Tomažević M. (1999). Earthquake-resistant design of masonry buildings. Vol. 1. World Scientific Publishing Company. London
- Tomažević M. (2000). Some aspects of experimental testing of seismic behavior of masonry walls and models of masonry buildings. *ISET journal of earthquake technology*, Vol. 37, No. 4, pp 101-117.
- Tomažević M. (2007). Damage as a measure for earthquake-resistant design of masonry structures: Slovenian experience. *Canadian journal of civil engineering*, Vol. 34, No. 11, pp 1403-1412.
- Tomažević M. and Gams M. (2012). Shaking table study and modelling of seismic behaviour of confined AAC masonry buildings. *Bulletin of Earthquake Engineering*, Vol. 10, No. 3, pp 863-893.
- Tomazevic M. and Klemenc I. (1997). Verification of seismic resistance of confined masonry buildings. *Earthquake Engineering & Structural Dynamics*, Vol. 26, No. 10, pp 1073-1088.
- Tomažević M., Klemenc I. and Weiss P. (2009). Seismic upgrading of old masonry buildings by seismic isolation and CFRP laminates: a shaking-table study of reduced scale models. *Bulletin of Earthquake Engineering*, Vol. 7, No. 1, pp 293-321.

- Tomazevic M., Lutman M. and Petkovic L. (1996a). Seismic behavior of masonry walls: experimental simulation. *Journal of Structural Engineering*, Vol. 122, No. 9, pp 1040-1047.
- Tomazevic M., Lutman M. and Weiss P. (1996b). Seismic upgrading of old brick-masonry urban houses: tying of walls with steel ties. *Earthquake Spectra*, Vol. 12, No. 3, pp 599-622.
- Tomažević M., Lutman M. and Weiss P. (1993). The seismic resistance of historical urban buildings and the interventions in their floor systems: an experimental study. *Journal of The Masonry Society* Vol. 12, No. 1.
- Tomažević M. and Weiss P. (2010). Displacement capacity of masonry buildings as a basis for the assessment of behavior factor: an experimental study. *Bulletin of Earthquake Engineering*, Vol. 8, No. 6, pp 1267-1294.
- Toranzo L. A., Restrepo J. I., Mander J. B. and Carr A. J. (2009). Shake-Table Tests of Confined-Masonry Rocking Walls with Supplementary Hysteretic Damping. *Journal of Earthquake Engineering*, Vol. 13, No. 6, pp 882-898.
- Tu Y. H., Chuang T. H., Liu P. M. and Yang Y. S. (2010). Out-of-plane shaking table tests on unreinforced masonry panels in RC frames. *Engineering Structures*, Vol. 32, No. 12, pp 3925-3935.
- Vasconcelos G., Alves P. and Lourenço P. B. (2012). Influence of distinct reinforcing schemes on the shear resistance of masonry. 15th international brick and block masonry conference. Florianopolis, Brazil.
- Vasconcelos G., Lourenço P. B., Mouzakis H. and Karapitta L. (2006). Experimental investigations on dry stone masonry walls. 1st International Conference on Restoration of Heritage Masonry Structures. Cairo, Egypt.
- Vecchio F. J. and McQuade I. (2011). Towards improved modeling of steel-concrete composite wall elements. *Nuclear Engineering and Design*, Vol. 241, No. 8, pp 2629-2642.
- Weihe S., Kröplin B. and De Borst R. (1998). Classification of smeared crack models based on material and structural properties. *International journal of solids and structures*, Vol. 35, No. 12, pp 1289-1308.
- Xuwei C., Xiaolei H., Cheang J., Shengyi L. and Guiniu M. (2008) Dynamic inelastic numerical simulation for a shaking table test of a full scale steel moment frame structure based on OpenSEES, *Proceedings of 14WCEE*. Beijing, China.
- Yi T., Moon F. L., Leon R. T. and Kahn L. F. (2006). Lateral load tests on a two-story unreinforced masonry building. *Journal of Structural Engineering*, Vol. 132, No. 5, pp 643-652.
- Žarnić R., Gostič S., Crewe A. J. and Taylor C. A. (2001). Shaking table tests of 1: 4 reduced-scale models of masonry infilled reinforced concrete frame buildings. *Earthquake Engineering & Structural Dynamics*, Vol. 30, No. 6, pp 819-834.
- Zhou X. and Li G. (2010). Shaking table model test of a steel-concrete composite high-rise building. *Journal of Earthquake Engineering*, Vol. 14, No. 4, pp 601-625.

Zonta D., Zanardo G. and Modena C. (2001). Experimental evaluation of the ductility of a reduced-scale reinforced masonry building. *Materials and Structures*, Vol. 34, No. 10, pp 636-644.

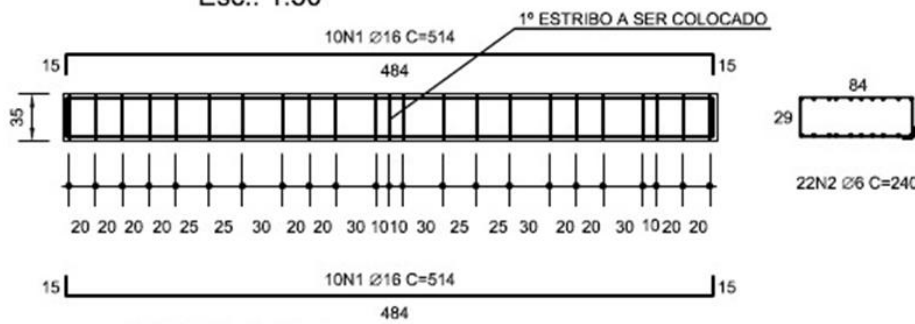
APPENDIX A

Final project for the construction of the symmetric buildings



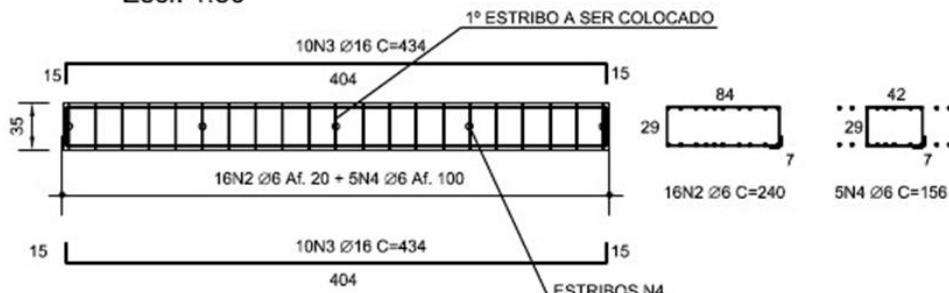
VIGAS DA BASE

Esc.: 1:50



VIGAS 1 E 4

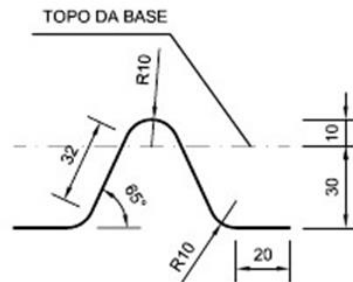
Esc.: 1:50



VIGAS 2 E 3

Esc.: 1:50

 <p>UNIVERSIDADE DO MINHO ENGENHARIA CIVIL</p>	<p>ENSAIO EM MESA SÍSMICA</p>	<p>Maio 2008</p>
<p>Escala: 1:50</p>	<p>MACIÇO DE FUNDAÇÃO -DEFINIÇÃO GEOMÉTRICA</p>	<p>01 / 11</p>

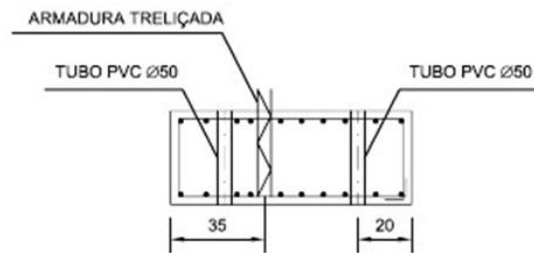


8 N8 Ø16 C=145

Obs.: Deve-se utilizar 2 peças por ponto de suspensão

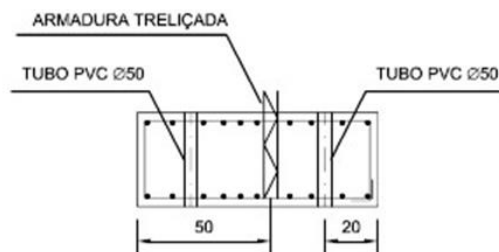
DETALHE 1

Esc.: 1:25



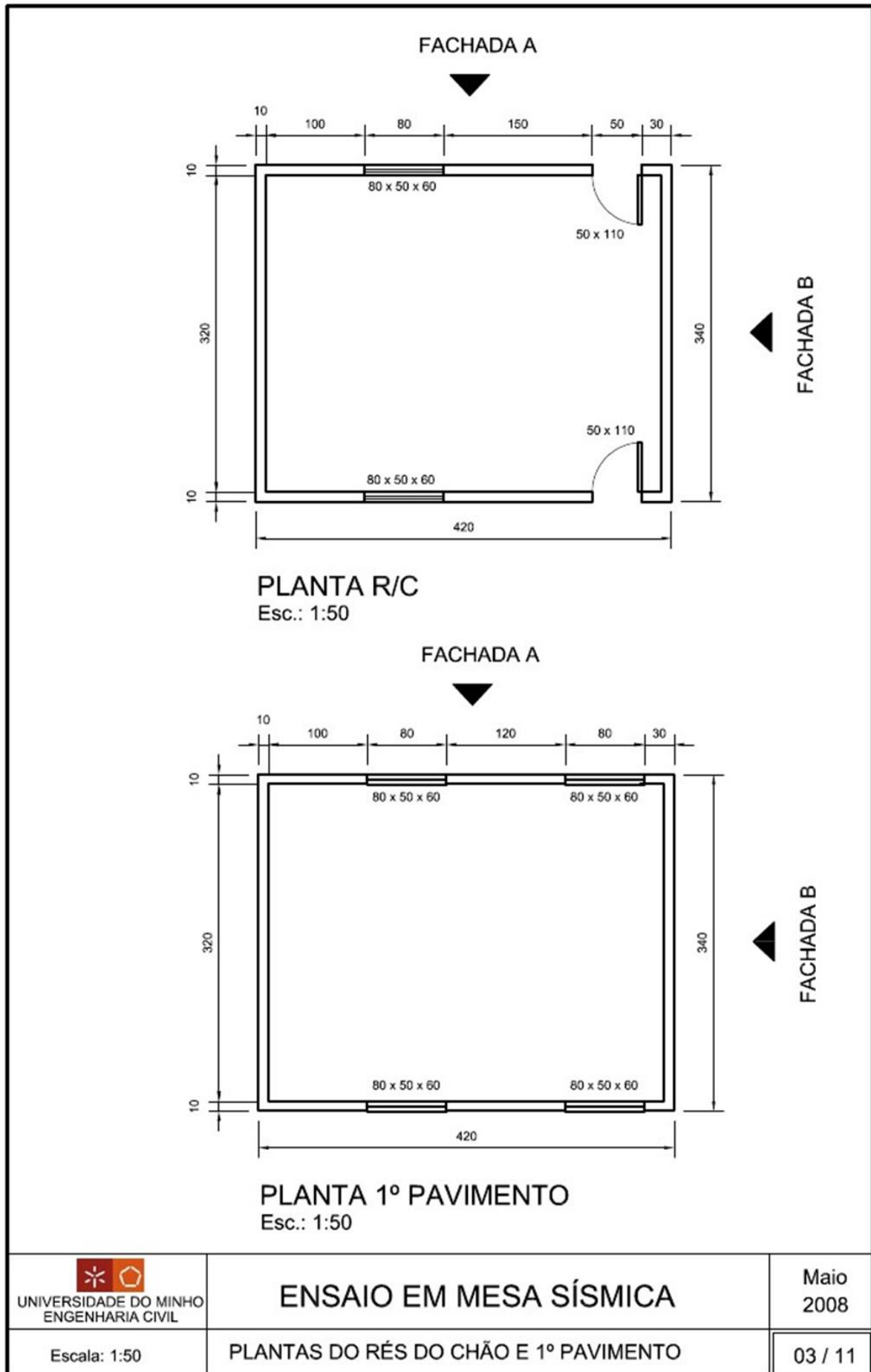
DETALHE 2

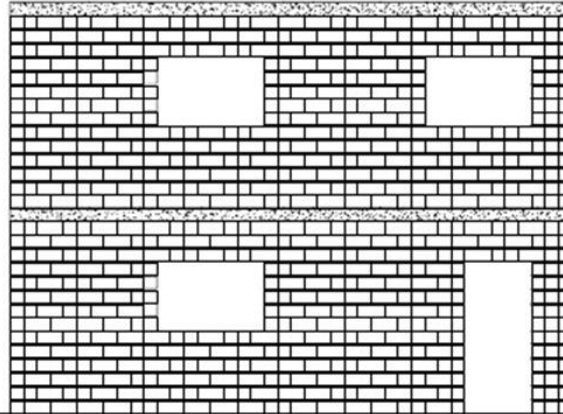
Esc.: 1:25



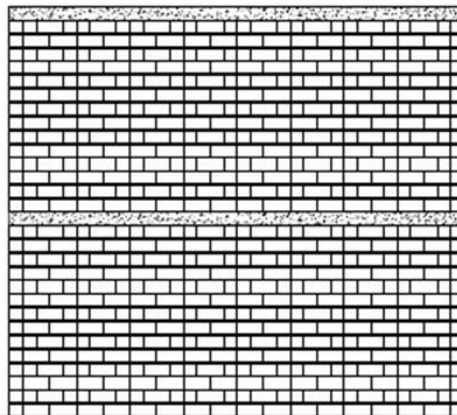
DETALHE 3

Esc.: 1:25



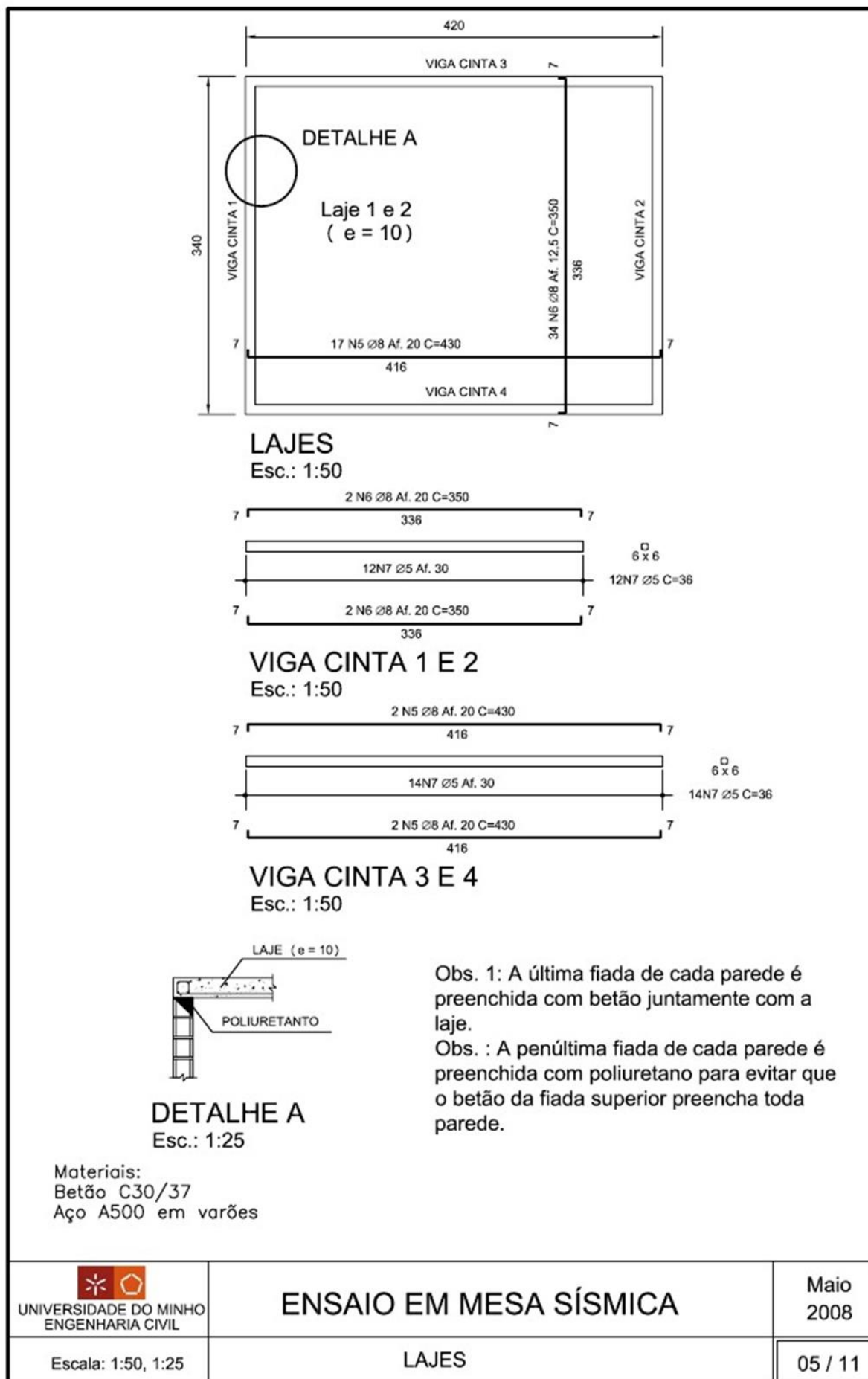


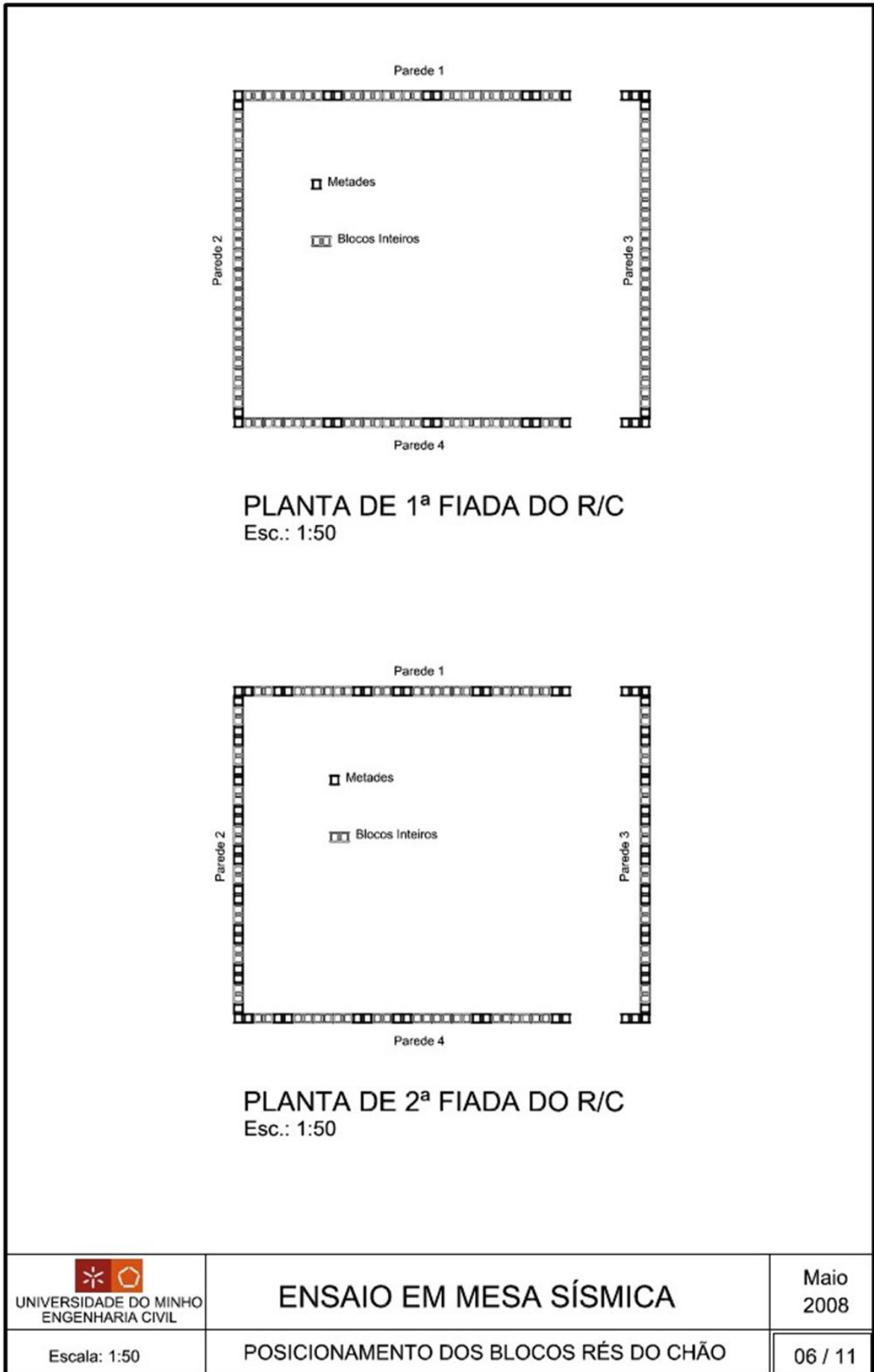
FACHADA A
Esc.: 1:50

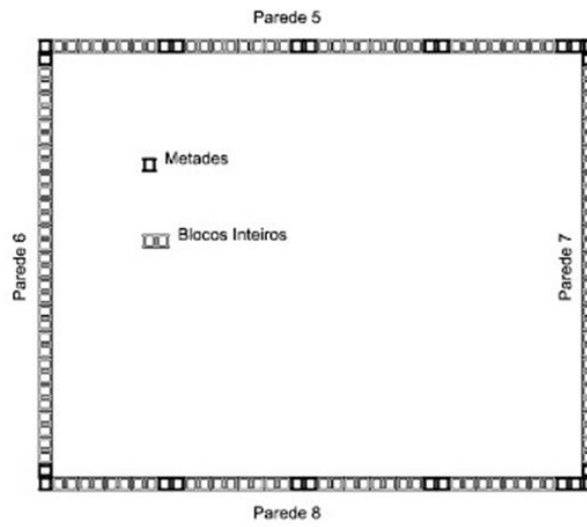


FACHADA B
Esc.: 1:50

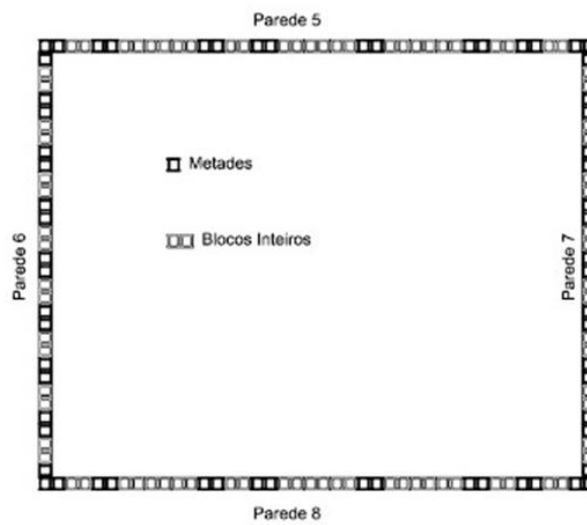
 UNIVERSIDADE DO MINHO ENGENHARIA CIVIL	ENSAIO EM MESA SÍSMICA	Maio 2008
Escala: 1:50	FACHADAS	04 / 11






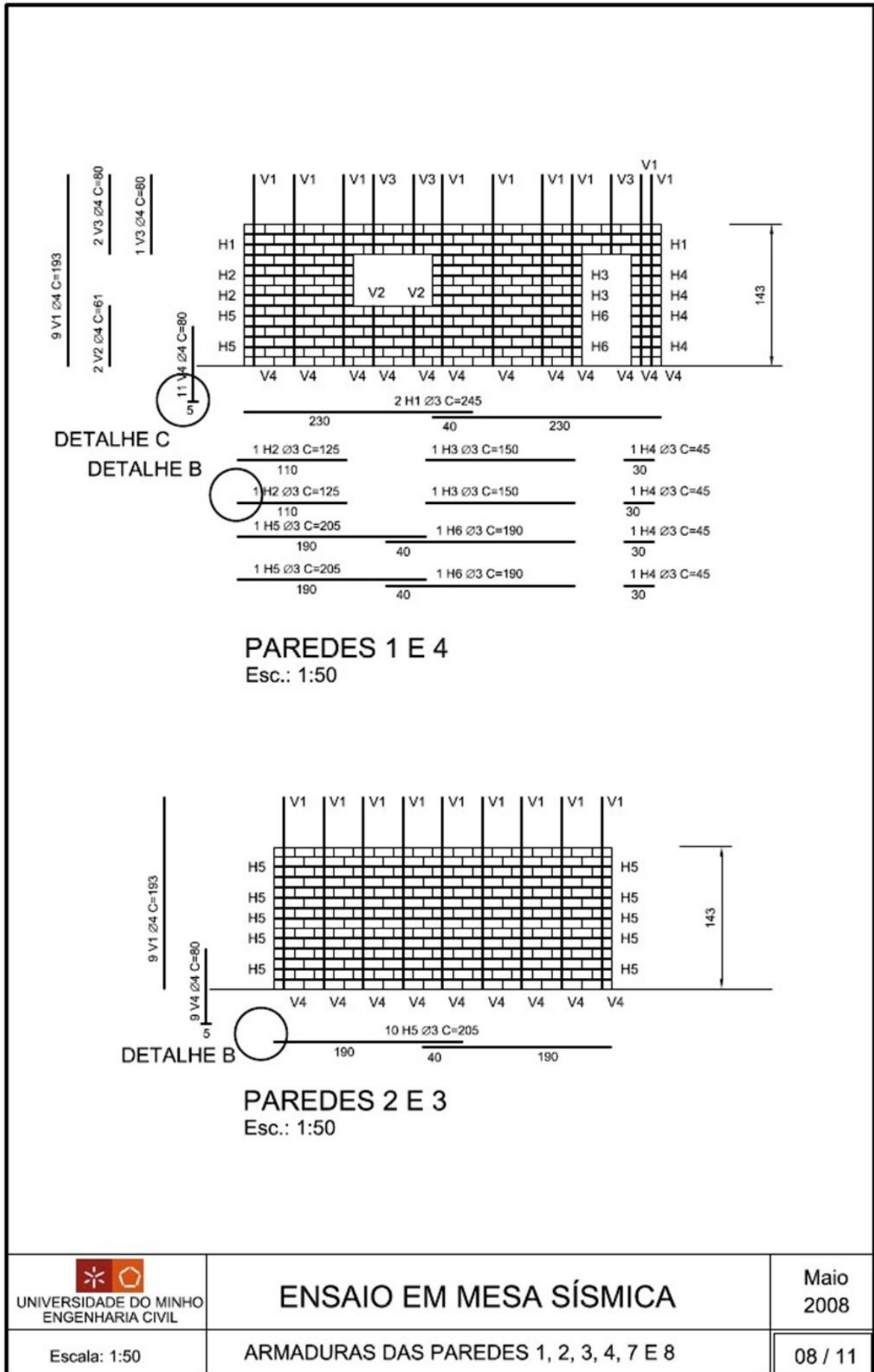


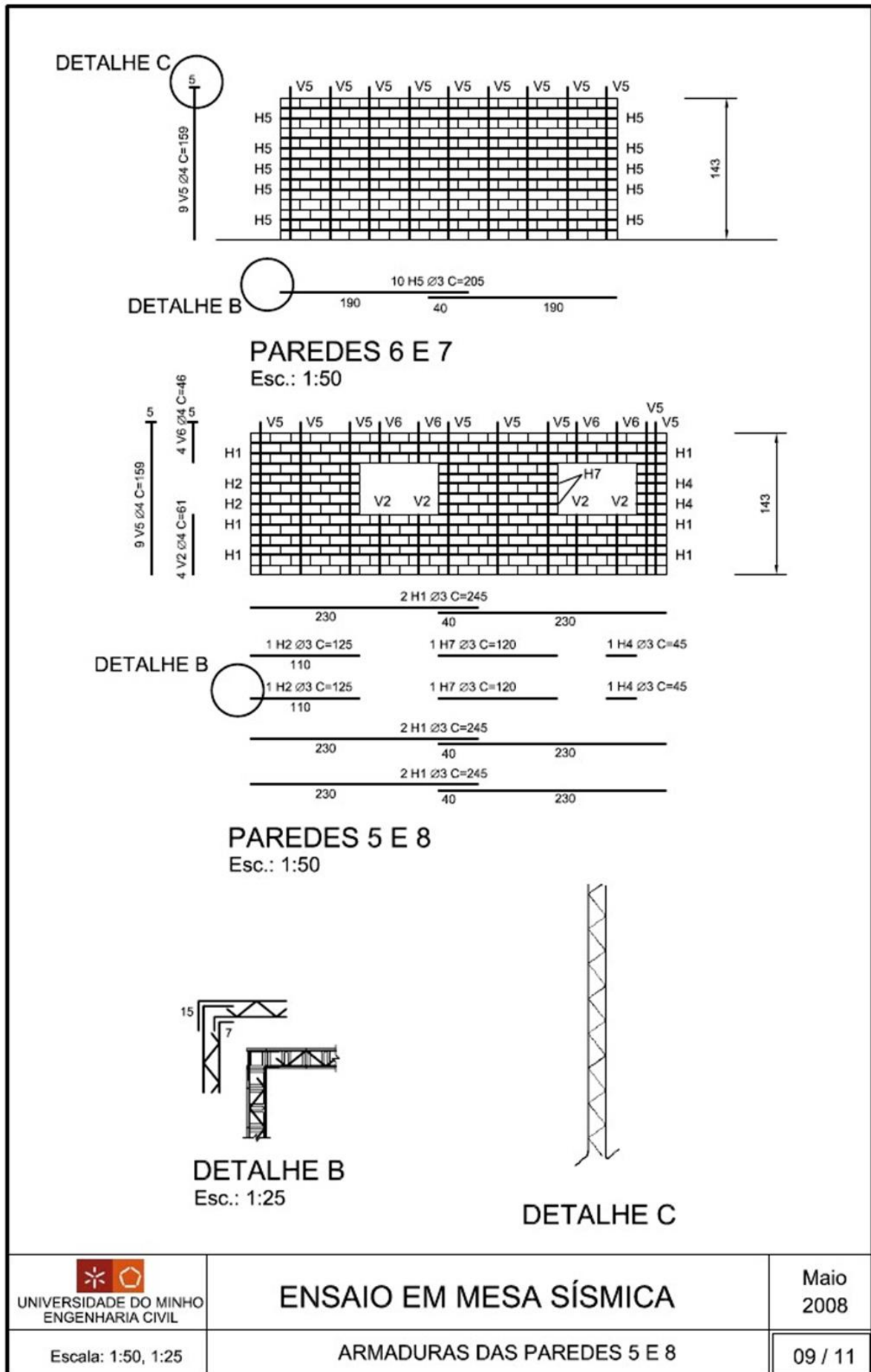
PLANTA DE 1ª FIADA DO 1º PAVIMENTO
Esc.: 1:50

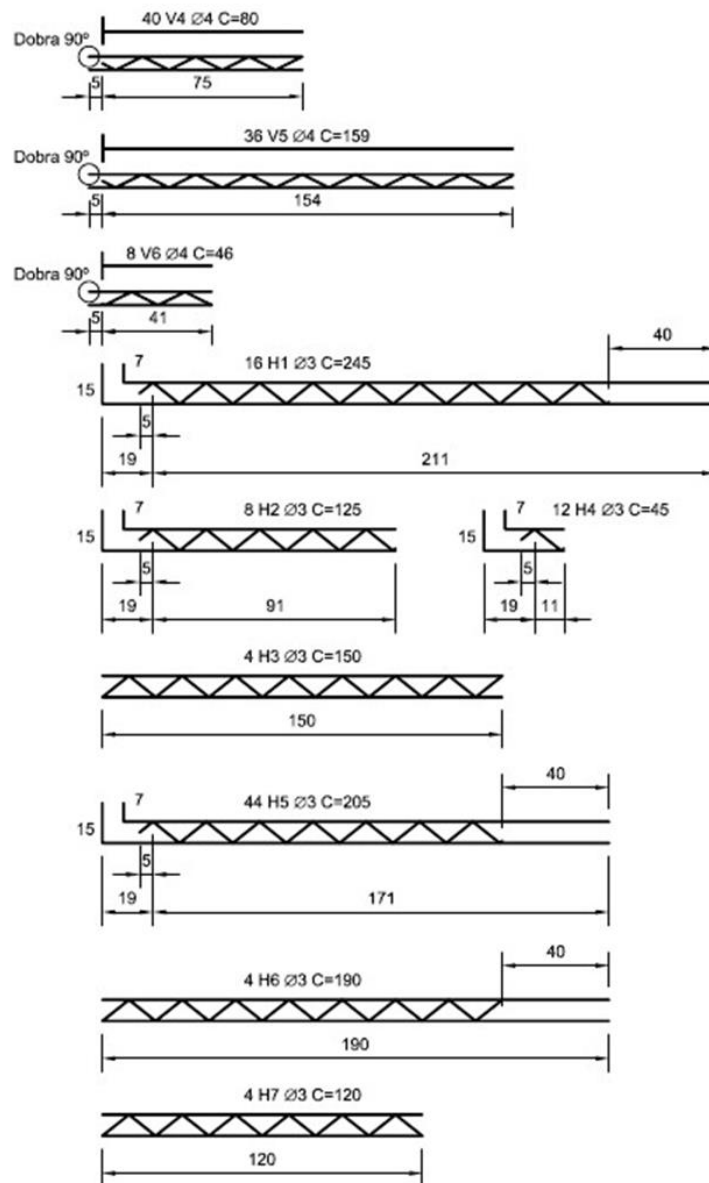


PLANTA DE 2ª FIADA DO 1º PAVIMENTO
Esc.: 1:50

 UNIVERSIDADE DO MINHO ENGENHARIA CIVIL	ENSAIO EM MESA SÍSMICA	Maio 2008
Escala: 1:50	POSICIONAMENTO DOS BLOCOS 1º PAVIMENTO	07 / 11








CORTE DAS ARMADURAS TRELIÇADAS

Esc.: 1:25

Obs. 1: As armaduras verticais V1, V2 e V3 pode ser cortadas independentemente da disposição das diagonais.

 UNIVERSIDADE DO MINHO ENGENHARIA CIVIL	<h2>ENSAIO EM MESA SÍSMICA</h2>	Maio 2008
Escala: 1:25	CORTE DAS ARMADURAS TRELIÇADAS	10 / 11

MATERIAISTABELA DE ARMADURAS

QUANTIDADE	TIPO	Ø (mm)	t (mm)	COMPRIMENTO (cm)	TOTAL (m)
36	V1	4	50	193	69.48
12	V2	4	50	61	7.32
6	V3	4	50	80	4.80
40	V4	4	50	80	32.00
36	V5	4	50	159	57.24
8	V6	4	50	46	3.68
16	H1	3	80	245	39.20
8	H2	3	80	125	10.00
4	H3	3	80	150	6.00
12	H4	3	80	45	5.40
44	H5	3	80	205	90.20
4	H6	3	80	190	7.60
4	H7	3	80	120	4.80
40	N1	16	-	514	205.60
86	N2	6	-	240	206.40
40	N3	16	-	434	173.60
8	N4	16	-	145	11.60
42	N5	8	-	430	180.60
76	N6	8	-	350	266.00
52	N7	5	-	36	18.72

t (mm) - distância entre longitudinais da armadura treliçada

UNIDADESRESUMO DA ARMADURA

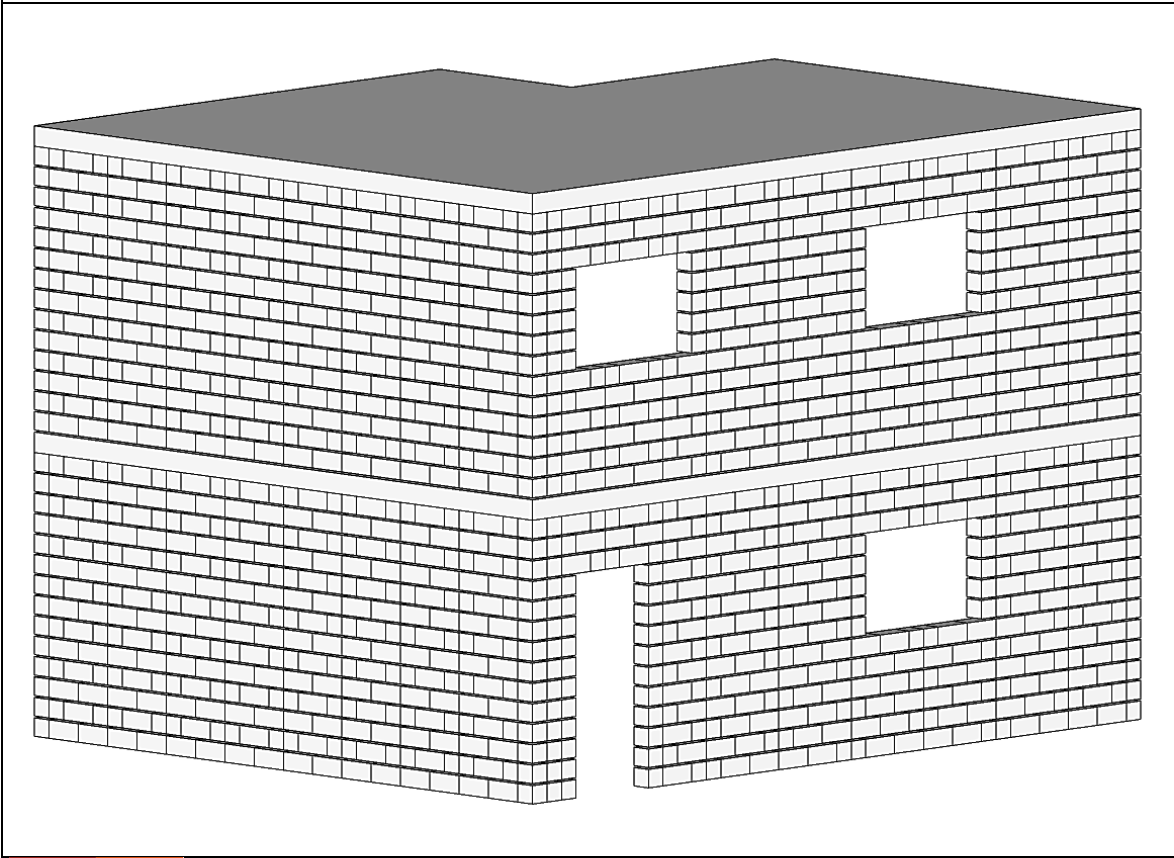
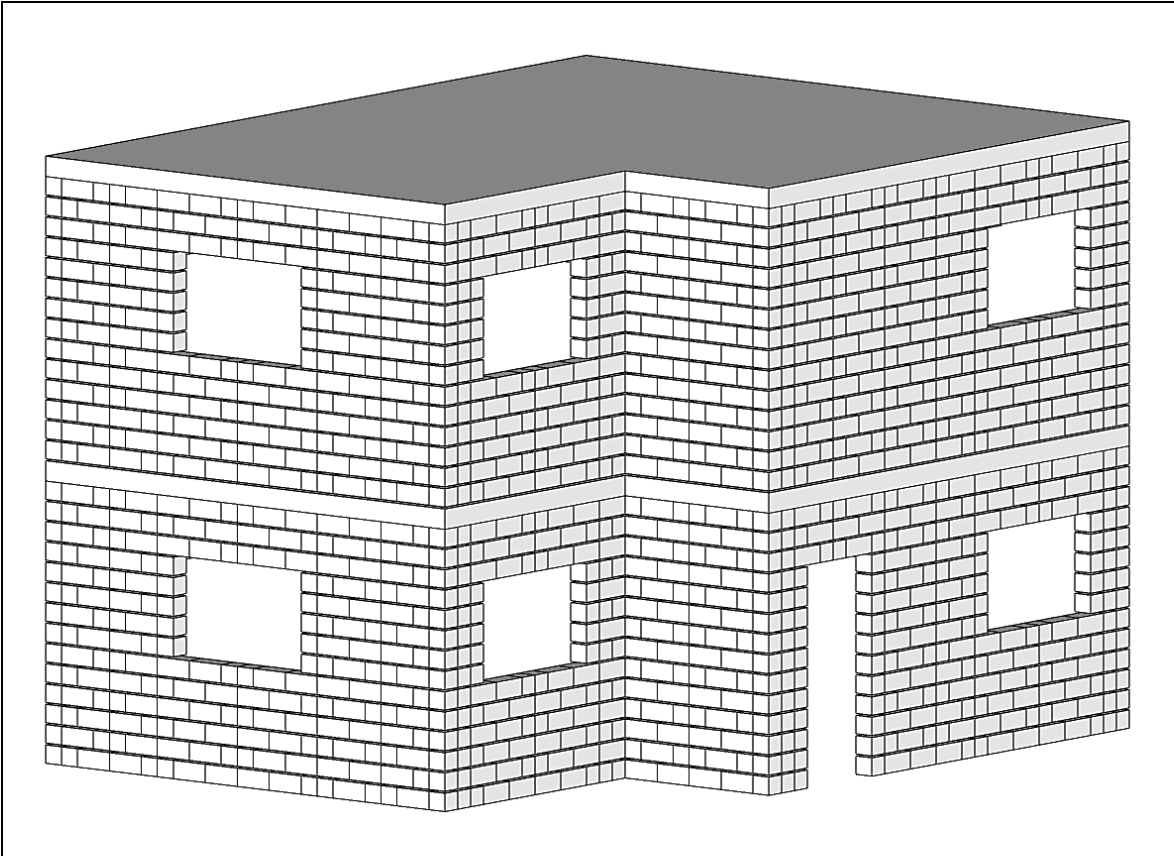
		Ø (mm)	t (mm)	TOTAL (m)
BLOCOS INTEIROS	1320			
METADES	1134	4	50	174.52
		3	80	163.20
		8	-	380.60
VOLUME PARA A BASE (m ³)	4.73	6	-	206.40
		5	-	18.72
		16	-	394.40


MICROBETÃO (30 MPa)ARGAMASSA

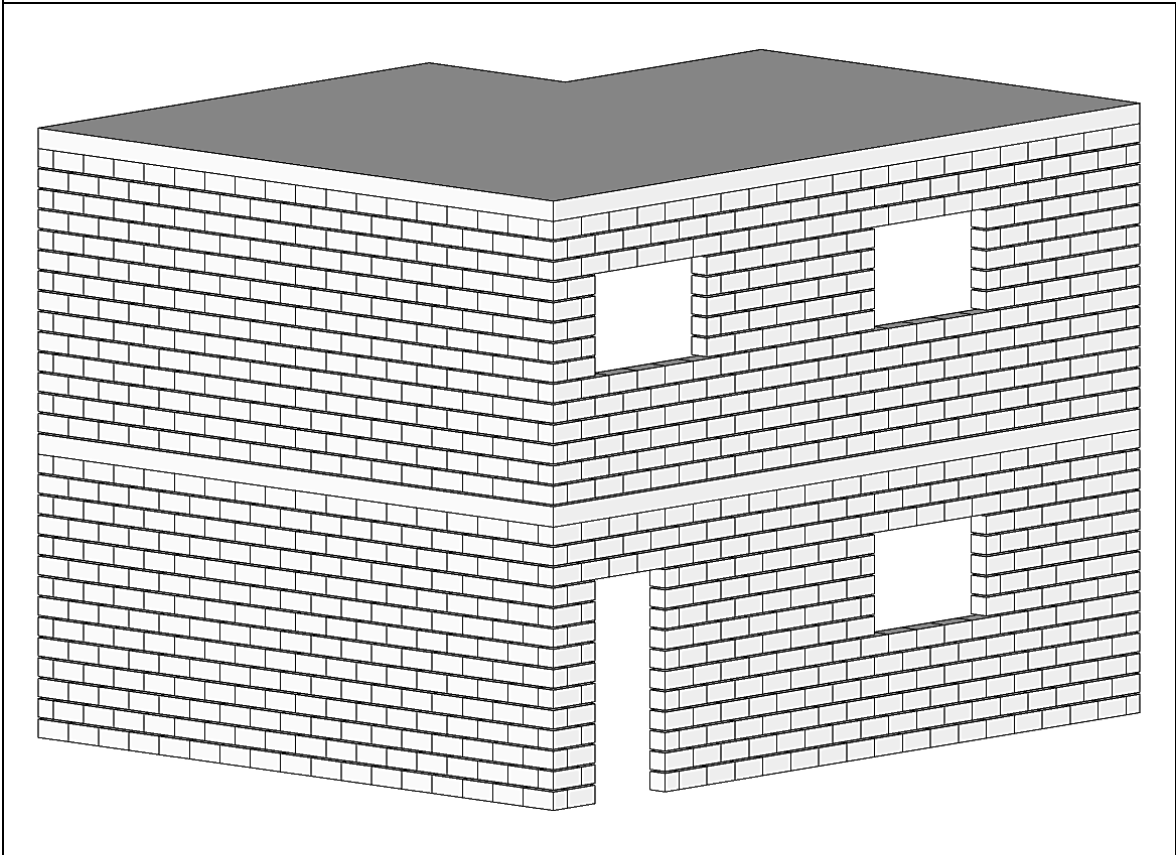
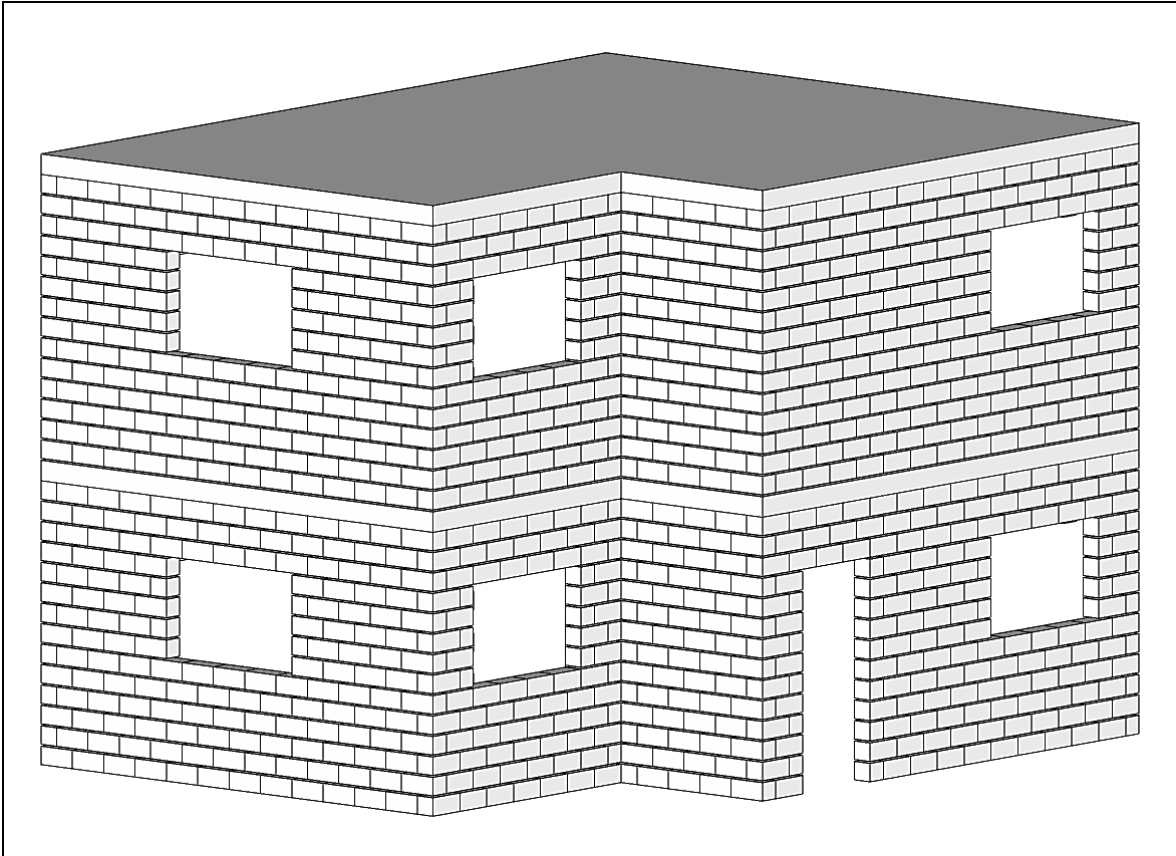
VOLUME EM CADA LAJE (m ³)	2.84	VOLUME (m ³)	1.50
---------------------------------------	------	--------------------------	------


APPENDIX B

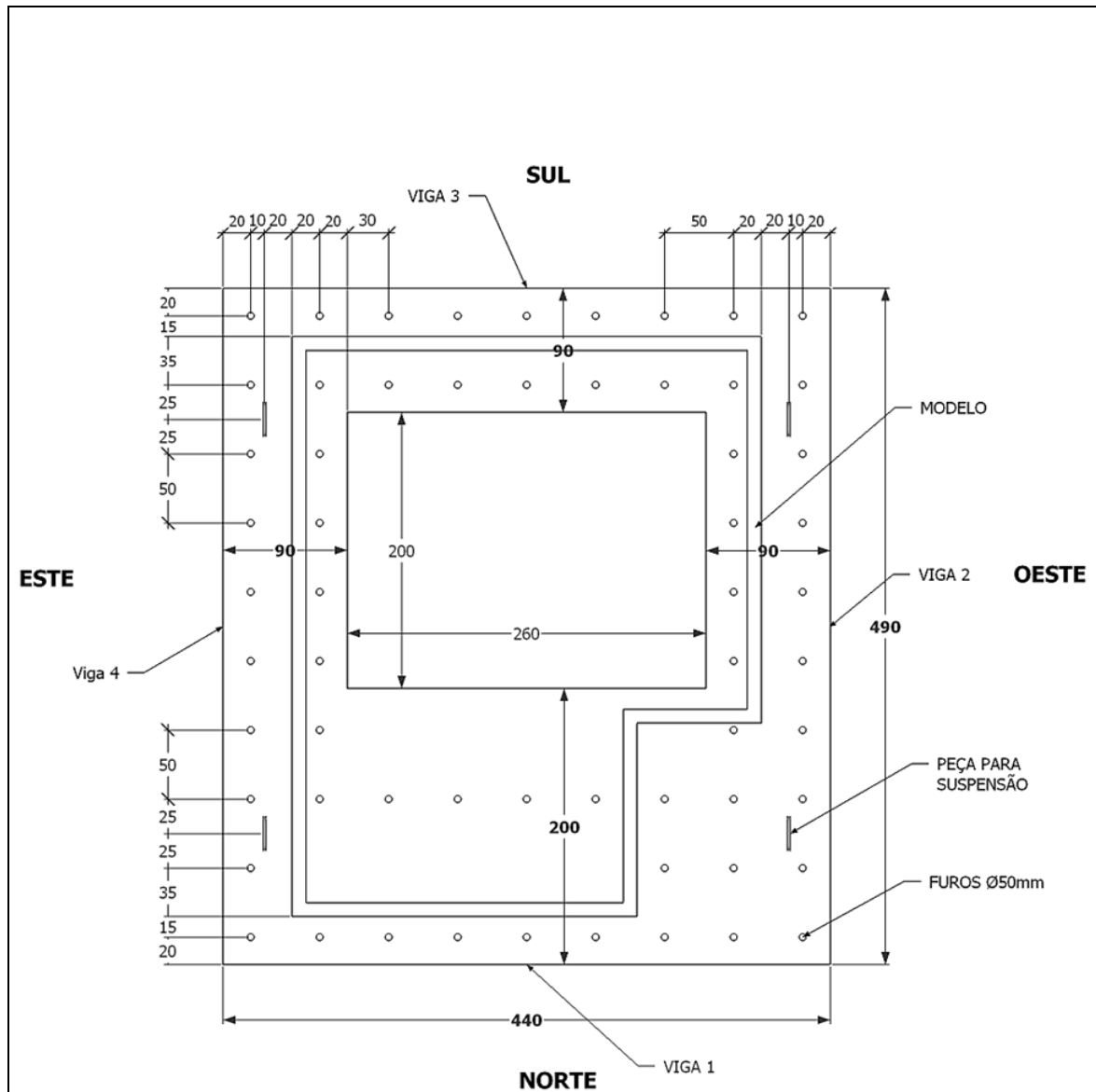
Final project for the construction of the asymmetric buildings



 Universidade do Minho	ENSAIO EM MESA SÍSMICA	Novembro 2011
	Edifício reforçado	1/33



 <p>Universidade do Minho</p>	<p>ENSAIO EM MESA SÍSMICA</p> <p>Edifício não reforçado</p>	<p>Novembro 2011</p> <p>2/33</p>
--	---	----------------------------------



Obs.:

Dimensões em cm

Materiais:

Betão C30/37

Aço A400

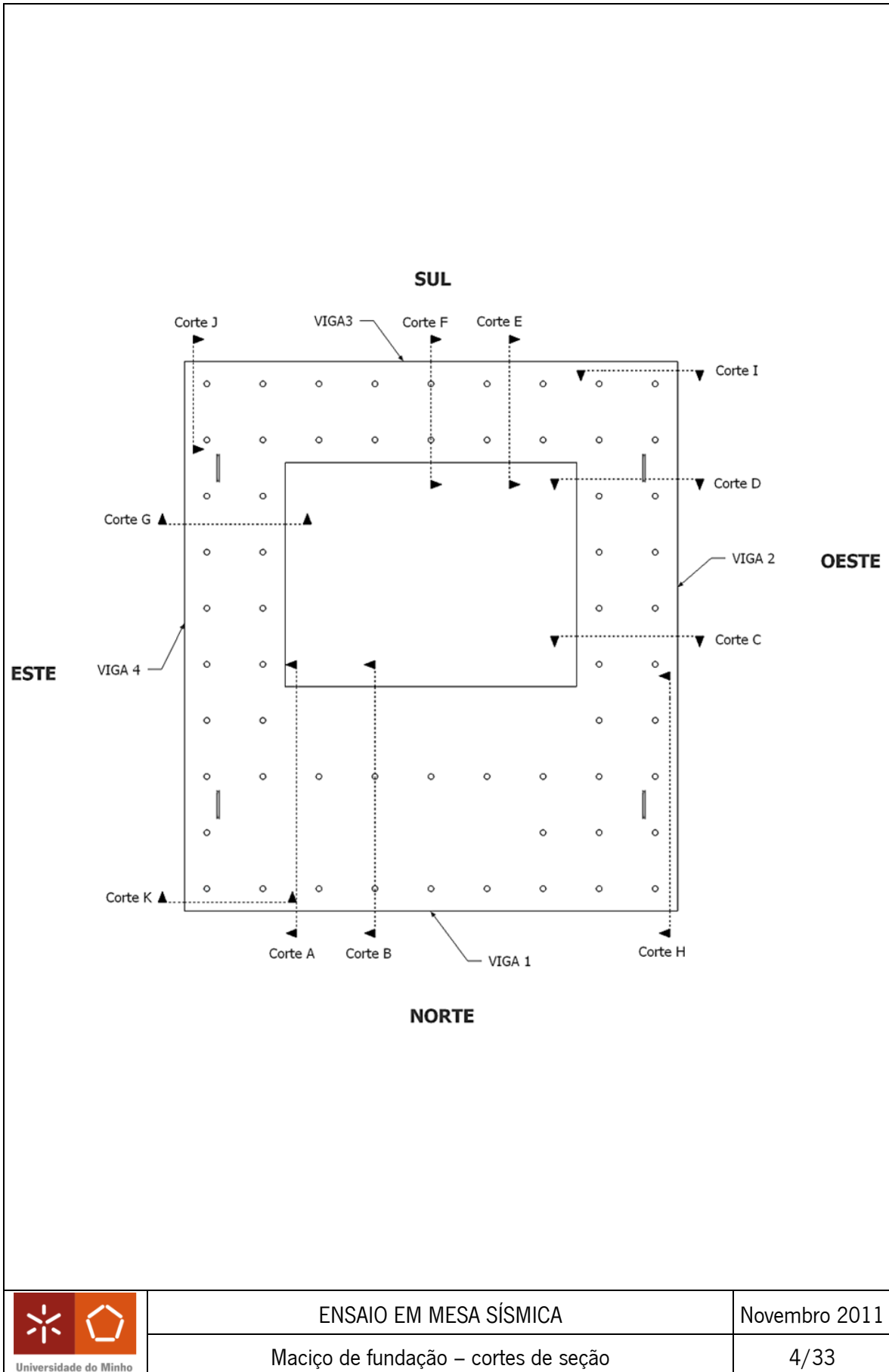


ENSAIO EM MESA SÍSMICA

Novembro 2011

Maciço de fundação - definição geométrica

3/33

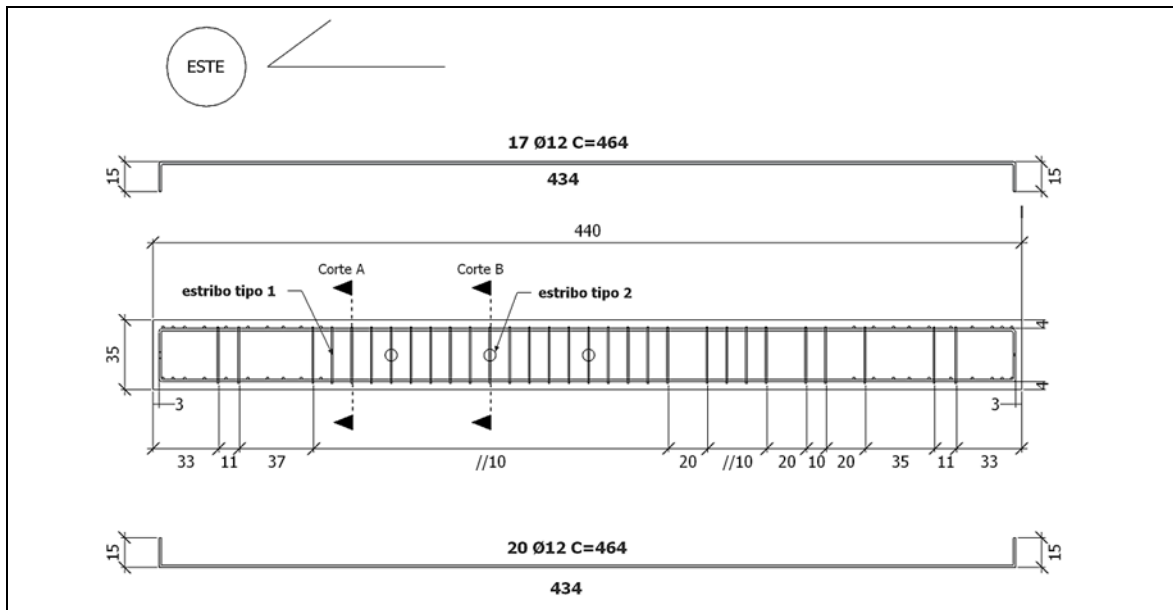


ENSAIO EM MESA SÍSMICA

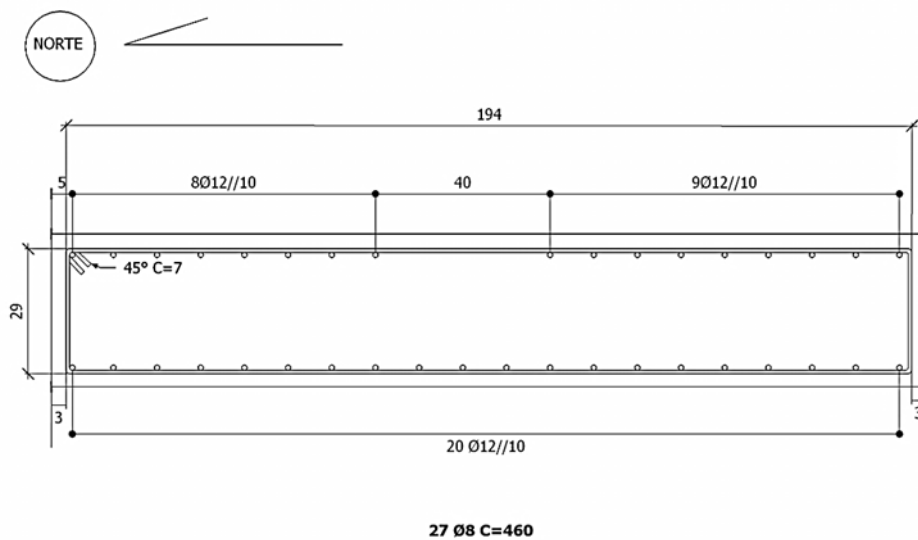
Novembro 2011

Maciço de fundação – cortes de seção

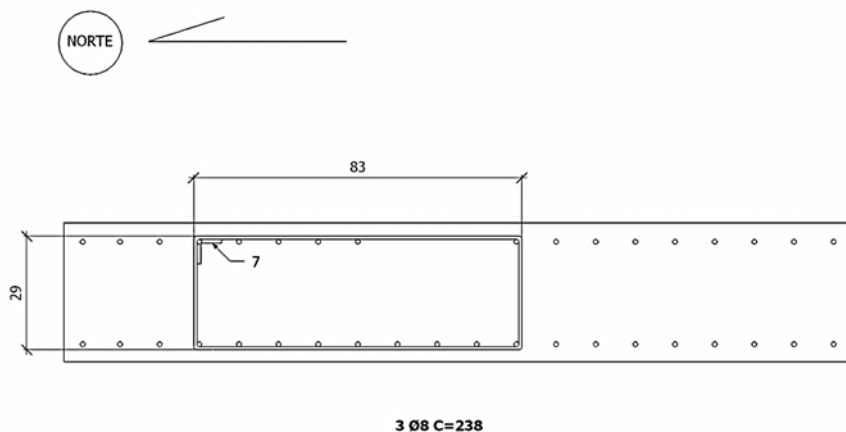
4/33



Corte A



Corte B



Obs.:

A

armadura da viga 1 é sempre colocada debaixo da armaduras das vigas 2 e 4

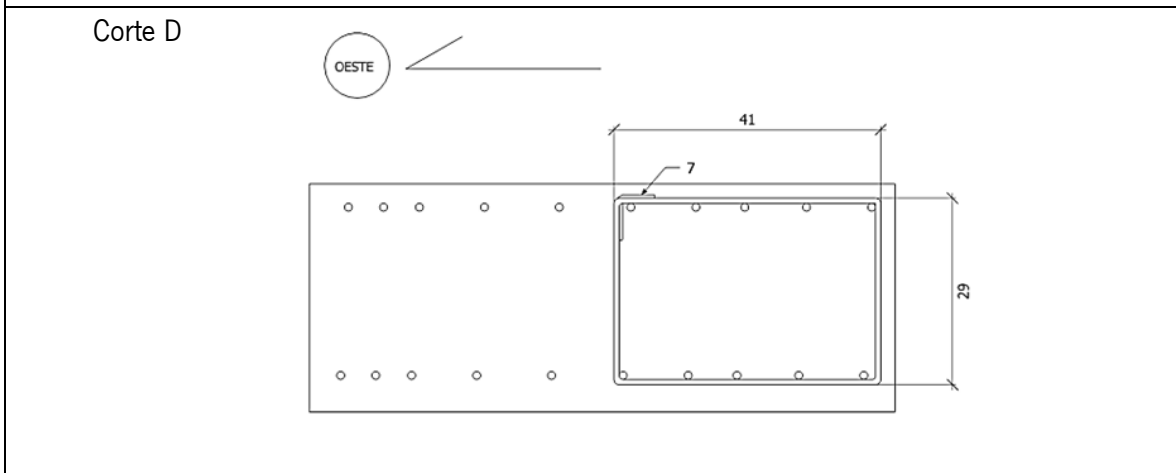
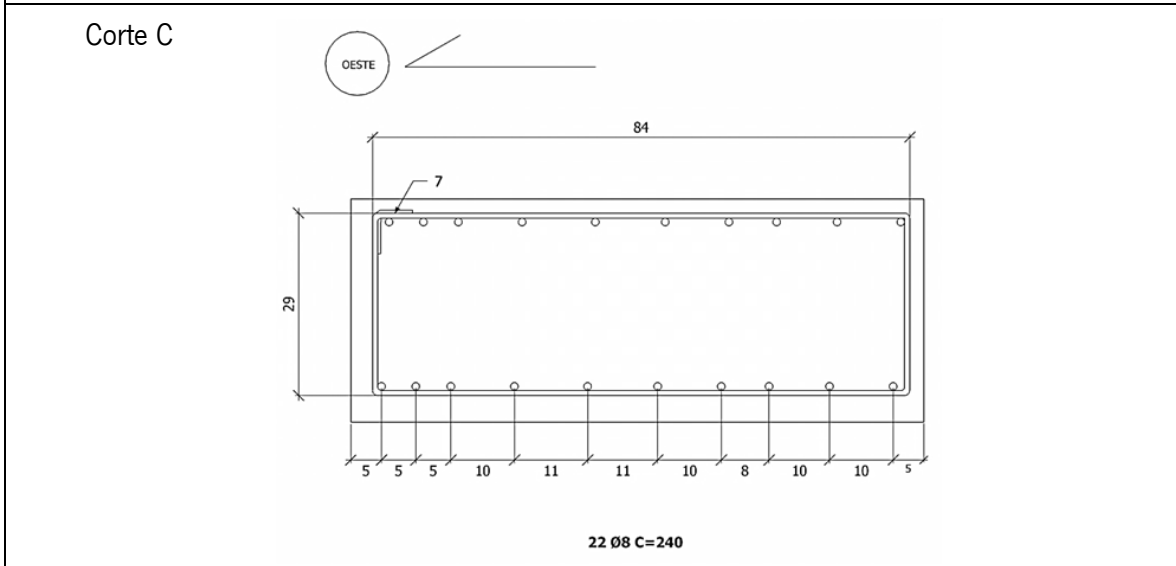
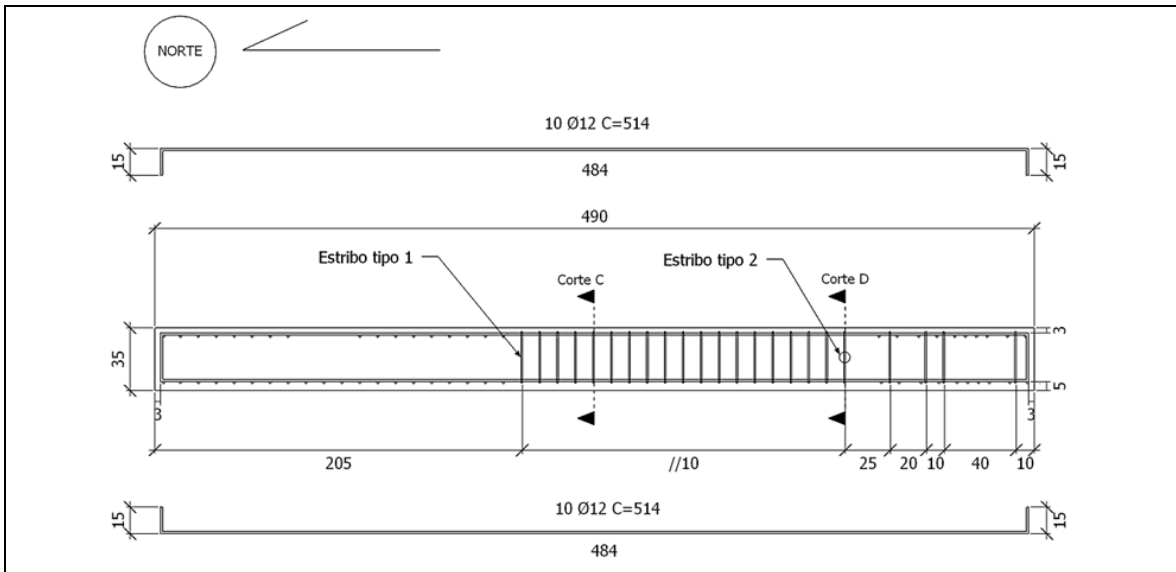


ENSAIO EM MESA SÍSMICA

Novembro 2011


Viga 1 – corte A e B

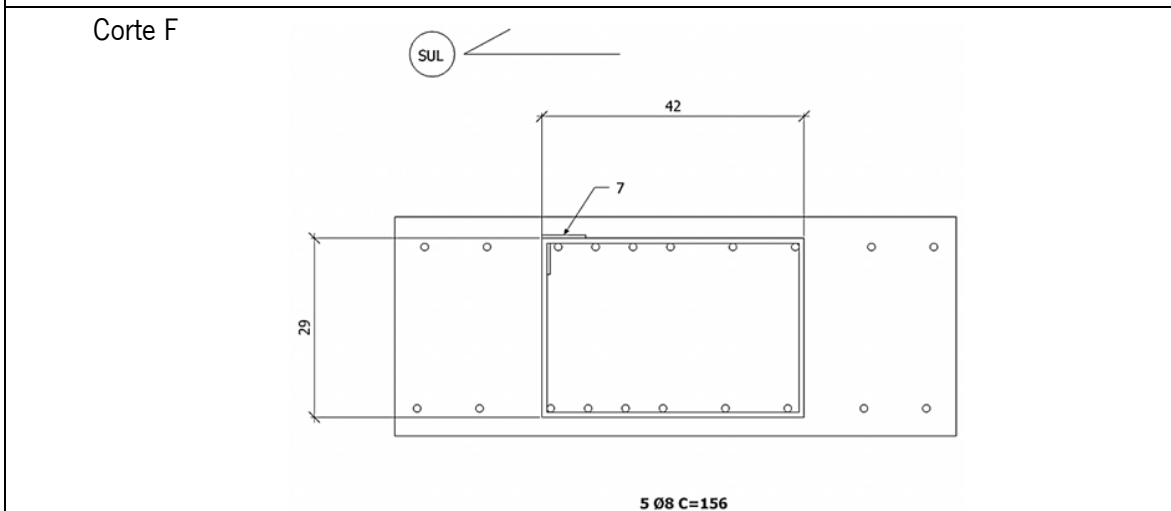
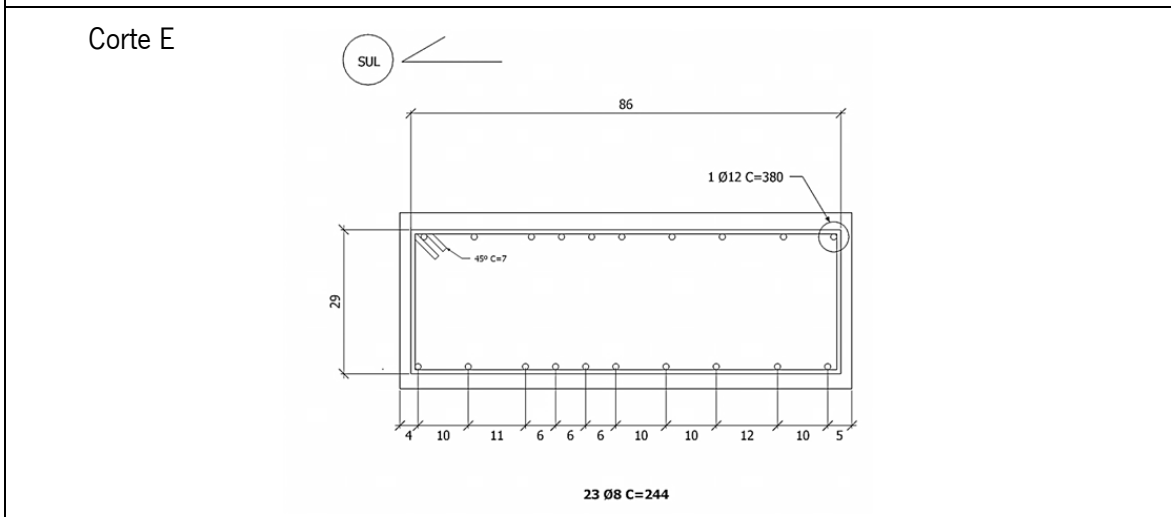
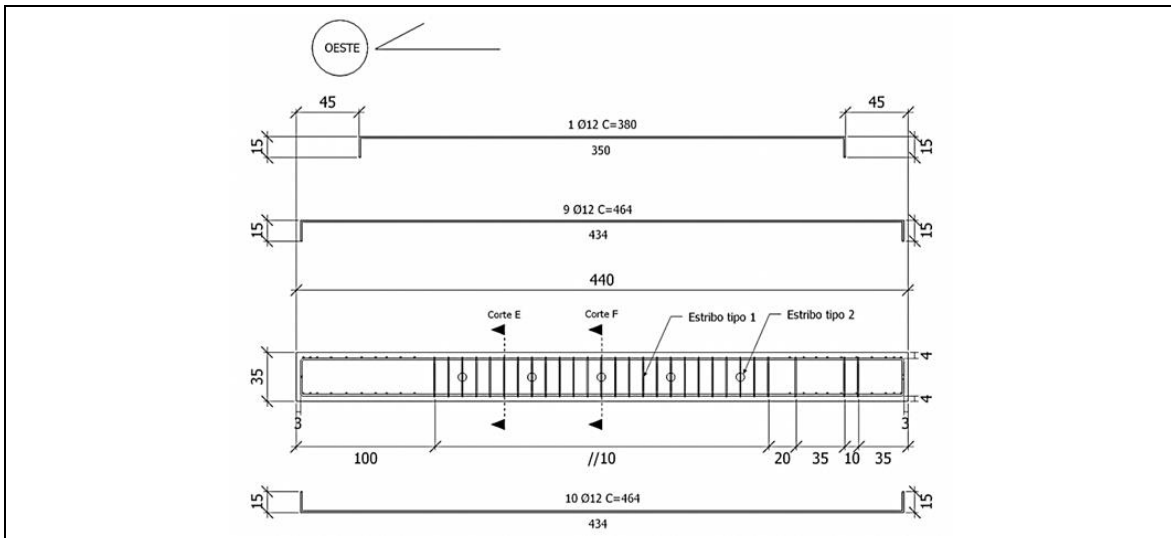
5/33



Obs.:


A armadura da viga 1 é sempre colocada debaixo da armaduras das vigas 2 e 4

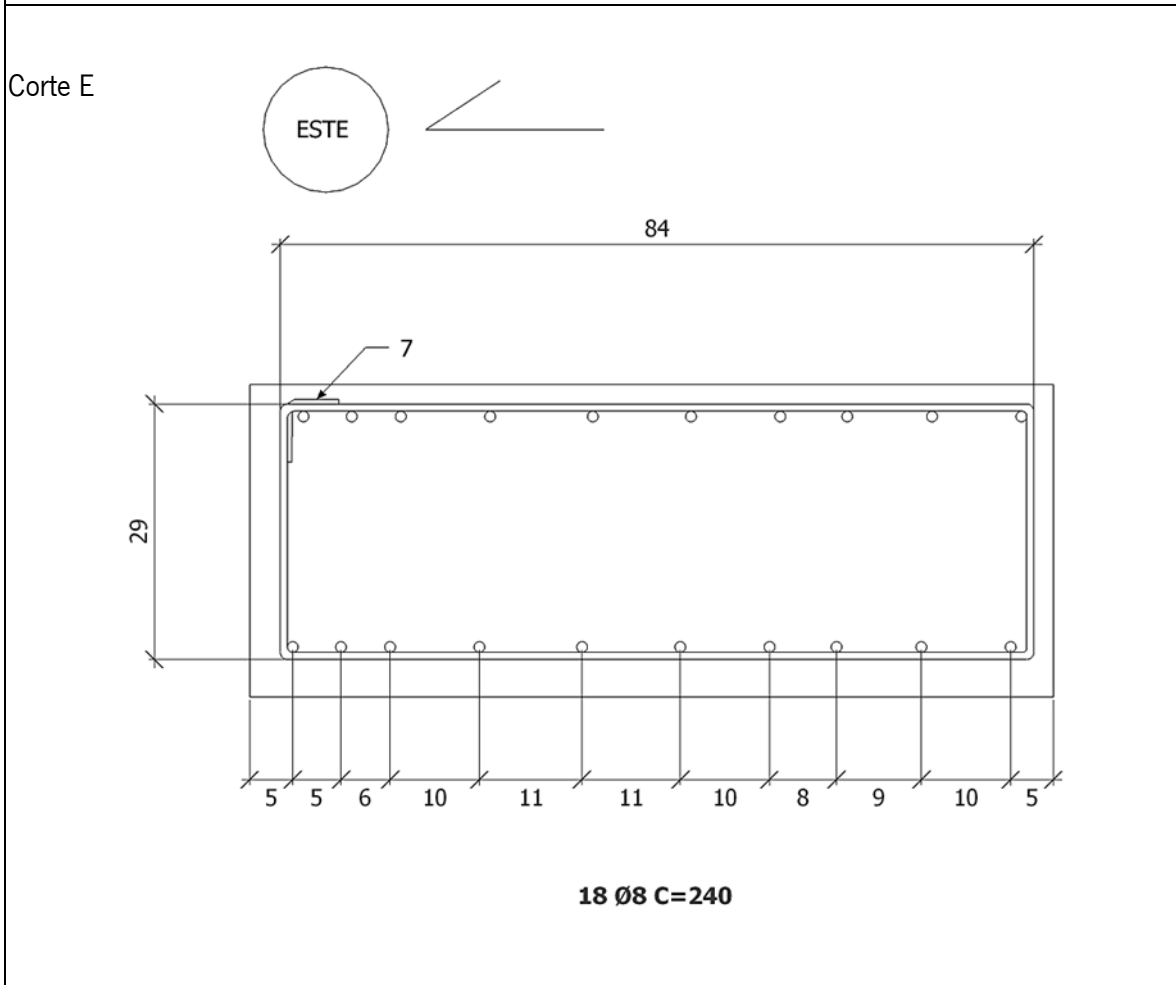
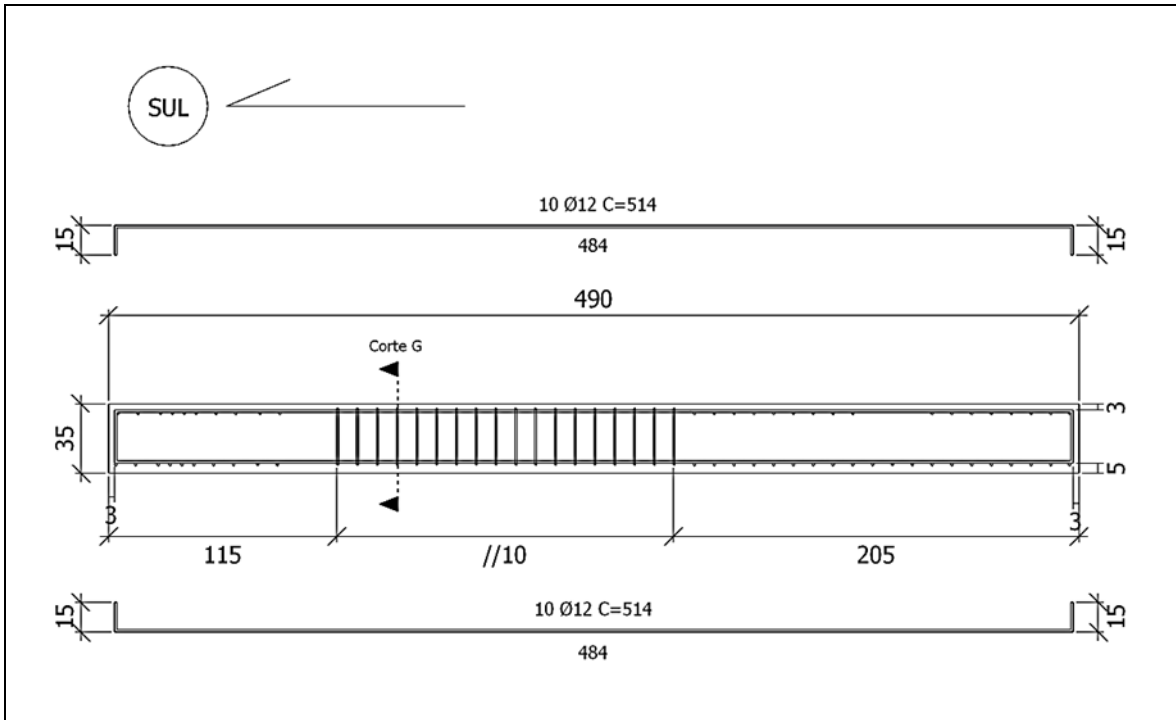
 <p>Universidade do Minho</p>	<p>ENSAIO EM MESA SÍSMICA</p>	<p>Novembro 2011</p>
	<p>Viga 2 – corte C e D</p>	<p>6/33</p>




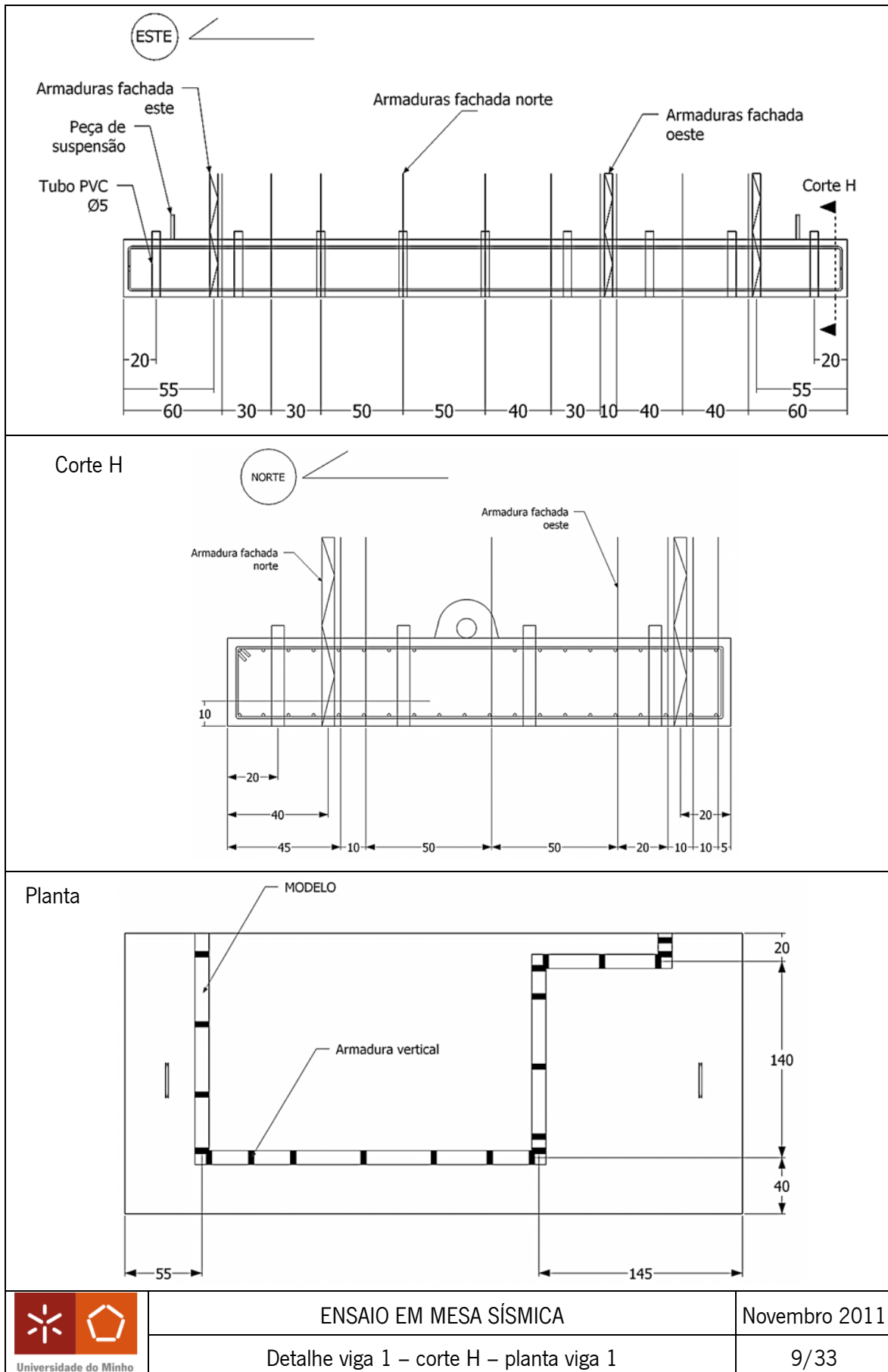
Obs.:

A armadura da viga 1 é sempre colocada debaixo da armaduras das vigas 2 e 4

	ENSAIO EM MESA SÍSMICA	Novembro 2011
	Viga 3 – corte E e F	7/33



	ENSAIO EM MESA SÍSMICA	Novembro 2011
	Viga 4 – corte G	8/33

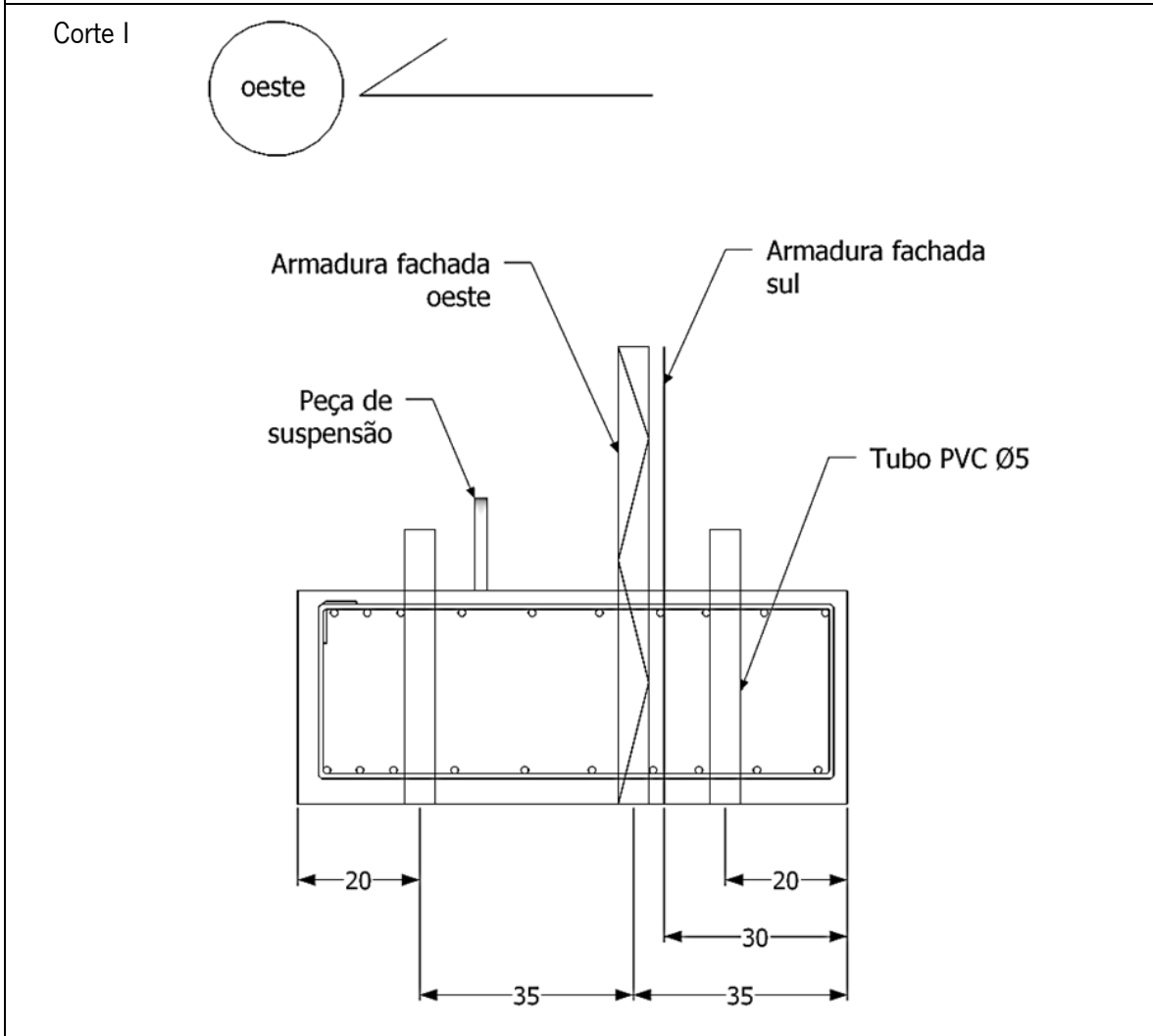
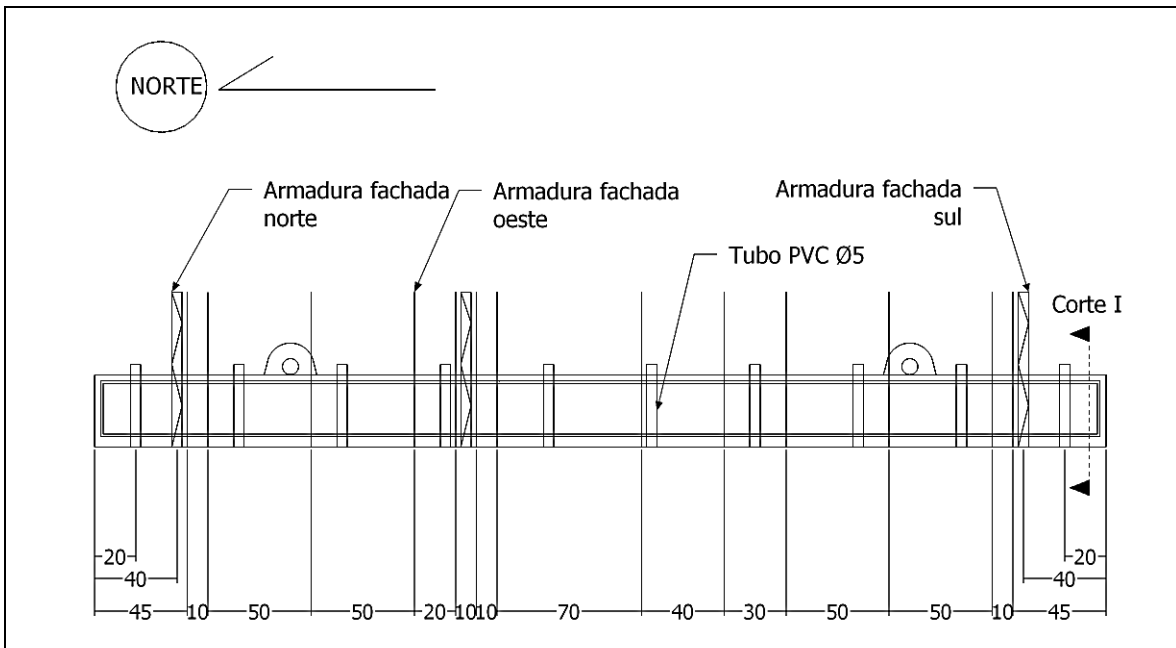



ENSAIO EM MESA SÍSMICA

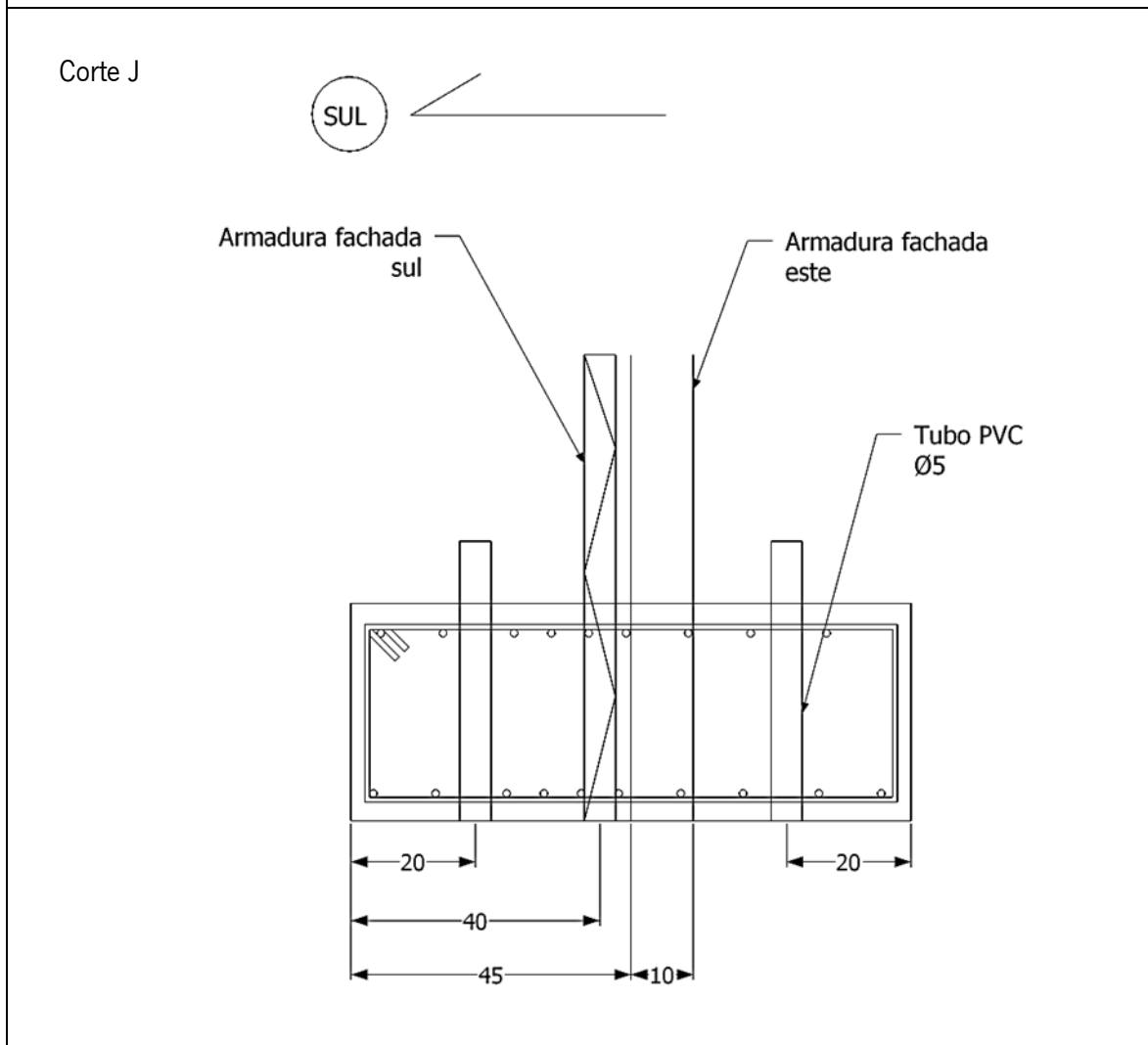
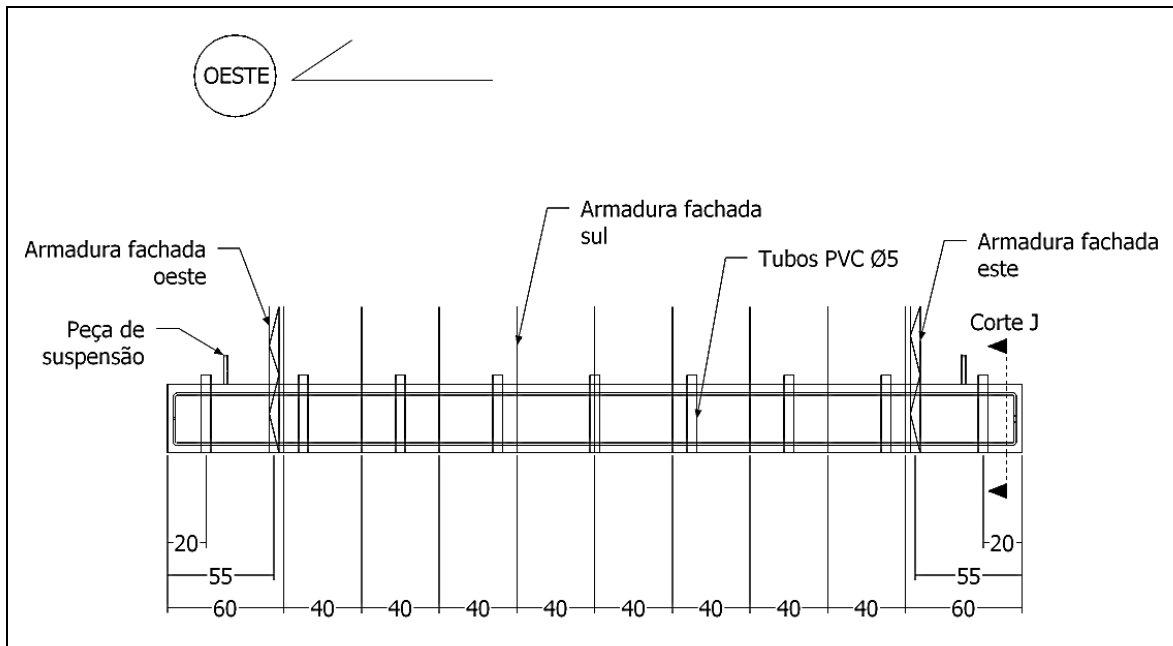
Novembro 2011

Detalhe viga 1 – corte H – planta viga 1

9/33



	ENSAIO EM MESA SÍSMICA	Novembro 2011
	Detalhe viga 2 – corte I	10/33

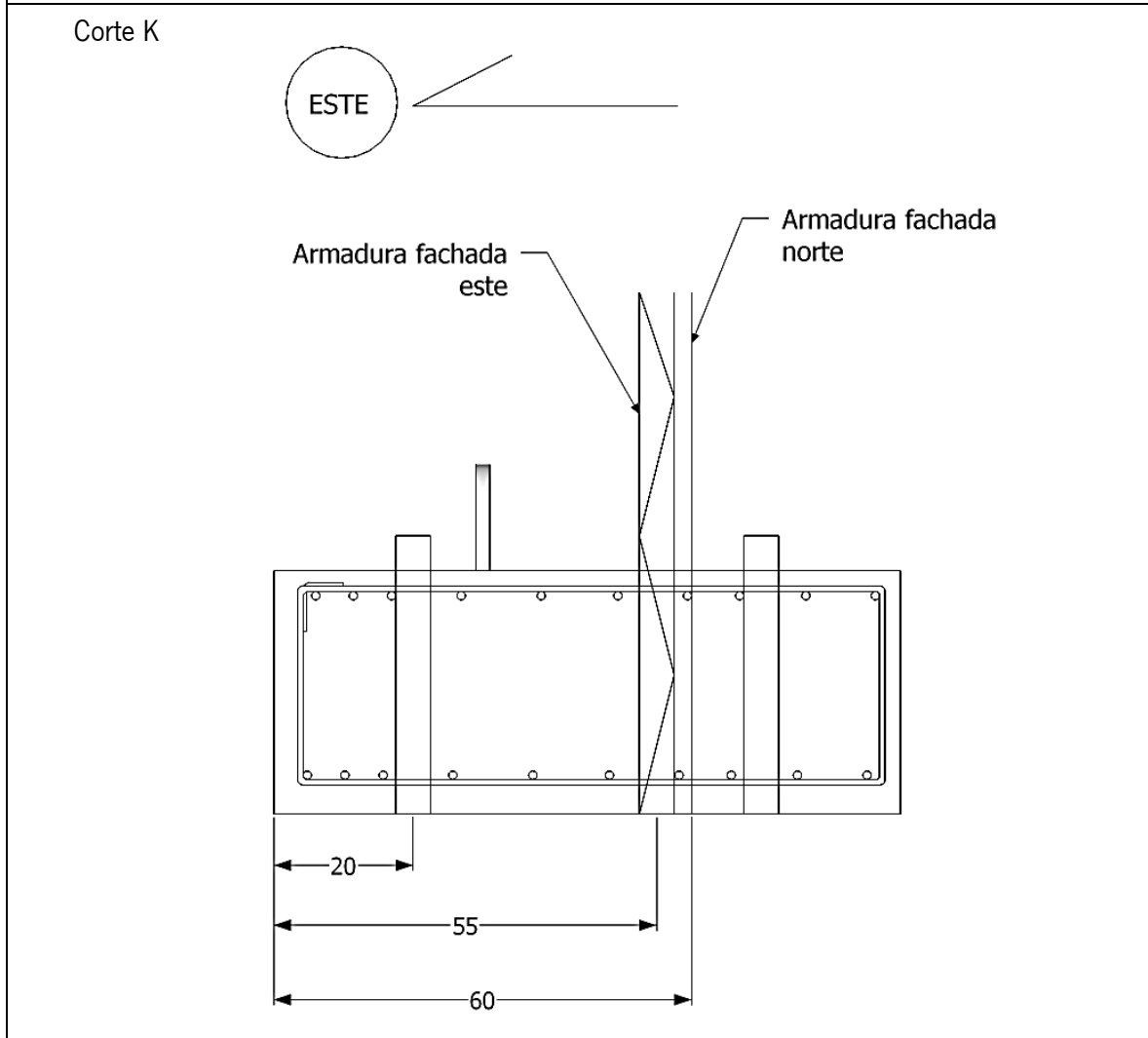
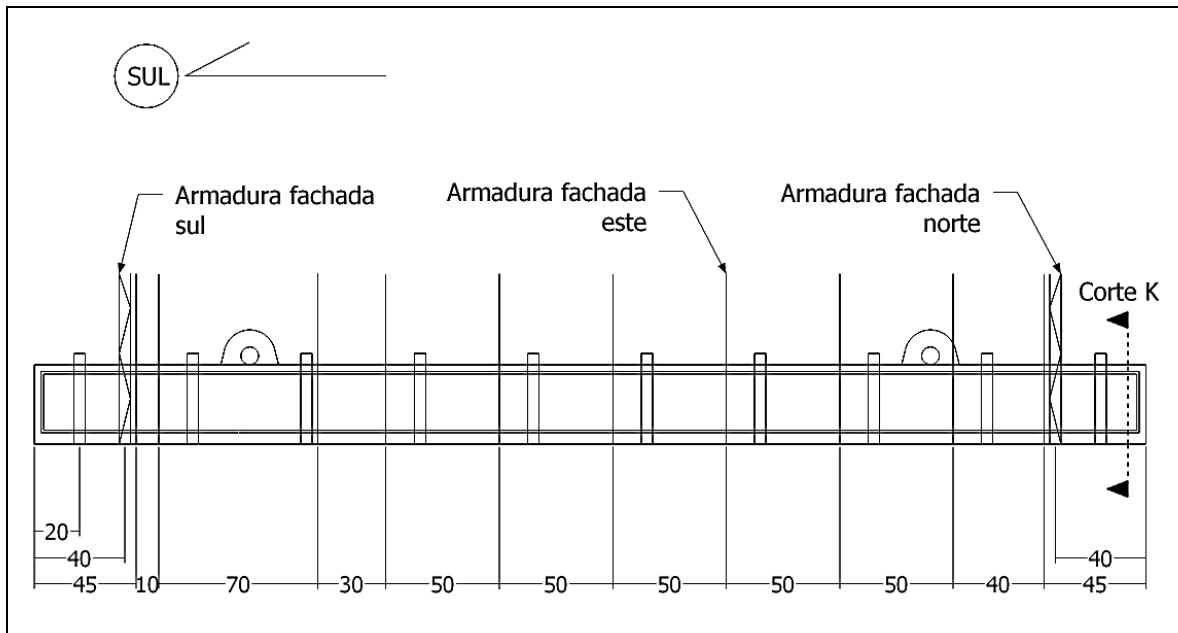


ENSAIO EM MESA SÍSMICA

Novembro 2011

Detalhe viga 3 – corte J

11/33



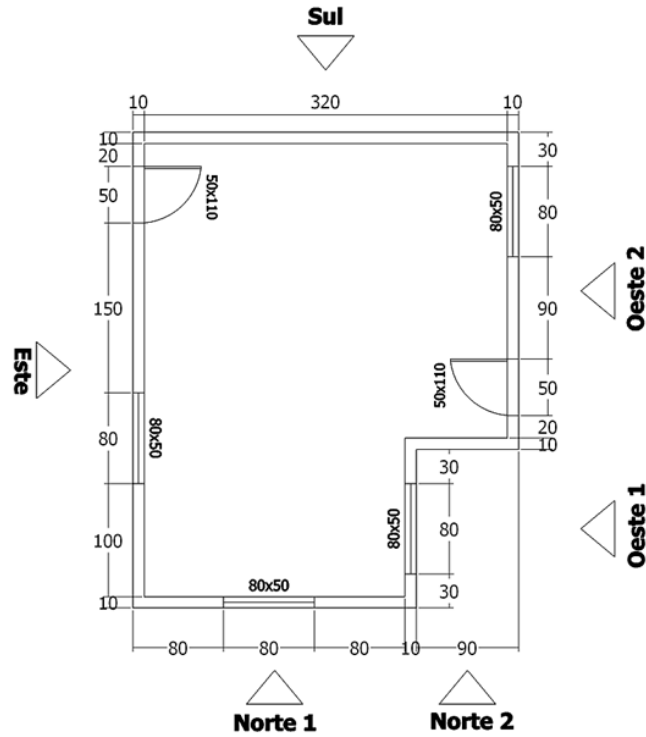
ENSAIO EM MESA SÍSMICA

Novembro 2011

Detalhe viga 4 – corte K

12/33

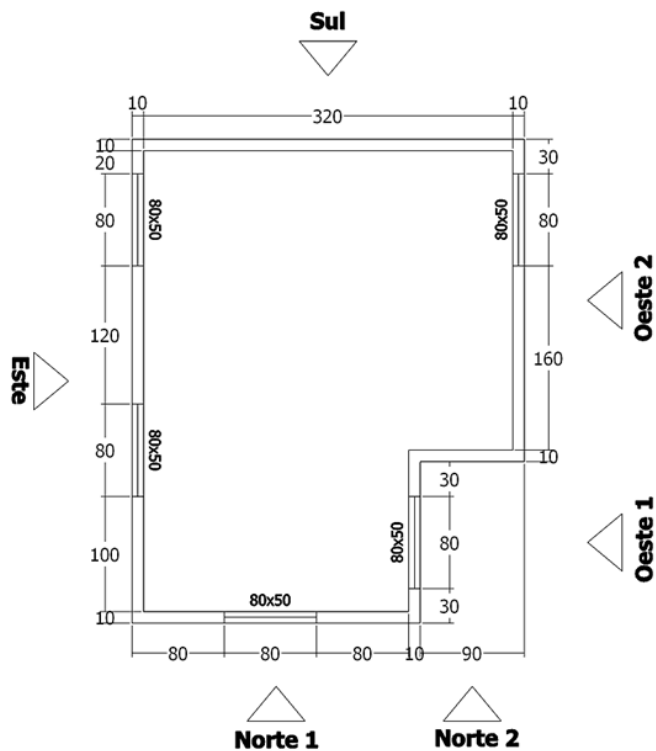
Primeiro piso



Obs.:

Altura até à soleira das janelas: 60cm desde a fundação

Segundo piso



Obs.:

Altura até à soleira das janelas: 60cm desde a primeira laje



Universidade do Minho

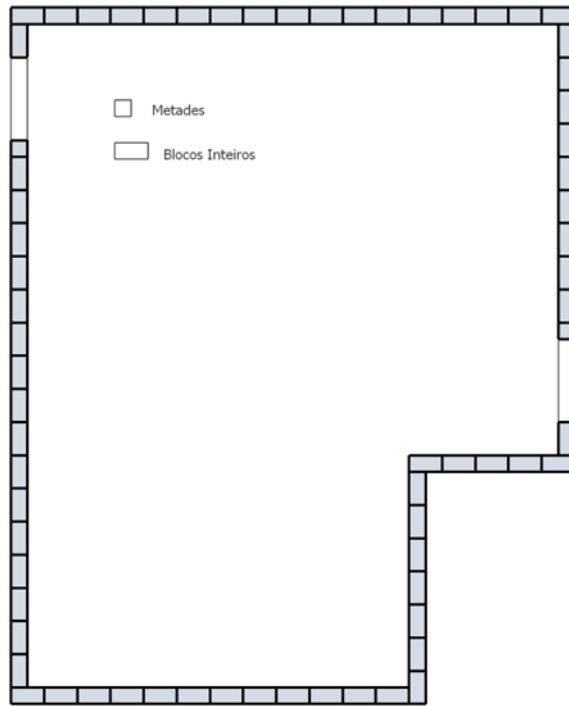
ENSAIO EM MESA SÍSMICA

Novembro 2011

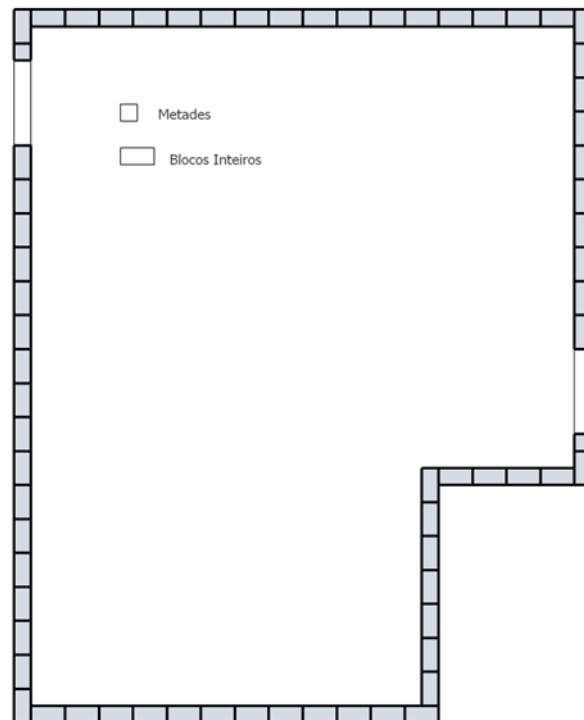
Plantas do primeiro e segundo pisos

13/33

Primeira fiada



Segunda fiada



Universidade do Minho

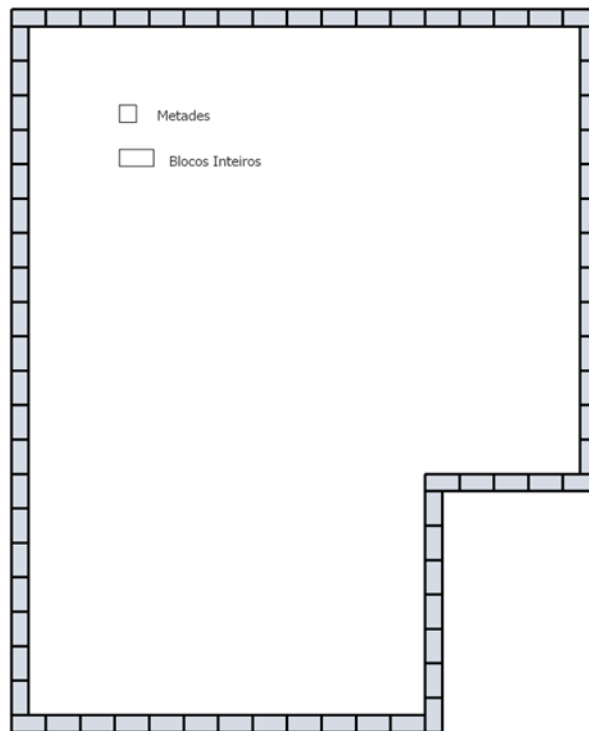
ENSAIO EM MESA SÍSMICA

Posicionamento dos blocos para o edifício não reforçado no primeiro piso

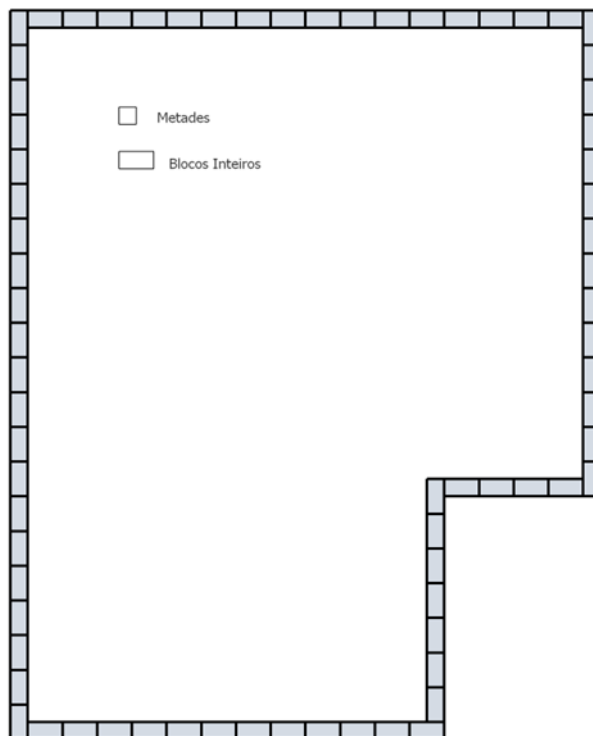
Novembro 2011

14/33

Primeira fiada



Segunda fiada

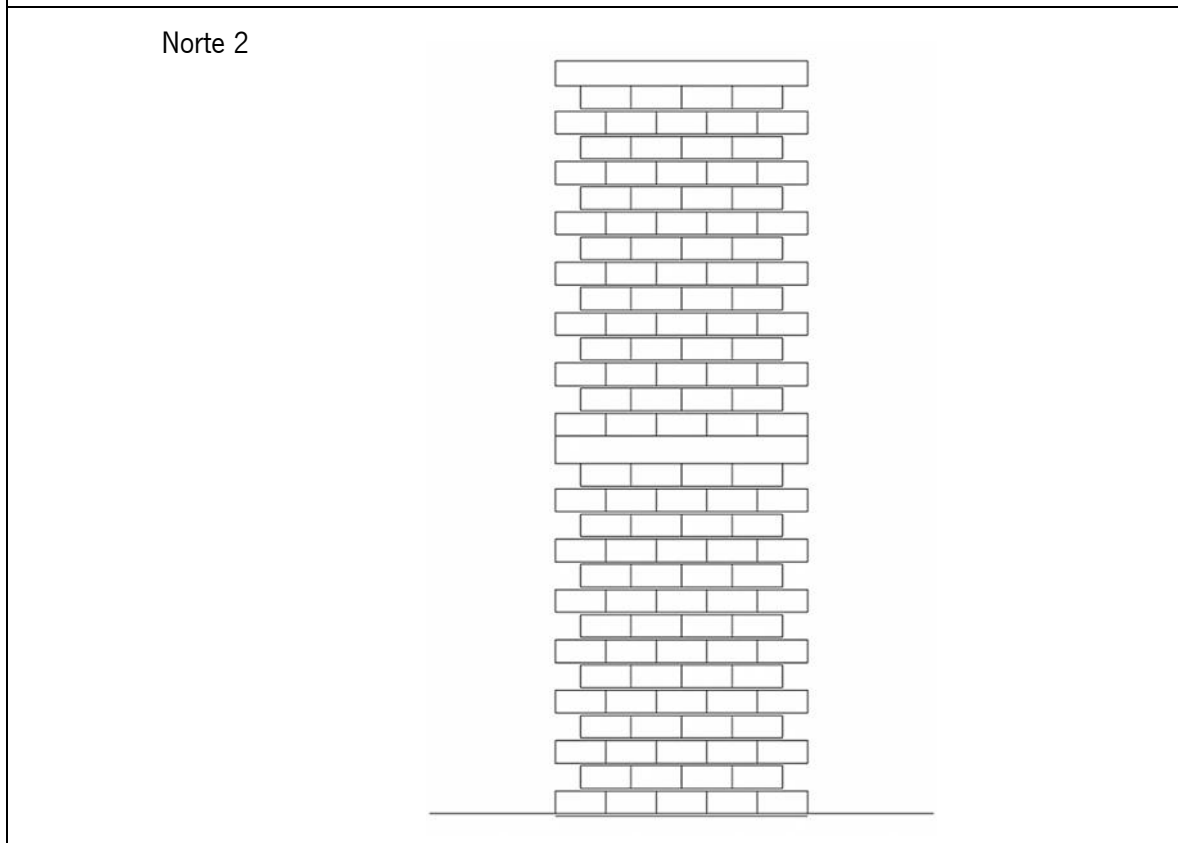
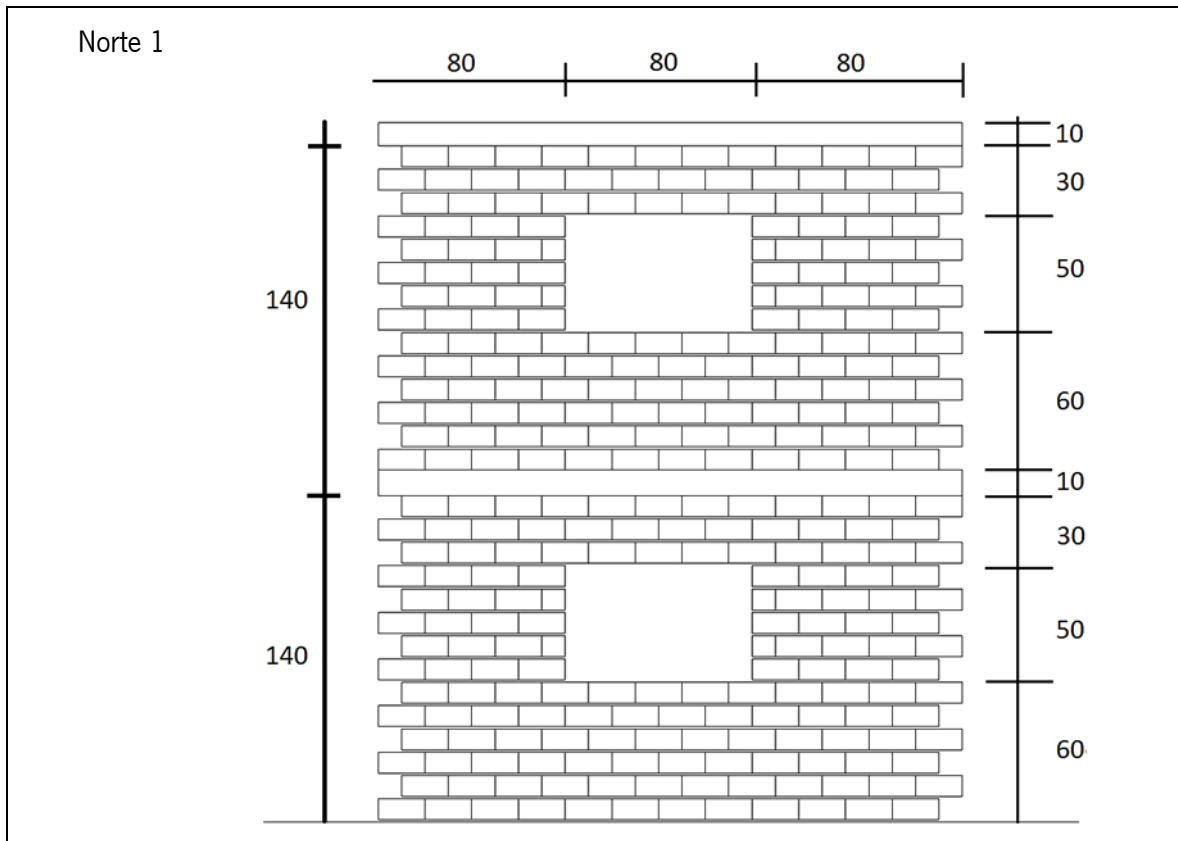


ENSAIO EM MESA SÍSMICA

Novembro 2011

Posicionamento dos blocos para o edifício não reforçado no segundo piso

15/33

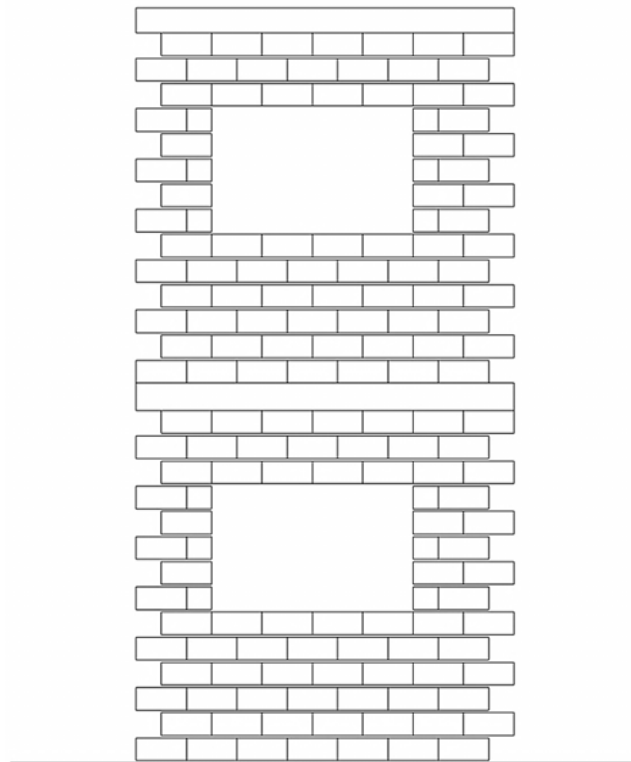


ENSAIO EM MESA SÍSMICA
 Posicionamento dos blocos do edifício não reforçado na fachada norte

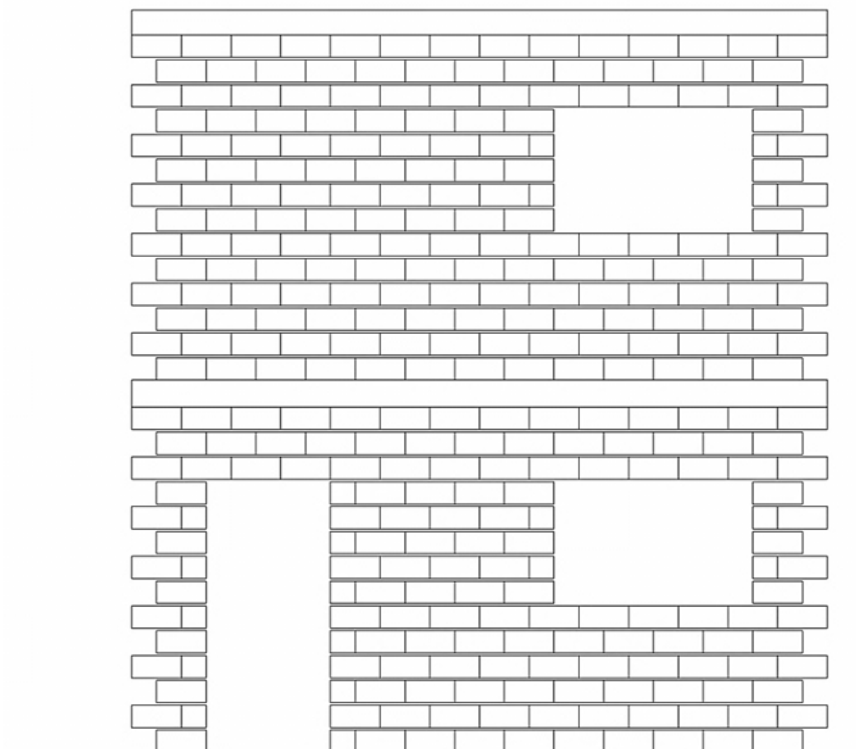
Novembro 2011

16/33

Oeste 1



Oeste 2



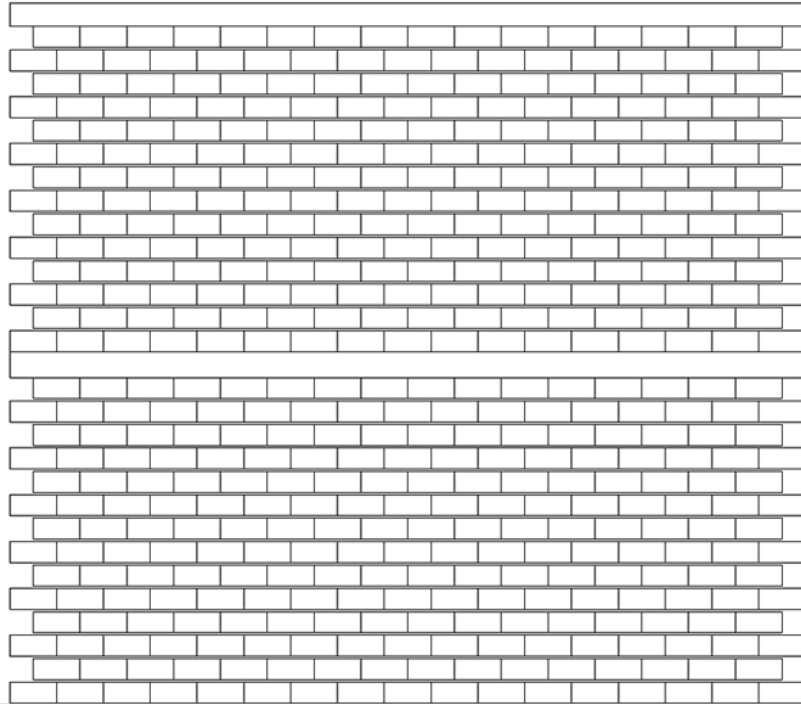
ENSAIO EM MESA SÍSMICA

Novembro 2011

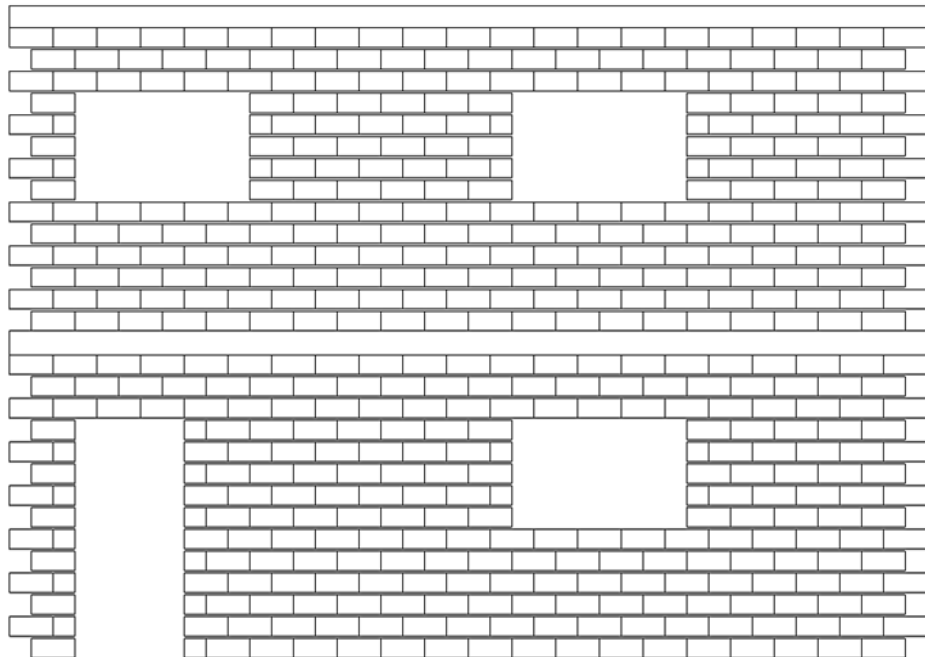
Posicionamento dos blocos do edifício não reforçado na fachada oeste

17/33

Sul



Este

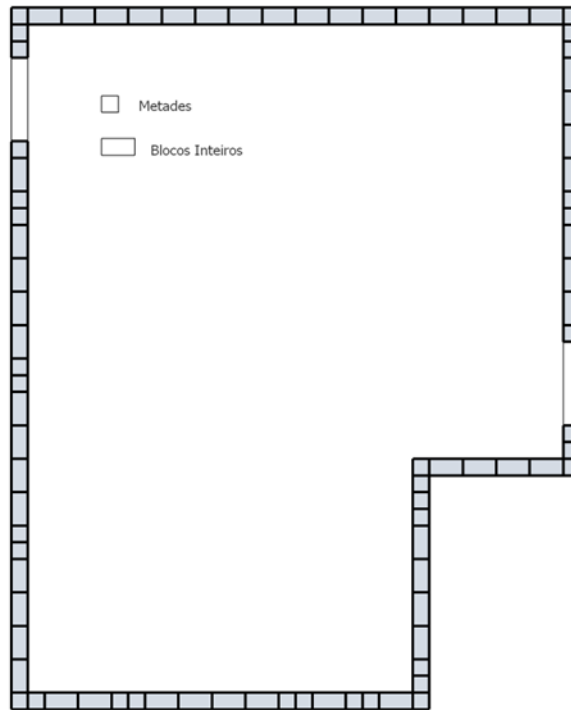


ENSAIO EM MESA SÍSMICA
 Posicionamento dos blocos do edifício não reforçado na fachada
 sul e este

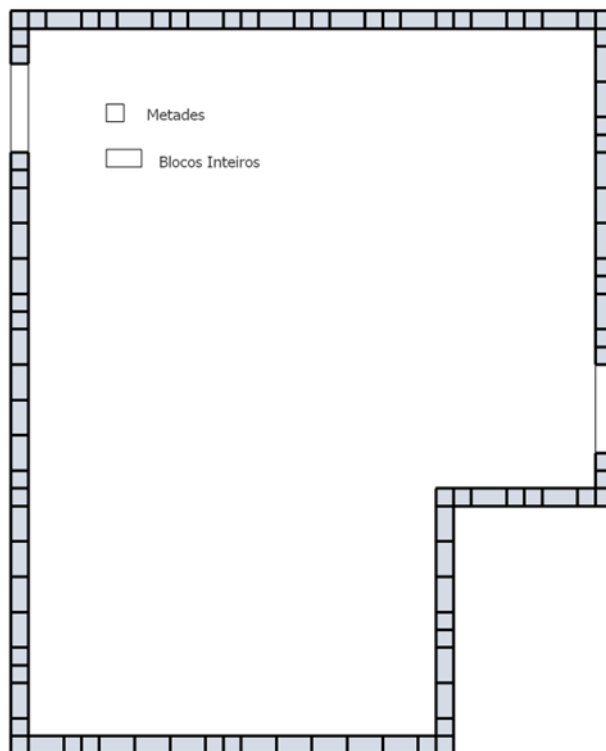
Novembro 2011

18/33

Primeira fiada



Segunda fiada

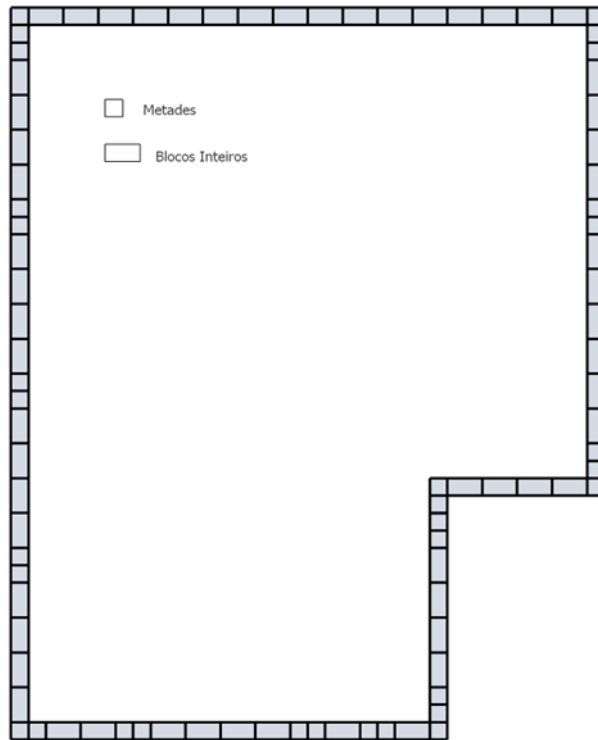


ENSAIO EM MESA SÍSMICA
 Posicionamento dos blocos para o edifício reforçado no primeiro
 piso

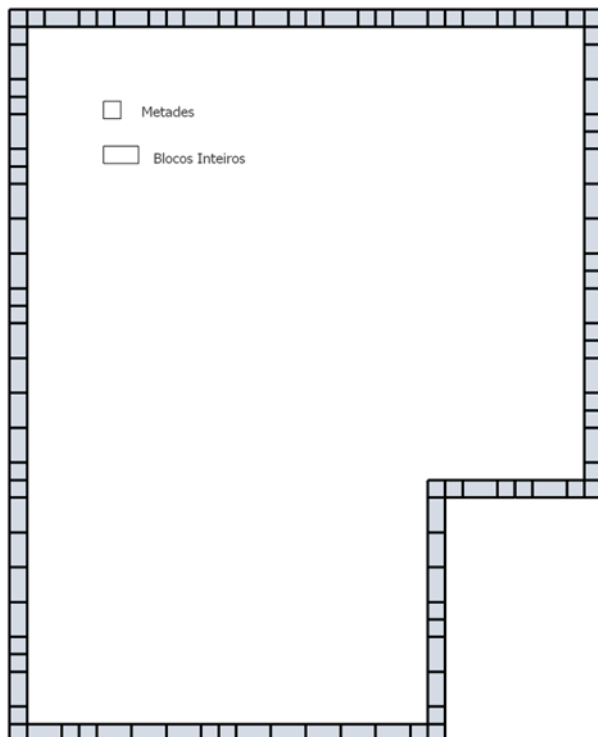
Novembro 2011

19/33

Primeira fiada



Segunda fiada

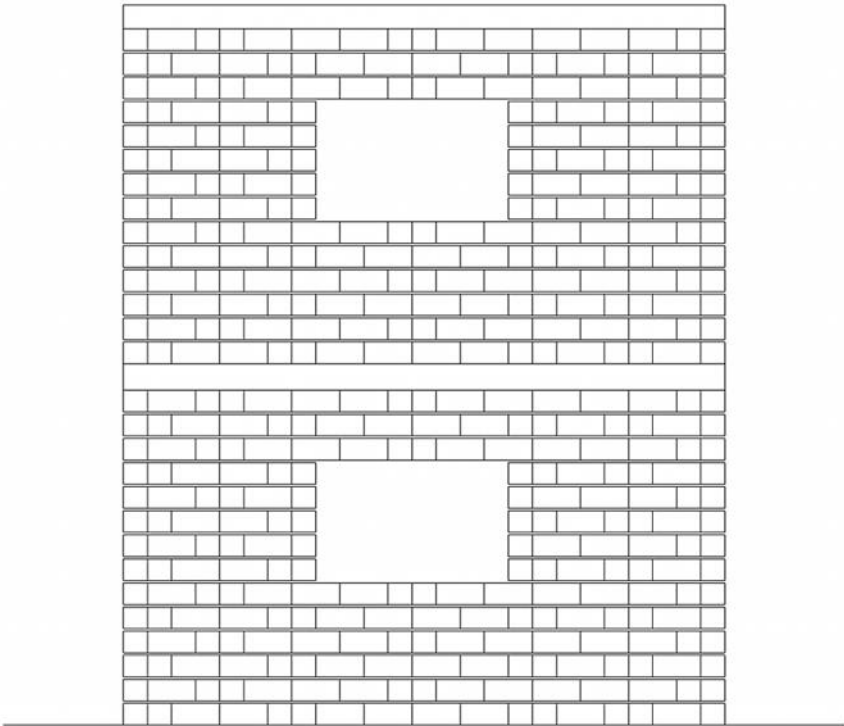


ENSAIO EM MESA SÍSMICA
 Posicionamento dos blocos para o edifício reforçado no segundo
 piso

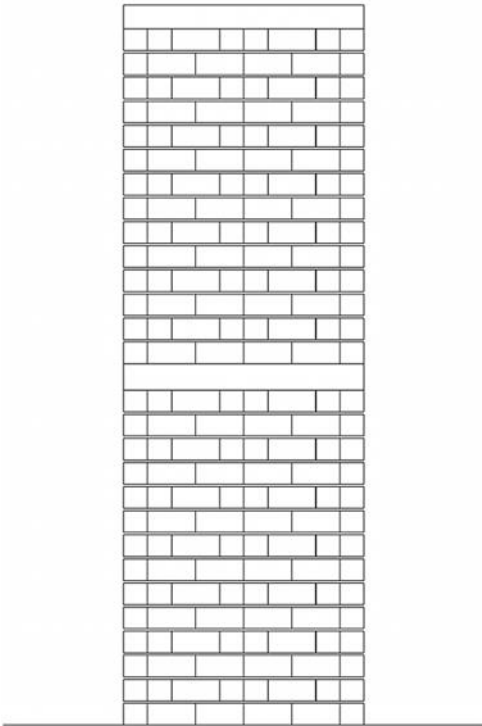
Novembro 2011

20/33

Norte 1



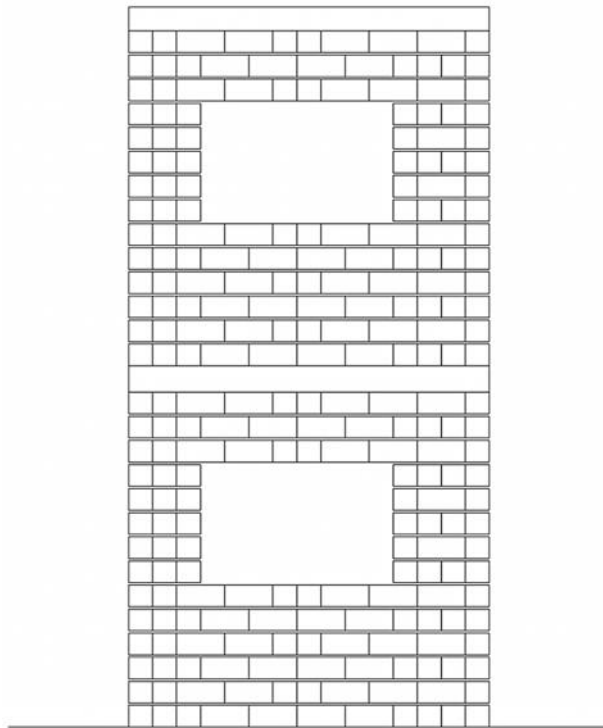
Norte 2



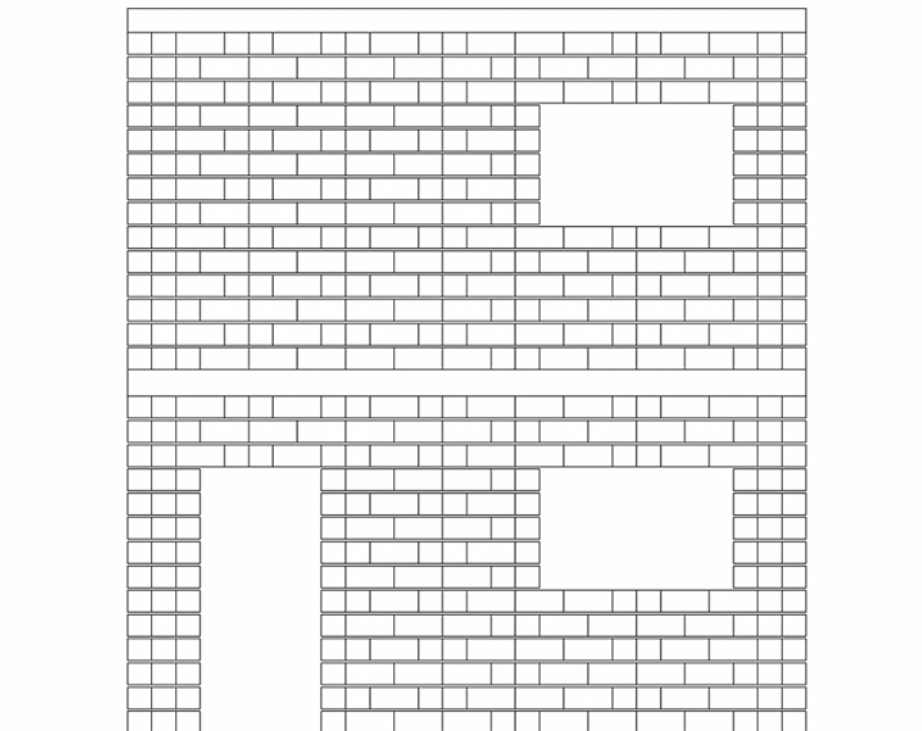
ENSAIO EM MESA SÍSMICA
Posicionamento dos blocos do edifício reforçado na fachada norte

Novembro 2011
21/33

Oeste 1



Oeste 2



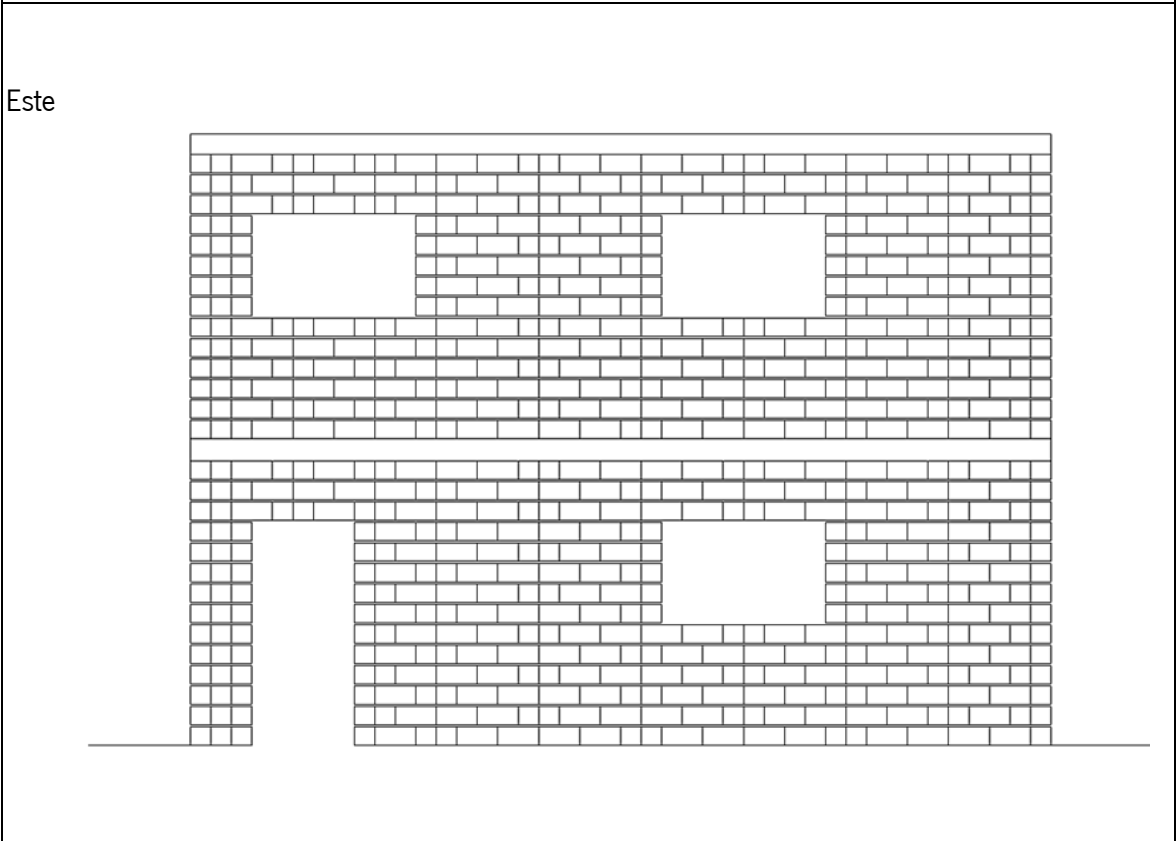
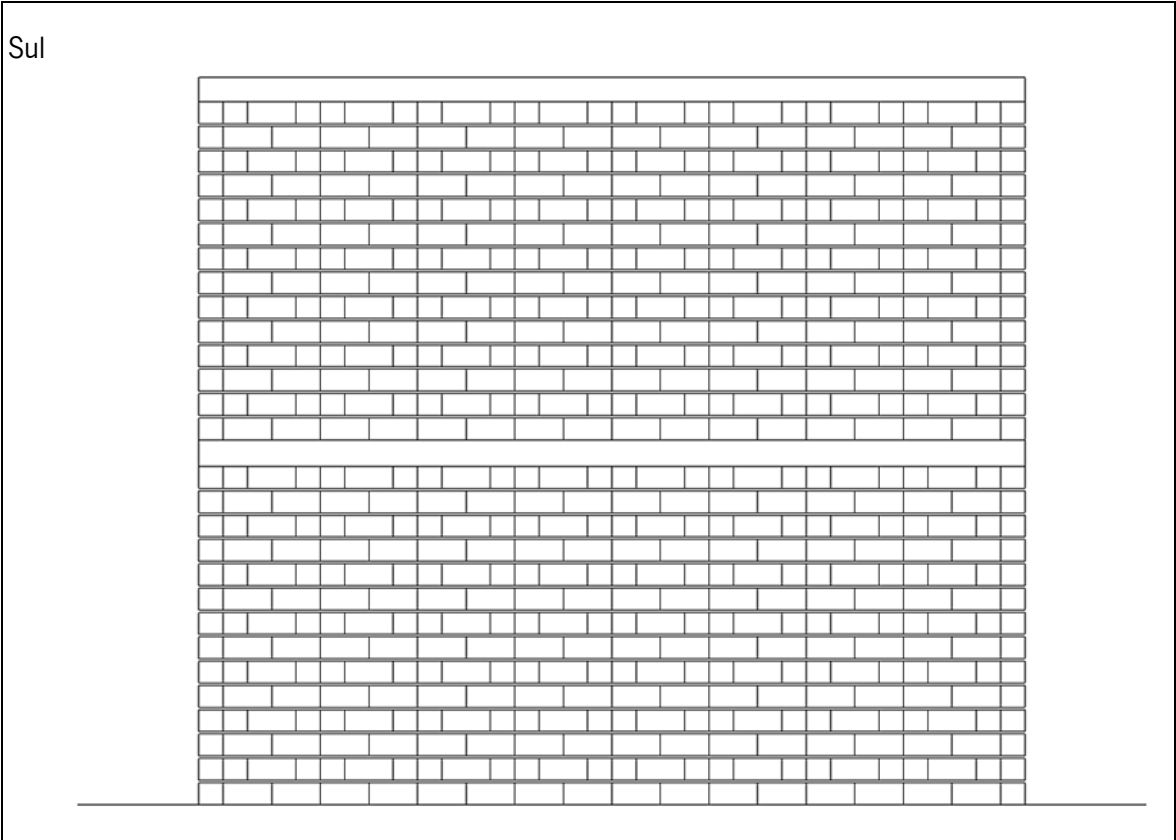
Universidade do Minho


ENSAIO EM MESA SÍSMICA

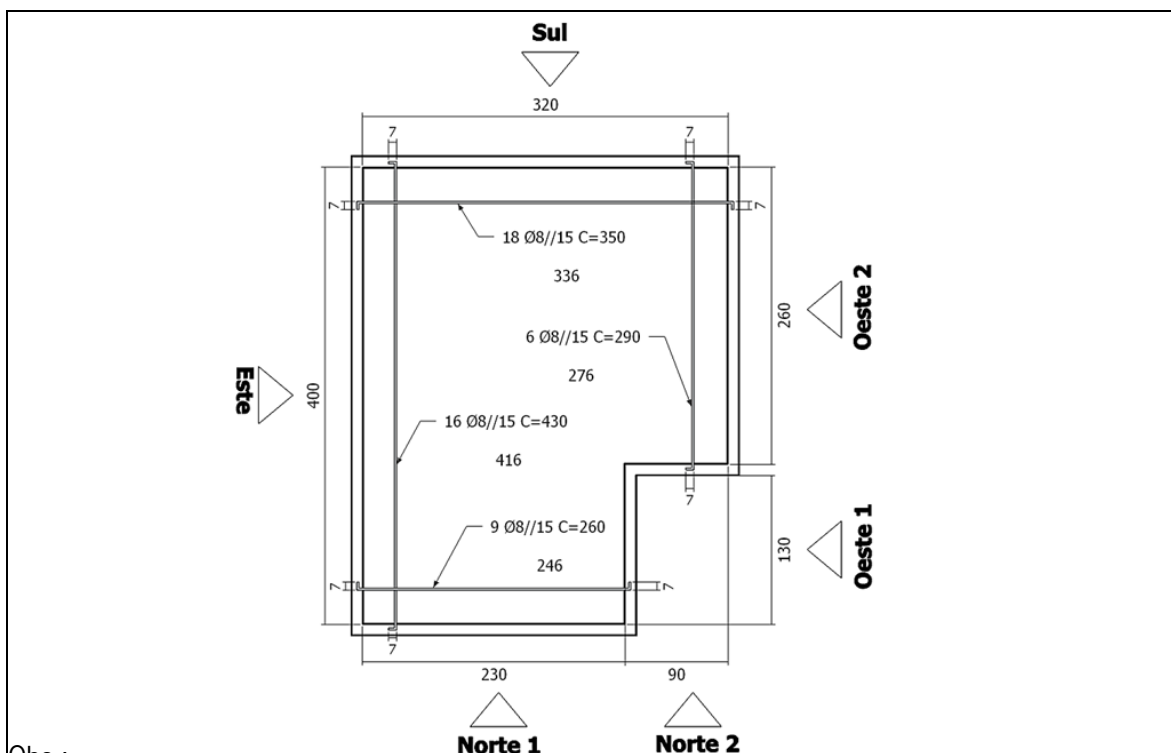
Posicionamento dos blocos do edifício reforçado na fachada oeste

Novembro 2011

22/33

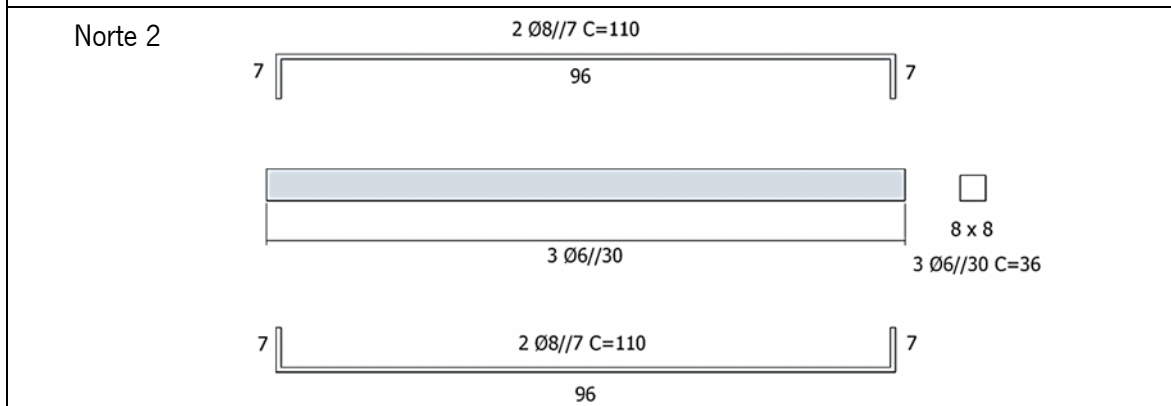
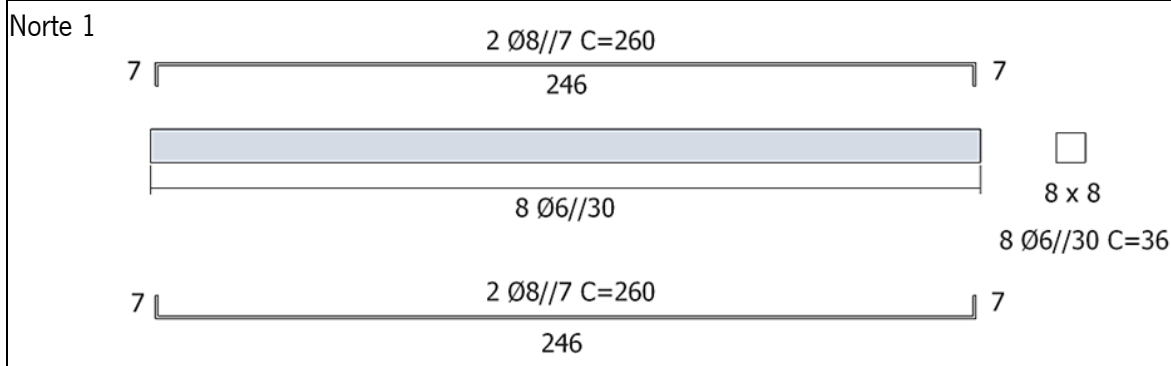


 Universidade do Minho	ENSAIO EM MESA SÍSMICA	Novembro 2011
	Posicionamento dos blocos do edifício reforçado na fachada sul e este	23/33



Obs.:

- A metade do bloco da ultima fiada de cada parede é preenchida com poliuretano, a outra metade é preenchida com betão juntamente com a laje.
- A armadura na direção este-oeste é sempre colocada debaixo da armadura na direção norte-sul




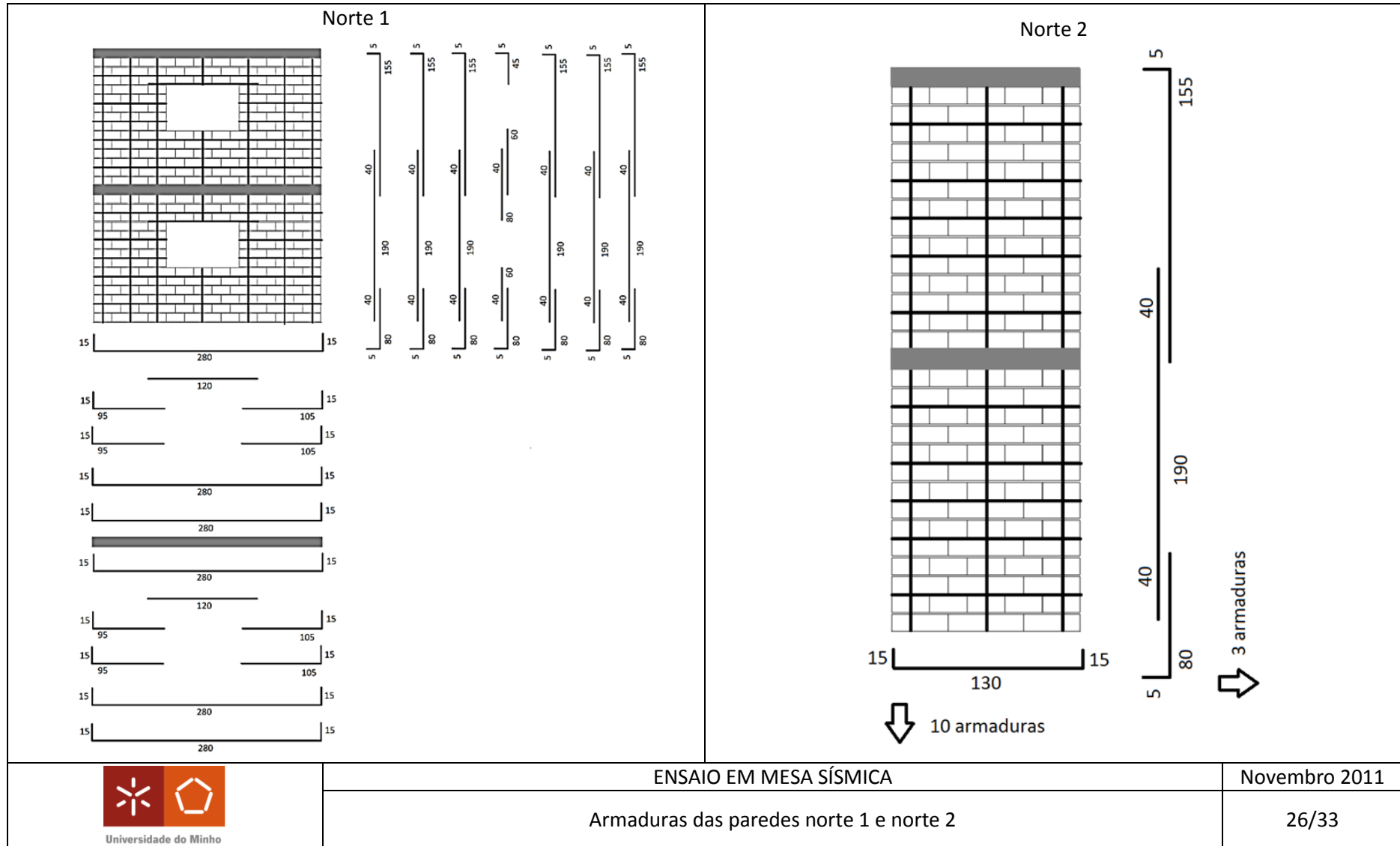
ENSAIO EM MESA SÍSMICA

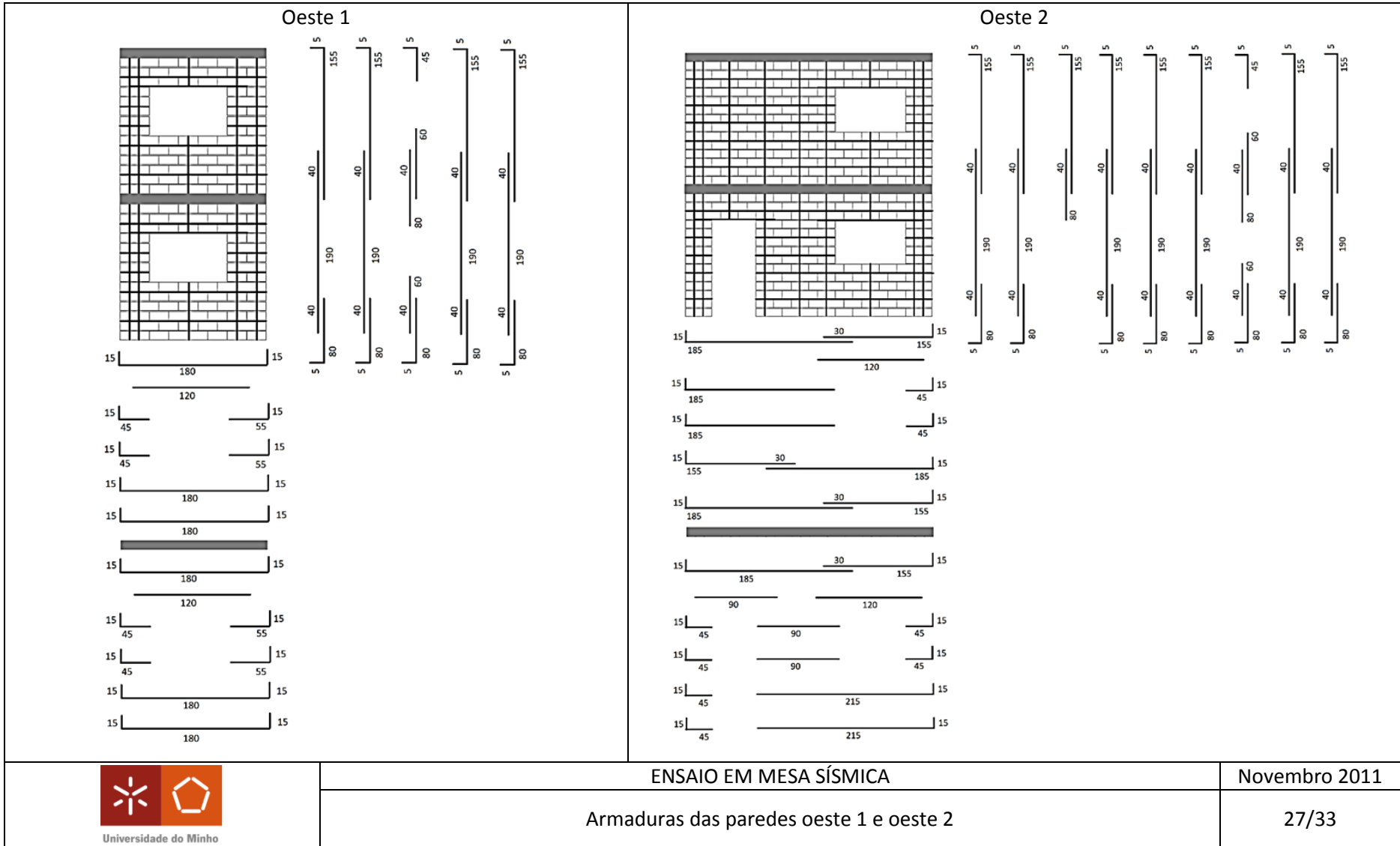
Novembro 2011

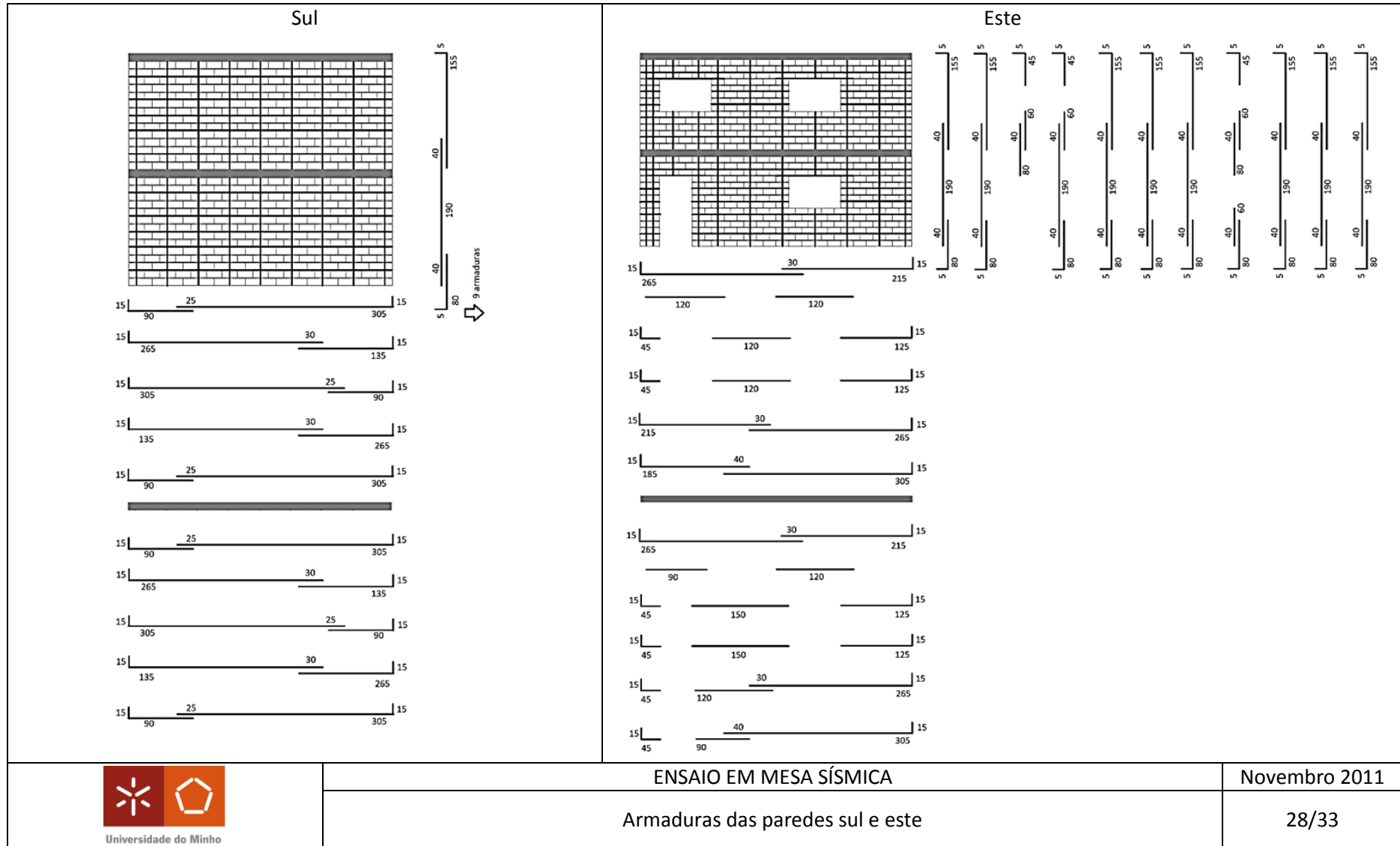
Laje e viga cinta norte 1 e norte 2

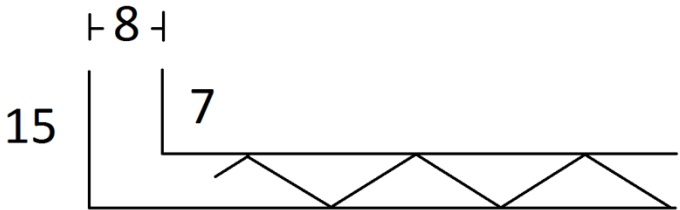
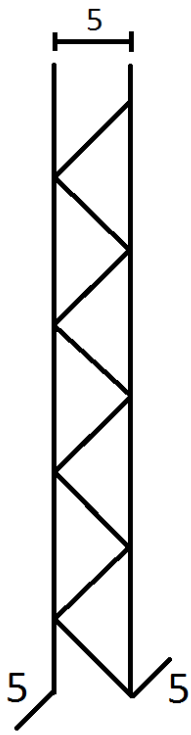
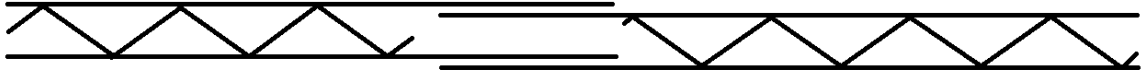

24/33


<p>Oeste 1</p>		<p>8 x 8 5 Ø6//30 C=36</p>
<p>Oeste 2</p>		<p>8 x 8 9 Ø6//30 C=36</p>
<p>Sul</p>		<p>8 x 8 11 Ø6//30 C=36</p>
<p>Este</p>		<p>8 x 8 14 Ø6//30 C=36</p>
	<p>ENSAIO EM MESA SÍSMICA Viga cinta oeste 1, oeste 2, sul e este</p>	<p>Novembro 2011 25/33</p>

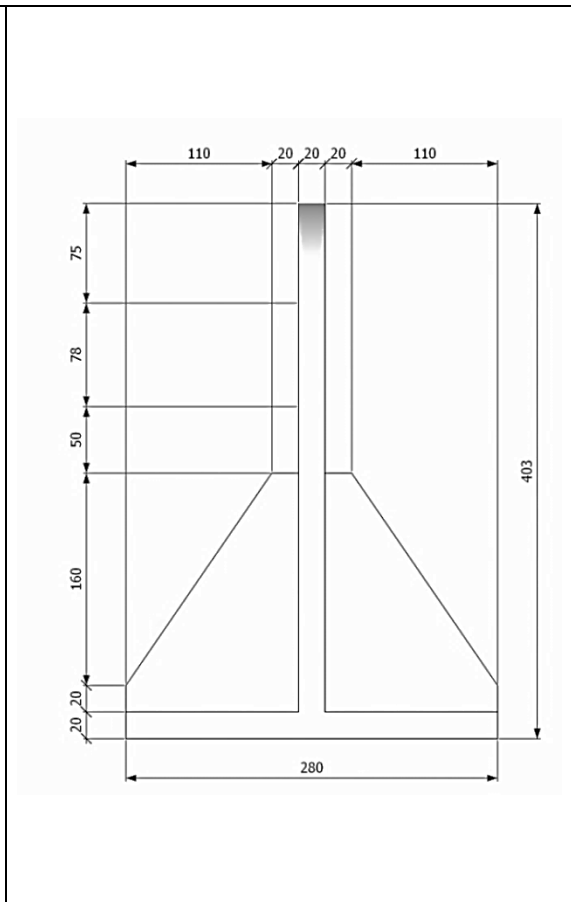
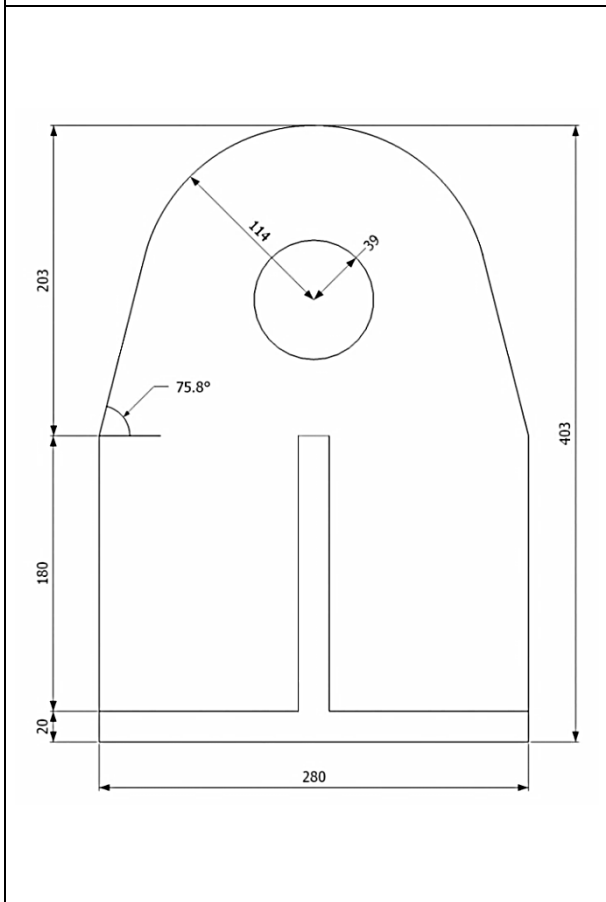
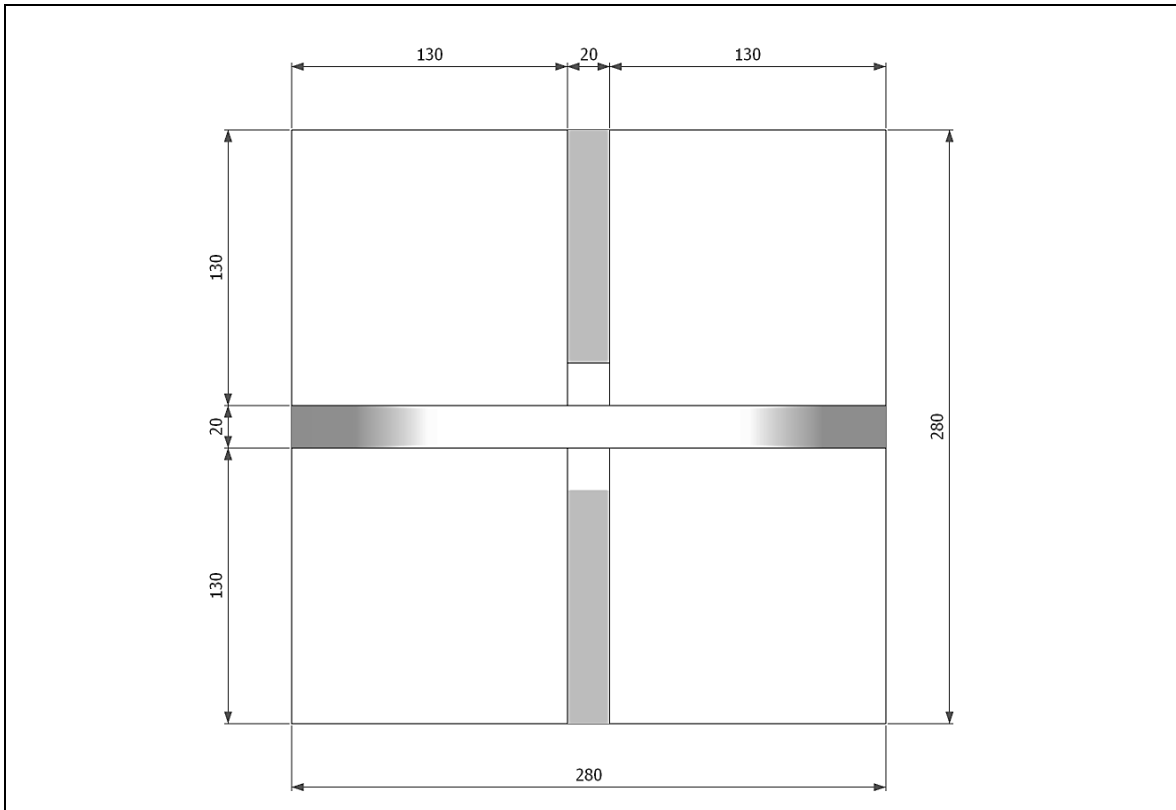







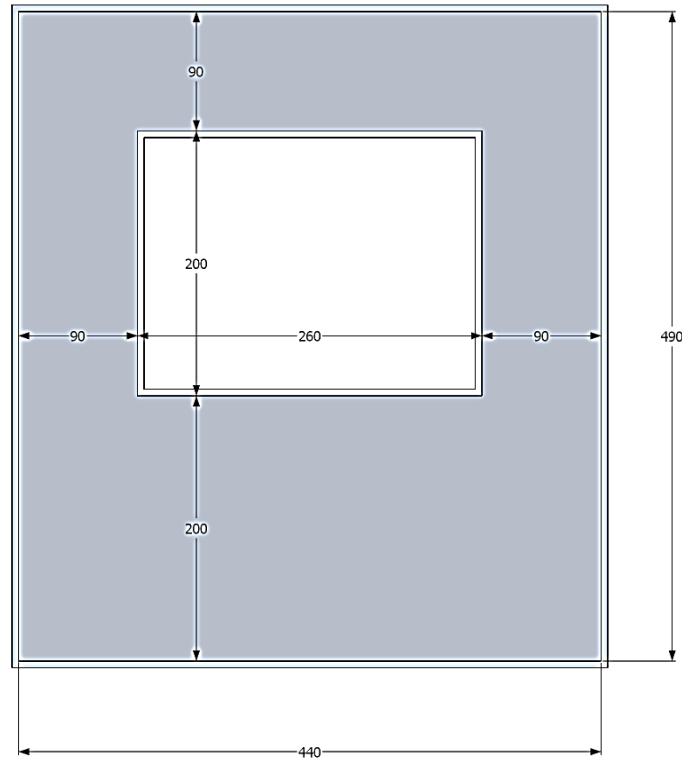
<p>Armadura horizontal (8cm entre longitudinaes)</p> 	<p>Armadura vertical (5cm entre longitudinaes)</p> 	
<p>Sobreposição</p> 		
 <p>Universidade do Minho</p>	<p>ENSAIO EM MESA SÍSMICA</p> <p>Detalhe das armaduras treliçadas</p>	<p>Novembro 2011</p> <p>29/33</p>

Betão (30MPA)		Argamassa	
Fundação	5.73 m ³	Edifício reforçado	0.81 m ³
Lajes	2.71 m ³	Edifício não reforçado	0.64 m ³
Total:	8.44 m ³	Total:	1.5 m ³
Blocos			
<u>Edifício refoçado</u>		<u>Edifício não reforçado</u>	
Inteiros	1223	Inteiros	1806
Metades	1245	Metades	62
Total:	Inteiros Metades	3029 1307	
Aço			
<u>Fundação</u>		<u>Lajes</u>	
Ø8	293 m	Ø6	36 m
Ø12	470 m	Ø8	474 m
Total:	Ø6 Ø8 Ø12	36 m 767 m 470 m	
<u>Armadura treliçada</u>			
Horizontal (8cm entre longitudinales)		Vertical (5cm entre longitudinales)	
<u>Comprimento</u>	<u>Quantidade</u>	<u>Comprimento</u>	<u>Quantidade</u>
45	18	45	6
55	4	60	10
90	11	80	48
95	4	155	38
105	4	190	38
120	12		
125	4		
130	10		
135	4		
150	2		
155	4		
180	6	Horizontal (8cm)	173 ml
185	7	Vertical (5cm)	179 ml
215	5		
265	8		
280	6		
305	8		
		Total:	
		Horizontal (8cm)	173 ml
		Vertical (5cm)	179 ml
		ENSAIO EM MESA SÍSMICA	Novembro 2011
		Quantidade de materiais	30/33




 Universidade do Minho	ENSAIO EM MESA SÍSMICA	Novembro 2011
	Peça de suspensão	31/33

Planta



Vista lateral



 Universidade do Minho	ENSAIO EM MESA SÍSMICA	Novembro 2011
	Formas da base	32/33

